acta physica slovaca vol. 58 No. 3, 243 – 486 **June 2008**

COHERENT MANIPULATIONS OF ATOMS USING LASER LIGHT

Bruce W. Shore[1]
618 Escondido Cir., Livermore, CA 94550, USA

Received 11 July 2008, accepted 18 July 2008

The internal structure of a particle – an atom or other quantum system in which the excitation energies are discrete – undergoes change when exposed to pulses of near-resonant laser light. This tutorial review presents basic concepts of quantum states, of laser radiation and of the Hilbert-space statevector that provides the theoretical portrait of probability amplitudes – the tools for quantifying quantum properties not only of individual atoms and molecules but also of artificial atoms and other quantum systems. It discusses the equations of motion that describe the laser-induced changes (coherent excitation), and gives examples of laser-pulse effects, with particular emphasis on two-state and three-state adiabatic time evolution within the rotating-wave approximation. It provides pictorial descriptions of excitation based on the Bloch equations that allow visualization of two-state excitation as motion of a three-dimensional vector (the Bloch vector). Other visualization techniques allow portrayal of more elaborate systems, particularly the Hilbert-space motion of adiabatic states subject to various pulse sequences. Various more general multilevel systems receive treatment that includes degeneracies, chains and loop linkages. The concluding sections discuss techniques for creating arbitrary pre-assigned quantum states, for manipulating them into alternative coherent superpositions and for analyzing an unknown superposition. Appendices review some basic mathematical concepts and provide further details of the theoretical formalism, including photons, pulse propagation, statistical averages, analytic solutions to the equations of motion, exact solutions of periodic Hamiltonians, and population-trapping "dark" states.

PACS: 01.30.Rr, 31.70.Hq, 32.80.Qk, 33.80.-b

KEYWORDS: Coherent excitation, Laser-induced excitation, Optical pumping, Adiabatic following, Stimulated Raman adiabatic passage, Coherent superpositions, Quantum state manipulation, Coherent control, Pulsed excitation, Dark quantum states

[1]E-mail address: bwshore@alum.mit.edu

Contents

1 Introduction

Atoms and molecules have long held interest, first of philosophers who debated their existence, then by spectroscopists who gained understanding of their internal structure, and more recently by physicists and chemists who use laser light to alter that structure, perhaps only briefly. This tutorial reviews some of the simplest notions of atomic and optical physics, namely how single atoms (or other simple quantum systems) are affected by laser light – a subject that is sometimes regarded as a part of quantum optics [1]. Starting with basic notions of atoms, quantum states and radiation, I will proceed to discuss the relevant equations of motion that govern alterations of atomic structure as a result of this interaction. Several examples illustrate the physics principles, those of coherent atomic excitation [2, 3, 4]. These principles have relevance to such basic concerns as the detection and quantitative analysis of trace amounts of chemicals [5], the catalysis or control of chemical reactions [6, 7], the alignment of molecules [8] and the processing of quantum information [9].

To place these contemporary applications into historical context I shall begin, in this introductory section and the next, by reviewing a few basic concepts: atoms as structured particles, and the clues to that structure provided by spectroscopy; quantum states and probabilities; and the parameters with which we characterize laser radiation. As will be emphasized, the underlying physics has broader application than atoms and molecules: a wide variety of quantum systems have the required discrete energies that enable coherent excitation of the sort described here.

The next sections, starting with Sec. 3, provide the mathematical foundation for describing the atom response to coherent radiation, first with a wavefunction (Sec. 3.2) and then with aid of abstract vector spaces for describing probability amplitudes (Sec. 3.4). These mathematical tools allow a discussion of the equations of motion needed to describe changes (Secs. 4 and 5).

Following these elementary notions will come the simplest of examples of the theory of radiation-induced changes to atomic structure, the "two-level atom" (or two-state quantum system) [10, 11], see Sec. 6. Section 7 offers an alternative view of the changes that take place within an atom as it acquires excitation energy.

Laser-induced excitation of free atoms or molecules inevitably deals with the effects of spherical or cylindrical symmetry, and the consequent degeneracy of energy levels [2]. Section 8 presents some of the basic theoretical principles needed to understand such symmetry-constrained excitation, based on the use of quantum states having well defined angular momentum. One consequence is the transfer of excitation probability by a combination of coherent excitation and incoherent excitation, known as optical pumping; cf. Sec. 8.3.

Section 9 mentions several important refinements of the simple theory, needed when describing the response of actual atoms: allowance for probability loss, treatment of ensemble averages that account for the distribution of attributes within an atomic beam (cf. also Appendix F), and extensions of the theory beyond the simple two-state rotating wave approximation (cf. also Appendix L).

The theoretical tools of the earlier sections – the essential-states approximation, rotating wave approximation and adiabatic changes – next find application, in Sec. 10, to three-state systems, with particular emphasis on stimulated Raman processes. These involve two independent fields,

[2] Quantum states that have the same energy are said to be *degenerate*, and are often termed *sublevels* of a given energy level.

often termed "pump" and "Stokes" fields. The process of stimulated Raman adiabatic passage (STIRAP) described there relies in part on the creation of a "dark" quantum state, a quantum-state superposition that is not excited by the radiation, cf. Sec. 10.6 and Appendix M.

Section 11 extends the theory to some simple examples of multilevel systems in which the linkage patterns form simple chains, branched chains or loops. Many of these cases have analytic solutions; some reveal unexpected dynamics.

Whereas the bulk of this review aims to describe complete alteration of atomic structure, from an initial state to a single final state, Sec. 12 discusses a few examples of excitation techniques that can create superpositions of quantum states or, from such superpositions, produce other predetermined superpositions. Section 13 discusses some procedures for analyzing such structures once they are created.

Apart from one section dealing with changes induced by incoherent interactions (Sec. 4), this article deals almost entirely with aspects of coherent excitation. It assumes that the responsible interaction is laser radiation. It is possible, under appropriate conditions, to achieve coherent changes in other ways. A simple example occurs in the idealized model of two trapped atoms, such as might be held within an optical lattice, cf. Sec. 2.3. By altering the separation between the two atoms in a controlled way one can produce coherent changes of the sort governed by the time-dependent Schrödinger equation, but for DC fields. Basically one considers the controlled formation of a molecule from two atoms. Such situations will not be considered explicitly here.

A series of appendices provides some mathematical background and further details on several of the topics. The bibliography, though lengthy, is not intended to be comprehensive, only indicative of available literature. The tools of internet search engines now make completeness less important.

The overall presentation emphasises theory, rather than experiment. It stresses the mathematical formulation, specifically the time-dependent Schrödinger equation, aimed at both computation and analytical solutions to the resulting coupled ordinary differential equations (ODEs). It particularly aims to provide ways of visualizing the excitation process using pictures involving abstract vector spaces.

1.1 Atoms: Structured particles

The 19th century saw the general acceptance of atoms as the smallest particles of matter that retained some of the chemical properties of aggregates. This notion, dating back to Greek philosophers, led to the fruitful quantitative explanation of vapor properties based upon atoms as moving mass points, the kinetic theory of gases [12].

But atom vapors have additional properties, made evident through observation of light emitted from hot gases or transmitted through cool vapor, see Fig. 1. Such properties underly the science of spectroscopy [13].

Spectroscopists recognized that the radiation emitted from an optically thin source of hot atoms contained features centered around discrete wavelengths, appearing as bright spectral lines [14]. By contrast, cooler atoms would absorb, from a continuous blackbody source, discrete wavelengths, appearing as dark spectral lines [3]. Figure 2 illustrates this property [2, §1.1].

[3] Although I have referred to spectral lines as having discrete frequencies, close examination reveals that the spectral features – the frequency distribution of light added or removed – occur over a small range of frequencies: the spectral lines have a finite width [2, §1.8]. These line widths convey useful information about the lifetime of the excited state and

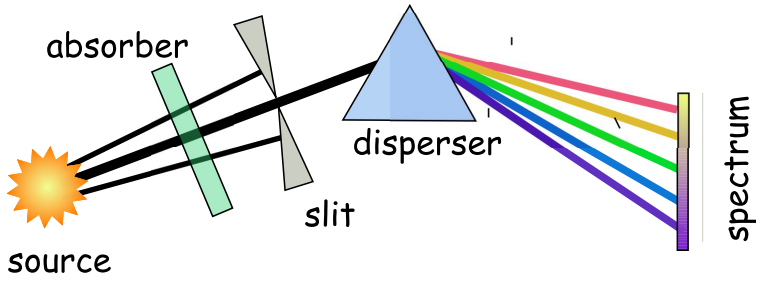

Fig. 1. Schematic definition of the spectroscopic atom: light from a source passes through a slit and then through a dispersing element (here a prism) which separates the radiation into constituent frequencies. An absorber, when present, removes selected frequencies. (after Fig. 1.1-2 of [2])

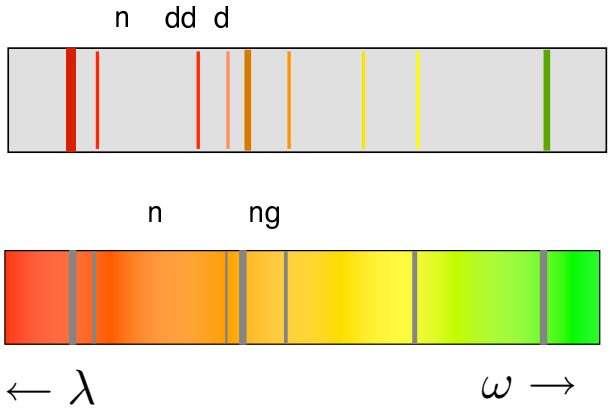

Fig. 2. Schematic illustration of emission spectra (comprising bright spectral lines) and absorption spectra (dark lines).

The wavelengths of these spectral lines were found to be uniquely characteristic of each chemical element, each different molecule, as suggested by Fig. 3. Evidently the vapor atoms carried with them, in some internal structure, the capability to produce these spectral lines as unique characteristic "fingerprints".

Detailed records of the wavelengths (or better, the *wavenumbers* – the inverses of vacuum-recorded wavelengths) of numerous spectra revealed that all spectral lines obeyed a spectroscopic *combination principle*: each wavenumber [4] $\tilde{\nu} \equiv 1/\lambda$ of a spectral line could be expressed as the difference of two spectroscopic *term values* $\tilde{E}$. That is, the wavenumbers were all expressible in

about the environment within which the emitting or absorbing atom resides [15]. Section 9 discusses some effects that act to broaden the range of frequencies for which atoms respond.

[4] Wavenumbers and term values have dimensions of inverse lengths, often expressed in units of Kayser, 1 cm^{-1} or kiloKayzer, kK.

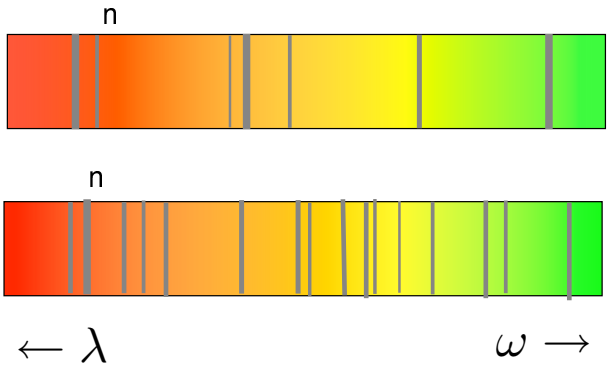

Fig. 3. Different elements, even different isotopes, have different spectra, here shown schematically. (after Fig. 1.1-3 of [2])

the form

$$\tilde{\nu} = \tilde{E}_i - \tilde{E}_j. \tag{1}$$

where the integers i and j identify the term values in a suitable ordered list. The explanation of this empirical rule emerged from several sources, including the Lorentz theory of electrons [16] – light negatively charged particles, bound to heavy positively charged nuclei, that absorb and emit radiation – together with the early quantum theory of Bohr, according to which the electron motion within an atom could have only discrete energies E_n. The index n here identifies a entry in an ordered list of energies, in which the lowest value is termed the *ground state* energy.

Taken together with the Planck theory of discrete radiation quanta, of energy $h\nu$, these theories provided an interpretation of the well established spectroscopic combination principle as a conservation of energy,

$$h\nu = E_i - E_j. \tag{2}$$

That is, the frequencies of spectral lines, multiplied by Planck's constant $h \equiv 2\pi\hbar$, corresponded to differences of excitation energies [5]. These discrete values are *Bohr frequencies*,

$$\omega_{ij} = |E_i - E_j|/\hbar. \tag{3}$$

Figure 4 illustrates this principle.

Spectroscopists found that not all possible pairs of energies produced spectral lines; they devised various empirical *selection rules* to classify "allowed" and "forbidden" transitions [6]. Drawing on the Lorentz theory of electrons [2, §8.2] (see Appendix I), the intensity of the spectral lines were parametrized by *oscillator strengths* [see eqn. (404)] [17].

[5] The discrete electromagnetic energy $h\nu \equiv \hbar\omega$ needed to produce excitation of a single atom, or emitted during deexcitation, defines a *photon*; cf. Appendix A.4.

[6] Spectroscopists, seeking patterns, found that the energy levels of free atoms could be classified as being one of two classes, termed *even parity* and *odd parity*. Transitions were generally not observed without a parity change.

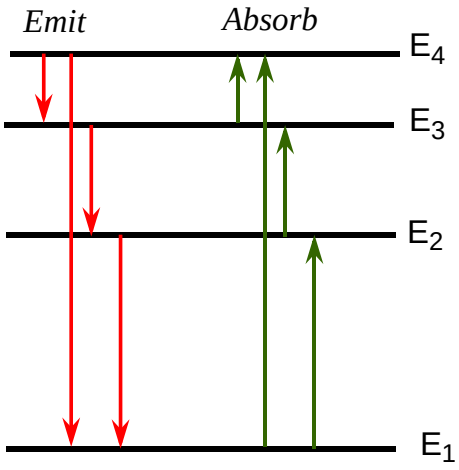

Fig. 4. Schematic illustration of the Bohr atom: internal energies are discrete; transitions to lower energies (left-hand arrows) produce emission lines, while absorption of discrete frequencies (right-hand arrows) produces excitation. (after Fig. 1.1-4 of [2])

The energy selectivity implied by the Bohr principle expressed with eqn. (2) – the unique association of specific energy states with specific frequencies – makes possible the quantitative analysis of atom samples to determine the relative abundance of constituent atoms and molecules, even allowing an experimenter to distinguish the several isotopes [7]. Traditional spectroscopy, making use of the distribution of frequencies absorbed and emitted by sources, provides a widely used tool for analytical chemistry [19], of forensic science [20], in archeology and art conservation [21], for industrial process control [22], for remote sensing of the environment [23] and has use in astrophysics for the study of distant stars [24]. These techniques use wavelengths ranging from x-rays [25] to radio [26]. When supplemented with symmetry-based constraints (e.g. angular momentum selection rules), and used with carefully timed pulses, the Bohr condition underlies the procedures presented in this review for manipulating internal motions of atoms. However, the theory presented in the present review deals with radiation whose properties (coherence) differ in an essential way from the radiation used in traditional spectroscopy [27]. This property makes possible a variety of improvements in the selectivity of traditional processes [28]. It also allows manipulations of quantum structures in ways that would be impossible with incoherent light sources.

Laser light sources provide important tools for spectroscopic studies of matter and for measuring pre-existing properties, but they also create opportunities to alter the internal structure of atoms. It is with such deliberate changes of atomic structure that the present article deals. Numerous books and reviews attest to the current interest in this subject [6, 7]. In turn, these laser-induced modifications permit one to produce, through emission of light from restructured atomic sources, tailored radiation fields, either in cavities [29] or propagating in free space; see

[7] The small but resolvable isotope shift of spectral lines underlies the procedures that make possible the separation of isotopes, even in commercially useful amounts [18].

Appendix A.1.

1.2 Atoms: Discrete quantum states

Basic quantum theory requires that when some motion is constrained within a finite region of space, and the system is isolated from uncontrollable external influences, the energy of that motion can take only discrete values – it is *quantized* [8]. Common examples of energy quantization include

- The motion of electrons bound to nuclei of atoms or molecules by Coulomb forces
- Vibrations of molecular parts
- Rotation of molecular frameworks
- The orientation energy of nuclear spins in an external magnetic field
- Energies of electrons and holes in quantum dots
- Center of mass motion of atoms or ions held in a trap.

In all these cases, and many others, the total energy of the constrained particle – the sum of kinetic and potential energies – is restricted to take only discrete values, between which radiative transitions can occur at discrete frequencies. It is these transitions, and the corresponding structure changes, that are the subject of the present article. Numerous textbooks present systematic discussions of atomic and molecular structure [30]; these details are not needed for the present discussion.

The discrete energies of electrons bound within atoms, revealed by spectroscopy, are associated with discrete states of motion – structures whose (internal) kinetic and potential energies combine in only specific discrete ways. Such motions, distinguishable by energy, are the *quantum states* [31] [2, § 1.3] with which we are here concerned [9]. These quantum states are the quantum mechanical counterparts of the states of motion that particularize, for specified initial conditions, the dynamics of classical systems – those whose behavior follows the laws of motion first enunciated by Newton, e.g. trajectories of planets, missiles and atoms in beams.

Although actual atoms and molecules have dimensions of nanometers or less, many larger objects are affected by quantum-mechanical behavior and have discrete energies. Quantum dots are macroscopic objects, composed of millions of atoms, in which electrons are confined and hence have discrete energy states [32]. Bulk superconductors are composed of many pairs of electrons that condense, as Cooper pairs, into a single quantum state; these allow the sort of discrete-state transitions, and quantum-state manipulation, discussed here [33].

In general quantum systems have several degrees of freedom. For example, a molecular framework has both rotational and vibrational motions, as well as alignments of each nuclear

[8] As discussed in textbooks on quantum theory, the discreteness is one consequence of the basic mathematical properties of the time-independent Schrödinger equation together with boundary conditions; cf. Sec. 3.2. It follows also from the non-commuting nature of the operators representing angular momentum.

[9] More particularly, we deal with information about the quantum system, as embodied in the wavefunctions and statevectors discussed in subsequent sections. Traditional classical descriptions of motion, by contrast, typically concern trajectories of particles: how positions vary with passing time under the influence of applied forces.

spin. The correlations between several degrees of freedom, whether in a single particle, several particles, or particles and photons, lead to useful applications of quantum mechanics. Appendix D.1 comments on an important property of systems with several degrees of freedom – correlation and entanglement. Throughout this review, however, I shall consider just a single degree of freedom.

To simplify the discussion, I shall refer specifically to atomic electrons as the system of interest, although the physics applies to any system for which discrete energy states exist. The discrete allowed energies (the internal energy of the atom) can be organized into an ordered list, a catalog in which integers form labels:

$$E_1,\ E_2,\ E_3,\ \cdots.$$

Several such discrete-energy systems typically form a part of courses in elementary quantum mechanics: the harmonic oscillator (a model of vibrating molecules), the rigid rotor (a model for molecular rotation) and the hydrogen atom [34]. The recognition of such quantization was important in the development of quantum theory during the first decades of the 20th century. It unified the work of spectroscopists by providing an explanation for the discreteness of the discrete frequencies seen in emission spectra or the corresponding dark spectral lines appearing in absorption spectra. Historically, spectroscopy offered the key experimental basis for understanding the internal structure of atoms and molecules. Nowadays atomic structure calculations and quantum chemistry calculations can provide detailed predictions of the discrete energies of a variety of atoms, starting with hydrogen, and of various molecules [35]. But for many purposes the details of the internal structure of atoms need not be considered; it is only necessary to have available a table of discrete energies (or wavenumbers) together with some parameters that express the intensity of each spectral line, such as the oscillator strength [36]. Indeed, only those simple parameters are needed for quantifying the theory of coherent excitation presented in this review.

1.3 Probabilities

A fundamental principle of quantum theory is that any single measurement of the internal energy of an atom must be one of the values from the allowed list of quantized energies. More generally, any single measurement of some attribute (e.g. orientation) can only show a value associated with one of the allowed discrete quantum states [10].

However, a succession of measurements will not always produce the same energy, or reveal the same quantum state. Typically the results will appear as a distribution of values, randomly occurring but with well defined statistical characteristics such as mean and variance. This distribution of many results, when normalized by dividing by the number of cases, bears interpretation as a distribution of probabilities for finding the allowable quantum states. A key observable for describing the effect of laser radiation on an atom is the probability P_n of excitation into state n, defined by considering numerous ensembles, in each of which there is observed N_n examples of state n. The probability that, in a series of measurements, each at time t following identical

[10] Unconstrained motion in free space has no such limitation to discrete values of observations; the energies and other observables are associated with a *continuum* of values rather than the discrete sets discussed here.

preparation, the observed system will be found in the quantum state bearing index n in some catalog, is

$$P_n(t) = \frac{N_n(t)}{N_1(t) + N_2(t) + \cdots}. \tag{4}$$

I will refer to $P_n(t)$ either as an excitation probability at time t or as a time dependent *population* in state n at time t, and to alterations of these probabilities as *population transfer*. Such probabilities form one of several key links between the formalism of quantum theory and the real world of experimental physics [11]. Other links include the effect of laser induced changes upon dipole moments, measurable by their effect on radiation propagating through a medium of altered atoms, cf. Appendix A.5.

1.4 Laser radiation

Visible light, in common with radio waves, x-rays and all other forms of electromagnetic radiation, is a manifestation of electromagnetic fields; cf. Appendix A.1. These, in turn, are subject to the laws of quantum mechanics, in the form of a quantum field theory [37]. Within this theory fields have a granularity: they have indivisible quanta of fixed energy increment. For the electromagnetic field the quantum is the photon [38]; a quantum of energy $\hbar\omega$, cf. Appendix A.4. Although it is tempting to attribute particulate attributes to photons, a photon is localized in space only upon being absorbed (destroyed) at the location of a detector. In emission, or in free space, it is delocalized, either as a wavepacket or an infinite train. Although the discreteness of photons has important implications, particularly for atoms in cavities [39], the fields of ordinary laser pulses contain such large numbers of photons that their quantization can be neglected. We therefore treat all excitation-producing laser fields as classical entities, whose time dependence can be specified without considerations of the underlying quantum nature [12]. Only when we discuss discrete excitation or de-excitation events does the mention of photons become useful.

Like all electromagnetic radiation in free space, laser radiation can be described as a traveling electric field (a vector $\mathbf{E}$ having magnitude and direction) paired with and perpendicular to a traveling magnetic field $\mathbf{B}$. Over the small size of an atom, these fields can generally be regarded as plane waves, meaning that all spatial variation occurs in a single direction, that of propagation [13]. In this (longitudinal) direction the electric and magnetic field vectors are periodic, with spatial period equal to the wavelength. The instantaneous direction of the electric vector $\mathbf{E}$, perpendicular (transverse) to the propagation direction, defines the *polarization* of the radiation [40]. Figure 5 illustrates the geometry of a laser-beam electric field for two common polarization choices, linear and circular.

[11] This operational definition of excitation probability rests on the implied assumption that every measurement occurs on a system that has undergone a specific common preparation procedure. Typically this preparatory step places the system in its lowest energy state, an assumption that holds for most of the present discussion. However, other preconditioning procedures are possible; one then must deal with conditional probabilities (transition probabilities) of finding the system in state n at time t, given that it was known to be in state m at time t_0.

[12] Single-photon fields occur in many applications of coherent excitation, notably those experiments involving single atoms in single-mode cavities. For discussions of such fully quantum-mechanical field-atom interactions see ref. [39] and Appendix L.2.

[13] As wavelengths become shorter, this approximation fails. The physics of x-ray interaction differs in detail from the formalism presented here for optical excitation.

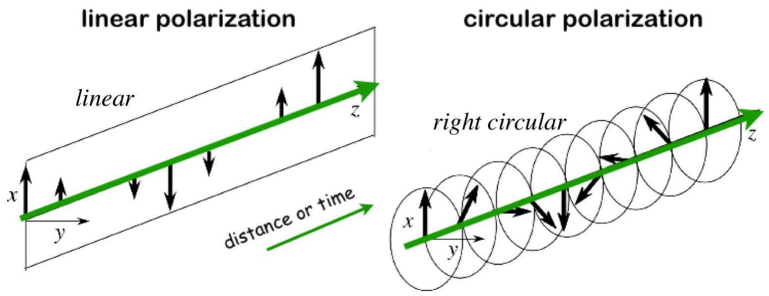

Fig. 5. A laser beam is a traveling electric and magnetic field. The direction of the electric vector (transverse to the propagation direction) defines the *polarization* direction. Shown here are examples of linear and circular polarization. (after Fig. 1.5-1) of [2])

The effects of radiation upon *unbound* particles are dominated by momentum considerations; one can regard each photon of a directed beam as carrying linear momentum, of magnitude $\hbar\omega/c$, in the direction of propagation. The absorption of radiation thereby introduces a momentum change $\Delta p = \hbar\omega/c$ that alters the velocity of an absorbing particle and which thereby acts on bulk matter as radiation pressure [41] or to cool and trap individual particles [42]. Appendix J mentions aspects of such interactions that have relevance to coherent excitation, particularly the correlation of internal excitation with center of mass motion.

However, *bound* particles (e.g. those responsible for internal structure and excitation) are affected primarily by the Lorentz force [43],

$$\mathbf{F} = e\mathbf{E} + (e/c)\mathbf{v} \times \mathbf{B}, \tag{5}$$

exerted on a charge e moving with velocity $\mathbf{v}$ by the electric and magnetic vectors of the radiation, evaluated at the origin of a coordinate system fixed to the atom center of mass.

The dominant such force, for transitions induced by radiation of optical frequencies, is that of the electric field acting on the charges [2, §3.3]. This produces an interaction energy $-\mathbf{d} \cdot \mathbf{E}$ proportional to the component of the electric dipole moment $\mathbf{d}$ along the direction of the electric field, evaluated at the atomic center of mass [14]. The corresponding magnetic interaction, $-\mathbf{m} \cdot \mathbf{B}$, is that of a magnetic moment $\mathbf{m}$ and a magnetic field [15]. Transitions involving this interaction typically occur in the radio-frequency regime and are observed as nuclear magnetic resonance (NMR) [26].

Our concern will be with optical frequencies and with the electric field acting on the bound constituents of an atom. For a stationary atom the electric field of a pulsed traveling plane wave has the form of a pulsed periodically oscillating electric field. Two cases have interest, distinguished by their polarization.

[14] This electric-field interaction is responsible for the Stark shift of energies in the presence of static electric fields; the dipole moment for such interactions is typically an *induced* dipole moment, proportional to the electric field strength.

[15] This magnetic-field interaction produces the Zeeman shift of energies in the presence of static magnetic fields.

1.4.1 Polarization

When the traveling-wave field is linearly polarized we can express the electric field at a fixed point (the atomic center of mass) as

$$\mathbf{E}(t) = \hat{\mathbf{e}}\mathcal{E}(t)\cos(\omega t - \varphi). \tag{6}$$

Here ω is the carrier frequency, φ is the phase, the unit vector $\hat{\mathbf{e}}$ defines the polarization direction (perpendicular to the propagation axis), and the real-valued function $\mathcal{E}(t)$ is the pulse envelope[16]. The force exerted by this field moves a charge back and forth along a line, in a plane perpendicular to the laser propagation axis. The alternating changes of linear momentum average to zero over one optical cycle.

To treat circularly polarized light we allow the unit vector and the envelope to be complex-valued, and we write the field as [17]

$$\mathbf{E}(t) = \mathrm{Re}\,[\hat{\mathbf{e}}\hat{\mathcal{E}}(t)\exp(-\mathrm{i}\omega t)]. \tag{7}$$

The complex-valued envelope $\hat{\mathcal{E}}(t)$ now incorporates the field phase $\mathrm{e}^{\mathrm{i}\varphi}$,

$$\hat{\mathcal{E}}(t) = |\hat{\mathcal{E}}|\mathrm{e}^{\mathrm{i}\varphi} = \mathcal{E}_R(t) + \mathrm{i}\mathcal{E}_I(t). \tag{8}$$

Taking the propagation direction to lie in the horizontal plane we introduce horizontal (H) and vertical (V) unit vectors, from which we construct *helicity* vectors [2, §1.5] [18]

$$\hat{\mathbf{e}}_{\pm 1} = \mp\frac{1}{\sqrt{2}}[\hat{\mathbf{e}}_H \pm \mathrm{i}\hat{\mathbf{e}}_V]. \tag{9}$$

The field now appears as the sum of two periodic exponentials; for a *single* helicity vector the field construction reads [19].

$$\mathbf{E}(t) = \tfrac{1}{2}\hat{\mathbf{e}}_q\hat{\mathcal{E}}(t)\exp(-\mathrm{i}\omega t) - \tfrac{1}{2}\hat{\mathbf{e}}_{-q}\hat{\mathcal{E}}^*(t)\exp(+\mathrm{i}\omega t). \tag{10}$$

To make evident the rotating nature of the electric field direction, in a vertical plane, we can write this as

$$\begin{aligned}\mathbf{E}(t) = &\frac{\mathcal{E}_R(t)}{\sqrt{8}}[\hat{\mathbf{e}}_H\cos(\omega t) + q\hat{\mathbf{e}}_V\sin(\omega t)] \\ &+\frac{\mathcal{E}_I(t)}{\sqrt{8}}[\hat{\mathbf{e}}_H\sin(\omega t) - q\hat{\mathbf{e}}_V\cos(\omega t)].\end{aligned} \tag{11}$$

When $q = +1$ this field produces a force that twists a charge distribution, at the steady rate of the carrier frequency ω, in a counterclockwise direction; the field exerts a *torque*. When $q = -1$ the

[16] Typically we choose the direction of linear polarization to be the Cartesian z axis, because this facilitates the evaluation of the dipole interaction when using eigenstates of angular momentum.

[17] The symbol i denotes the imaginary number $\mathrm{i} = \sqrt{-1}$.

[18] The field associated with *positive helicity*, $\hat{\mathbf{e}}_{+1}$, undergoes rotation of a positive screw as it propagates. When the field travels toward the observer this appears as a counter-clockwise rotation. In optics this is termed *left-circular* polarization. The negative helicity field, associated with unit vector $\hat{\mathbf{e}}_{-1}$, corresponds to right-circularly polarized light. cf. J. D. Jackson, *Classical Electrodynamics*, (Wiley, New York, 1962), p. 274

[19] The amplitude $\hat{\mathcal{E}}(t)$ associated with $\exp(-\mathrm{i}\omega t)$ is traditionally known as the *positive frequency part*, while $\hat{\mathcal{E}}^*(t)$ is known as the *negative frequency part*.

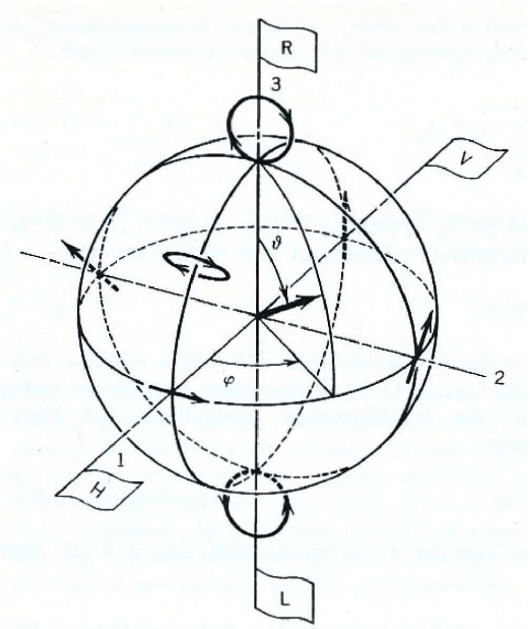

Fig. 6. The Poincaré sphere, with labels of particular polarizations: right circular (R), left circular (L), linear horizontal (H) and linear vertical (V). [after Fig. 9-3 of E. L. O'Neil, *Introduction to Statistical Optics*, (Addison-Wesley, Reading, Mass., 1963); cf. [2] Fig. 1.5-2.]

twisting force is in a clockwise direction. The twisting motion tends to impart angular momentum to the charge, as it moves in a circular path under the influence of such a field. Unlike the linear motion forced by linear polarization, the torque and the ensuing circular motion is always in the same sense – clockwise or counterclockwise.

The unit vector for the most general field, *elliptical polarization*, is expressible as a superposition of any two independent unit vectors in the plane transverse to the propagation direction. A useful choice is the two helicity vectors, with a superposition parametrized by two angles,

$$\hat{\mathbf{e}}(\vartheta,\varphi) = \cos(\vartheta/2)\hat{\mathbf{e}}_{+1} + \mathrm{e}^{\mathrm{i}\varphi}\sin(\vartheta/2)\hat{\mathbf{e}}_{-1}. \tag{12}$$

The display of these angles, and the resulting polarization, appears on the *Poincaré sphere*, shown in Fig. 6. Points at opposite sides of the sphere represent independent, orthogonal unit vectors.

For monochromatic light the motion of the electric field vector, along a line or on a more general ellipse, occurs at the carrier frequency of the light, ω. However, when an experimenter introduces modulation of the field this exactly periodic motion need not occur. For example, the modulation may cause the electric vector, while predominantly linearly polarized, to undergo a slow, controlled, rotation of the plane of polarization.

When the fields are those within a cavity, or between reflecting surfaces, they are subject to boundary conditions that select standing waves rather than running waves. Typically the bound-

aries impose nodes of the electric field at the cavity walls. Within such a bounded region, of length L in the x direction, the field has the structure [20]

$$\mathbf{E}(x,t) = \text{ Re } \hat{\mathbf{e}} \exp(-\mathrm{i}\omega t)\sqrt{2}\mathcal{E}(t)\sin(kx), \tag{13}$$

where k is restricted to discrete values $k = \pi m/L$ for positive integer n.

1.4.2 Intensity

The field constructed in this way is parametrized, in part, by the carrier frequency and the polarization direction (or, for elliptically polarized light, the ratio of the two field amplitudes associated with helicity vectors $\hat{\mathbf{e}}_{\pm 1}$). To quantify the strength of the field-induced force we use the intensity (see Appendix A.2),

$$I(t) = \tfrac{1}{2} c\epsilon_0 |\mathcal{E}(t)|^2. \tag{14}$$

Each of these parameters is, in principle, under the control of an experimenter, and can have predetermined time dependence. Detectors exist that can measure each of these parameters, and techniques exist for crafting pulses with nearly any desired time-dependent combination of these characteristics [48].

1.4.3 Phase

In practice all laser radiation only maintains purely sinusoidal oscillations for a finite time. Inevitably flucutations in the phase or frequency alter these after a finite *coherence time*. The inverse of this time, the laser bandwidth, characterizes the range of frequencies that contribute to the radiation. Various models and theoretical techniques exist for treating the random fluctuations that underlie this incoherence [44][2, Chap. 23]. For the present article I shall assume that the coherence time is much longer than any time interval of interest for radiation-induced changes (but generally also much shorter than the radiative lifetime).

The phase φ originates from several sources. When we idealize the radiation as a beam we typically express the travelling-wave nature of the field at a point with spatial coordinates x, y, z through a function such as $\exp[\mathrm{i}\Phi(x,y,z,t)]$ where

$$\Phi(x,y,z,t) = k_x(x-x_0) + k_y(y-y_0) + k_z(z-z_0) - \omega(t-t_0) + \chi \equiv \varphi - \omega t \tag{15}$$

describes the moving wavefronts of the field, periodic in space and time. The real numbers k_x, k_y, k_z form Cartesian components that define the *wave vector* $\mathbf{k}$.

The value of this function, and hence the phase φ, depends, in part, on the choice of reference position x_0, y_0, z_0; away from this location there occurs a position-dependent phase. When one compares the field at the centers of mass for several atoms, there will occur a different phase for each atom. If the atoms are moving, then there will occur a time dependent phase from the changing values of atom position. When the atoms are separated by distances comparable to a wavelength, then deviations from plane-wave behavior (e.g. the curved wavefronts of Gaussian beams) introduces additional phase differences.

[20] The factor $\sqrt{2}$ is introduced so that in all cases the mean value of $|\mathbf{E}|^2$, averaged over space and time, is $|\mathcal{E}|^2/2$.

The constant χ together with the temporal phase ωt_0 describes the moment when the electric vector of a linearly polarized field passes through zero or, for a circularly polarized field, points in a specified direction. This moment is not controllable experimentally, although as long as the field remains that of a (modulated) sinusoid of the sort assumed here, this phase remains constant, and can be taken to be zero.

Such conditions, and the assumed null phase, can hold only for time intervals shorter than the coherence time of the laser. For longer times the phase φ must be regarded as random. Such is the case for the phases of pulses that are well separated in time. It is also the case for fields of different carrier frequency; it is not possible to assign both fields the same moment of zero-crossing.

The real number χ parametrizes the intrinsic phase of the field emerging from the laser. It can be regarded as an (unknown) constant for the duration of a coherence time, but over longer time intervals it describes the inevitable randomness of a laser field.

Although an experimenter is unable to fix the absolute value of the constant phase φ, it is possible to impose phase modulation upon the laser field, e.g. sinusoidal modulation. Such manipulation alters the frequencies present in the laser spectrum.

1.5 Restrictions

The limitation to discrete quantum states implies a limit on the radiation wavelength of the laser excitation: bound particles become unbound as their excitation energy increases beyond some limit, the *binding energy*. For an electron bound within an atom the result is *photoionization*. For an atom vibrating within a molecule the result is *photodissociation*. Energies beyond the ionization or dissociation limit are not constrained to be discrete – they can take any value within a continuum. In turn, the particle is no longer localized; it is not constrained to be found within a finite volume.

To avoid such situations, and deal only with discrete quantum states, the wavelength of the radiation must be sufficiently long that the photon energy $\hbar\omega$ does not exceed the binding energy of the excited state (or states). The limitation to long wavelengths (i.e. laser radiation in the visible or infrared regions of the spectrum), and correspondingly low-energy photons, allows us to employ a nonrelativistic description of the system: particle velocities are all much slower than the speed of light. This approximation is implicit in all of the present discussion.

We must also require that the electric field of the radiation be weaker than the Coulomb field that holds the electron within the atom, so that the behavior of the bound electron will be dominated by the forces that provide the structure of the free atom. In the opposite extreme, of a very intense pulse, the behavior is predominantly that of a charge moving under the influence of the laser field, and perturbed by a Coulomb force [45]. A relativistic description is then needed.

2 Interacting with single atoms

Quantum theory offers the basic formalism for dealing with individual atoms exposed to controlled radiation fields. Several experimental techniques provide acceptable approximations to this ideal. The following paragraphs note some of these examples.

2.1 Particle beams

The simplest experimental realization of a single atom or molecule occurs in particle beams [46]. These are produced by allowing a suitable vapor source – say a noble gas or vaporized solid – to expand through a nozzle into a vacuum chamber. The atoms pass through a series of apertures, from which emerges a collimated beam, as shown in Fig. 7. Typically the density of the beam is sufficiently low that collisions are infrequent, and so the result is an ensemble of essentially free particles, localized in position and momentum, moving on average with velocity v.

This atomic beam then passes across one or more laser beams, usually at right angles to the laser-propagation axes. In moving with velocity v across the spatially varying laser-beam profile (typically a Gaussian) of electric field $\mathcal{F}(x)$, an atom experiences a time varying electric field $\mathcal{E}(t) = \mathcal{F}(x/v)$. (Appendix F.1 provides more details.)

Because there is a distribution of velocities within the atomic beam, not all atoms experience the same field duration. Furthermore, because of velocity-imparted Doppler shifts, proportional to the velocity $v_\perp$ transverse to the beam, the atoms experience different laser frequencies. In consequence, one observes an average over various atomic conditions. Appendix F discusses these and other aspects of beam interactions that lead to averages.

2.2 Trapped particles

Numerous techniques exist to obtain single isolated ions or atoms, held in place (in vacuum) by suitable electric and magnetic fields [47]. Beams of charged particles can, by use of suitably controlled electromagnetic fields, be slowed and brought to rest, held by electric and magnetic

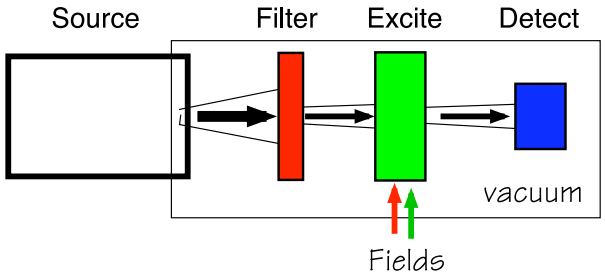

Fig. 7. Schematic presentation of atomic beam excitation: Atoms emerge from a vapor source into vacuum, through apertures (a spatial filter), forming a collimated beam. This passes through a laser beam (the excitation region), which produces changes in the atom internal structure. A beam detector monitors the result.

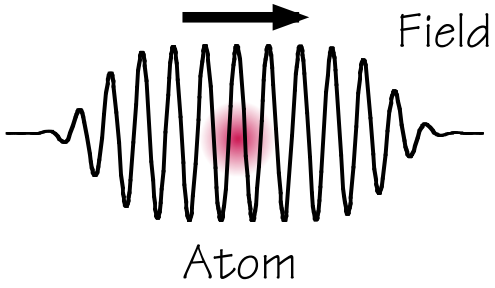

Fig. 8. Schematic presentation of trapped atom excitation: A travelling pulse of near-monochromatic radiation passes a stationary (trapped) atom. The travelling field appears, to the fixed atom, as a time-dependent electric field transverse to the propagation direction.

forces within a confined region. Alternatively, neutral beams can be photoionized within regions where trapping fields are present, and held there by suitable fields. Conceptually simpler are the various magneto-optical traps that can, when present within a cold sample of gas, trap an individual atom. Section 2.3 below mentions arrays of traps for neutral particles.

Once a particle is trapped, it can be placed within the relatively narrow waist of a focused laser beam, and there be subject to controlled radiation. It is possible, with suitable pulse-shaping techniques, to irradiate a single trapped atom with a pulse whose temporal and frequency characteristics are crafted to produce a desired result [48]. Figure 8 shows the essential elements of the interaction: a travelling electromagnetic wave and a stationary atom.

In this way it is possible to make repeated observations upon a single atom. Quantum theory provides predictions of time averages of such observations – of sets of histories that provide the counterpart of ensemble averages.

2.3 Optical lattices

An electric dipole in an inhomogeneous electric field possesses a spatially varying potential energy $-\mathbf{d}\cdot\mathbf{E}(\mathbf{r})$. Thus it experiences a force (the negative gradient of the energy) in the direction of the field gradient. When the dipole is an induced moment, proportional to the electric field, then the force is proportional to the gradient of the square of the electric field, i.e. to the gradient of the intensity. This is termed variously, the gradient force and the ponderomotive force.

The required potential energy of the induced dipole is obtained from the cycle-averaged square of the electric field as

$$U = -\tfrac{1}{2}\alpha(\omega)\{|\mathbf{E}|^2\}_{av}, \tag{16}$$

where $\alpha(\omega)$ is the the frequency-dependent (dynamic) polarizability; cf. Sec. 10.3.2. The force

resulting from this energy is [21]

$$\mathbf{F} = -\nabla U = \tfrac{1}{2}\alpha(\omega)\nabla\{|\mathbf{E}|^2\}_{av}. \tag{17}$$

Macroscopic dielectric particles are typically attracted into regions of high field. It is this behavior that makes possible the use of tightly focused laser beams as "optical tweezers". For an atom or molecule the frequency dependence of the polarizability changes sign as the frequency varies from red to blue about a resonance, and so the force can either repel the particle from regions of intense field or attract the particle toward a high field region.

For light near resonant at a Bohr frequency ω_B, the induced dipole will be in phase with the electric field if the carrier frequency ω is smaller than the resonant frequency, i.e. it is "red-detuned". The gradient force will then be in the direction of increasing field, and the particle will be drawn toward regions of high intensity. A "blue-detuned" laser field induce a force that repels the particle from the high-field region. A standing-wave optical field will, through this mechanism, provide a periodic array of potential troughs in which cold atoms will be trapped. A combination of two orthogonal standing waves will create an optical lattice of wells in which cold atoms, or Bose-Einstein condensates, can be trapped [49].

2.4 Atoms in solids

Stationary quantum systems described by a few discrete quantum states can be obtained in various other ways. For example, suitable chemical preparations can create impurity atoms held within a solid matrix. The electrons of such atoms are held by both Coulomb attraction to a nucleus and repulsion from nearby atomic electrons. Although experiments may not distinguish between individual atoms, each one can have well-characterized discrete energies, and can be regarded as a simple atom of the sort discussed here [50]. To describe the aggregate collection of atoms one must include an average over the various atom environments, as discussed in Sec. 9.1.

Other techniques are used to fabricate small solid regions in which electron-hole pairs are localized – quantum dots [32]. Because the excitations involve confined motion, the energies are discrete. The theory presented here provides a description of the laser-induced changes to such excitations.

2.5 The isolated-atom idealization

The discussion that follows will be based on several assumptions about quantum systems interacting with optical radiation.

- No collisions
- No radiative decay
- No interruptions of strict laser periodicity
- No thermal surroundings

[21] The derivative operator ∇, used to produce the gradiant of a scalar field is a vector with Cartesian components $\{\partial/\partial x, \partial/\partial y, \partial/\partial z\}$.

- No random long range interactions.

Given these assumptions, we deal with coherent excitation of a single atom [22]. The relevant equation of motion is the time dependent Schrödinger equation (TDSE) for the statevector, discussed in Sec. 5.

2.6 Simple questions

Numerous questions come to mind when considering an atom exposed to radiation, most notably: What is the effect of a particular pulse of radiation? Alternatively, one might ask: Given some initial probability distribution of quantum states, how can one produce a desired final distribution? That is, what choice of radiation parameters – carrier frequency, pulse duration, peak intensity, etc. – will produce some desired change in the quantum state [23].

To answer such questions quantitatively it is necessary to have an equation of motion for the probabilities, i.e. some differential equation of the form

$$\frac{d}{dt}P_n(t) = ?\ ? \tag{18}$$

in which the right-hand side depends upon radiation parameters as well as a set of populations. Given such a set of differential equations we can, in principle, carry out the implied integration, starting from specified initial conditions, say $P_n(0)$. Section 4.2 and Appendix H.1 provide examples of these equations.

Several forms of these equations have merit; the choice depends, in part, upon which of several regimes of laser intensity holds interest. The coherent-excitation regimes, and the associated idealized physical descriptions, fit generally into three classes:

> **Weak**: In this regime an individual pulse has very little effect upon the initial probability distributions; it represents a *perturbation* of the initial state, and can be treated by time-dependent perturbation theory, as mentioned in Sec. 6.1.
>
> **Strong**: In this regime there occurs a significant change in probability distributions; Rabi oscillations, discussed in the following sections, are an example. Perturbation theory fails, and one must find alternative approaches. This is the regime treated in the present review, based on equations of motion for a few selected quantum-state probabilities.
>
> **Ultrastrong**: When the pulse is sufficiently intense, the electric field of the laser overwhelms the Coulomb field that binds the electrons to the nucleus, and photoionization can occur within a few optical cycles [24]. The use of a few essential bound quantum states, and their equations of motion, no longer provides a satisfactory description and new models, alternative approaches, are needed [52], often based on numerical evaluation of wavefunctions [53]. I will not discuss this regime.

[22] It proves convenient to refer to the system as an "atom", though the descriptions apply equally well to other systems with discrete bound energies.

[23] Traditionally the change was from an initially populated ground state, but more recent interest lies with other states, even superpositions of states.

[24] Under suitable conditions stabilized bound states may exist even in such very strong fields [51].

3 Picturing changes

Because the uncertainty principle limits the simultaneous measurement of position and momentum (hence velocity), it is not possible to follow any details of particle trajectories within the small confines of an atom; only statistical properties of motion have possibility of observation. I will offer several ways of visualizing the effect of optical radiation, starting from a rather classical portrait of the sort that Lorentz might have used, relating this to the wavefunction portraits that form the basis of quantum chemistry, and concluding with a rather abstract description based on the use of statevectors in Hilbert space.

3.1 Classical force

To picture most graphically the effect of laser radiation upon an atom we can consider the effect of an electric field acting upon an electron bound within an atom. Lorentz suggested picturing the electron, a point particle, as subject to a steady Coulomb binding force which holds the electron in an equilibrium position, a picture that can be made exact with the aid of quantum theory (cf. Appendix I). The inevitable wavelike properties of a bound electron, imposed by quantum theory, forces us to picture a distribution of negative electric charges – an electron cloud.

Acting upon such a charge cloud the electric field produces a time varying force. The simplest illustration is the force produced by linearly polarized light, say in the x direction, as in eqn. (6) with unit vector $\hat{\mathbf{e}}_x$. This field exerts a periodic force, alternately in the $+x$ direction and then in the $-x$ direction, see Fig. 9. Responding to this force, the electron cloud must move, periodically toward $+x$ and then toward $-x$. This motion appears as a "shaking" of the charge cloud at the radiation frequency ω [25].

When the frequency of the radiation satisfies the Bohr condition, eqn. (2), this simple periodic motion of the charge cloud undergoes a gradual *secular* change, a distortion of the charge cloud into a distribution recognizable as the result of an atomic transition – a gain of internal energy, from the field.

The effect of a classical periodic force upon harmonic motion is well known, familiar to every child who has mastered the art of a playground swing: when the force is in phase with the motion, then there occurs an increase in the amplitude of the motion – an increase of swing energy. When the force is timed to oppose the velocity, then the motion diminishes – the swing energy decreases. Similar effects are to be expected, and are observed, in the action of a periodic electric field upon the motion of a charge cloud. Specifically the atom, having gained energy from the field, then proceeds to lose it and return to the initial unexcited state. This gain and subsequent loss occurs periodically; the frequency is known as the *Rabi frequency* [2, §3.4].

3.2 The wavefunction

The charge-cloud picture of an atomic transition is most directly presented by means of a *wavefunction* [54]. For a particle obeying quantum mechanics (say an atomic electron), all measurable

[25] Circularly polarized light forces a "spinning" motion of the charge cloud, about an axis through the center of mass. This motion is not evident for a charge distribution that has cylindrical symmetry about the rotation axis, as does the $1s$ state of hydrogen, but it becomes evident for excited states whose charge distributions have angular nodes.

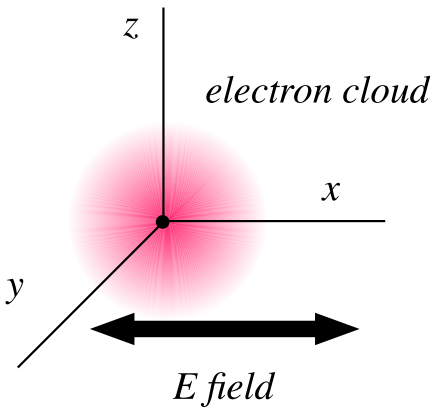

Fig. 9. The electric field of the laser forces oscillations of the electron cloud

properties are deducible from a wavefunction $\Psi(t, \mathbf{r})$ such that the probability of electron being at position $\mathbf{r}$ at time t is proportional to the absolute square

$$P(t, \mathbf{r}) = |\Psi(t, \mathbf{r})|^2. \tag{19}$$

The electron must be somewhere, and so the spatial integral, at any time, must be unity,

$$\int d\mathbf{r}\, |\Psi(t, \mathbf{r})|^2 = 1. \tag{20}$$

The electron carries an electric charge, and so the probability density $|\Psi(t, \mathbf{r})|^2$ times the electron charge e bears interpretation as the charge density. The expectation value of the electric dipole moment, needed for evaluating the influence of the atom upon radiation (see Appendix A.5), is evaluated from the integral

$$\langle \mathbf{d}(t) \rangle = e \int d\mathbf{r}\, \mathbf{r}\, |\Psi(t, \mathbf{r})|^2. \tag{21}$$

The exact distribution of charge probability, often termed an electron *orbital* [55] [2, §19.1] $\psi(\mathbf{r})$, is a solution to the time-*independent* Schrödinger equation, a second-order partial differential equation supplemented by boundary conditions, whose multiple solutions I here label by a simple integer n, [26]

$$\left[-\frac{\hbar^2}{2m} \nabla^2 + V(\mathbf{r}) - (E_n - E_\infty) \right] \psi_n(\mathbf{r}) = 0. \tag{22}$$

[26] The presence of the constant E_∞ here is in keeping with the convention that bound energies E_n should be positive, measured from the smallest value E_1. The combination $E_n - E_\infty$ is therefore negative for bound states; positive values represent scattering states, available for any energy.

The second-order spatial derivative expresses kinetic energy; the potential energy – responsible for the binding force – is $V(\mathbf{r})$. Here E_∞ is the minimum energy required for photoionization and E_n, the energy of state n, is the energy of excitation above the ground state.

To complete the mathematical definition of the quantum system we require boundary conditions. For bound states (those for which $E_n < E_\infty$) these are that the wavefunction should be confined in space,

$$\psi_n(\mathbf{r}) \to 0 \text{ as } \mathbf{r} \to \infty. \tag{23}$$

With this constraint the solutions for positive values of $(E_n - E_\infty)$ exist only for particular discrete values (the *eigenenergies*).

For a particle that can exist in two, and only two, quantum states, we describe the possible probability distributions with two single-particle wavefunctions (orbitals), $\psi_1(\mathbf{r})$ and $\psi_2(\mathbf{r})$, such that, if the particle is known to be in state n, and is free from external disturbances, its spatial distribution is (independent of time),

$$P_n(t, \mathbf{r}) = |\psi_n(\mathbf{r})|^2. \tag{24}$$

Because, by assumption, the particle can only be found in one of these two quantum states, then even when external forces are present the wavefunction must always be some superposition,

$$\Psi(t, \mathbf{r}) = c_1(t)\psi_1(\mathbf{r}) + c_2(t)\psi_2(\mathbf{r}), \tag{25}$$

with time-varying complex-valued coefficients $c_n(t)$. The probability of the electron being in state n at time t is

$$P_n(t) = |c_n(t)|^2, \tag{26}$$

and hence the $c_n(t)$ are *probability amplitudes*. The probability of the electron being at position $\mathbf{r}$ at time t is

$$P(t, \mathbf{r}) = P_1(t)|\psi_1(\mathbf{r})|^2 + P_2(t)|\psi_2(\mathbf{r})|^2 + 2 \text{ Re } [c_1(t)^* c_2(t)\, \psi_1(\mathbf{r})^* \psi_2(\mathbf{r})]. \tag{27}$$

The first two terms are recognizable as expressing the individual charge distributions – these one expects from classical probabilities. The final term expresses quantum mechanical interference; it makes possible nodes of zero probability from individual orbitals whose probabilities are everywhere nonzero.

Free-space orbitals can be classified according to their spatial symmetries, such as are labeled with orbital angular momentum and parity. (By definition, odd parity wavefunctions undergo a sign change when the coordinates are reversed.) These labels permit statements of selection rules governing transitions; cf. Sec 8.1.

3.3 Wavefunction changes: Distortion and excitation

A simple semiclassical description [27] of laser radiation acting upon an atom is as follows. The laser provides a periodic electric field. This periodic field in turn exerts a periodic force upon

[27] The term "semiclassical" appears often; it refers to physics in which the atom or other quantum system obeys laws of quantum mechanics, while the radiation field obeys only the classical Maxwell field equations (cf. Appendix A.1) and is not quantized.

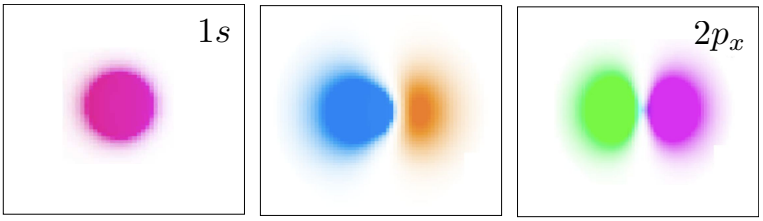

Fig. 10. Slow transformation of orbital in $1s \rightarrow 2p_x$ transition. The frame at the left shows the initial charge distribution for the $1s$ orbital, the frame at the right shows the charge distribution for the $2p_x$ orbital. The middle frame shows a superposition of these two orbitals. With time the charge distribution proceeds through each of these frames, from left to right, and then from right to left, as the excitation probability underges Rabi oscillations. Colors indicate phase. [after pictures generated using the Java applet from http://www.falstad.com/qmatomrad/]

bound electrons. (Because the atom nucleus is much more massive, it remains essentially stationary.) Over time this periodic force adds energy to the bound electrons – a transition occurs between discrete states of internal energy of the atom, see Fig 10. Subsequently a reversing transition occurs as energy leaves the bound electrons.

A very nice graphical illustration of this process, an animated version of Fig. 10, has been created by Paul Falsted, available from his web site,

`http://www.falstad.com/qmatomrad/`. (28)

There one can see, for example, the effect of a periodic electric field, directed along the x axis and resonant with the $1s-2p$ transition of hydrogen, on the two relevant hydrogenic orbitals: the ground state $1s$ orbital (null orbital angular momentum, even parity) and the excited-state $2p_x$ orbital (unit orbital angular momentum, odd parity, selected by electric field polarization from the three possible degenerate $2p$ orbitals p_x, p_y, p_z appropriate to linear polarization; the orbitals p_{-1}, p_0, p_{+1} are appropriate to angular momentum) [28].

One sees, in the Java applet, at first a small periodic wiggling of the spherically symmetric charge cloud of the $1s$ state. These are small perturbations of the otherwise stationary charge distribution at the radiation frequency ω. It is during this initial time that the Lorentz model applies: the electron behaves like a driven harmonic oscillator, moving about an equilibrium position under the influence of a periodic force.

Over many cycles at the driving frequency ω one observes a distortion of the cloud: a nodal surface appears, and the cloud takes on an increasingly bimodal appearance, though still subject to a continual small oscillation along the x axis. The charge distribution is distinctly asymmetric. A diagram shows the internal energy steadily increasing.

[28] The wavelength of the $1s-2p$ transition in hydrogen, responsible for the "Lyman α" spectral line, lies in the far ultraviolet, at 121.6 nm; it has not been possible to demonstrate Rabi oscillations with this short wavelength. Amongst other problems, the radiation will simultaneously photoionize the excited state. Rydberg atoms, those with large principal quantum number, offer better choices for demonstrations but not for simplest picturing of wavefunctions because they have more nodes [56].

In time the charge distribution becomes that of the $2p_x$ orbital of hydrogen: two lobes of equal probability but opposite sign. At this moment a transition has been completed, $1s \rightarrow 2p$, and the internal energy is that of a $2p$ state.

But, with continued presence of the periodic driving field, the wavefunction continues to respond. It continues to undergo small oscillations together with a gradual change of form, until it appears once more as the spherical $1s$ distribution, and the energy has returned to that of the ground state.

These effects continue as long as the field is present: a rapidly varying perturbation at the driving frequency ω (i.e. a shaking of the charge cloud), together with a slower periodic variation of excitation probability (a distortion of the charge cloud), at the *Rabi frequency* Ω [57] [2, §2.7]. As will be noted below, the latter is a measure of the cycle-averaged interaction energy between atom and field, and can be altered by changing the intensity of the light. If the field is that of eqn. (6) then the Rabi frequency is $\Omega = -d_{12}\mathcal{E}/\hbar$, where d_{12} is the electronic transition-dipole moment. The square of the Rabi frequency is proportional to the oscillator strength and the intensity. Subsequent sections of the present review provide the theoretical basis for understanding the quantitative properties of Rabi oscillations and other manifestations of coherent excitation.

The picture presented here, of periodic linear displacements of the electron charge-cloud and slower distortions, holds for an electric field that is linearly polarized. When the field is circularly polarized there is no linear displacement. Instead the atom undergoes rotation under the influence of the field-induced torque. Again slow distortions occur, at the Rabi frequency, but these changes occur in a framework that rotates steadily at the carrier frequency.

Periodic distortion of an electron cloud, as discussed here, relies on the two-state approximation. When the electric field becomes sufficiently strong (i.e. the interaction energy exceeds the binding energy), this simple picture fails. Instead, one must include an infinite number of additional quantum states, including an ionization continuum, in order to depict more extensive distortion of the wavefunction (cf. Sec 10.3.2). These additional states allow a portrait in which, for example, a single cycle of the field forces the electron cloud to leave the vicinity of the nucleus and move away – ionization occurs [58].

3.4 The statevector; Hilbert spaces

The wavefunction of a single particle offers a simple interpretation of the particle as a probability cloud – a distribution of electric charge when the particle is an electron. When one considers the several electrons that comprise all atoms heavier than hydrogen, there is a challenge to depict the resulting multi-dimensional wavefunction: for two electrons it is a function of six spatial dimensions and two spin coordinates. The description of atoms within a molecule requires an even larger number of dimensions, associated with rotational and vibrational degrees of freedom. Thus for all but the simplest systems, those whose important properties are associated with only one or two spatial coordinates, there is little possibility of extracting simple pictures of excitation dynamics from wavefunctions [29]. An alternative approach has therefore found favor, one based

[29] An important exception occurs with descriptions of wavepackets formed from molecular vibrational states. Pictures of these provide valuable insight into the dynamics of laser-induced unimolecular reactions, such as photodissociation; cf. Sec. refsec-wavepackets.

on the use of an abstract vector space to represent probability amplitudes. This approach forms the basis of the present review.

The needed quantum mechanics is based upon the recognition that, whatever the electron trajectories may be within the confines of an atom, whatever may be the rotational and vibrational motions of the molecular framework, the internal energies of atoms and molecules form a discrete set that can be ordered, in part, by increasing value, E_1, E_2, ..., together with a continuum for energies above some limit. For any atom or molecule there are an infinite number of discrete internal energy states. Each can often be assigned various identifying quantum-number labels, such as those associated with angular momentum; the single index 1 or 2 would then be understood as standing for the more complete list of identifying labels.

Because the quantum states of interest here are discrete, they can be associated with an abstract vector space, a mathematical construct in which each individual coordinate is associated with one of the possible quantum states. There are as many dimensions as there are quantum states; in many situations there is an infinite number of these.

The multidimensional vector spaces of interest in quantum mechanics have several distinguishing properties that mark them as *Hilbert spaces* [59]. Appendix B.2 discusses the basic properties of such constructs and summarizes relevant notation. In such a space lengths and angles are well defined, and the coordinates, along the coordinate axes, are complex-valued numbers, i.e. with real and imaginary parts. At the heart of the mathematics of quantum mechanics there is therefore the connection [30]

$$\text{quantum states} \leftrightarrow \text{Hilbert-space unit vectors.} \tag{29}$$

As it turns out, most coherent excitation by lasers, and the consequent state manipulation, involves relatively few quantum states – primarily only those for which the laser frequencies satisfy (at least approximately) the Bohr resonance condition (2). Thus the Hilbert space of interest has finite dimension, say N.

A basic postulate of quantum theory is that, because the possible internal structures of the atom – the quantum system – must be expressible as one of the allowed quantum states any particular quantum state can be represented as a single point in this abstract space. This *system point* can be regarded as a vector from the coordinate origin: the *statevector* Ψ.

The connection between the abstract mathematics of a Hilbert space and the world of experimental physics occurs through the coordinates of the statevector: the projection of vector Ψ on axis ψ_n, denoted $\langle\psi_n|\Psi\rangle$ or $\langle n|\Psi\rangle$, when squared absolutely, is the probability P_n,

$$P_n = |\langle\psi_n|\Psi\rangle|^2. \tag{30}$$

This equation lies at the heart of the association of quantum theory with the mathematics of Hilbert space – the mapping of physically observable sets of atomic properties that distinguish each quantum state, onto the mathematics of an abstract vector space in which the coordinates are complex numbers. It is notable that this postulated connection leaves the phase of the probability amplitude unspecified; only its magnitude has direct connection with probability.

[30] For greatest clarity one should distinguish the unit vectors in Hilbert space with the quantum states with which they are associated, but common usage applies the term "state" to both concepts, quantum state and Hilbert-space unit vector, speaking of the latter as *basis states*.

3.5 Hilbert-space coordinates and probability amplitudes

As is the case with any vector, in any mathematical space, the statevector must be expressible by its coordinates. With the present notation this construction reads

$$\Psi = c_1\,\psi_1 + c_2\,\psi_2 + \cdots, \tag{31}$$

where c_n is a complex-valued number, the *probability amplitude*, whose absolute square is the probability, $P_n = |c_n|^2$. Because probabilities should sum to unity [31], the numbers c_n are constrained by the normalization

$$|c_1|^2 + |c_2|^2 + \cdots = 1, \tag{32}$$

and the statevector has unit length,

$$|\Psi| = 1. \tag{33}$$

It may happen that the system is known to be in a single quantum state, say state 1. Then the statevector has the form

$$\Psi = \mathrm{e}^{\mathrm{i}\phi_1}\psi_1, \tag{34}$$

where ϕ_1 is a real-valued phase [32]. In all other cases the statevector is a superposition of basis states. Because the complex-valued probability amplitudes c_n require not only magnitudes $|c_n|$ but phases ϕ_n for complete definition, the statevector generally incorporates phase relationships between its constituent coordinates. These have no counterpart in conventional probability theory: the statevector generally is a *coherent superposition* of quantum states, as expressed by eqn. (31).

When one deals with degenerate quantum states, i.e. states sharing a common energy, the choice of unit vectors is somewhat arbitrary [33]. This flexibility in choosing a Hilbert-space coordinate system means, for example, that what appears to be a superposition of two states may, by suitably redefining basis states, appear as a single quantum state. Such coordinate transformations are an example of a traditional goal of physics: to find a simple way of expressing complicated behavior. I will discuss several examples.

3.6 Time dependence

When excitation occurs, the state of motion changes; there occurs a corresponding time dependence of the statevector, indicated by including a time argument, $\Psi(t)$. When the statevector varies with time, then the projections onto the fixed reference frame also change with time, thereby providing the time-dependent probabilities

$$P_n(t) = |\langle\psi_n|\Psi(t)\rangle|^2. \tag{35}$$

[31] Section 5.8 discusses situations which violate this requirement.

[32] The overall phase of the statevector, ϕ_1 in this case, is not observable. Thus it is usually convenient to omit it. As will be noted, this overall phase choice is related to the arbitrariness in setting the zero of energy.

[33] When external fields act on the atom the degeneracy is less (is at least partially "lifted"). It is common to use the symmetry properties of such a field, expressed using the mathematics of group theory, to label the resulting quantum states. In the absence of any external field we are at liberty to use any convenient group representation to classify the degenerate states; each such classification leads to a different Hilbert-space basis of unit vectors; cf. Appendix C.4.

It is customary to assume, as I shall, that the N quantum states associated with N-dimensional Hilbert space are complete, meaning that certainly, with unit probability, the system will be found in one of these states. This requirement means that the individual-state probabilities sum to unity

$$\Sigma_{n=1,N} P_n(t) = 1. \tag{36}$$

It follows that the statevector has unit length at all times,

$$|\Psi(t)|^2 \equiv |\langle\Psi(t)|\Psi(t)\rangle|^2 = \left|\Sigma_n \langle\Psi(t)|\psi_n\rangle\langle\psi_n|\Psi(t)\rangle\right|^2 = \Sigma_{n=1,N} P_n(t) = 1. \tag{37}$$

Thus any change to the statevector must be characterizable as a generalized rotation in Hilbert space [34]. The unit sum property is often expressed as a *completeness* relationship, in which N orthonormal unit vectors provide an expansion of unity,

$$\Sigma_{n=1,N} |\psi_n\rangle\langle\psi_n| \equiv \Sigma_{n=1,N} |n\rangle\langle n| = 1. \tag{38}$$

3.7 Two-state Hilbert spaces

The simplest example of a Hilbert-space description is that of a two-state system (or two-level atom) [10, 60], as in the hydrogenic excitation example discussed above. We have two fixed unit vectors, ψ_1 and ψ_2, and the statevector must be some superposition of these, say [35]

$$\Psi(t) = c_1(t)\psi_1 + c_2(t)\psi_2. \tag{39}$$

The two corresponding propabilities $P_1(t)$ and $P_2(t)$ are the squared projections of the statevector upon the Hilbert-space axes,

$$P_1(t) = |c_1(t)|^2, \qquad P_2(t) = |c_2(t)|^2. \tag{40}$$

Figure 11 illustrates this abstract space.

3.7.1 The Bloch sphere

The time dependent coordinates $c_n(t)$ are generally complex-valued functions of time; we therefore require four real numbers to specify the projections of the statevector. However, the condition of unit norm, eqn. (33), provides one real number, so that only three real-valued parameters are required. One way to choose these is to write the statevector in a form akin to eqn. (12),

$$\Psi = \exp(-i\zeta)\Big[\cos(\theta/2)\psi_1 + \sin(\theta/2)\mathrm{e}^{-i\phi}\psi_2\Big], \tag{41}$$

meaning

$$c_1 = \exp(-i\zeta)\cos(\theta/2), \quad c_2 = \exp(-i\zeta - \mathrm{i}\phi)\sin(\theta/2). \tag{42}$$

[34] The motion may appear as a rotation in the full N-dimensional Hilbert space, but the overall effect of pulsed change may appear as a reflection within a subspace .

[35] When dealing with quantum information such a system is known as a *qubit*; the states are conventionally denoted $|0\rangle$ and $|1\rangle$. When treating spin-half particles the states are typically denoted $|\uparrow\rangle$ and $|\downarrow\rangle$. .

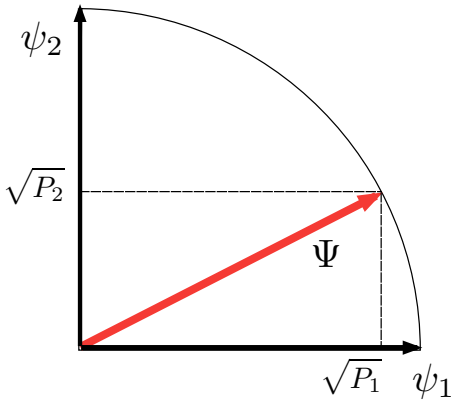

Fig. 11. The statevector for two dimensions, showing projections onto the two unit vectors ψ_1 and ψ_2. Although two dimensions – a single angle and fixed unit length – often suffice to describe a statevector, more generally a third dimension is needed, to describe the relative phase between two projections, as discussed in the following section.

The probabilities associated with this expression,

$$P_1 = \cos^2(\theta/2) = \tfrac{1}{2}[1+\cos\theta], \tag{43}$$

$$P_2 = \sin^2(\theta/2) = \tfrac{1}{2}[1-\cos\theta], \tag{44}$$

are independent of the relative phase ϕ (and of the overall phase ζ), and sum to unity. The connection between the angle parametrization and the probability amplitudes can be seen from the following table.

θ	c_1	c_2
0	1	0
$\pi/2$	$1/\sqrt{2}$	$e^{i\phi}/\sqrt{2}$
π	0	$e^{i\phi}$
$3\pi/2$	$-1/\sqrt{2}$	$e^{i\phi}/\sqrt{2}$
2π	-1	0
4π	1	0

The two angles represent a statevector as a point on a unit sphere, the *Bloch sphere* [36] [2, §8.1]. The south pole of this sphere represents population entirely in state 1, while the north pole represents population in state 2. The equator represents a phased 50:50 coherent superposition of the two states. This parametrization is similar to that used with the Poincaré sphere, Fig. 6,

[36] This abstract vector space has real-valued coordinates; it is an example of a *state space* rather than a Hilbert space. Mathematicians refer to the Bloch sphere, or the Poincaré sphere, as *Riemann spheres* that provide a "compactification of the complex-number line".

for describing general elliptical polarization of light, as shown in eqn. (12). As with that picture, points on opposite sides of the Bloch sphere represent orthogonal states.

The connection between the Bloch angles and the probability amplitudes c_n is often expressed through bilinear products of the two probability amplitudes (see also Appendix H.1):

$$\begin{array}{lll} 2c_1c_1^* = & 2\cos^2(\theta/2) & = 1+\cos\theta = 2P_1, \\ 2c_2c_2^* = & 2\sin^2(\theta/2) & = 1-\cos\theta = 2P_2, \\ 2c_1c_2^* = & 2\mathrm{e}^{\mathrm{i}\phi}\cos(\theta/2)\,\sin(\theta/2) & = \mathrm{e}^{\mathrm{i}\phi}\sin\theta. \end{array} \tag{45}$$

Section 7 illustrates the usefulness of the Bloch sphere for presenting a simple visualization of various pulse effects.

3.7.2 Multiple states and the Bloch sphere

The general construction of a statevector involves N quantum states and a corresponding N-dimensional Hilbert space,

$$\Psi = c_1\psi_1 + c_2\psi_2 + \cdots + c_N\psi_N. \tag{46}$$

This specification involves N complex-valued amplitudes c_N, meaning $2N$ real numbers. The overall normalization requirement $\Sigma_n|c_n|^2 = 1$ provides one number, and the overall phase, unobservable, provides a second number. Thus we require $N-1$ pairs of real numbers. For this purpose it is possible to generalize the two Bloch-sphere angles (θ,ϕ) to a set of $N-1$ angle pairs,

$$(\theta_1,\phi_1),\cdots,(\theta_{N-1},\phi_{N-1}).$$

In this way we expect that a statevector in N dimensions can be represented by $N-1$ points on the Bloch sphere.

One way to associate the states of certain classes of N-state systems with sets of two-state systems follows from the use of a Morris-Shore (MS) transformation, as described in Appendix M. In the MS basis each point on the Bloch sphere moves independently, in accord with well defined two-state equations. But their connection with the original N-state description is through a transformation that makes evolution indirectly associated with the original Hamiltonian.

More generally one can use a mathematical device used by Majorana to express the connection between a set of $2S$ particles, each a two state system (and hence representable as spin one half cf. Appendix C.2), and a statevector having $2S+1$ Hilbert-space coordinates (and hence a representation of total spin S) [61]. Applied to the present case the Majorana approach considers the $N = 2S+1$ roots x_n of the polynomial equation [37]

$$\Sigma_{n=1}^{N} c_n\, h_{n-1}x^{n-1} = 0. \tag{47}$$

Majorana chose the parameters h_n to be

$$h_n = \frac{(-1)^{n+1}}{\sqrt{(N-n)!(n+1)!}}, \tag{48}$$

[37] The statevector coefficients c_n have indices $n = 1,\ldots,N-1$. These are associated in the polynomial with powers $x^{N-1},\cdots,x^0$.

but other choices can be used (e.g. $h_n = 1$). Each complex-valued root can be expressed as a pair of angles,

$$x_n = \tan(\theta_n/2)\mathrm{e}^{\mathrm{i}\phi_n}. \tag{49}$$

Each of these define a point on a unit sphere – the Bloch sphere The complete description of the statevector consists of $N-1$ points on the Bloch sphere. This association, between the N probability amplitudes c_n and the set of $N-1$ Bloch angles, holds for any statevector.

The Majorana decomposition, eqn. (47) taken with the parameters of eqn. (48), is particularly useful when the N-state RWA Hamiltonian is expressible using matrix representations of angular momentum, i.e. spin matrices, as defined in Appendix C.2. Sec. 11.3 discusses this case. With such a Hamiltonian the motion of the statevector in N dimensions has portrayal as a rotation, defined by three Euler angles [38]. The motion of the points on the Bloch sphere therefore undergo rotations defined by these same Euler angles. Thus for this class of N-state Hamiltonians there is a simple portrait of time evolution of $N-1$ points on the Bloch sphere.

3.8 Typical goals

Traditional goals for pulsed excitation include the production of complete population transfer, from the initially populated state 1 to the excited state 2,

$$\Psi = \psi_1 \rightarrow \mathrm{e}^{\mathrm{i}\varphi}\,\psi_2. \tag{50}$$

When the phase φ is zero this corresponds to a rotation of the statevector by 90 degrees (a rotation of the Bloch angle θ by π). Alternatively, we might wish to maximise the induced dipole moment (for use with nonlinear optics, cf. Appendix A.5), by producing the coherent superposition

$$\Psi = \psi_1 \rightarrow \beta\psi_1 + \alpha\psi_2, \qquad |\alpha|^2 + |\beta|^2 = 1. \tag{51}$$

For null phase this corresponds to a rotation of the statevector by 45 degrees (a rotation of the Bloch angle by $\pi/2$).

Each of these objectives can be obtained by producing a predetermined portion of a Rabi oscillation. However, other procedures are possible, often providing advantages. In particular, alternative schemes based upon adiabatic changes are much less sensitive to details of the pulse; they are basically independent of the time integral of the Rabi frequency, for example, and are therefore termed *robust*. Later sections will discuss some of these alternatives.

Although population changes have traditionally drawn attention, the more detailed manipulation of quantum states needed for quantum information processing require the ability to alter phases. One might then wish to produce the change

$$\Psi = \psi_1 \rightarrow \mathrm{e}^{\mathrm{i}\varphi}\,\psi_1. \tag{52}$$

Such a phase change only becomes observable when there are several states; it might be implemented in a two-state system as the alteration

$$\Psi = c_1\psi_1 + c_2\psi_2 \rightarrow \mathrm{e}^{\mathrm{i}\varphi}c_1\psi_1 + c_2\psi_2. \tag{53}$$

This is a special case of the general quantum-state manipulation

$$\Psi = c_1\psi_1 + c_2\psi_2 \rightarrow c_1'\psi_1 + c_2'\psi_2. \tag{54}$$

[38] In this context the Euler angles have no connection with rotations of objects in ordinary Euclidean space; they are simply three parameters.

3.9 Equations of motion for changes

To describe changes of an atom subject to external fields we require an equation of motion for the probabilities – or for probability amplitudes. There are two regimes of excitation that have simple equations.

- Historically, the first regime to be considered was that of thermal radiation or, more generally, *incoherent* light sources – those having broad bandwidth, such as occur in the atomospheres of stars or laboratory plasmas. The approach was first suggested by Einstein, and leads to a set of first-order ordinary differential equations for probabilities – *rate equations* for changes in probabilities [2, §2.2].

- The second regime, that of *coherent excitation*, became of practical interest with the introduction of laser light sources. It relies on differential equations for probability amplitudes – the time dependent Schrödinger equation [2, Chap. 3].

Each of these sets of equations is an idealization, appropriate to different assumptions about the excitation. A more generally applicable approach requires a formalism that bridges these two extremes, a *density matrix*, cf. Sec. H.1.

4 Incoherence: the Einstein equations

The early discussions of radiative transitions followed the approach of Einstein, who postulated that one could describe the effects of resonant radiation by means of simple rate equations that express rates of change of number densities as being the difference between gains and losses [2, §2.2]. Three mechanisms contribute to this change:

I. The absorption of radiation, proportional to the radiation intensity

II. Stimulated emission, proportional to the intensity;

III. Spontaneous emission of radiation, independent of intensity and parametrized by the Einstein A coefficient A_{21}.

The resulting radiative rate equations provide a set of coupled ordinary differential equations for the probabilities $P_n(t)$, having the form

$$\frac{d}{dt}P_n(t) = \Sigma_m R_{mn}(t)P_m(t), \tag{55}$$

where $R_{mn}(t)$ is the rate of change in level n produced by level m, i.e. the transition probability per unit time for $m \to n$. These coefficients incorporate the three mechanisms itemezed above. These coupled linear differential equations take simplest form when we place the probabilities into a *column vector* (cf. Appendix B.1)),

$$\mathbf{P}(t) = \begin{bmatrix} P_1(t) \\ P_2(t) \\ \vdots \end{bmatrix}. \tag{56}$$

The equations then appear as a matrix equation [cf. eqn. (416)]

$$\frac{d}{dt}\mathbf{P}(t) = \mathsf{R}(t)\mathbf{P}(t), \tag{57}$$

where R is the square matrix of rate coefficients [39].

4.1 The Einstein rates

Rather than deal with radiation beams, and intensity, Einstein considered steady broadband spectral radiation energy density $u(\nu)$ in a cavity (with dimension of energy per unit volume per Hz), and wrote the rate of excitation, from state 1 to state 2, in the form

$$R_{12} = B_{12}u(\nu). \tag{58}$$

The radiative deexcitation transitions, $2 \to 1$, combining stimulated and spontaneous emission, were postulated to occur at the rate

$$R_{21} = B_{21}u(\nu) + A_{21}. \tag{59}$$

[39] The matrix element R_{nm} is the rate R_{mn}

The connection between the Einstein A and B coefficients, deduced originally from thermodynamic arguments, is

$$B_{21} = \frac{(\lambda_0)^3}{4\hbar} A_{21} \tag{60}$$

where $\lambda_0 = 2\pi c/\omega_0$ is the resonance wavelength of the transition.

Although rate equations, and A and B coefficients, remain widely used, the original equations require modification for use with narrow-bandwidth radiation. This proceeds by considering the absorption of a directed beam, such as eqn (6). The relevant rate equation for the incremental reduction of steady intensity along the propagation axis z, through cold matter, is

$$\frac{d}{dz} I(z) = -\alpha(\omega) I(z). \tag{61}$$

Resonant excitation from state 1 to state 2 occurs when a pulse, of carrier frequency ω, passes through matter. Let the number density of absorbers (atoms in state 1 per unit volume) be $\mathcal{N}_1$. In the absence of any previous excitation (i.e. $\mathcal{N}_2 = 0$), the linear absorption coefficient $\alpha(\omega)$, with dimensions of inverse length, is expressible in terms of an absorption cross section $\sigma(\omega)$, with dimensions area per atom,

$$\alpha(\omega) = \mathcal{N}_1 \frac{\sigma(\omega)}{\hbar\omega}. \tag{62}$$

In turn, the explicit frequency dependence can be placed into a single function, either $s(\omega)$ or $s(\nu) = s(\omega)/2\pi$, by writing

$$\sigma(\omega) = \sigma_{tot} s(\nu), \qquad \text{with} \int_0^\infty d\nu \; s(\nu) = 1. \tag{63}$$

The frequency-integrated cross section can be written in terms of Einstein A and B coefficients as

$$\sigma_{tot} = \frac{(\lambda_0)^2}{8\pi} A_{21} = \frac{\hbar\omega_0}{c} B_{21}. \tag{64}$$

Appendix A.6 defines additional parameters with which to express the ability of an atom to absorb or emit radiation.

4.2 The two-state rate equations

The radiative rate equations can be expressed in several ways. Expressed in terms of laser intensity $I(t)$ the relevant equations for a two-state atom subjected to narrow-bandwidth near-resonant radiation read [62]

$$\frac{d}{dt} P_1(t) = -B_{12} s(\nu) \frac{I(t)}{c} P_1(t) + [A_{21} + B_{21} s(\nu) \frac{I(t)}{c}] P_2(t), \tag{65}$$

$$\frac{d}{dt} P_2(t) = -\frac{d}{dt} P_1(t). \tag{66}$$

The radiative rates appearing here can be expressed in several ways, e.g.

$$R_{12}(t) = B_{12}s(\nu)\frac{I(t)}{c} = \sigma(\omega)\frac{I(t)}{\hbar\omega}, \tag{67}$$

$$R_{21}(t) = A_{21} + 2B_{21}s(\nu)\frac{I(t)}{c} = A_{21}[1 + 2\bar{n}(t)] = A_{21}\left[1 + \frac{I(t)}{I^{sat}}\right]. \tag{68}$$

Here $\bar{n}(t)$ is the mean number of interacting photons, i.e. the photon flux $I(t)/\hbar\omega$ within the cross section $\sigma(\omega)$,

$$\bar{n}(t) = \frac{B_{21}s(\nu)I(t)}{cA_{21}} = \frac{s(\nu)I(t)\lambda^2}{4\hbar\omega} = \sigma(\omega)\frac{I(t)}{\hbar\omega}, \tag{69}$$

and I^{sat} is the *saturation intensity* appropriate to the carrier frequency ω,

$$I^{sat} = \frac{\hbar\omega A_{21}}{2\sigma(\omega)} = \frac{cA_{21}}{2B_{21}s(\nu)} = \frac{2\hbar c}{\lambda^3 s(\nu)}. \tag{70}$$

4.3 Solutions to the rate equations

The effects of radiation take simpler form when expressed in terms of the *population inversion*,

$$w(t) \equiv P_2(t) - P_1(t). \tag{71}$$

With the assumption $B_{12} = B_{21}$ appropriate for nondegenerate transitions the rate equation for population inversion reads

$$\frac{d}{dt}w(t) = -R(t)\, w(t) - A_{21}. \tag{72}$$

where

$$R(t) = R_{12}(t) + R_{21}(t). \tag{73}$$

The solution to this equation is

$$w(t) = [w(0) - w(\infty)] \exp\left[-\int_0^t dt'\, R(t')\right] + w(\infty). \tag{74}$$

For steady illumination this solution monotonically approaches the asymptotic value

$$w(\infty) = \frac{-A_{21}}{A_{21} + 2B_{21}s(\nu)I(t)} = \frac{-1}{1 + I(t)/I^{sat}} = \frac{-1}{1 + 2\bar{n}}. \tag{75}$$

That is, the populations *saturate* at constant values. The inversion approaches the final equilibrium value $w(\infty)$ at a rate that increases with intensity $I(t)$ (or mean photon number $\bar{n}$) but which is never less than the spontaneous emission rate A_{21}. The instantaneous excitation, at time t, depends on the time integrated intensity (known as pulse *fluence*),

$$\int_0^t dt'\, R(t') = A_{21}t + \frac{\sigma(\omega)}{\hbar\omega}\int_{-\infty}^t dt'\, I(t'). \tag{76}$$

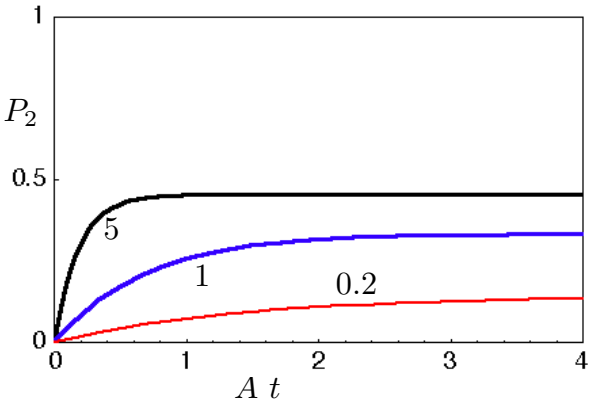

Fig. 12. Excitation probability P_2 vs. decay lifetimes $A\,t$ for various intensities of the radiation, as measured by the mean photon number, $\bar{n} = 0.2, 1, 5$. There is initially no excitation. (after Fig. 2.2-2 of [2])

This behavior contrasts with that of coherent excitation, for which the relevant parameter is the time integral of the electric field amplitude; cf. Sec. 6.2.

The final saturated inversion $w(\infty)$ depends upon the ratios of the several rates, but if $B_{12} = B_{21}$, as is the case for nondegenerate transitions, then the inversion can never exceed $w(\infty) = 0$, meaning in turn that the excitation probability P_2 can never exceed $P_2 = 0.5$. This value is only approached if the stimulated rate is much larger than the spontaneous rate, $B_{21}s(\nu)I(t) \gg A_{21}$ or, equivalently, $\bar{n} \gg 1$, as will occur for sufficiently high intensity $I(t)$. Figure 12 illustrates the behavior.

4.4 Comments

Such radiative rate equations, supplemented with additional rates for collision-induced population changes, have been adequate for the description of numerous environments in which the radiation is incoherent. Examples include hot dense gases or the atmospheres of stars [63]. But they are not applicable to excitation of isolated atoms by laser radiation. Such radiation has a long coherence time; during shorter intervals its effects cannot be described adequately by rate equations that assume random environmental fluctuations. Instead we require the apparatus of quantum mechanics, not only to explain the existance of discrete energy levels but also to describe the changes induced by coherent radiation; cf. Sec. 5 below.

Although the Einstein B coefficients play no direct role in the description of excitation by coherent light, the notion of *spontaneous* emission remains of importance. For isolated atoms in free space the possibility of radiative excitation to a selected quantum state implies an ever present possibility of spontaneous emission, with a lifetime equal to the inverse of the sum of all possible spontaneous emission rates from that state. Only laser-induced procedures that are significantly shorter in duration than the spontaneous-emission lifetime will be considered in most of the present article (an exception is the discussion of optical pumping, Sec. 8.3). Because the spontaneously radiated field is that of a single photon – a single increment of an electromagnetic

field mode – these rates can be altered by modifying the field modes, say by placing the atom in a suitable cavity [64], or into a solid whose structure has been designed to allow only selected radiation modes to propagate (a *photonic crystal*) [65]. Such techniques allow extension of coherent excitation to various discrete states of solids.

5 Coherence: The Schrödinger equation

Information about a quantum system that remains free of randomizing disturbances [40] resides not with probabilities but within a statevector $\Psi(t)$, as discussed in Sec. 3.4. Effects of coherent changes are therefore described by an equation of motion for $\Psi(t)$,

$$\frac{d}{dt}\Psi(t) = ?? \tag{77}$$

As with rate equations, the equation should be linear, thereby allowing superpositions. Because probabilities must sum to unity [41], the statevector remains of unit length during any procedure. Changes to the statevector, in its Hilbert-space setting, must therefore fit the form of multidimensional unitary transformations (e.g. rotations or reflections). The relevant equation of motion, governing the changes induced in the system by laser pulses, as represented by motion of the statevector in Hilbert space, is the time-dependent Schrödinger equation (TDSE) [42],

$$\frac{d}{dt}\Psi(t) = -\frac{\mathrm{i}}{\hbar}\mathsf{H}(t)\Psi(t), \tag{78}$$

involving, on the right-hand side, the imaginary unit $\mathrm{i} \equiv \sqrt{-1}$ and the time-dependent Hamiltonian energy operator $\mathsf{H}(t)$ (cf. Appendix B.4). The Dirac constant, $\hbar = 1.054 \times 10^{-34}$ Joule sec, serves merely to convert energy units into angular frequency units; many authors choose time scales such that they set $\hbar = 1$.

We wish to find the time dependent statevector $\Psi(t)$, an $N-$dimensional column vector in the Hilbert space of physical states, cf. Appendix B.2. To do so we must solve the TDSE subject to initial conditions that specify the statevector at some time t_i, typically taken either as $t_i = 0$ or $t_i \to -\infty$, before the laser field appears. Usually the required condition is that the statevector should initially align with one of the unit vectors (i.e. it should represent a single unperturbed state), say that associated with the quantum state having energy E_1.

When used to describe laser-induced changes, the Hamiltonian has two parts:

$$\mathsf{H}(t) = \mathsf{H}^{at} + \mathsf{H}^{int}(t). \tag{79}$$

The first, constant, contribution, H^{at}, incorporates the energies of the (*bare*) atom in the absence of the laser radiation. The Hilbert-space unit vectors are eigenvectors of this operator,

$$\mathsf{H}^{at}\psi_n = E_n\psi_n. \tag{80}$$

Its eigenvalues are the observable energies $E_1, E_2, \cdots$, of the free, undisturbed atom. Thus, by construction, the matrix H^{at} is *diagonal* (in the basis of physical states); the elements of H^{at} are the unperturbed energies of the system, E_n.

The matrix elements of the interaction $\mathsf{H}^{int}(t)$ can, in principle, be obtained from the wavefunctions of the system. Suppose, for example, that we deal with a single electron, and that the

[40] The succession of measurements on any quantum system produces random results, unless the system is in an eigenstate of the measurement operator. The randomness mentioned here is additional beyond that intrinsic randomness of quantum measurement, and refers to the Hamiltonian itself having random fluctuations.

[41] Section 5.8 discusses situations which violate this requirement.

[42] Traditionally the time derivative appears in the TDSE as a partial derivative, $\partial/\partial t$, to allow the inclusion of spatial coordinates; the equation then applies to a wavefunction $\Psi(\mathbf{r}, t)$.

interaction energy of this electron with the field, at position $\mathbf{r}$ and time t is $V(\mathbf{r},t)$. Using the discrete wavefuntions $\psi_n(\mathbf{r}) \equiv \langle \mathbf{r}|\psi_n\rangle$ one can evaluate the matrix elements of the interaction Hamiltonian as the integral

$$H_{ij}^{int}(t) = \int d\mathbf{r}\, \psi_i(\mathbf{r})^* V(\mathbf{r},t)\psi_j(\mathbf{r}). \tag{81}$$

As noted in the following section, the interaction typically allows parametrization in terms of experimentally measurable quantities (e.g oscillator strengths and intensities) and so it is not necessary to have any wavefunctions.

An aside: this review concerns excitation by laser radiation, and hence the appropriate form of the interaction is one in which there is a carrier at the laser frequency ω. All of the mathematical machinery presented below, with rotating coordinate frames and the rotating-wave approximation, hold for DC fields ($\omega = 0$) if we take the Bohr frequency to be zero, $E_2 - E_1 = 0$, i.e. if we consider degenerate states. Then the interaction strength $d_{12}\mathcal{E}(t)/\hbar$ is termed the *Majorana frequency* and the population oscillations are termed *Majorana oscillations*[2, §3.4].

5.1 Essential states

Only if the carrier frequency nearly matches a Bohr frequency will any appreciable population ever appear in an quantum state other than those initially populated (cf. Sec. 7.3). Thus although there may be an infinite number of quantum states, very few of those participate in the excitation dynamics. We can therefore restrict attention to a finite subspace of the infinite Hilbert space, say one of N dimensions – the N *essential states*. In this subspace the statevector has the expression

$$\Psi(t) = c_1(t)\psi_1 + c_2(t)\psi_2 + \cdots + c_N(t)\psi_N. \tag{82}$$

Although only N states appear explicitly here, the other states have important effects. They are responsible for the polarizability of the atom, i.e. for the occurrence of an induced dipole moment which, when the laser field is present, supplements the direct transition dipole moment. These produce multiphoton transitions and laser-induced energy shifts. Section 10.3.2 discusses simple examples.

The expansion displayed in eqn. (82) holds in a fixed Hilbert space, spanned by N unit vectors ψ_n whose coordinates are the time-varying complex numbers $c_n(t)$. Although we speak of N dimensions, each of the coordinate vectors can be considered as comprising a two-dimensional space in the complex plane; we require $2N$ real numbers to specify the location of the statevector.

The probability amplitudes $c_n(t)$ of eqn. (82) must be chosen such that the resulting statevector satisfies the TDSE, eqn. (78). To assure this behavior we substitute the construction (82) into eqn. (78) and require that the resuting equation be fulfilled along each coordinate. We thereby obtain a set of N coupled ordinary differential equations for the probability amplitudes. For two states these are [43]

$$\frac{d}{dt}c_1(t) \;=\; -\frac{\mathrm{i}}{\hbar}\left[E_1 c_1(t) + V(t)^* c_2(t)\right], \tag{83}$$

[43] Although the distinction between V and V^* for a classical field involves only a phase, when one treats quantized radiation the interaction V^*, originating with the negative-frequency part of the field, is associated with the creation of a photon, while V, based on the positive-frequency part of the field, is associated with photon annihilation. I have followed this convention when using complex-valued Rabi frequencies: $\hat{\Omega}^*$ is associated with an increase of field energy while $\hat{\Omega}$ accompanies radiation absorption; see Appendix A.4.

$$\frac{d}{dt}c_2(t) \quad = \quad -\frac{\mathrm{i}}{\hbar}\left[E_2 c_2(t) + V(t)c_1(t)\right], \tag{84}$$

where $V(t)$ is the interaction energy $\mathsf{H}^{int}(t)$ evaluated between states 2 and 1. In general this may be a complex number, but the Hamiltonian must be Hermitian (meaning $H_{ij} = H^*_{ji}$) in order that the statevector should retain unit length; cf. Appendix B.5.

It is important to recognize that, unlike rate equations, the Schrödinger equation treats single quantum states, not degerate states. To treat degeneracy when describing coherent excitation it is necessary to treat each quantum state separately; cf. Sec. 9.1.

5.2 Undisturbed statevectors: rotating axes

In the absence of any interaction $V(t)$ the equations for the probability amplitudes are, for each state,

$$\frac{d}{dt}c_n(t) = -\frac{\mathrm{i}}{\hbar}E_n c_n(t). \tag{85}$$

These have the simple solutions

$$c_n(t) = \exp(-\mathrm{i}E_n t/\hbar)c_n(0), \tag{86}$$

and thus the statevector at time t is expressible as

$$\Psi(t) = \Sigma_n \exp(-\mathrm{i}E_n t/\hbar)c_n(0)\psi_n. \tag{87}$$

This construction can be regarded as expressing a fixed superposition,

$$\Psi(t) = \Sigma_n c_n(0)\psi'_n(t), \tag{88}$$

of time-dependent basis vectors $\psi'_n(t)$,

$$\psi'_n(t) \equiv \exp[-\mathrm{i}E_n t/\hbar]\psi_n. \tag{89}$$

Each of these unit vectors rotates, with constant angular velocity $E_n/\hbar$, in a complex-number plane. To visualize the resulting Hilbert-space motion we can express the unit vectors as two-dimensional axes in the complex plane, $\psi_n = \psi^R_n + \mathrm{i}\psi^I_n$ and, with the abbreviation $\omega_n = E_n/\hbar$ write

$$\begin{aligned}\exp(-\mathrm{i}E_n t/\hbar)\psi_n \quad = \quad & [\cos(\omega_n t)\psi^R_n - \sin(\omega_n t)\psi^I_n] \\ & -\mathrm{i}[\sin(\omega_n t)\psi^R_n - \cos(\omega_n t)\psi^I_n],\end{aligned} \tag{90}$$

thereby displaying explicitly the steady turning of the rotating coordinate axes.

In such a rotating coordinate system the expansion coefficients c_n remain fixed, in the absence of any interaction. More generally, for a constant Hamiltonian that includes interaction it is similarly advantageous to use a rotating frame to present the description of the statevector. The particular rotating-coordinate choice of eqn. (89) is known as the *Dirac picture* or *interaction picture*, in contrast to the original rigid framework, known as the *Schrödinger picture*. The Dirac picture has the property that the Hamiltonian matrix, in this picture, has no diagonal elements. In recompense, the off-diagonal elements have exponential phases that vary with time.

We shall find it more convenient to introduce, in subsequent sections, a third class of frameworks, known as the *rotating-wave picture* (see Sec 5.6 below). With this choice the Hamiltonian matrix has, as diagonal elements, differences between Bohr frequecies and carrier frequencies, i.e. *detunings*. Furthermore, under suitable conditions, the off-diagonal elements vary only slowly with time.

5.3 The electric-dipole interaction

The interaction of bound particles with laser light almost always originates with the electric-dipole interaction [44] [66]. This means that the interaction energy operator is the projection of the electric dipole moment $\mathbf{d}$ onto the electric field [45],

$$\mathsf{H}^{int}(t) = -\mathbf{d} \cdot \mathbf{E}(t). \tag{91}$$

Here $\mathbf{E}(t)$ is the time varying electric field at the center of mass of the atom. This expression applies to nearly all commonly considered (i.e. "allowed") transitions. For a single laser beam we write the field $\mathbf{E}(t)$ as in eqns. (6) or (7).

Typically there exist selection rules [67] (see Sec. 8.1) such that, for a given pair of states i, j only one polarization direction $\hat{\mathbf{e}}$ gives a nonzero transition moment. I shall refer to the possible nonzero array of values for the interaction Hamiltonian, fixed by nonzero dipole transition moments, as a *linkage pattern* [46]. The possible dipole transition moments – the possible linkages – are fixed for any given atom or molecule; statevector manipulation takes place through control of the magnitude and direction of the electric field $\mathbf{E}(t)$.

The dipole transition moment between states i and j, projected onto the field unit vector $\hat{\mathbf{e}}$, is

$$d_{ij} = \langle \psi_i | \mathbf{d} \cdot \hat{\mathbf{e}} | \psi_j \rangle. \tag{92}$$

For a single-electron orbital this is obtainable from the spatial integral

$$d_{ij} = e \int d\mathbf{r}\, \psi_i(\mathbf{r})^* \mathbf{r} \cdot \hat{\mathbf{e}} \psi_j(\mathbf{r}), \tag{93}$$

where e is the electron charge. Alternatively, the magnitude of the dipole moment (but not the phase) can be extracted from experimental spectroscopic data such as oscillator strengths or Einstein A coefficients; see Appendix A.6.

The directional properties of the electric field, relative to a coordinate system fixed with the atom, appears here embodied in the scalar product of $\mathbf{d}$ with $\mathbf{E}$. For linear polarization we can write the two-state interaction as

$$V(t) = -d_{12}\mathcal{E}(t)\cos(\omega t - \varphi) \equiv \hbar\Omega(t)\cos(\omega t - \varphi), \tag{94}$$

[44] These produce the "allowed" transitions of spectroscopy. Other possibilities include magnetic dipole, electric quadrupole and induced electric-dipole interactions [2, § 2.8]; these are responsible for some, but not all, "forbidden" transitions.

[45] Because orientations are quantized, there occur discrete values for this interaction; see Sec. 8.1.

[46] This pattern has the properties of a *graph*; see Appendix B.8.

where, by suitable choice of phase φ, the field amplitude $\mathcal{E}(t)$ can be taken as real [47]. For circular polarization, of helicity q, the needed expression is the sum of two terms,

$$V(t) = \hbar\Omega_q(t)\exp(-\mathrm{i}\omega t) + \hbar\Omega_{-q}(t)\exp(+\mathrm{i}\omega t). \tag{95}$$

Typically selection rules pick just one of these; cf. Sec. 8.1 and Sec. 8.2. More generally, for elliptical polarization, the interaction is the sum of two helicity components.

When the field is that of a standing wave, e.g. eqn. (13), rather than a traveling wave, the field structure leads to spatial dependence of the Rabi frequency, which becomes $\Omega(x,t) = d_{21}\mathcal{E}(t)\sqrt{2}\sin(kx)/\hbar$. A stationary atom positioned at a field node will experience no excitation, whereas an atom at an antinode will be be subject to maximum interaction.

5.4 Excitation viewed in rotating coordinates

For an idealized monochromatic interaction the function $V(t)$ changes periodically at the carrier frequency ω. As discussed in Sec. 3.3, when the polarization is circular the effect is a steady torque – a steady rotation at the carrier frequency ω – that tends to alter angular momentum, first adding and then subtracting as a series of transitions. When the polarization is linear the relatively rapid field variation produces a shaking of the charge distribution; much more slowly there occurs a distortion of the charge distribution attributable to a transition. It is this latter aspect of the motion that concerns us.

To view the two-state transition most clearly for circular polarization, and to eliminate the relatively uninteresting small variations at the carrier frequency induced by linear polarization, we introduce a rotating Hilbert-space coordinate,

$$\psi_2'(t) = \exp(-\mathrm{i}\omega t)\psi_2, \tag{96}$$

that rotates at the carrier frequency ω [48]. In this rotating reference frame the statevector appears as

$$\Psi(t) = C_1(t)\psi_1 + C_2(t)\psi_2'(t). \tag{97}$$

The probabilities are independent of the phases,

$$P_n(t) = |\langle\psi_n|\Psi(t)\rangle|^2 = |C_n(t)|^2 = |c_n(t)|^2, \tag{98}$$

but other quantities, such as the induced dipole moment, exhibit them [49],

$$\text{Re}\,\langle\mathbf{d}(t)\rangle = \langle\psi_1|\mathbf{d}|\psi_2\rangle\, C_1(t)^* C_2(t)\exp[-i\omega t]. \tag{99}$$

[47] The absolute phase of the field, as parametrized with the time of electric field zero crossing, is not controllable. During time shorter than the coherence time of the laser field it is permissible, and useful, to regard the phase as zero. However, it is then essential to maintain this convention during subsequent time evolution, particularly if controlled phase changes occur, as in Sec. 7.1.2.

[48] The coordinate change can be designed to incorporate the full local variation of the field phase $\Phi(x,y,z,t)$, as defined in eqn. (15).

[49] The frequency associated with a dipole moment picks out the carrier frequency of a field that will be modified, during propagation; cf. Appendix A.5. The time-varying dipole moment will create a field at this frequency, if it is not already present, and will alter existing fields at this frequency.

The resulting pair of coupled ODEs read, in vector and matrix form,

$$\frac{d}{dt}\begin{bmatrix} C_1(t) \\ C_2(t) \end{bmatrix} = -\frac{\mathrm{i}}{\hbar}\begin{bmatrix} E_1 & V(t)^* \mathrm{e}^{-\mathrm{i}\omega t} \\ V(t)\mathrm{e}^{+\mathrm{i}\omega t} & E_2 - \hbar\omega \end{bmatrix}\begin{bmatrix} C_1(t) \\ C_2(t) \end{bmatrix}. \tag{100}$$

These equations are exact (in a coordinate frame rotating with angular velocity ω), within the idealization of an isolated two-state atom that undergoes no spontaneous emission.

When the light is circularly polarized, the interaction is that of eqn. (95). When, in addition, the transition takes place between suitable magnetic sublevels (cf. Sec. 8.1), then the interaction $V(t)$ embodies an exponential $\exp(\mathrm{i}\omega t)$ that exactly cancels the exponentials appearing in in these equations [50]. It then becomes a straightforward exercise in numerical integration to obtain the solutions, starting e. g. with the initial conditions

$$C_1(0) = 1, \quad C_2(0) = 0. \tag{101}$$

In principle, there is no difficulty in integrating numerically the exact two-state differential equations for any reasonable time variation of $\Omega(t)$, using appropriate numerical tools [68].

Alternatively, when the light is linearly polarized, so the interaction $V(t)$ is that of eqn. (94), one can again numerically integrate the coupled equations. However, it is necessary to use integration time steps that allow sufficient resolution of the fastest changes, i.e. those at the carrier frequency. The equations are, in fact, examples of *stiff* ordinary differential equations – ODEs that have a wide range of characteristic time scales. It is not always practical to follow the relatively rapid oscillations of the carrier frequency in order to evaluate much slower transition changes at the Rabi frequency. Simplification then proves desirable. The following section discusses the traditional approach.

5.5 Two-state example

Solutions to the two-state equations presented here underly the calculations used to display wavefunction changes discussed in Sec. 3.3. To illustrate that example we consider resonant excitation by monochromatic laser light of a two-state atom that is initially unexcited. Figure 13 illustrates one example of the resulting probabilities, when the radiation is linearly polarized. In this example one sees very clearly the rapid linear oscillations associated with the carrier frequency, together with the slower Rabi oscillations, at the constant Rabi frequency. Excitation by circularly polarized light exerts a steady torque that produces the Rabi oscillations but not the rapid variation at the carrier frequency.

5.6 The rotating wave approximation (RWA)

For optical radiation of commonly used laser pulses, the Rabi frequency Ω is typically 4 or 5 orders of magnitude smaller than the carrier frequency ω. That is, the photon energy $\hbar\omega$ is much

[50] The use of magnetic sublevels always involves more than two quantum states. When some of these are degenerate then frequency alone does not limit the linkages. In addition to the link described here, say from an initial state having magnetic quantum number M to one with quantum number $M+1$ via interaction $V(t)$, there will also occur a potential linkage to state $M-1$ via interaction $V(t)^*$. One of these, in rotating coordinates, will involve a counter-rotating term $\exp(\pm 2\mathrm{i}\omega t)$. The neglect of this term, through the RWA, reduces the system, for example, from three states to two; see Sec. 8.2.

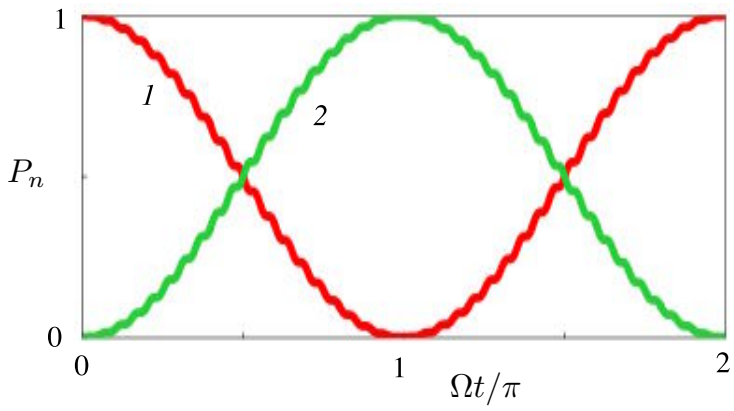

Fig. 13. Plot of probabilities $P_n(t)$ vs. Rabi cycles $\Omega\, t/\pi$ for linearly polarized monochromatic excitation with $\omega = 20\Omega$. Initially the system is in state 1. Note the rapid small oscillations (these are at the carrier frequency) that slowly lead to a transition into state 2.

larger than the interaction energy $\hbar\Omega$. Typical optical frequencies (the carrier) are

$$\omega \;=\; 2\pi c/\lambda \approx 5\times 10^{15}\ \text{sec}^{-1} \tag{102}$$

while typical Rabi frequencies (the interaction energy / $\hbar$) are less than

$$|\Omega_0| \;=\; |d\mathcal{E}|/\hbar = 2.2\times 10^{8}\ \text{sec}^{-1}\sqrt{I[\text{W cm}^{-2}]}\times\frac{|d|}{(ea_0)} \tag{103}$$

$$\approx\; 2\times 10^{11}\ \text{sec}^{-1}\ \text{for}\ I = 1\ \text{Gw/cm}^2. \tag{104}$$

Thus for optical excitation the inequality $\omega \gg \Omega_0$ applies. Therefore the small carrier-frequency oscillations hold no interest; we are instead concerned with activity that takes place only over very many optical cycles. We therefore consider probability amplitudes that are averaged over many optical cycles. In the Schrödinger equation we make the *rotating wave approximation* (RWA) [51] [2, §3.9], neglecting terms that vary as $2\omega t$ (*counter-rotating* terms) when added to constant terms

$$\cos(\omega t-\varphi)\mathrm{e}^{-i\omega t} = \tfrac{1}{2}\left[e^{-\mathrm{i}\varphi} + \mathrm{e}^{-2\mathrm{i}\omega t+i\varphi}\right] \to \tfrac{1}{2}\mathrm{e}^{-\mathrm{i}\varphi}. \tag{105}$$

The result is the two-state RWA Schrödinger equation

$$\frac{d}{dt}\begin{bmatrix} C_1(t)\\ C_2(t)\end{bmatrix} = -\mathrm{i}\begin{bmatrix} 0 & \frac{1}{2}\Omega(t)\mathrm{e}^{-\mathrm{i}\varphi}\\ \frac{1}{2}\Omega(t)\mathrm{e}^{\mathrm{i}\varphi} & \Delta\end{bmatrix}\begin{bmatrix} C_1(t)\\ C_2(t)\end{bmatrix}. \tag{106}$$

The Rabi frequency $\Omega(t)$ appearing here is the slowly varying real-valued function of time

$$\Omega(t) = -d_{12}\mathcal{E}(t)/\hbar. \tag{107}$$

[51] The use of Hilbert-space coordinates that rotate at a carrier frequency dates back to early work with microwave resonances, [69].

There occurs a phase φ associated with the interaction, shown here explicitly [52]. At times it proves convenient to incorporate the phase into the Rabi frequency, and regard that as a complex-valued quantity $\hat{\Omega}(t) = \mathrm{e}^{\mathrm{i}\varphi}\Omega(t)$. Alternatively, one can place the phase into the Hilbert-space unit vector, by defining $\hat{\psi}_2 = \mathrm{e}^{-\mathrm{i}\varphi}\psi_2$.

Written more compactly in matrix form the Schrödinger equation reads

$$\frac{d}{dt}\mathbf{C}(t) = -\mathrm{i}\mathsf{W}(t)\mathbf{C}(t), \tag{108}$$

where $\mathbf{C}(t)$ is a two-component column vector comprising the elements $C_n(t)$ and the 2×2 matrix $\mathsf{W}(t)$ is the RWA Hamiltonian, in frequency units,

$$\mathbf{C}(t) = \begin{bmatrix} C_1(t) \\ C_2(t) \end{bmatrix}, \qquad \mathsf{W}(t) = \begin{bmatrix} 0 & \frac{1}{2}\Omega(t)\mathrm{e}^{-\mathrm{i}\varphi} \\ \frac{1}{2}\Omega(t)\mathrm{e}^{+\mathrm{i}\varphi} & \Delta \end{bmatrix}. \tag{109}$$

Like eqn. 57, the RWA Schrödinger equation (109) presents symbolically a set of linear ordinary differential equations. It differs from the rate equations by the presence of the imaginary unit $\mathrm{i} \equiv \sqrt{-1}$. This difference appears in the solution forms: rate equations have exponentials where the Schrödinger equation has sinusoids.

The basic controls appearing here are the time-dependent Rabi frequency $\Omega(t)$ and the detuning Δ, defined through the equation

$$\hbar\Delta \quad \equiv \quad E_2 - E_1 - \hbar\omega. \tag{110}$$

It is through manipulation of these quantities that we control the time evolution of the statevector. Both the electric field envelope $\mathcal{E}(t)$ and the Rabi frequency $\Omega(t)$ can be taken as real valued at some specific time, but in general they may be complex-valued functions of time.

5.7 Integral form of the equations

Rather than present the description of excitation in the form of ordinary differential equations, as was done above, it sometimes proves useful to cast these into the form of integrals. For the two state system in the RWA the integral equations read

$$C_2(t) = \mathrm{e}^{-\mathrm{i}\Delta t}\left[C_2(t_0) - \frac{\mathrm{i}}{2}\int_{t_0}^{t} dt'\ \Omega(t')\mathrm{e}^{\mathrm{i}\Delta t' + \mathrm{i}\varphi}C_1(t')\right], \tag{111}$$

$$C_1(t) = C_1(t_0) - \frac{\mathrm{i}}{2}\int_{t_0}^{t} dt'\ \Omega(t')\mathrm{e}^{-\mathrm{i}\varphi}C_2(t'). \tag{112}$$

These incorporate the initial conditions $C_n(t_0)$ at the initial time t_0 prior to the arrival of the excitation pulse. By taking the derivative with respect to time t one recovers the coupled ordinary differential equations of the RWA. Like the equivalent ODEs, the integral equations involve on the right-hand side the as yet unknown solutions, and so they are of use only with the introduction of some further assumptions or with an iterative algorithm. Section 6.1 discusses an example of such an approach.

[52] The absolute value of the phase is not controllable, and can be taken as zero at any convenient time. Only when one compares two pulses, both within a coherence time, or pulses affecting two locations, does one need to keep track of phases.

5.8 Probability loss

All excited states – states whose energy exceeds that of the ground state – will eventually impart this energy to surroundings. When collision partners are present, these can carry of the internal energy as increased kinetic energy of the projectile, or can themselves lose kinetic energy to produce excitation. Whenever radiative excitation is possible between two states, then spontaneous emission can transfer excitation energy from the atom to radiation. Often the result of such emission, seen as fluorescence, is one of several possible final states. These need not be amongst the set of essential states – they may be unaffected by the particular active laser fields. Because they are not included amongst our limited set of basis states, any transition to one of them represents a loss of probability for finding the atom in an essential state.

When the time scale of interest – that of pulsed excitation – is much shorter than the lifetime of any of the essential states, then we can neglect spontaneous emission. But when we consider short-lived species, or long pulse durations, then the effects of spontaneous emission must be included in the dynamics. This can be done rigorously with the use of a density matrix (see Appendix H.1). However, a simpler description, using only the statevector, is possible under some circumstances: If nearly all spontaneous-emission transitions take the system out of the limited Hilbert subspace spanned by the essential states, then these events can be regarded as simple probability losses. The underlying physics relies on the following observations.

Although we here treat an idealized system comprising a single isolated atom, having only a few discrete states of interest, in reality this atom has additional states that form a continuum, e.g. ionization or dissociation states. To treat these we imagine the atom (an ion and its associated bound electron) to be contained within a very large but finite box, so that its wavefunction is constrained by boundary conditions. It then has discrete but closely spaced energies rather than a continuum (the spectrum is a *quasicontinuum* [70]). By superposing such states we can construct a state whose associated wavefunction is localized at a given time; the electron, though possessing energy above the ionization limit, has not yet departed from the ion. With passing time this wavepacket will move into other portions of the box, spreading as it does so. When we view only a small volume around the original location of the wavepacket we have the impression that the particle has vanished; its probability, measured by the square of a wavefunction, is spread throughout other regions of the box.

It may very well happen that, after a *recurrence time*, the particle is once again seen to be localized [53]. But until then the electron behaves as a free particle. This simple picture preserves overall probability – the electron that is removed from the atom is still within the large box. But the probability of finding it in the immediate vicinity of the ion core has diminished. By directing attention to only a small region of the large confining box we regard this as "lost" probability. More precisely, the electron is not in one of the small set of discrete states (e.g. two) that we have taken as our Hilbert space.

There exist straightforward mathematical techniques for treating situations in which a continuum of energies occur and in which, as a consequence, there appears to be probability loss from a set of discrete states. In essence, we deal with a weak interaction linking a discrete state with a near-continuum of excited state. We regard the time evolution as unidirectional, e.g. we

[53] This behavior occurs when intense laser radiation removes a bound electron and places it, as a wavepacket, onto an elliptical trajectory that returns regularly to the ion [58]. Modelings of intense field response often rely on simulations within a finite box; recurrences then are avoided by making the boundary have absorbing walls [53].

include photoionization but not its inverse, radiative recombination. Under these conditions the continuum structure retains no memory; changes are irreversable. The portion of the system that is described by a few discrete states then appears to undergo exponential decay. That is, they cause probability decays described by the equation

$$P_n(t) = \exp(-\Gamma_n t) P_n(0), \tag{113}$$

where Γ_n is the decay rate for state n. Such processes, irreversible probability loss from the system of interest, make this an example of an *open* system [71]. Although proper treatment requires a density matrix, they can be treated by replacing the real-valued energy E_n by the complex-valued number $E_n - \mathrm{i}\Gamma_n/2$.

The extension of the resonant two-state TDSE equation for the excited-state probability amplitude provides the equations

$$\frac{d}{dt}C_1(t) \quad = \quad -\frac{\mathrm{i}}{2}\Omega \mathrm{e}^{-\mathrm{i}\varphi} C_2(t), \tag{114}$$

$$\frac{d}{dt}C_2(t) = -\frac{\mathrm{i}}{2}\Omega e^{\mathrm{i}\varphi} C_1(t) - \tfrac{1}{2}\Gamma C_2(t). \tag{115}$$

These two coupled first-order equations can be replaced by a single second-order differential equation; each amplitude $C_n(t)$ obeys the same equation, recognizable as that of a damped harmonic oscillator,

$$\frac{d^2}{dt^2}C_n(t) + \tfrac{1}{2}\Gamma \frac{d}{dt}C_n(t) + \tfrac{1}{4}\Omega^2 C_n(t) = 0. \tag{116}$$

The system is completely described by this ODE together with the initial values $C_n(0)$ of the two probability amplitues.

To find solutions we test the trial solution $C_n(t) = A_n \exp(-\mathrm{i}Zt)$ and find that Z must satisfy the quadratic equation

$$Z^2 + \mathrm{i}\tfrac{1}{2}\Gamma Z - \tfrac{1}{4}\Omega^2 = 0. \tag{117}$$

Two regimes exist [2, §3.10] : a regime of *underdamped* oscillation when the loss rate is small, $\Omega > \Gamma/2$, and a regime of *overdamping* when the loss rate is large, $\Omega < \Gamma/2$. The two regimes are separated by the condition of *critical damping*, when $\Omega = \Gamma/2$. Figure 14 shows examples of the three regimes. I shall treat primarily situations in which the damping is slight.

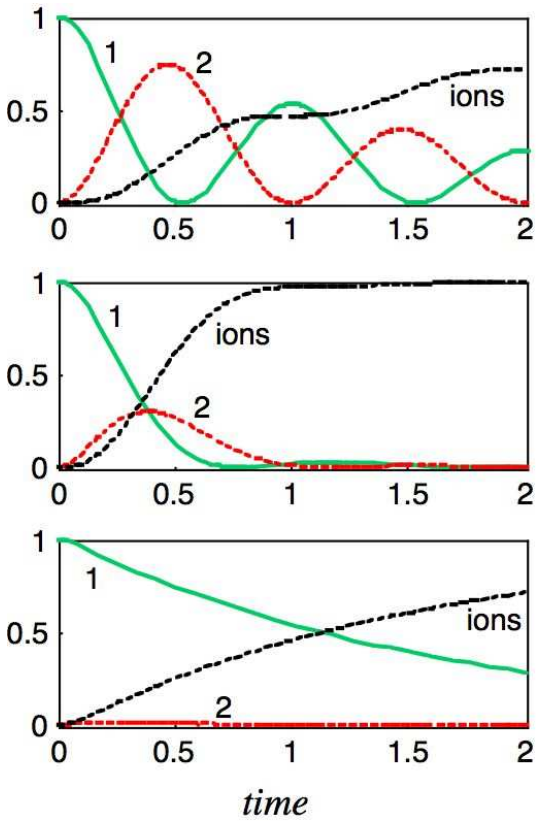

Fig. 14. Effect of ionization loss on two-state excitation. Top frame: population histories of states 1 and 2 with weak loss; behavior is underdamped Rabi oscillations. Each burst of probability into state 2 produces a corresponding burst of ionization loss; the cumulation ionization population is shown by a dashed line. Middle frame: critical damping: the populations undergo no oscillations. Bottom frame: overdamped behavior; the population flows from state 1 directly into the ionization state. (after Fig. 3.10-2 of [2])

6 Two-state coherent excitation examples

For many years the primary emphasis in textbooks on quantum mechanics was on relatively weak fields, and the resultant slight excitation, rather than on the Rabi oscillations that attend contemporary coherent excitation. I will comment briefly on this weak-excitation regime in Sec. 6.1. I will then consider two specific classes of more general two-state coherent excitation, each illustrating a form of excitation that has numerous applications and which generalizes to more complicated multi-level systems. The first examples treat impulsive excitation, in which a field of constant intensity suddenly turns on. Such excitation produces Rabi oscillations; cf. Secs. 6.2 and 6.3. The second class occurs when there is slow variation of the detuning (e.g. a *frequency chirp*) along with variation of the intensity, and population transfer occurs without oscillations; cf. Sec. 6.5. For each of these classes I offer Hilbert-space pictures of the excitation. These are particular cases of the many two-state models which allow solution in terms of conventional special functions; cf. Appendix E.

6.1 Weak pulse: Perturbation theory

The model of excitation by monochromatic light is an idealization that neglects any fluctuations in the phase or amplitude of the field, properties that affect the frequency content of the field. One way to characterize modulated radiation is by means of Fourier transforms, expressing in this way the distribution of frequencies present in the illumination. To examine the connection between field frequencies and excitation we introduce the Fourier transform (FT) of the interaction Hamiltonian (i.e. the transform of the electric field amplitude, not the intensity), expressed via the FT of the pulsed Rabi frequency:

$$\widetilde{\Omega}(\Delta) = \frac{1}{2\pi}\int_{-\infty}^{\infty} dt\, \mathrm{e}^{\mathrm{i}\Delta t + \mathrm{i}\varphi}\, \Omega(t). \tag{118}$$

The inverse transform provides the time varying Rabi frequency,

$$\Omega(t) = \int_{-\infty}^{\infty} d\Delta\, \mathrm{e}^{-\mathrm{i}\Delta t - \mathrm{i}\varphi}\, \widetilde{\Omega}(\Delta). \tag{119}$$

The peak value of the Rabi frequency $\Omega_0 \equiv \Omega(t=0)$ provides one measure of the strength of the interaction; a second measure is the *temporal pulse area* (or *Rabi angle*), expressible as the resonant ($\Delta = 0$) contribution to this Fourier transform [54],

$$A_\infty \equiv \int_{-\infty}^{\infty} dt\, \Omega(t) = 2\pi\widetilde{\Omega}(0)\mathrm{e}^{-\mathrm{i}\varphi}. \tag{120}$$

The pulse duration τ can be regarded as the ratio of temporal pulse area to peak Rabi frequency,

$$\tau \equiv |A_\infty/\Omega_0| = 2\pi|\widetilde{\Omega}(0)/\Omega_0|. \tag{121}$$

An important idealization of the radiation interaction occurs when conditions are such that there is little excitation. Changes to the atom can then be regarded as small perturbations. The resulting simplified mathematics, *time dependent perturbation theory* [72] [2, §4.5,17.1], starts

[54] Note that this quantity can be positive, negative or zero.

from the exact relationship of eqn. (111) with $C_2(t_0) = 0$. Although this expression, when differentiated, yields the time-dependent Schrödinger equation, it is not of immediate use because it involves the as yet unknown ground-state amplitude $C_1(t)$. However, because the radiative interaction produces, by assumption, little change in the statevector, we approximate that amplitude as the initial value

$$C_1(t) \approx C_1(-\infty) = 1. \tag{122}$$

This approximation produces the *first-order perturbation theory* result

$$C_2(t) \approx -\frac{\mathrm{i}}{2}\int_{-\infty}^{t} dt'\ \Omega(t')\,\mathrm{e}^{\mathrm{i}\Delta(t'-t)+\mathrm{i}\varphi}. \tag{123}$$

In particular, the completed pulse produces an amplitude proportional to the FT of the Rabi frequency,

$$C_2(\infty) \approx -\frac{\mathrm{i}}{2}\mathrm{e}^{-\mathrm{i}\Delta t}\int_{-\infty}^{+\infty} dt'\ \Omega(t')\,\mathrm{e}^{\mathrm{i}\Delta t'+\mathrm{i}\varphi} = -\frac{\mathrm{i}}{2}\mathrm{e}^{-\mathrm{i}\Delta t}\widetilde{\Omega}(\Delta). \tag{124}$$

In turn, the excitation probability $|C_2(\infty)|^2$ produced by the completed pulse, to first order and for given detuning Δ, is the absolute square of the Fourier transform of the Rabi frequency,

$$\mathcal{P}^I(\Delta) = \frac{1}{4}\left|\int_{-\infty}^{+\infty} dt\ \Omega(t)\,\mathrm{e}^{\mathrm{i}\Delta t}\right|^2 = \tfrac{1}{4}|\widetilde{\Omega}(\Delta)|^2. \tag{125}$$

In this first-order perturbation-theory result the cumulative excitation produced by a pulse depends only on the frequency content, not at all on any details of the temporal pulse shape. An important consequence of this result is that when a pulse has no frequency component at the given detuning, then it produces (in first order) no lasting excitation, $\mathcal{P}^I(\Delta) = 0$. The population transfer produced by any resonant pulse ($\Delta = 0$) is proportional to the square of the temporal pulse area,

$$\mathcal{P}^I(0) = (A_\infty/2)^2, \qquad \text{for } \Delta = 0. \tag{126}$$

This result holds only for small values of the temporal pulse area, $A_\infty \ll 1$. For resonant excitation this absence of frequency content means the pulse has zero temporal pulse area: the electric field has equal positive and negative contributions to this area.

It is not difficult to construct counter examples, in which permanent excitation occurs despite the absence of resonant frequencies. One in which complete population inversion can take place even though there are no resonant components in the field, occurs with bichromatic light, as discussed in Appendix E.6.

The evident lack of excitation predicted (to first order) by eqn. (125) does not mean that a pulse has no lasting effect upon the atom. Indeed, exact numerical evaluation of the TDSE may reveal complete population transfer for a pulse for which $\mathcal{P}^I(\Delta) = 0$. To treat such situations within the context of perturbation theory it is necessary to improve the estimate of $C_1(t)$ by using an approximation to the exact expression

$$C_1(t) = 1 - \frac{\mathrm{i}}{2}\int_{-\infty}^{t} dt'\ \Omega(t')\mathrm{e}^{-\mathrm{i}\varphi}C_2(t'). \tag{127}$$

When the radiative interaction is that of an electric-dipole moment of a free atom, the second-order estimate requires an integral involving the product of two successive interactions, i.e. two photons. For free atoms this vanishes exactly because of parity constraints. Then the next contributory order to the probability amplitude is third-order theory. When the first-order contribution vanishes this gives the prescription

$$\mathcal{P}^{III}(\Delta) = \frac{1}{2^6}\left|\int_{-\infty}^{\infty} dt' \int_{-\infty}^{t'} dt'' \int_{-\infty}^{t''} dt''' \,\Omega(t')\Omega(t'')\Omega(t''')\,\mathrm{e}^{\mathrm{i}\Delta t' - \mathrm{i}\Delta t'' + \mathrm{i}\Delta t'''}\right|^2 . \quad (128)$$

The evaluation of this triple integral is daunting, but is possible in simple cases [73].

Time dependent perturbation theory has its most important application to the evaluation of transitions produced by broadband radiative excitation or between a discrete state and a continuum of final states, such as occurs with photoionization. Applied to such situations it produces the traditional transition rates associated with the Fermi Golden Rule and described in basic textbooks on quantum mechanics [34] [2, §4.5].

6.2 Resonant CW excitation

When the excitation is resonant (meaning $\hbar\omega = E_2 - E_1$), the two coupled RWA equations read

$$\frac{d}{dt}C_1(t) = -\frac{\mathrm{i}}{2}\Omega(t)\mathrm{e}^{-\mathrm{i}\varphi}\,C_2(t), \quad (129)$$

$$\frac{d}{dt}C_2(t) = -\frac{\mathrm{i}}{2}\Omega(t)\mathrm{e}^{\mathrm{i}\varphi}\,C_1(t). \quad (130)$$

Analytic solutions are readily found, for any variation of the pulsed Rabi frequency, by introducing a new time scale $d\tau = |\Omega(t)|dt$, cf. Appendix E.1. The result, for a system known to be in state 1 at time $t = 0$, as specified by the initial conditon $C_1(0) = 1$, is

$$C_1(t) = \cos[A(t)/2], \qquad C_2(t) = -\mathrm{i}\,\mathrm{e}^{\mathrm{i}\varphi}\,\sin[A(t)/2]. \quad (131)$$

Here $A(t)$ is the Rabi angle (temporal pulse area), the integral to time t of the (real-valued) Rabi frequency,

$$A(t) = \int_{-\infty}^{t} dt\,\Omega(t). \quad (132)$$

The resulting populations read, independent of the field phase φ,

$$P_1(t) = \tfrac{1}{2}[1 + \cos A(t)], \quad P_2 = \tfrac{1}{2}[1 - \cos A(t)]. \quad (133)$$

When the Rabi frequency remains constant, the Rabi angle is $A(t) = |\Omega t|$, and the populations undergo periodic Rabi oscillations at the Rabi frequency Ω. In general, for any t, the angle $A(t)$ can be positive, negative or zero. Figure 15 illustrates this behavior.

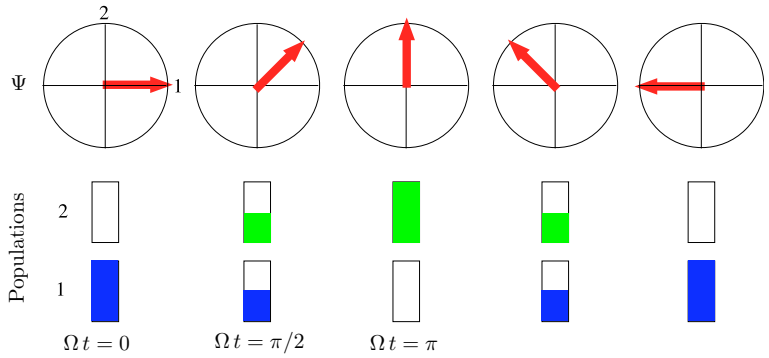

Fig. 15. Rabi oscillations: top frames show statevector Ψ, bottom frames show histograms of population, for a succession of times

6.3 Detuned CW excitation

When steady nonzero detuning occurs, along with steady intensity, then the solutions are again oscillatory. Appendix E.2 provides exact analytic solutions for the two-state atom subject to constant non-resonant intensity. When the population initially occupies state 1 the excited-state RWA amplitude, from eqn. (500) of Appendix E.2, is

$$C_2(t) = U_{21}(t) = \mathrm{i}\frac{\hat{\Omega}}{\sqrt{\Delta^2 + |\hat{\Omega}|^2}} \sin(\widetilde{\Omega} t/2), \tag{134}$$

where $\hat{\Omega}$ is allowed to be complex-valued, thereby incorporating the laser phase, and

$$\widetilde{\Omega} \equiv \sqrt{\Delta^2 + |\hat{\Omega}|^2} \tag{135}$$

is the *nonresonant Rabi frequency*. The resulting excited-state population is

$$P_2(t) = \frac{|\hat{\Omega}|^2}{2(\Delta^2 + |\hat{\Omega}|^2)}[1 - \cos(\widetilde{\Omega} t)]. \tag{136}$$

When the field is not resonant the population transfer is never complete; the maximum excitation diminishes with increasing detuning and the oscillations become more rapid. Figure 16 illustrates this behavior.

The oscillatory behavior continues indefinitely, as long as the radiation remains constant and coherent, and no interruptions occur. Over many Rabi cycles the time-averaged excitation, obtained by averaging the sinusoid (to zero), is

$$\bar{P}_2 = \frac{|\hat{\Omega}|^2}{2(\Delta^2 + |\hat{\Omega}|^2)}. \tag{137}$$

On resonance, $\Delta = 0$, this average, $\bar{P}_2 = \frac{1}{2}$, is the value obtained from the rate-equation model for a strong field and no degeneracy, in the limit of long times. In the limit of large detuning

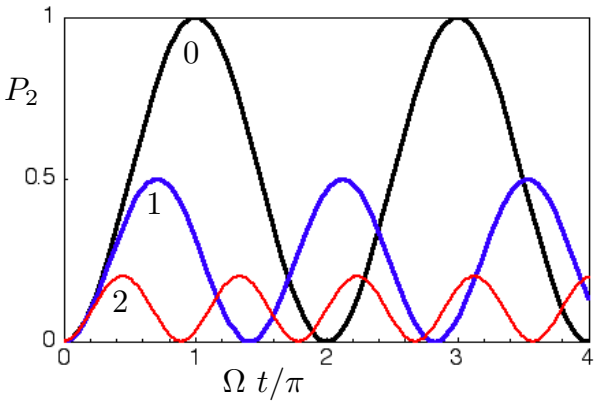

Fig. 16. Excitation probability $P_2(t)$ vs. Rabi cycles $\Omega t/\pi$, showing population oscillations for constant Rabi frequency Ω with detunings 0, 1 and 2 times Ω_0. (after Fig. 3.7-1 of [2])

(i.e. much larger than the Rabi frequency) the excitation is negligible at all times. The range of detunings where appreciable excitation can occur, on average, is roughly bounded by the Rabi frequency: with larger Rabi frequencies larger detuning can contribute to excitation.

6.4 Explaining oscillations: Dressed states

Simple analytic solutions to the nonresonante two-state RWA are known for a number of analytic forms of the time dependent Rabi frequency and detuning; see Appendix E. However, it is also possible to find solutions in a form that readily generalizes to multilevel excitation.

We consider here excitation by a constant real-valued Rabi frequency and nonzero detuning. The constant two-state RWA Hamiltonian matrix is that of eqn. (109.) We proceed, as suggested in 19th century texts on ordinary differential equations with constant coefficients [68], by introducing eigenvectors of the coefficient matrix,

$$\mathsf{W}\Phi_\pm = \varepsilon_\pm \Phi_\pm. \tag{138}$$

The matrix W has, for the present discussion, dimension 2, and so there are two of these eigenvectors, labeled here with $\pm$. Because W is, apart from conversion to frequency units, the RWA Hamiltonian, the eigenvalues are often termed energy eigenvalues, and the eigenvectors are known as energy eigenstates. (They are also known as *dressed states* [74, 75]; the original basis states ψ_n are termed *bare states*).

The energy eigenvalues are readily found as

$$\varepsilon_\pm = \tfrac{1}{2}[\Delta \pm \widetilde{\Omega}], \quad \text{where } \widetilde{\Omega} = \sqrt{\Delta^2 + \Omega^2}. \tag{139}$$

To find expressions for the eigenvectors we introduce an angle Θ through the definition

$$\cot(2\Theta) = \Delta/\Omega \tag{140}$$

and rewrite the Hamiltonian, using trigonometric identities, as

$$\begin{aligned} \mathsf{W} &= \frac{\widetilde{\Omega}}{2}\begin{bmatrix} 0 & \sin(2\Theta)\,\mathrm{e}^{-\mathrm{i}\varphi} \\ \sin(2\Theta)\,\mathrm{e}^{\mathrm{i}\varphi} & 2\cos(2\Theta) \end{bmatrix} \\ &= \widetilde{\Omega}\begin{bmatrix} 0 & \sin\Theta\cos\Theta\,\mathrm{e}^{-\mathrm{i}\varphi} \\ \sin\Theta\cos\Theta\,\mathrm{e}^{\mathrm{i}\varphi} & \cos^2\Theta - \sin^2\Theta \end{bmatrix}. \end{aligned} \tag{141}$$

It then follows that the eigenvectors are [55]

$$\Phi_+ = \begin{bmatrix} \sin\Theta\,\mathrm{e}^{-\mathrm{i}\varphi} \\ \cos\Theta \end{bmatrix}, \qquad \Phi_- = \begin{bmatrix} \cos\Theta \\ -\sin\Theta\,\mathrm{e}^{\mathrm{i}\varphi} \end{bmatrix}. \tag{142}$$

To picture these with the Bloch sphere of Sec. 3.7.1 we write (using alternative overall phases)

$$\Phi_\pm = \sin(\theta_\pm/2)\psi_1 + \cos(\theta_\pm/2)\,\mathrm{e}^{\pm\mathrm{i}\varphi}\psi_2 \tag{143}$$

where

$$\cot(\theta_+) = \Delta/\Omega, \qquad \theta_- = \theta_+ - \pi. \tag{144}$$

The two points on the Bloch sphere representing these two eigenstates are opposite one another.

These are stationary states; they evolve in time with only a phase change. If the initial state coincides with one of these, say $\Psi(0) = \Phi_k$, then

$$\Psi(t) = \exp(-\mathrm{i}\varepsilon_k t)\Phi_k. \tag{145}$$

Usually, however, the initial statevector is a superposition of energy eigenstates. For example, when the system is known to be in state 1 at time $t = 0$ the superposition is

$$\Psi(0) = \psi_1 = \mathrm{e}^{\mathrm{i}\varphi}\sin\Theta\,\Phi_+ + \cos\Theta\,\Phi_-. \tag{146}$$

The energy eigenstates that contribute to this construction evolve in time with simple phases; the effect on $\Psi(t)$ is

$$\Psi(t) = \mathrm{e}^{\mathrm{i}\varphi}\sin\Theta\,\mathrm{e}^{-\mathrm{i}\varepsilon_+ t}\,\Phi_+ + \cos\Theta\,\mathrm{e}^{-\mathrm{i}\varepsilon_- t}\,\Phi_-. \tag{147}$$

This equation presents an exact analytic solution to the posed two-state Schrödinger equation with initial condition (146). Expressed in (rotating) bare states, through the use of eqn. (142), the construction reads

$$\begin{aligned} \Psi(t) \;=\; \mathrm{e}^{-\mathrm{i}\Delta t/2}\;\Big[&\Big(\cos(\widetilde{\Omega}t/2) + \mathrm{i}\cos(2\Theta)\;\sin(\widetilde{\Omega}t/2)\Big)\;\psi_1 \\ &- \mathrm{i}\;\sin(2\Theta)\sin(\widetilde{\Omega}t/2)\,\mathrm{e}^{\mathrm{i}\varphi}\psi_2'(t)\Big]. \end{aligned} \tag{148}$$

The individual bare-state populations evidently undergo oscillations. These Rabi oscillations, at frequency $\widetilde{\Omega}$, are here seen to be manifestations of interference between two energy eigenstates formed into a coherent time-dependent superposition, as required by the initial conditions: the initial state is not an eigenstate of the Hamiltonian, and so the statevector cannot remain aligned with it.

Although the population returns periodically to the ground state, the statevector acquires a new phase with each return, namely

$$\Psi(t) = \mathrm{e}^{-\mathrm{i}\Delta t/2}\,\psi_1. \tag{149}$$

[55] The overall phase of each of these is arbitrary and is here chosen for convenience.

6.5 Chirped frequency: Adiabatic passage

The production of specific changes in the statevector by resonant excitation requires careful control of the temporal pulse area. Furthermore, such excitation has limited use when the ensemble includes a range of detunings, such as occur with Doppler shifts. An alternative pulsed excitation procedure overcomes such limitations; it can produce equal excitation for a distribution of Doppler-induced detunings, independent of the temporal pulse area. Specifically, the excitation pulse includes not only a variation of the Rabi frequency but a monotonic sweep of the detuning.

The technique, *rapid adiabatic passage* (RAP) [3, 76], requires that statevector changes must be completed during a time interval that is shorter than any incoherence-producing processes, such as spontaneous emission – the overall action is rapid on that time scale – but that within that time interval the detuning should change slowly with time, i.e. adiabatically. The resulting The resulting motion of the statevector is an example of *adiabatic following* [77] in which the statevector follows a path in Hilbert space defined by an adiabatic state [2, §3.6], as discussed in Sec. 6.6 below.

The simplest idealization of RAP takes the detuning to vary linearly in time [56]. The RWA equation then reads, for real-valued Rabi frequency ($\varphi = 0$),

$$\frac{d}{dt}C_1(t) = -\frac{\mathrm{i}}{2}\Omega(t)\mathrm{e}^{-\mathrm{i}\varphi}\,C_2(t), \tag{150}$$

$$\frac{d}{dt}C_2(t) = -\frac{\mathrm{i}}{2}\Omega(t)\mathrm{e}^{\mathrm{i}\varphi}\,C_1(t) - \mathrm{i}(\Delta_0 + rt)C_2(t), \tag{151}$$

where r is the rate at which the detuning changes and Δ_0 is a fixed detuning, such as might occur from a single Doppler shift. Such a situation occurs if the laser frequency varies linearly with time, i.e. the frequency is *chirped* (basically sweeping from $-\infty$ to $+\infty$).

Solutions of these coupled equations obtained by direct numerical integration reveal that, if the chirp takes place over a sufficiently long time interval, all population will transfer from the initial state, say state 1, to the excited state, for any value of the static detuning. Indeed, the value of Δ_0 merely sets the time at which resonance occurs, $t = \Delta_0/r$. Figure 17 illustrates this behavior. Analytic results confirm this behavior; see Appendix E.3.

6.6 Explaining adiabatic passage: adiabatic states

When the atom is subjected to a swept detuning the behavior of the population histories, or the statevector underlying them, can best be understood with the aid of an alternative Hilbert-space coordinate system, one in which the needed unit vectors are chosen as instantaneous eigenvectors $\Phi_n(t)$ of the time varying Hamiltonian $\mathsf{W}(t)$,

$$\mathsf{W}(t)\Phi_n(t) = \varepsilon_n(t)\Phi_n(t). \tag{152}$$

These are *adiabatic* states [3, 78], contrasted with the *diabatic* states $\psi_n(t)$ that form the original basis states (in a rotating frame). We allow time variation of both the Rabi frequency (taken to

[56] Obviously this cannot continue indefinitely. The infinite limit is a mathematical artifice; it is only necessary that the initial detuning be much larger than the range of static detunings of the ensemble, and that the frequency sweep continue until the desired changes of the statevector are completed.

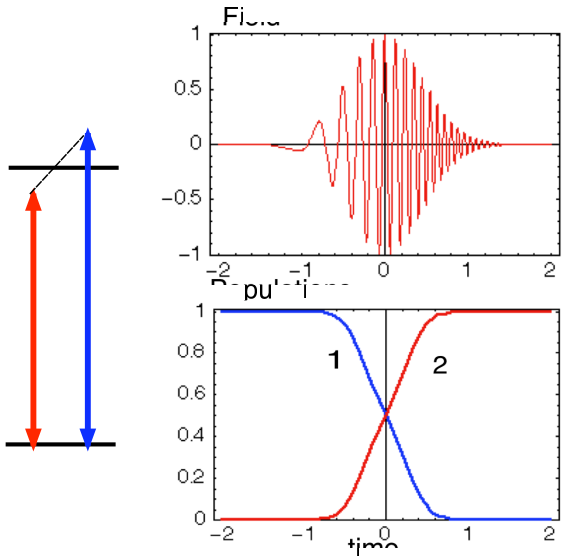

Fig. 17. Example of chirped rapid adiabatic passage. Above: the electric field. Below: the population histories. As the detuning sweeps through resonance, here at time $t = 0$, population transfer occurs from initial state 1 to final state 2.

be real-valued) and the detuning. The two-state RWA Hamiltonian of eqn. (109) becomes

$$\mathsf{W}(t) = \begin{bmatrix} 0 & \frac{1}{2}\Omega(t)\mathrm{e}^{-\mathrm{i}\varphi} \\ \frac{1}{2}\Omega(t)\mathrm{e}^{\mathrm{i}\varphi} & \Delta(t) \end{bmatrix}. \tag{153}$$

For the two-state system the two eigenvalues, *adiabatic eigenvalues* or *adiabatic energies*, are

$$\varepsilon_{\pm}(t) = \tfrac{1}{2}[\Delta(t) \pm \widetilde{\Omega}(t)], \qquad \text{where } \widetilde{\Omega}(t) = \sqrt{\Delta(t)^2 + \Omega(t)^2}. \tag{154}$$

The original diagonal elements of the RWA Hamiltonian, 0 and $\Delta(t)$ in the present example, are known as *diabatic* energies. The adiabatic states are as presented in eqn. (142) but now with time varying elements, resulting from a time dependent angle $\Theta(t)$.

When the statevector initially aligns with one adiabatic state, and the RWA Hamiltonian changes slowly, then the statevector remains aligned with this single adiabatic state; cf. Appendix K. The adiabatic state changes with time, and so the statevector construction changes when viewed with bare-state coordinates. The result is a transfer of population. Figure 18 illustrates the behavior.

The following paragraphs offer further discussion of adiabatic changes, with specific reference to chirped adiabatic passage of a two-state system. Appendix K.3 discusses the conditions needed to ensure the evolutio is adiabatic.

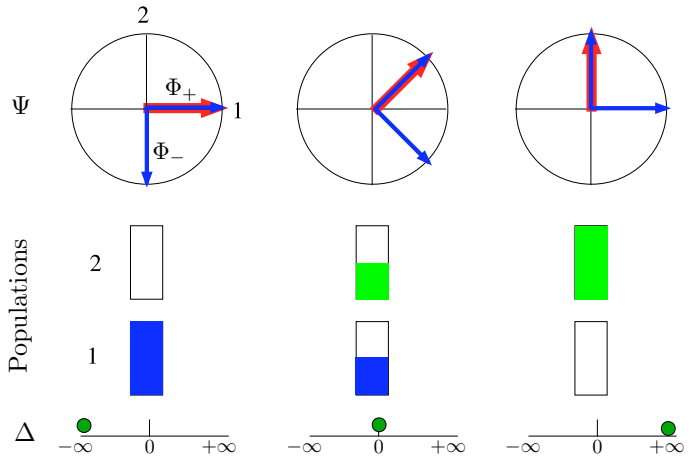

Fig. 18. Top frames show statevector Ψ and two adiabatic eigenvectors $\Psi_\pm$, bottom frames show histograms of population, for three values of the detuning Δ.

6.6.1 Asymptotic forms

The adiabatic states of eqns. (142) have the property that, for extremely large positive or negative values of the detuning $\Delta(t)$ they become aligned with the diabatic states $\psi'_n(t)$. When $\Delta \to -\infty$, then $\Theta \to 0$ and the adiabatic states become

$$\Phi_+(t) = \psi'_2(t), \qquad \Phi_-(t) = \psi_1. \tag{155}$$

When $\Delta \to +\infty$, then $\Theta \to \pi/2$, and the adiabatic states become

$$\Phi_+(t) = \mathrm{e}^{-\mathrm{i}\varphi}\psi_1, \qquad \Phi_-(t) = -\mathrm{e}^{\mathrm{i}\varphi}\psi'_2(t). \tag{156}$$

From these asyptotic forms we can deduce the effect of sweeping the detuning.

Suppose that initially $\Psi(t)$ is aligned with ψ_1 and that the detuning is large and negative. Then the state ψ_1 is, in turn, aligned with Φ_+. That adiabatic state will, when $\Delta \to +\infty$, be aligned with ψ_2. If the statevector remains always aligned with this adiabatic state then a transition from $1 \to 2$ will occur as the detuning sweeps from $-\infty$ to $+\infty$.

Alternatively, suppose the detuning is initially large and positive, but again $\Psi(t)$ is aligned with ψ_1. This state, for $\Delta \to +\infty$, is aligned with adiabatic state $\Psi_-(t)$. As the detuning sweeps from $+\infty$ to $-\infty$ this adiabatic state will become aligned with ψ_2. Again a transition occurs from $1 \to 2$, if the statevector remains aligned with an adiabatic state.

Thus it does not matter whether the detuning sweep is positive or negative; in all cases adiabatic evolution will produce the complete interchange of population (with a possible phase change)

$$\Psi(t) = \psi_1 \to -\mathrm{e}^{\mathrm{i}\varphi}\psi_2(t), \qquad \Psi(t) = \psi_2(t) \to \mathrm{e}^{-\mathrm{i}\varphi}\psi_1. \tag{157}$$

This is (chirped) rapid adiabatic passage. The process, though adiabatically slow, so that the statevector remains aligned wiht an adiabatic state, must nevertheless be completed before decoherence effects disrupt the coherent excitation; it must be rapid compared with any spontaneous emission lifetime of the excited state. Although the linear time dependence of the detuning provides a simple model, adiabatic passage occurs with any detuning variation that changes slowly from very large negative to very large positive or vice versa. It is not necessary that the change be linear or even monotonic with time.

The effects of swept detuning is easy to portray using adiabatic states. There remains a concern: under what conditions can the statevector maintain its alignment with an adiabatic state as the Hamiltonian varies. Appendix K.3 offers quantitative guidance. The following paragraphs present qualtitative considerations.

6.6.2 Energy curves: crossings and avoided crossings

The constraints on adiabatic passage are often presented by viewing plots of adiabatic energies along with plots of diabatic energies (the diagonal elements of the RWA Hamiltonian). For a two-state system these diabatic energies are 0 and $\Delta(t)$ or, alternatively, $\pm\frac{1}{2}\Delta(t)$. When there is a sweep of detuning, then the (bare) *diabatic* energy curves cross – this occurs at the time when $\Delta(t) = 0$. However, the (dressed) *adiabatic* curves do not share this instantaneous degeneracy: if there is any Rabi frequency present, however small, the adiabatic curves do not cross; they have an *avoided crossing*; see Appendix K.

Figure 19 illustrates the behavior of these curves, and the corresponding population histories during adiabatic evolution, for two examples of a two-state system subject to a pulsed Rabi frequency. The left-hand pair of frames illustrate the case when the detuning is constant. The diabatic energies remain constant horizontal lines, while the adiabatic energies exhibit reversible changes produced by the Rabi-frequency variation with time. With the choice of parameters here, there occurs complete population return (CPR); cf. Appendix E.5

The right-hand pair of frames show the effect on these curves of a chirped detuning. The diabatic curve for state 2 varies linearly with time, crossing that of state 1 at $t = 0$. For large values of $|t|$, far from $t = 0$, the Rabi frequency is negligible, and the adiabatic curves follow the diabatic curves 0 and $\Delta(t)$. However, as the Rabi frequency grows larger, the two sets of curves differ.

To interpret the population histories associated with such curves we begin by considering the system at early times – the left-hand side of the figures. Suppose the statevector is initially a single bare diabatic state, ψ_1. At these times there is no Rabi interaction, and so the diabatic and adiabatic states coincide. The initial statevector is therefore aligned with a single adiabatic state; it is represented by a system point on the coinciding diabatic and adiabatic curves.

As time increases and the energies change this system point moves across the figure, from left to right, expressing the changes of the energies with time. Its association with a *single* curve can continue only for two extreme idealizations, corresponding to either fast (diabatic) or slow (adiabatic) changes of the RWA Hamiltonian.

During *rapid* change the statevector will remain aligned with the original bare *diabatic* state, and the system point will therefore follow the (dashed) diabatic curve, always associated with the energy of bare diabatic state 1, a horizontal line in this figure. The system point moves steadily

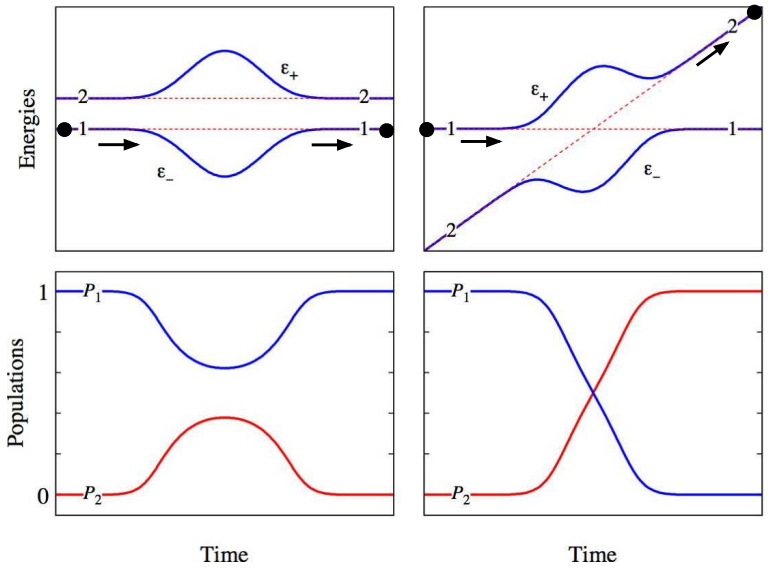

Fig. 19. Top frames: diabatic and adiabatic energies for two-state system. Bottom frames: population histories. Left: adiabatic evolution with constant detuning. Right: adiabatic evolution with chirped detuning. Large dots on the energy curves show those associated with initial and final states; arrows show the motion of these system points. [after Fig. 4 of Vitanov et al. Adv. Atomic Mol. Opt. Phys. bf 46 55 (2001)]

along this line, crossing the bare diabatic curve for state 2. At the end the system will still be in bare state 1; it follows a straight-line path on the energy vs. time plot, and no transition occurs.

By contrast, when the changes occur sufficiently slowly (*adiabatically*) the statevector will remain aligned with the *adiabatic* state. The system point will move along the (full) adiabatic curve that initially connects with state 1. During the time when the two sets of curves differ the system point will follow the dressed adiabatic curve, on a path that does not cross any other curve. Initially this path is horizontal, but at later times the path changes direction, eventually heading upward to join the diabatic curve for bare state 2 at large times; a transition will then have occurred.

The choice between the two paths depends on how rapidly the system point moves through the region where the interaction occurs, where the two sets of curves are not the same. If the point moves slowly then it follows the dressed adiabatic curve and a transition occurs. If it moves rapidly then it follows the bare diabatic curve; a curve-crossing occurs, but no transition. When the changes cannot be clearly classified as fast or slow, the population becomes divided between paths, and at the end the statevector is a coherent superposition of the two diabatic states.

However, if the chirp rate is *too* slow then the adiabatic and diabatic curves will run nearly parallel for a long time interval. It is then not possible to regard the system point as being associated with a single state, either diabatic or adiabatic, and the simple picture of an avoided crossing is not appropriate; see Appendix K.4.

A quantitative description of the relative probabilities for these two extreme possibilities

obtains from the Landau-Zener model [79] of a two-state system subject to linearly varying detuning $\Delta(t) = rt$ and constant Rabi frequency Ω; see Appendix E.3. When the population initially resides in state 1, the probability of finding the system in state 2 at the conclusion of the interaction is

$$P_2(\infty) = \exp(-\pi\Omega^2/|r|). \tag{158}$$

When $\Omega^2 \gg |r|$, as occurs for small chirp rate, the motion is adiabatic, and a transition occurs. When $\Omega^2 \ll |r|$, as occurs for rapid change, the motion is diabatic, and no transition occurs.

6.7 Stark-chirped rapid adiabatic passage (SCRAP)

To produce complete population transfer via adiabatic passage the detuning should sweep slowly through resonance. Because the detuning is the difference between the Bohr transition frequency of the atom and the laser carrier frequency, an alteration of either of these two frequencies will produce the desired result. The Bohr frequency, being proportional to the energy difference between two stationary states, can be altered by imposing any slowly varying *nonresonant* electric or magnetic field. Quasi-static electric fields, inducing Stark shifts of the energies, offer one possibility. Pulses of nonresonant laser light offer another means of subjecting the atom to a slowly varying electric field and there by producing a (dynamic) Stark shift [80] [2, §4.3]. (Section 9.3 discusses the origin of these shifts.)

Figure 20 shows a pulse sequence that will produce population transfer by RAP. It involves a Stark-shifting laser pulse (S) that sweeps the Bohr frequency through resonance with the fixed laser carrier while a transition-inducing laser (P) acts. This P pulse terminates before the S pulse ends. The resulting adiabatic passage is, in theory, identical with that produced by a chirped pulse; it has been called Stark-chirped rapid adiabatic passage (SCRAP) [81].

As in all adiabatic processes, the final result does not depend on details of the pulse envelope. It does not depend on the peak value of the Rabi frequency or the temporal pulse area nor on the details of the detuning variation with time; in this sense it is *robust*.

6.8 Comparison of excitation methods

Preceding sections have presented three classes of two-state excitation: incoherent, impulsive and adiabatic. Each is associated with different forms of radiation and produces different results; each has application to particular requirements. Figure 21 presents illustrative examples of these three mechanisms for producing excitation.

The first, appropriate for broadband incoherent light (not monochromatic laser light) draws on rate equations. These predict that, at most, half of the population can be transferred to the excited state, and that this saturation value is approached exponentially, at a rate that increases with increasing intensity. Althouth the transfer is incomplete, the result is not a coherent superposition; it is an incoherent mixture.

The second, resonant coherent excitation, can produce relatively rapid complete population transfer, but the pulse must be terminated with precision if exact inversion is desired. This constraint requires careful control of pulse amplitude and duration (i.e. of integrated Rabi frequency) as well as avoidance of Doppler-shifts of detunings. It can produce a coherent superposition of the two states.

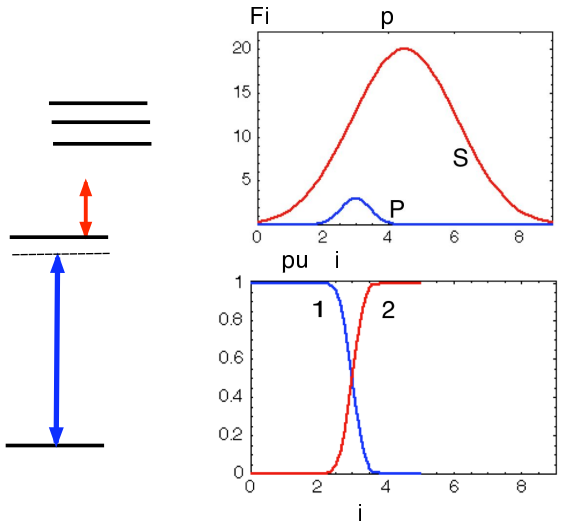

Fig. 20. Example of Stark-shifted rapid adiabatic passage. Left: a schematic diagram of energy levels, showing near resonant P field, responsible for transitions, and nonresonant S field, producing dynamic Stark shifts. Upper right frame: the S and P pulses, with P occurring during the rising portion of the S pulse. Lower right: the population histories, showing complete adiabatic transfer from state 1 to state 2.

The third option, adiabatic passage, requires a larger temporal pulse area than does resonant Rabi oscillation, but in the end it can produce a more robust result, insensitive to details of the pulse. It too can produce a coherent superposition.

6.9 Sequential pulses

The statevector resulting from a single pulse can provide the initial state for a second pulse; the effect of a sequence of pulses can be treated as a succession of statevector rotations. The cumulative effect is best presented with the aid of the time evolution matrix $\mathsf{U}(t)$, a solution to the Schrödinger equation that reduces to the unit matrix at the initial time, say $t = 0$. For a constant interaction the relevant defining equations are

$$\frac{d}{dt}\mathsf{U}(t) = -\mathrm{i}\mathsf{W}\mathsf{U}(t), \qquad \mathsf{U}(0) = 1. \tag{159}$$

We write the effect of a single constant interaction as

$$\mathbf{C}(t) = \mathsf{U}(t)\mathbf{C}(0). \tag{160}$$

Let a constant interaction, described by RWA Hamiltonian $\mathsf{W}^{(1)}$, persist for an interval T_1 after time t_1. Let this interval be followed by a succession of contiguous intervals T_m, during each of which the interaction is treated as constant. During the mth interval the RWA Hamiltonian is a

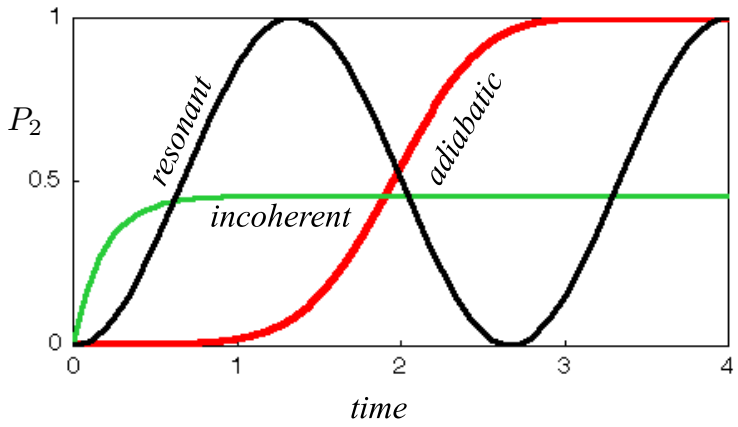

Fig. 21. Examples of excitation probability P_2 vs. time for incoherent excitation (with $A = 1$), adiabatic passage (with $\Omega = 1$) and resonant excitation (with $\Omega = 3\pi/4$).

constant matrix $\mathsf{W}^{(m)}$ and the time evolution operator is the associated matrix $\mathsf{U}^{(m)}(t)$. Figure 22 illustrates a succession of four such intervals.

The effect of these successive interactions upon the probability amplitudes is expressible as a succession of matrix multiplications that carry the statevector through a succession of generalized rotations. For the three intervals of Fig. 22 the result, at the end of the pulse sequence, has the form

$$\mathbf{C}(t) = \mathsf{U}^{(4)}(T_4)\mathsf{U}^{(3)}(T_3)\mathsf{U}^{(2)}(T_2)\mathsf{U}^{(1)}(T_1)\mathbf{C}(t_1), \quad t = t_1 + T_1 + T_2 + T_3 + T_4. \quad (161)$$

The intervals may be of arbitrary duration consistent with the requirement that the system remain unaffected by interruptions. In particular, by breaking the description of a general pulse into a succession of small contiguous increments, one can describe its effect by means of a succession of evolutions with constant interactions [57]. This construction, when automated, provides a very effective algorithm for evaluating numerically the effect of an arbitrary pulse. The intervals T_n need not be of uniform duration, although that constraint simplifies the construction of numerical procedures.

6.10 Pulse trains

The description of time evolution by means of independent interactions applies to any succession of pulses [82]. In particular, there can be time intervals between the interactions, i.e. the system is subjected to a train of pulses, separated by interaction-free intervals τ_n. Figure 23 illustrates an example of such a sequence, for three pulses.

Although there is no interaction during the pauses between pulses, it is essential to account for these intervals. Let t_0 be the reference time for expressing the sinusoidal time variation of the

[57] The motion of the tip of the statevector can be regarded as a *quantum walk*.

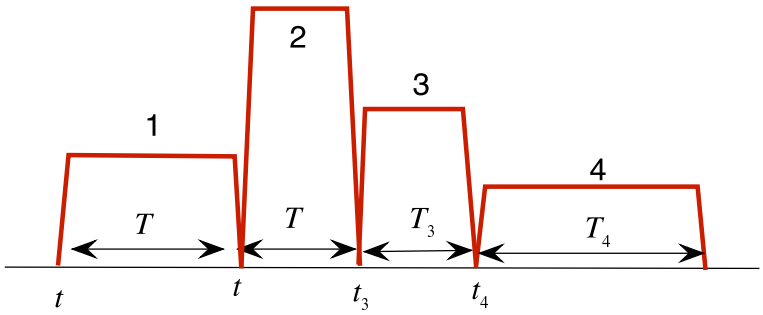

Fig. 22. A succession of four contiguous constant interactions. To clarify the extent of the separate pulses they are shown as turning on and off during small intervals.

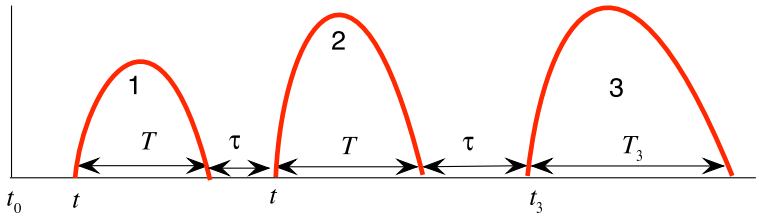

Fig. 23. A succession of three nonoverlapping pulses, of duration T_n and separated by intervals τ_n.

field as $\mathcal{E}(t)\cos(\omega t-\varphi)$. That is, the field phase is $\varphi=\omega t_0$. This reference time t_0 also serves to define a rotating coordinate system, earlier written as

$$\psi_1(t)=\psi_1,\qquad \psi_2(t)=\exp(-\mathrm{i}\omega t)\psi_2, \tag{162}$$

and to express the RWA interaction energy as $(\hbar/2)\mathcal{E}(t)\exp(i\varphi)$. In this reference frame the statevector has the construction

$$\Psi(t)=\Sigma_n C_n(t)\psi_n(t). \tag{163}$$

We now wish to consider a succession of independent interactions, each described by a slowly varying RWA Hamiltonian matrix $\mathsf{W}^{(m)}(t)$. Traditionally, and conveniently, one takes the start of a pulse as the reference time for the rotating Hilbert space coordinates during a pulse, rather than maintaining an ongoing reference system. This means that during the mth pulse we write the statevector as

$$\Psi(t)=\Sigma_n C'_n(t)\psi_n^{(m)}(t) \tag{164}$$

where the basis states

$$\psi_1^{(m)}(t)=\psi_1,\qquad \psi_2^{(m)}(t)=\exp[-\mathrm{i}\omega(t-t_m)]\psi_2, \tag{165}$$

provide the reference system appropriate to the interval that begins at time t_m. That is, at time $t = t_m$ the rotating coordinates $\psi_n^{(m)}(t)$ coincide with the static basis ψ_n. The probability amplitudes in the pulse-centric basis of eqn. (164) incorporate phases from the ongoing carrier frequency:

$$\mathbf{C}'(t) = \mathsf{T}(t)\mathbf{C}(t), \tag{166}$$

where

$$\mathsf{T}(\tau) = \begin{bmatrix} 1 & \exp(-\mathrm{i}\omega\tau) \\ \exp(+\mathrm{i}\omega\tau) & 1 \end{bmatrix}. \tag{167}$$

The RWA Hamiltonian $\mathsf{W}^{(m)}(t)$ must incorporate the rotation of the coordinates in defining the Rabi frequency. Typically this is taken to be a real-valued quantity at some reference time, say t_0. The ongoing rotation of the Hilbert-space coordinates then introduces phases that must be incorporated into the Hamiltonian at the start of each pulse.

During interactionless intervals the RWA Hamiltonian is a simple diagonal matrix W^0. When detuning is present this can introduce important phase factors in the probability amplitudes.

Given these properties of the successive time evolutions, we can write the time evolution as the product of pulse interactions, $\mathsf{U}^{(m)}(t)$, free evolution $\exp[-\mathrm{i}\mathsf{W}^0\tau_m]$ and revisions of the coordinate system phases, $\mathsf{T}(\tau)$. For the three pulses of Fig. 23 the construction is

$$\begin{array}{rcll} \mathbf{C}(t) & = & \exp[-\mathrm{i}\mathsf{W}^0(t-t_3)] & \textit{interval 3} \\ & \times & \mathsf{U}^{(3)}(T_3) & \textit{pulse 3} \\ & \times & \mathsf{T}(t_3-t_2) & \textit{update coordinates} \\ & \times & \exp[-\mathrm{i}\mathsf{W}^0\tau_2] & \textit{interval 2} \\ & \times & \mathsf{U}^{(2)}(T_2) & \textit{pulse 2} \\ & \times & \mathsf{T}(t_2-t_1) & \textit{update coordinates} \\ & \times & \exp[-\mathrm{i}\mathsf{W}^0\tau_1] & \textit{interval 1} \\ & \times & \mathsf{U}^{(1)}(T_1) & \textit{pulse 1} \\ & \times & \mathsf{T}(t_1-t_0)\mathbf{C}(t_0) & \textit{preliminary} \end{array} \tag{168}$$

The individual evolution matrices $\mathsf{U}^{(n)}(t)$ appearing here may be composites, constructed as in eqn. (161), or they may be analytic constructions appropriate to one of the many interactions for which there exist analytic solutions to the Schrödinger equation; cf. Appendix E.

An interesting application of pulse sequences occurs with two pulses, each of which produces a Bloch-vector rotation of $\pi/2$, i.e. a 50:50 superposition. The overall effect depends explicitly on the phase change during the pause (cf. Sec. 7.1.2). The resulting variation of excitation, between constructive and destructive interference is analogous to the bright and dark intensity fringes viewed in the traditional two-slit interference experiment.

The preceding discussion assumes that there is no external field present during the pauses between pulses. If, instead, there occurs a static energy-shifting field, perhaps differing from pulse to pulse, then this must be regarded as a detuning and treated as in eqn. (161).

Another interesting example occurs when the pulse train consists of contiguous identical pulses (i.e. the pauses are regarded as part of the pulse). Let the RWA Hamiltonian be written

$$\mathsf{W} = \tfrac{1}{2}\begin{bmatrix} -\Delta(t) & \Omega(t) \\ \Omega(t)^* & \Delta(t) \end{bmatrix}. \tag{169}$$

Let the effect of a single pulse be expressed by the unitary matrix

$$\mathsf{U}^{(1)} = \begin{bmatrix} (a_1 + \mathrm{i}b_1) & (c_1 + \mathrm{i}d_1) \\ -(c_1 - \mathrm{i}d_1) & (a_1 + \mathrm{i}b_1) \end{bmatrix}. \tag{170}$$

Then, as shown by Vitanov and Knight [82], the effect of N pulses is obtained from the matrix

$$\mathsf{U}^{(N)} = (\mathsf{U}^{(1)})^N = \begin{bmatrix} \cos(N\vartheta) + \mathrm{i}b_1 f_N(\vartheta) & (c_1 + \mathrm{i}d_1) f_N(\vartheta) \\ -(c_1 - \mathrm{i}d_1) f_N(\vartheta) & \cos(N\vartheta) - \mathrm{i}b_1 f_N(\vartheta), \end{bmatrix} \tag{171}$$

where

$$f_N(\vartheta) \equiv \frac{\sin(N\vartheta)}{\sin\vartheta}, \qquad \cos\vartheta = a_1, \qquad \sin\vartheta = \sqrt{1 - a_1^2}. \tag{172}$$

Thus if population is in state 1 prior to the arrival of the pulse train, the excited state population after N pulses is

$$P_2^{(N)} = P_2^{(1)} \frac{\sin^2(N\vartheta)}{\sin^2\vartheta}. \tag{173}$$

This is the quantum analog of the pattern of optical intensity fringes produced by a diffraction grating.

Trains of short pulses, each different and each producing only a small change (a "kick" in system space), have been suggested as a means of crafting specified Hilbert-space rotations [83].

7 The vector model

As noted in Sec. 3.7.1, a simple description of a two-state system presents the statevector as a point on a two-dimensional sphere, the Bloch sphere, parametrized by two angles. This description has several useful applications, and allows a useful generalization in which incoherent processes are treated. The resulting formalism, in which the system properties are represented by a vector in a three-dimensional abstract space, was first described by Feynman, Vernon and Hellwarth [58] [84] [2, §8.5]. The following paragraphs discuss the model, equivalent to the two-state RWA Schrödinger equation, with its simple means of depicting the dynamics of a two-state atom. Appendix H.4 discusses an N-state generalization.

7.1 The Bloch equations

The statevector for a two-state system involves two complex-valued probability amplitudes $C_n(t)$. With rotating coordinate 2 the construction is

$$\Psi(t) = C_1(t)\psi_1 + C_2(t)\psi_2'(t). \tag{174}$$

The two complex amplitudes are constrained by the requirement $\Sigma_n |C_n(t)|^2 = 1$. Furthermore, the overall phase is not of interest. Therefore, as discussed in Sec. 3.7.1, we need only two real-valued time-varying parameters to characterize the statevector.

The parametrization of the two-state RWA Hamiltonian of eqn. (153) requires a real-valued detuning and a real-valued Rabi frequency with phase φ (or a complex-valued Rabi frequency) [59]. Therefore this requires three real-valued functions for complete characterization. One may well ask, how best to choose the several real variables for this purpose.

A very satisfactory choice of variables for the two-state atom are the three real-valued quantities now known as *Bloch variables* [84], cf. Sec. 3.7.1[2, §8.1]. These are often denoted u, v, w. To emphasize their interpretation as components of a vector $\mathbf{r}$ in an abstract three-dimensional space I shall use the notation r_1, r_2, r_3 and the Bloch angles θ and ϕ of eqn. (45),

$$\begin{array}{llll} u(t) \equiv r_1(t) & = \text{Re } \tilde{\rho}_{12}(t) & = \text{Re } [C_2(t)^* C_1(t)] & = \cos\phi \, \sin\theta, \\ v(t) \equiv r_2(t) & = \text{Im } \tilde{\rho}_{12}(t) & = \text{Im } [C_2(t)^* C_1(t)] & = \sin\phi \, \sin\theta, \\ w(t) \equiv r_3(t) & = P_s(t) - P_1(t) & = |C_2(t)|^2 - |C_1(t)^2 & = \cos\theta. \end{array} \tag{175}$$

Here $\tilde{\rho}(t)$ is the density matrix, in rotating coordinates; cf. Appendix H.1. In the absence of probability loss this Bloch vector maintains unit length,

$$|\mathbf{r}(t)|^2 = r_1(t)^2 + r_2(t)^2 + r_3(t)^2 = 1, \tag{176}$$

and hence it maps the statevector onto a point on a unit sphere (the Bloch sphere). Figure 24(a) illustrates the Bloch vector. The $1, 2$ axes are set by the initial E field phase. It is customary, and convenient, to take this as zero, thereby fixing the relative orientation of the coordinate systems. From the Bloch vector we evaluate the populations as

$$P_2(t) = \tfrac{1}{2}\left[1 + r_3(t)\right], \qquad P_1(t) = \tfrac{1}{2}\left[1 - r_3(t)\right], \tag{177}$$

[58] The model results rather simply from the two-state density matrix, cf. Sec. H.1.

[59] Because the absolute phase of the field is uncontrollable, it is convenient to set this to zero at the start of a pulse. But subsequent manipulation of the laser field may require a later nonzero value.

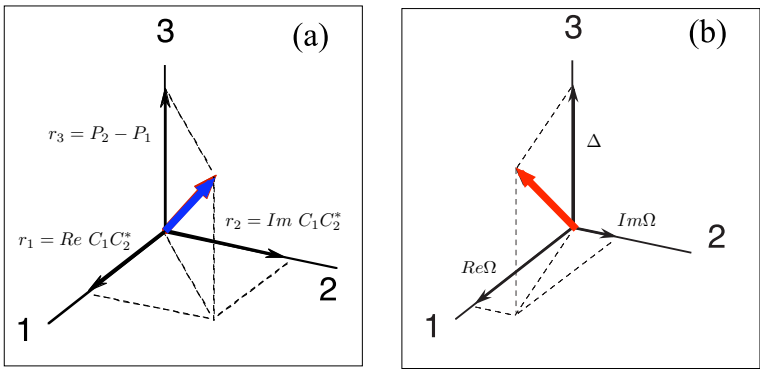

Fig. 24. (a) The Bloch vector. The $1, 2$ axes are set by the initial phase. (b) The angular velocity vector. The projection into the $1, 2$ plane is determined by the field phase φ.

and the dipole moment as

$$\begin{aligned} \langle d(t) \rangle &= 2\,\mathrm{Re}\,\left[d_{12} C_1(t)^* C_2(t) \exp(-\mathrm{i}\omega t) \right] && (178) \\ &= |d_{12}|\,\left[r_1(t)\cos(\omega t) - r_2(t)\sin(\omega t) \right]. && (179) \end{aligned}$$

When the RWA applies, as here assumed, variables $C_n(t)$ and $r_j(t)$ vary more slowly than the carrier frequency ω. Bloch-vector component $r_1(t)$ is *in phase* with the electric field of the laser, while component $r_2(t)$ is *in quadrature* with this field.

The two-state RWA Hamiltonian can be similarly parametrized by the real-valued coordinates of a vector $\widetilde{\Omega}$ in a three-dimensional abstract space,

$$\begin{array}{lll} \widetilde{\Omega}_1(t) & = Re[\hat{\Omega}(t)] & = \Omega\cos\varphi, \\ \widetilde{\Omega}_2(t) & = -Im[\hat{\Omega}(t)] & = -\Omega\sin\varphi, \\ \widetilde{\Omega}_3(t) & = \Delta & = \omega_0 - \omega. \end{array} \qquad (180)$$

The length of this vector is the root-mean-square of the Rabi frequency (i.e. the interaction energy) and the detuning. The polar angle of the vector is defined by the relationship

$$\cot\theta = \Delta/\Omega. \qquad (181)$$

Figure 24(b) shows this vector.

Using the TDSE it is straightforward to find equations of motion for the three Bloch variables:

$$\frac{d}{dt}\begin{bmatrix} r_1 \\ r_2 \\ r_3 \end{bmatrix} = \begin{bmatrix} 0 & -\Delta & \Omega\sin(\varphi) \\ \Delta & 0 & \Omega\cos(\varphi) \\ -\Omega\sin(\varphi) & -\Omega\cos(\varphi) & 0 \end{bmatrix} \begin{bmatrix} r_1 \\ r_2 \\ r_3 \end{bmatrix}. \qquad (182)$$

These are the RWA *Bloch equations*, in a Hilbert-space reference frame rotating with angular velocity ω [2, §8.4].

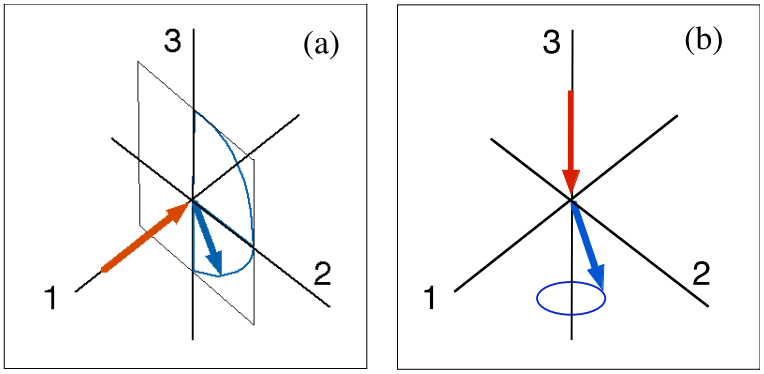

Fig. 25. Two-state vector model, showing the action of an angular velocity vector on the Bloch vector. (a) Resonant excitation ($\Delta = 0$) the angular velocity vector lies along the 1 axis. The Bloch vector follows a circular path in the $2, 3$ plane. (b) The angular velocity vector lies along the 3 axis, and moves the Bloch vector in a cone about this axis.

A useful presentation of these equations occurs when we describe the RWA Hamiltonian by means of the vector $\widetilde{\Omega}$. Then the equation of motion for the Bloch vector **r**, eqn. (182), appears as a torque equation,

$$\frac{d}{dt}\,\mathbf{r}(t) = \widetilde{\Omega}(t) \times \mathbf{r}(t), \tag{183}$$

in which the elements of the RWA Hamiltonian appear organized into an *angular velocity* vector $\widetilde{\Omega}$ (often termed the *torque vector*). The Bloch vector rotates, at the instantaneous rate

$$|\widetilde{\Omega}| = \sqrt{\Delta^2 + |\Omega|^2}, \tag{184}$$

about an axis defined by the components of the angular velocity vector. Figure 24(b) illustrates the angular velocity vector, parametrizing the RWA Hamiltonian. The projections onto the $1, 2$ axes are set by the E field phase φ.

By regarding the action of the angular velocity vector as producing a torque that turns the Bloch vector it is straightforward to visualize the dynamics resulting from a simple pulse, as Fig. 25 illustrates. Frame (a) shows the Bloch vector motion for resonant excitation. Frame (b)shows the Bloch vector motion for excitation with constant detuning.

7.1.1 Examples: Steady field

Although the torque equation for the Bloch vector holds for any pulsed excitation (within the RWA), it is most useful when applied to situations when the RWA Hamiltonian has constant elements. We here consider some examples.

When the excitation is resonant, and the initial state is that of population entirely in state 1, the tip of the Bloch vector moves along a great-circle path, in the plane normal to the angular velocity vector. The projections of this motion onto the 3 axis are the Rabi oscillations of population inversion. Figure 26 illustrates this behavior.

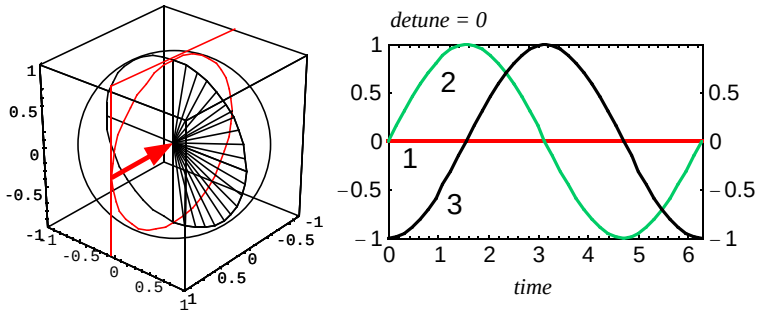

Fig. 26. Left: depiction of rotating Bloch vector for resonant excitation. Right: plots of the time dependence of the three components of the Bloch vector

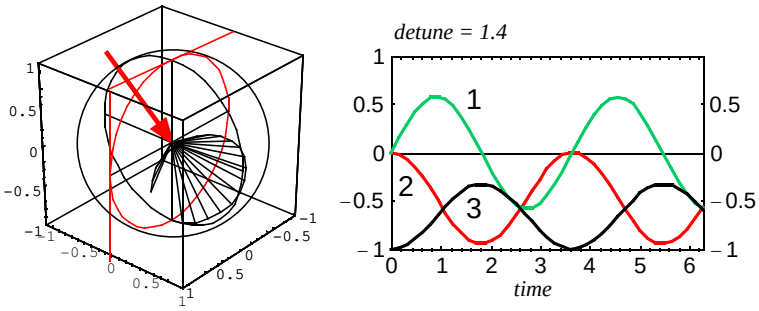

Fig. 27. As in the previous figure 26, but with detuning.

When the excitation is nonresonant the angular velocity vector lies out of the equitorial plane of the Bloch sphere. It produces motion of the Bloch vector on a conical surface, as shown in Fig. 27.

7.1.2 Examples: Sequential pulses

The Bloch vector and the torque equation of motion for it provide a very simple interpretation of sequential-pulse excitation effects [82]. One of these occurs when a first pulse, of constant Rabi frequency, ceases for some time interval before resuming. During the illumination halt there occurs no change of the Bloch vector, but there does occur an ongoing accumulation of phase, originating with the rotating coordinate system; cf. Sec. 6.10. This affects the orientation of the angular velocity vector when it next acts.

Figure 28 illustrates this scenario: a pulse of constant amplitude acts for a definite time interval, and then ceases. What do we expect the plots will be when the excitation resumes?

To analyze the effect of successive pulses we write the initial pulsed field as

$$\mathbf{E}^{(1)}(t) = \mathrm{Re}\,\left[\hat{\mathbf{e}}\mathcal{E}(t-t_1)\mathrm{e}^{-\mathrm{i}\omega(t-t_1)+\mathrm{i}\varphi_1}\right], \tag{185}$$

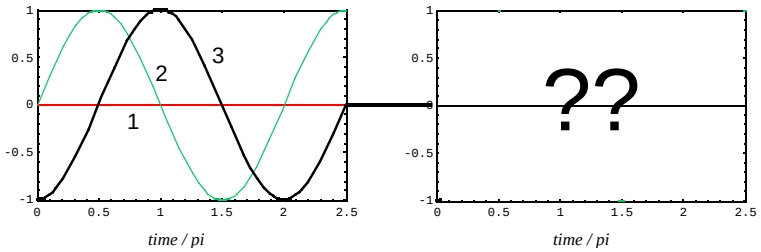

Fig. 28. Left frame: plot of time dependence of the three components of the Bloch vector, as produced by a resonant pulse of constant amplitude. Following the termination of this pulse there is a pause, and then the pulse resumes. The effect of the second pulse, indicated here with question marks, depends upon the phase change $\Delta\varphi$.

with t_1 as the time when the pulse envelope starts. That is, the envelope function appearing in the Bloch equation is a function of the time interval $\tau = t - t_1$ measured from the pulse start; it vanishes for $t - t_1 < 0$. The rotating Hilbert-space coordinate associated with this field is

$$\psi_2'(t) = \mathrm{e}^{-\mathrm{i}\omega(t-t_1)}\ \psi_2. \tag{186}$$

The second pulse begins at a later time t_2, and we write the resulting field as

$$\mathbf{E}^{(2)}(t) = \mathrm{Re}\ \left[\hat{\mathbf{e}}\mathcal{E}(t-t_2)\mathrm{e}^{-\mathrm{i}\omega(t-t_2)+\mathrm{i}\varphi_2}\right]. \tag{187}$$

To place these two expressions on a common time scale, one associated with the rotating coordinate of eqn. (186), we rewrite eqn. (187) as

$$\mathbf{E}^{(2)}(t) = \mathrm{Re}\ \left[\hat{\mathbf{e}}\mathcal{E}(t-t_2)e^{+\mathrm{i}\Delta\varphi}\ \mathrm{e}^{-\mathrm{i}\omega(t-t_1)+\mathrm{i}\varphi_1}\right]. \tag{188}$$

The phase increment appearing here,

$$\Delta\varphi = \omega(t_2 - t_1) - \varphi_1 + \varphi_2, \tag{189}$$

acts as a modifier of the field envelope $\mathcal{E}(t)$. We see that, in addition to any specific phase change $\varphi_1 - \varphi_2$ between pulses there occurs an inevitable change $\omega(t_2 - t_1)$ associated with the translation of the time scale used for the rotating coordinate system. This dynamic phase is directly proportional to the steady carrier frequency ω and to the time interval $t_2 - t_1$ between the pulses

Thus the effect of a second pulse depends on the phase of the field envelope, as parametrized here by the phase shift $\Delta\varphi$. Figure 29 shows two examples. In the first (top row) there occurs no pause between pulses, $\Delta\varphi = 0$. In the lower row, a phase delay of $\Delta\varphi = 0.3\pi$ occurs. As can be seen, the result is a much smaller modulation of the population oscillations: little excitation occurs. Instead, Bloch-vector component r_1 begins to oscillate.

Figure 30 shows two more examples of possible phase increments. In the first case (top row), for phase increment 0.55π, there is little excitation produced by the second pulse. As the phase increment changes, to π, we see that the effect of the delay interval has been to reverse the excitation process – essentially to reverse time.

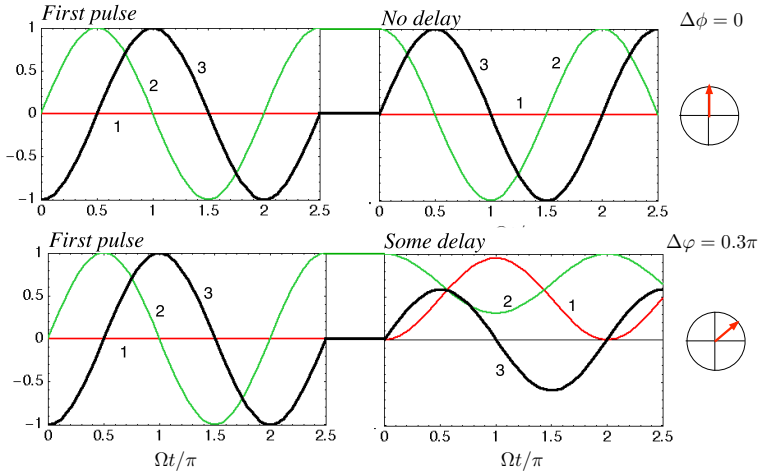

Fig. 29. Two possible continuations of the excitation; here there pause introduces a phase change $\Delta\varphi = 0$ (top row) or 0.3π (lower row). To the right are clock faces indicating the phase change during the pulse-free interval.

An interesting situation occurs when the phase increment is exactly $\pi/2$. Then the second pulse has no effect upon the Bloch vector: none of the components change, even though a pulsed field is present. Figure 31 illustrates this behavior.

This can be understood by considering the combination of Bloch vector and angular velocity vector. For the present example, the effect of the first pulse appears as the Bloch vector rotation from the south pole to the equator, as shown in Fig. 32 (a).

With the phase change $\pi/2$ the second angular velocity vector acts along the 2 direction. This is the direction of the Bloch vector, as seen in Fig. 32 (b). That is, the angular velocity vector and the Bloch vector are parallel. Therefore this pulse produces no visible effect

In summary, the effect of the pause prior to resumption of the pulse, is as follows:

- The envelope phase shift $\Delta\varphi$ shifts the phase of the complex-valued Rabi frequency, and hence the orientation of the angular velocity vector [60]
$$\widetilde{\Omega} = [\Omega\cos\varphi, \quad \Omega\sin\varphi, \quad \Delta]^T.$$
- Subsequent population change may be zero. If the angular velocity vector aligns with Bloch vector (this occurs if $\Delta\varphi = \pi/2$ when resonant, $\Delta = 0$).
- A phase change $\Delta\varphi = \pi$ is equivalent to time reversal.

Such effects occur only if the laser field remains coherently phased. When the delay interval is longer than the coherence time, then the phase becomes random. The resulting effect on the atom can only be evaluated statistically: the Bloch vector components are averages of those for a distribution of phase changes. Rabi oscillations will not then be seen at long times.

[60] Here the superscript T denotes matrix transpose, i.e. replacing rows by columns.

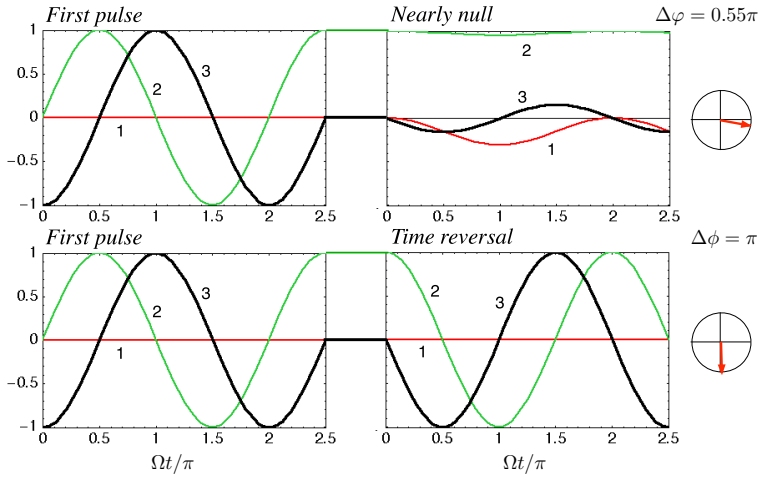

Fig. 30. Other possible continuations of the excitation; here the pause introduces a phase change $\Delta\varphi = 0.55\pi$ (top row) or π (lower row).

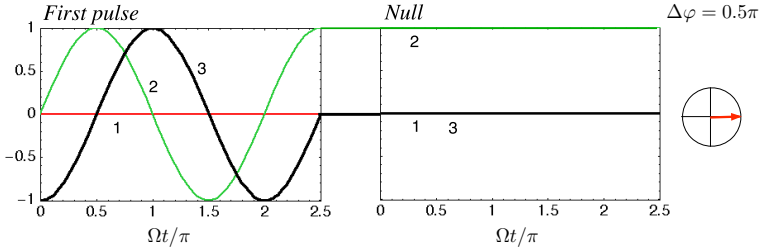

Fig. 31. Effect of second pulse when phase delay is $\Delta\varphi = 0.5\pi$. The second pulse has no effect.

7.2 Including relaxation

The presence of spontaneous emission between states 2 and 1 causes a loss of coherence as well as a transfer of population. Other processes, such as collisions, also produce this coherence loss. To account for such effects the needed revision of the Bloch equations are often written (here the Rabi frequency is taken to be real valued, $\varphi = 0$)

$$\frac{d}{dt}r_1 = -\Delta\, r_2 - \frac{1}{T_2}r_1,$$

$$\frac{d}{dt}r_2 = +\Delta\, r_1 - \Omega\, r_3 - \frac{1}{T_2}r_2, \tag{190}$$

$$\frac{d}{dt}r_3 = \Omega\, r_2 - \frac{1}{T_1}(r_3 + 1). \tag{191}$$

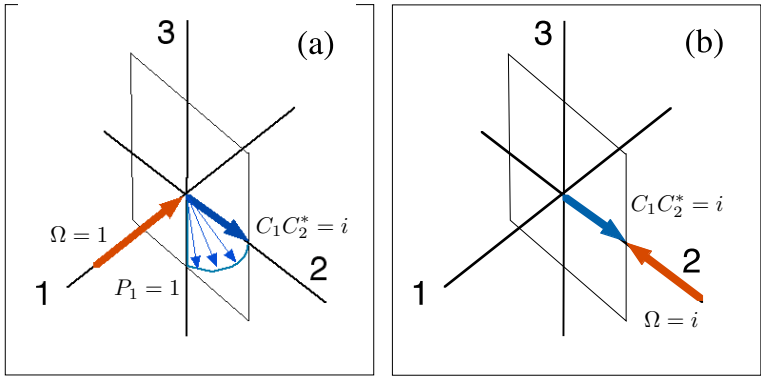

Fig. 32. (a) The Bloch vector rotation produce by the first pulse, of Rabi angle $\pi/2$. (b) The rephased pulse has no effect

Here the incoherent processes are parametrized by two times, traditionally denoted T_1 and T_2. The *longitudinal* relaxation time T_1 expresses population-changing events: spontaneous emission and inelastic (energy-changing) collisions; it is the average time required for the atom to change states (e.g. decay from the excited state to the ground state or collisional excitation). The *transverse* relaxation time T_2 expresses events that alter phases; it is the average time required for spontaneous emission or elastic collisions to alter phases.

The effect of T_2 is to pull the Bloch vector toward the vertical axis, towards $r_1 = r_2 = 0$. The effect of T_1 is to pull the Bloch vector toward the south pole of the Bloch sphere, towards $r_3 = -1$. In the absence of coherent excitation, $\Omega = 0$, this point is the ultimate resting point of the Bloch vector – all population resides in the ground state.

These equations model a closed system: there is no radiative decay from state 2 except to state 1. When spontaneous emission is the only relaxation process the two relaxation times have the connection $T_2 = 2T_1 = 2/A_{21}$. More generally there exists the constraint

$$T_2 \leq 2T_1. \tag{192}$$

7.3 Steady-state excitation

When the illumination of the atom is steady then spontaneous emission provides a balance to the excitation, as recognized by Einstein, and the various elements of the Bloch vector reach a steady state. More generally, when the relaxation time T_2 is short the variables r_1 and r_2 equilibrate with the instantaneous value of the inversion. By setting the time derivatives [61] to zero, $\dot{r}_1 = \dot{r}_2 = 0$, we obtain expressions appropriate to adiabatic elimination,

$$\bar{r}_1 = -(\Delta T_2)\bar{r}_2, \qquad \bar{r}_2 = -\frac{(\Omega T_2)}{1 + (\Delta)^2 T_2} r_3. \tag{193}$$

[61] The overhead dot on a function of time, used for typographical simplification, denotes the time derivative.

The inversion then obeys the rate equation

$$\frac{d}{dt}r_3 = -\frac{1}{T_1}\left[\frac{1+(\Delta T_2)^2+(\Omega T_1)(\Omega T_2)}{1+(\Delta T_2)^2}r_3+1\right]. \tag{194}$$

This has the structure of eqn. (72); it can be directly integrated, allowing for time-dependent rates, to produce an expression of the form of eqn. (74). When the rate is constant the equilibrium solution to this equation, obtained by setting $\dot{r}_3 = 0$, is

$$\bar{r}_3 = -\frac{1+(\Delta T_2)^2}{1+(\Delta T_2)^2+(\Omega T_1)(\Omega T_2)}. \tag{195}$$

When the Rabi frequency is small, $|\Omega T_1| \ll 1$, the equilibrium inversion approaches the value $\bar{r}_3 = -1$ descriptive of an unexcited atom. When the Rabi frequency is large, $|\Omega T_1| \gg 1$, the equilibrium inversion vanishes, $\bar{r}_3 = 0$, meaning the two populations are equal. It is not possible to obtain positive equilibrium inversion; the equilibrium populations must satisfy the inequality $\bar{P}_2 < \bar{P}_1$.

When spontaneous emission, at rate A, provides the only incoherent process the relaxation times are $T_2 = 2/A$ and $T_1 = 1/A$. Then the equilibrium solutions are

$$\bar{r}_1 = -(2\Delta/A)\bar{r}_2, \qquad \bar{r}_2 = -\frac{(\Omega A/2)}{(A/2)^2+(\Delta)^2}\bar{r}_3, \tag{196}$$

$$\bar{r}_3 = -\frac{(A/2)^2+(\Delta)^2}{(A/2)^2+(\Delta)^2+(1/2)(\Omega)^2}. \tag{197}$$

Under these conditions the steady-state excited-state population is

$$\bar{P}_2 = \frac{(\Omega/2)^2}{(\Delta)^2+(A/2)^2+(1/2)(\Omega)^2}. \tag{198}$$

That is, the excitation is greatest, as one expects, for resonance, $\Delta = 0$, where it can be no larger than $\bar{P}_2 = 0.5$. The dependence of this equilibrium population on detuning Δ, the *excitation spectrum*, is a *Lorentz profile* whose full width at half maximum (FWHM) is

$$\Delta_{1/2} = \tfrac{1}{2}\sqrt{A^2+2\Omega^2}. \tag{199}$$

In the absence of the laser radiation this is the *natural line width* $\Delta_{1/2} = A/2$. But as the excitation becomes stronger, as parametrized by the radiation power, the width increases; it exhibits *power broadening*. In the limit of strong excitation the width is directly proportional to the Rabi frequency, i.e. to the square root of the intensity.

The occurrence of power broadening depends upon the conditions of excitation, here taken to be steady illumination with damping. When the excitation is pulsed, and observations take place after the pulse, then power broadening does not occur [85].

This steady-state model provides a description of excitation that is useful for understanding the frequency variation of excited-state photoionization – the *excitation spectrum*. By contrast, the fluorescence radiation has its own distribution of frequencies. A spectroscopist, collecting the fluorescence, passes this radiation through a spectrometer to determine the traditional *fluorescence spectrum*. The totality of this radiation, into all solid angles and integrated over all

frequencies, is proportional to the product of the emission rate A and the excited state population, a quantity available from the Bloch equation. However, the simple Bloch-vector model presented here does not give a description of the fluorescence spectrum. When the laser field becomes sufficiently strong that Rabi oscillations dominate the atom dynamics – coherent excitation – the periodic variation of the dipole moment creates sidebands to the fluorescent signal. These are offset from the carrier frequency and are separated by the Rabi frequency. The spectrum appears as a *Mollow triplet* [86] [2, §11.6]. The treatment of such observations requires a more elaborate treatment than the simple average excitation probability.

8 Degeneracy

The discrete energies E_n of bound states are not the only symptoms of quantum-mechanical properties and quantization. Rotational motion of particles, associated with angular momentum, is also quantized; only discrete orientations differing by $\hbar$ are allowed with respect to any selected (but arbitrary) axis of quantization [2, §18.1].

For angular momentum characterized by the quantum number J there exist $2J + 1$ distinguishable orientations. Because rotations imply electrical currents, and consequent magnetic moments, different orientations correspond to different interactions with electric and magnetic fields – either fields imposed externally or fields that originate with electronic motion. These interactions alter the energy of the particle, in discrete increments associated with the discrete orientations.

The overall angular momentum of an atom or molecule has discrete orientation energies in an external field. These are the Zeeman energy shifts associated with static magnetic fields [87] and Stark shifts produced by static electric fields [88]. In the absence of such external fields the energy of a confined quantum-mechanical particle is unaffected by orientation; all $2J + 1$ orientations have the same energy, and the associated quantum states are degenerate. It is common practice, based upon terminology from atomic spectroscopy, to refer to a set of degenerate quantum states as an *energy level*. The individual constituents, distinguishable by orientation, are magnetic or Zeeman *sublevels*.

An important class of magnetic-moment interactions are those arising from nuclear spin. The possible orientations of nuclear spin relative to electronic structure produces hyperfine splitting [89], cf. Appendix G. Within a molecule the nuclear orientation energy is observed as a chemical shift that motivates the practical use of nuclear magnetic resonance [90].

As with the quantized energies, it is possible to place the discrete set of quantum states into a catalog, a list labeled by integers. Often it is convenient to use several quantum-number labels for each individual state. These may identify the energy, the total angular momentum (J) and the projection (M) of that angular momentum upon some (arbitrary) reference axis, traditionally chosen as the Cartesian z axis . However, for present purposes it is more convenient to use single indices, and to express the condition of degeneracy as $E_i = E_j$.

When degeneracy occurs, polarization provides a means of more specifically controlling the laser-induced excitation. Because the states of free atoms can be taken as states with well defined angular momentum, simple selection rules on the magnetic quantum number M are associated with particular polarizations.

8.1 Radiation polarization and selection rules

Laser-induced transitions originate, in the dipole approximation, with transition dipole-moments within the atom. These can either emit or absorb electric dipole radiation. Typically one regards the free atom as existing in an angular momentum state defined by the pair of quantum numbers J, M. The formula for evaluating the dipole-transition moment between angular momentum states is given by the Wigner-Eckert theorem, discussed in treatises on angular momentum [91] [2, §20.5] :

$$\langle J'M'|\hat{\mathbf{e}}_q{\cdot}\mathbf{r}|JM\rangle = (-1)^{J'-M'} \begin{pmatrix} J' & 1 & J \\ -M' & q & M \end{pmatrix} ea_0\sqrt{S(J,J')}, \tag{200}$$

where $(:::)$ is a three-j symbol (cf. Appendix C.3), $S(J, J')$ is the dimensionless transition strength of eqn. (400) and $ea_0 = 2.542$ debye is the atomic unit of dipole moment [2, §2.9]. The unit vectors $\hat{\mathbf{e}}_q$, for $q = -1, 0, +1$, used to define the directions of a three-dimensional vector in a spherical basis, have the following relationship to the three unit vectors $\hat{\mathbf{e}}_x$, $\hat{\mathbf{e}}_y$, and $\hat{\mathbf{e}}_z$ of Cartesian coordinates:

$$\hat{\mathbf{e}}_{\pm 1} = \mp \frac{1}{\sqrt{2}} [\hat{\mathbf{e}}_x \pm \mathrm{i}\hat{\mathbf{e}}_y], \qquad \hat{\mathbf{e}}_0 = \hat{\mathbf{e}}_z. \tag{201}$$

The six arguments of the three-j symbol incorporate basic selection rules for dipole radiation (electric or magetic) [67]. First, the two atomic angular momentum quantum numbers J and J' must form a triangle with unity as the third side. This constraint is because the dipole field has unit angular momentum, and this must equal the change in atomic angular momentum [62]. Thus it is not possible to have a radiative transition, via single photon, between two states that each have angular momentum $J = 0$. Nor is it possible to have a transition, via dipole radiation, in which $|J - J'| > 1$. Such transitions occur with quadrupole or higher multipole radiation.

The nonzero linkages amongst sublevels are restricted by the requirement

$$M - M' + q = 0. \tag{202}$$

Thus the magnetic quantum numbers M and M' can similarly differ by no more than 1; the choice $q = 0$ requires $M = M'$. This constraint expressed the fact that the projection of angular momentum onto the propagation axis (the helicity q) cannot exceed unity. When the two angular momenta are the same, $J = J'$, an additional restriction occurs: no transitions occur from $M = 0$ or $M' = 0$ without a change in magnetic quantum number, i.e. there is no interaction link $M = 0 \leftrightarrow M' = 0$.

These geometrically based selection rules are

$$|J - J'| = 0, \pm 1, \qquad \text{but not } J = 0 \leftrightarrow J' = 0 \tag{203}$$

$$|M - M'| = 0, \pm 1, \qquad \text{but not } M = 0 \leftrightarrow M' = 0 \text{ when } J = J' \tag{204}$$

A further selection rule applies to transitions between states of free atoms, though not to transitions in atoms held within a crystalline environment: the electric dipole transition moment is nonzero only between states of opposite parity. This attribute refers to symmetry under coordinate inversion: odd-parity states change sign whereas even parity states remain unchanged.

8.1.1 Emission: Angular momentum fields

The radiation spontaneously emitted during a transition between atomic states of well defined angular momentum quantum numbers J, M carries also angular momentum; the relevant fields are the angular momentum fields of Appendix A.3 [2, § 19.4]. There are three basic angular momentum multipole fields that can be created, conventionally denoted σ_+, σ_- and π, each identified with as specific change of magnetic quantum number, ΔM. The association is

$$\Delta M = 0 \quad \text{for } \pi, \tag{205}$$

$$\Delta M = +1 \quad \text{for } \sigma_+, \tag{206}$$

$$\Delta M = -1 \quad \text{for } \sigma_-. \tag{207}$$

[62] The electromagnetic field, being a vector field in three-dimensional Euclidean space, has intrinsic angular momentum (i.e. spin) of one. Particular fields may also carry orbital angular momentum about a reference axis.

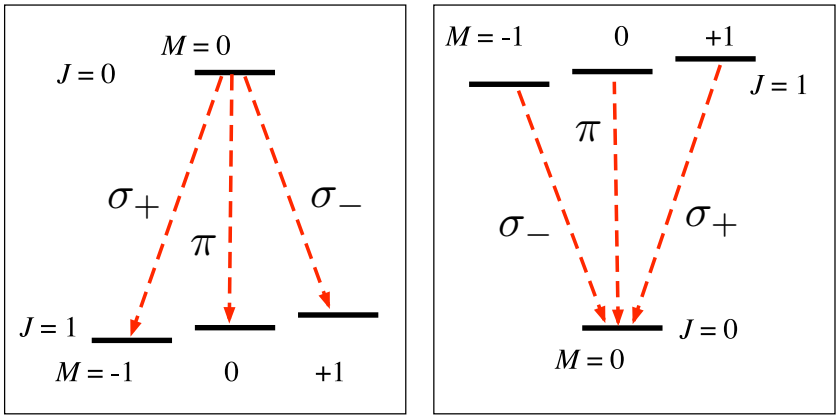

Fig. 33. Transitions between magnetic sublevels create one of three electric dipole fields, denoted σ_+, σ_- and π

Figure 33 shows examples of the transitions that produce these emission fields.

The three basic dipole fields produced by these transitions are shown in Fig. 34. The π field vectors remain fixed in direction, although oscillating in length. The $\sigma_\pm$ fields have vectors that rotate about the z axis, with frequency ω.

8.1.2 Absorption: Linear momentum fields

To excite an atom with laser radiation it is necessary to associate these emission fields, which are multipole fields characterised by unit angular momentum, with laser fields, which are characterized by *linear momentum*, cf. Appendix A.3. The laser fields typically are idealized as plane waves, meaning spatial and temporal properties governed by the phase function of eqn. (15).

A general polarization vector can be written, using Cartesian coordinates, as

$$\hat{\mathbf{e}} = \epsilon_z \hat{\mathbf{e}}_z + \epsilon_x \hat{\mathbf{e}}_x + \epsilon_y \hat{\mathbf{e}}_y. \tag{208}$$

Because the electric and magnetic fields of radiation must be transverse to the propagation direction it proves useful to identify these unit vectors in a coordinate system aligned with the propagation direction. For radiation propagating along the z axis (the quantization axis) we use orthogonal complex spherical unit vectors (helicity states of the field), as given by eqn. (201) and instead of eqn (208) we have the corresponding expansion

$$\hat{\mathbf{e}} = \epsilon_0 \hat{\mathbf{e}}_0 + \epsilon_+ \hat{\mathbf{e}}_+ + \epsilon_- \hat{\mathbf{e}}_-. \tag{209}$$

Figure 35 sketches the three polarization choices available with this basis.

The appearance of the three components of the polarization vector $\hat{\mathbf{e}}$ depend explictly upon the choice of coordinate orientation, e.g. whether the z axis lies along the propagation direction or along the direction of linear polarization. The choice of orientation is best described by the three Euler angles α, β and γ [91],

$$\hat{\mathbf{e}}_{q'} = \exp(i\gamma q')\Sigma_{q=-1,0,+1}\hat{\mathbf{e}}_q \exp(-\mathrm{i}\gamma q) d^{(1)}_{q,q'}(\beta). \tag{210}$$

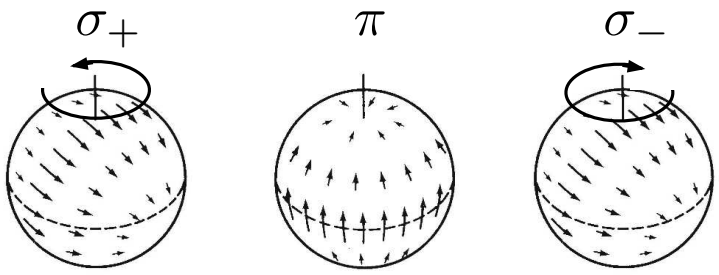

Fig. 34. Basic electric-dipole fields with definite angular momentum Left: the σ_+ field appears along the polar axis as circularly polarized, while when viewed in the equatorial plane it is horizontally linearly polarized; center: the π field vanishes in polar directions, and is vertically polarized in the equatorial plane; right: the σ_+ field is similar to the σ_+ field but has opposite sense of polarization rotation. [after Fig. 2.7 of B. W. Shore and D. H. Menzel, *Principles of Atomic Spectra* (Wiley, N.Y., 1968)]

Here $d^{(1)}_{M,M'}(\beta)$ is the reduced rotation matrix of order 1 [2, §18.5].

The most general polarization, elliptical polarization, can be expressed as a superposition of any two independent unit vectors that are perpendicular to the propagation direction; cf. eqn. (12) and Fig. 6.

8.1.3 Connection, linear and angular momentum fields

The combination of energy selectivity, associated with the monochromatic nature of laser light, and sublevel selectivity, associated with polarization, provides controls with which to manipulate the quantum states of an atom. Figure 36 shows possible connections between the polarization of a directed beam and the multipole fields needed for inducing transitions between angular momentum states. By using all three independent polarization fields, each specified by a complex amplitude, we have at most six control parameters with which to create, and detect, degenerate superpositions, as discussed in the present article.

It is important to recognize that any rotation of the coordinates alters the apparent identification of individual magnetic sublevels. Under rotation, parametrized by Euler angles α, β and γ, a single angular momentum state appears as a coherent superposition of states having the same J [91][2, §18.4],

$$|J, M\rangle_{rot} = \Sigma_{M'} \mathcal{D}^{(J)}_{M,M'}(\alpha, \beta, \gamma)|J, M'\rangle. \tag{211}$$

Similarly, the complex-valued unit vectors that describe the direction of the electric field undergo the transformation

$$\hat{\mathbf{e}}_q = \Sigma_{q'} \mathcal{D}^{(1)}_{q,q'}(\alpha, \beta, \gamma)\hat{\mathbf{e}}_{q'}, \qquad q, q' = 0, \pm 1. \tag{212}$$

As an example, the rotation of $J = 1$ from x to z produces the result

$$|1, 0\rangle_{rot} = \frac{1}{\sqrt{2}} \left[|1, -1\rangle - |1, +1\rangle\right]. \tag{213}$$

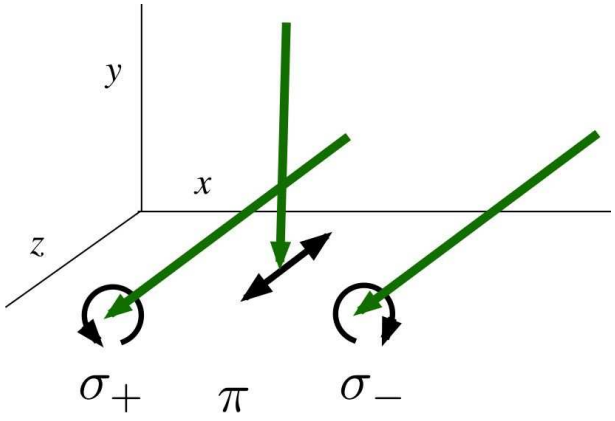

Fig. 35. Examples of polarizations based on helicity, eqn. (209). Long (green) arrows show propagation direction, shorter (black) arrows indicate polarization plane for linear (π) or circular ($\sigma_\pm$) polarizations.

A single state becomes a superposition, and vice versa. Figure 37 illustrates the effect on a linkage pattern of this coordinate change.

8.2 The RWA with degeneracy

The RWA for circularly (or elliptically) polarized light requires consideration of linkages involving all magnetic sublevels. As an example, the interaction Hamiltonian for positive helicity is

$$\mathsf{H}^{int}(t) = -\,\mathrm{Re}\,[d_{+1}\hat{\mathcal{E}}(t)\mathrm{e}^{-\mathrm{i}\omega t}] = -\tfrac{1}{2}d_{+1}\hat{\mathcal{E}}(t)\mathrm{e}^{-\mathrm{i}\omega t} + \tfrac{1}{2}d_{-1}\hat{\mathcal{E}}^{*}\mathrm{e}^{+\mathrm{i}\omega t}. \tag{214}$$

Consider a degenerate ground level having angular momentum $J = 1$ linked by this Hamiltonian to an excited state having $J = 0$, as in Fig. 37. Three states are coupled by this interaction; let us label them by their magnetic quantum numbers. Set the zero of energy to be $E_{-1} = E_{+1} = 0$ and express the statevector as

$$\Psi(t) = C_{-1}(t)\psi_{-1} + C_0(t)\,\mathrm{e}^{-\mathrm{i}\omega t}\psi_0 + C_{+1}(t)\psi_{+1}. \tag{215}$$

Using angular momentum selection rules we obtain from the TDSE the three coupled equations

$$\hbar\frac{d}{dt}C_{-1} = -\frac{\mathrm{i}}{2}[\langle -1|d_{-1}|0\rangle\hat{\mathcal{E}}^{*}\mathrm{e}^{+\mathrm{i}\omega t}]\,\mathrm{e}^{-\mathrm{i}\omega t}C_0, \tag{216}$$

$$\hbar\frac{d}{dt}C_0 = -\mathrm{i}(E_2 - \hbar\omega)C_0 + \frac{\mathrm{i}}{2}\mathrm{e}^{+\mathrm{i}\omega t}[\langle 0|d_{+1}|-1\rangle\hat{\mathcal{E}}\mathrm{e}^{-\mathrm{i}\omega t}]\,C_{-1} - \frac{\mathrm{i}}{2}\mathrm{e}^{+\mathrm{i}\omega t}[\langle 0|d_{-1}|+1\rangle\hat{\mathcal{E}}^{*}\mathrm{e}^{+\mathrm{i}\omega t}]\,C_{+1}, \tag{217}$$

$$\hbar\frac{d}{dt}C_{+1} = \frac{\mathrm{i}}{2}[\langle -1|d_{+1}|0\rangle\hat{\mathcal{E}}\mathrm{e}^{-\mathrm{i}\omega t}]\,\mathrm{e}^{-\mathrm{i}\omega t}C_0. \tag{218}$$

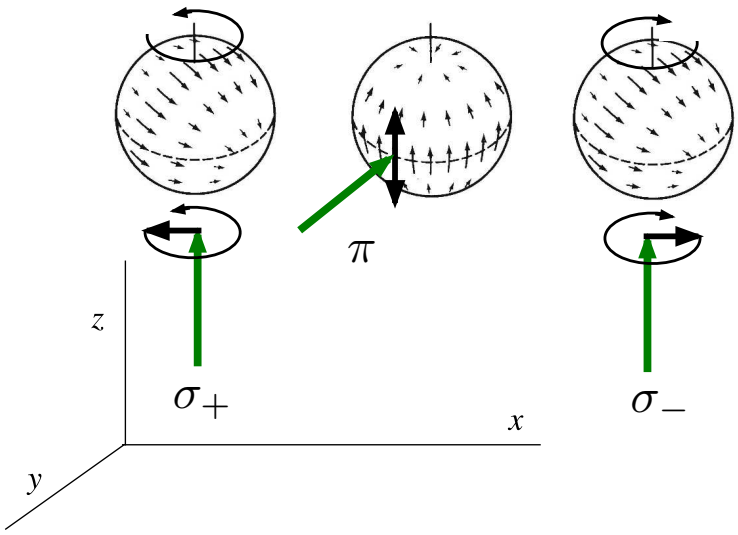

Fig. 36. Electric dipole fields in absorption. The $\sigma_\pm$ fields at the left and right are most strongly coupled to circularly polarized plane waves propagating vertically. The π field at the center has strongest coupling to a vertically polarized field incident in the equatorial plane.

These equations can be written more simply as

$$\frac{d}{dt}C_{-1} = -\frac{\mathrm{i}}{2}\Omega_P^* C_0, \tag{219}$$

$$\frac{d}{dt}C_0 = -\mathrm{i}\Delta C_0 - \frac{\mathrm{i}}{2}\Omega_P C_{-1} - \frac{\mathrm{i}}{2}\Omega_S^* \mathrm{e}^{+2\mathrm{i}\omega t} C_{+1}, \tag{220}$$

$$\frac{d}{dt}C_{+1} = -\frac{\mathrm{i}}{2}\Omega_S \mathrm{e}^{-2\mathrm{i}\omega t} C_0, \tag{221}$$

where the Rabi frequencies are

$$\hbar\Omega_P^* \equiv \langle -1|d_{-1}|0\rangle\hat{\mathcal{E}}^*, \qquad \hbar\Omega_S \equiv -\langle +1|d_{+1}|0\rangle\hat{\mathcal{E}}. \tag{222}$$

The RWA neglects terms that vary as twice the carrier frequency. When we omit these terms we obtain the two-state RWA equations

$$\frac{d}{dt}C_{-1} = -\frac{\mathrm{i}}{2}\Omega_P^* C_0, \tag{223}$$

$$\frac{d}{dt}C_0 = -\mathrm{i}\Delta C_0 - \frac{\mathrm{i}}{2}\Omega_P C_{-1}. \tag{224}$$

More generally, when the radiation is elliptically polarized then the Hamiltonian will have the form

$$\mathsf{H}^{int}(t) = -\,\mathrm{Re}\,[d_{+1}\hat{\mathcal{E}}_P(t)\mathrm{e}^{-\mathrm{i}\omega t} + d_{-1}\hat{\mathcal{E}}_S(t)\mathrm{e}^{-\mathrm{i}\omega t}]. \tag{225}$$

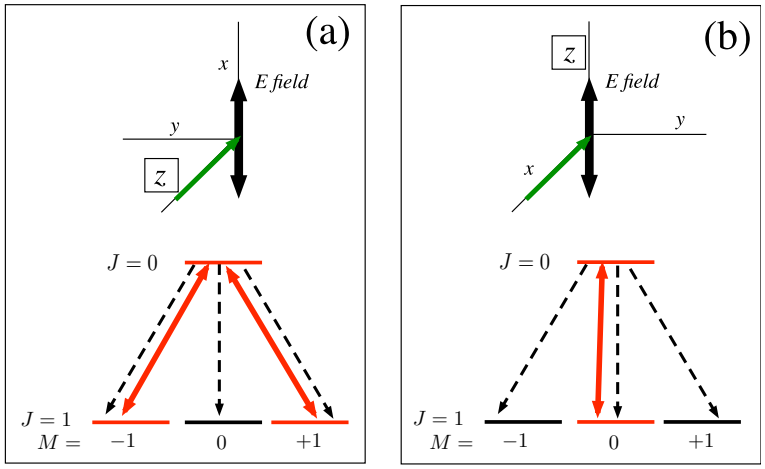

Fig. 37. (a) Upper frame shows Cartesian coordinate system with z axis (the quantization axis) aligned with polarization. Lower frame shows resulting coupling of laser interaction (solid arrow) and spontaneous emission (dashed arrows). (b) Upper frame shows Cartesian coordinate system with x axis aligned with linear polarization. Lower fram shows couplings of laser field (solid lines), using helicity vectors (circular polarization) to describe the electric field. Dashed lines show spontaneous emission linkages.

There will now be linkages to C_0 involving both C_{-1} and C_{+1}. Each linkage will have counter-rotating terms involving $\exp(\pm \mathrm{i}2\omega t)$. The RWA neglects these, and provides a three-state equation, for ladder linkage, of the form

$$\begin{aligned}
\frac{d}{dt}C_{-1} &= -\frac{\mathrm{i}}{2}\Omega_P^* C_0, \\
\frac{d}{dt}C_0 &= -\mathrm{i}\Delta C_0 - \frac{\mathrm{i}}{2}\Omega_P C_{-1} - \frac{\mathrm{i}}{2}\Omega_S^* C_{+1}, \\
\frac{d}{dt}C_{+1} &= -\frac{\mathrm{i}}{2}\Omega_S C_0.
\end{aligned} \tag{226}$$

These equations, based on the TDSE, do not account for spontaneous emission; they only treat the laser-induced transitions. To account for spontaneous emission, an incoherent process, it is necessary to employ a density matrix, as discussed in Appendix H.1. Nevertheless, even without displaying and solving the required equations of motion it is possible to make some qualitative observations about some effects of spontaneous emission. The following sections present some examples.

8.3 Optical pumping

Under conditions of thermal equilibrium populations are evenly distributed amongst magnetic sublevels; each sublevel of a given J has population $1/(2J+1)$. Various laser-induced processes alter this uniform distribution. Distributions of magnetic sublevels, whether coherent or incoherent, are commonly classed as being either *oriented* or *aligned* [2, § 21.9]. Orientation

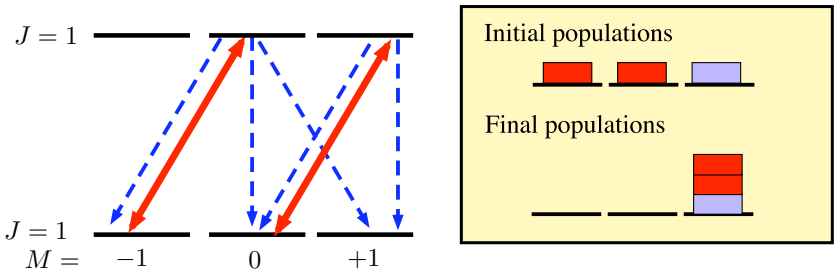

Fig. 38. Optical pumping can produce complete transfer into a single quantum state. Left frame: Linkage pattern for radiative transitions for $J = 1 \rightarrow J = 1$ using circularly polarized light. Solid (red) line: linkage of circularly polarized laser radiation. Dashed lines: allowed linkages of spontaneous emission. Right frame: Population distributions before (above) and after (below) many optical pumping cycles of excitation and spontaneous emission. Initially all sublevels are equally populated. Dark red fill marks the portion affected by laser radiation, light blue fill marks the portion unaffected by laser radiation. After optical pumping (below) all population is placed into sublevel $M = +1$.

means that there is a nonzero averaged magnetic moment. Alignment means that the averaged magnetic moment is zero but the population is not uniformly distributed amongst magnetic sublevels – although sublevels of $+M$ and $-M$ have equal population.

The redistribution often takes place by a combination of coherent and incoherent processes. Illumination of a resonant transition will transfer population into an excited state, from which it will decay by spontaneous emission. When the ground level is degenerate (say, angular momentum $J = 1$) then spontaneous emission from an excited quantum state (a sublevel) will proceed by all three polarization fields, in accord with selection ruless $\Delta M = 0, \pm 1$, each with equal probability. When the illumination is steady and polarized, then there will occur cycling of population: each absorption from a ground sublevel will be followed by spontaneous return to another low-lying sublevel. The result, after many excitation-deexcitation cycles, will be a redistribution of population amongst the ground sublevels – an example of *optical pumping* [92], illustrated by the following figures.

As a first example, Fig. 38 illustrates how optical pumping with circularly polarized light produces complete population transfer into a single quantum state, the sublevel having maximum magnetic quantum number – in this case $M = +1$. The laser-induced excitation obeys the selection rule $\Delta M = +1$, while spontaneous emission returns population to all three sublevels. Population eventually accumulates in sublevel $M = J$, on which the illumination has no effect. Complete transfer will occur if, and only if, there are no spontaneous emissions other than those that return population to the initially populated Zeeman sublevels.

As a second example, Figure 39 illustrates the redistribution that occurs when linearly polarized light excites atoms from angular momentum $J = 1$ to $J = 0$. The quantization axis here is taken along the direction of linear polarization, so that the selection rule $\Delta M = 0$ holds for excitation. Radiative decay, by contrast, returns population to all three sublevels. Population eventually accumulates into sublevels $M = \pm 1$, which do not undergo laser-induced excitation. After many optical cycles the population is entirely removed from $M = 0$. However, the final

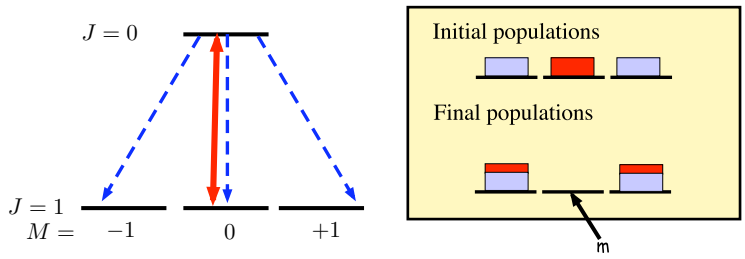

Fig. 39. Optical pumping can produce complete depletion. Left frame: Linkage pattern for radiative transitions for $J = 1 \rightarrow J = 0$. Solid (red) line: linkage of linearly polarized laser radiation, in a reference system aligned with the polarization axis. Dashed lines: allowed linkages of spontaneous emission. Right frame: As in Fig. 40, population distributions before (above) and after (below) many cycles of optical pumping. After optical pumping (below) all population is removed from sublevel $M = 0$.

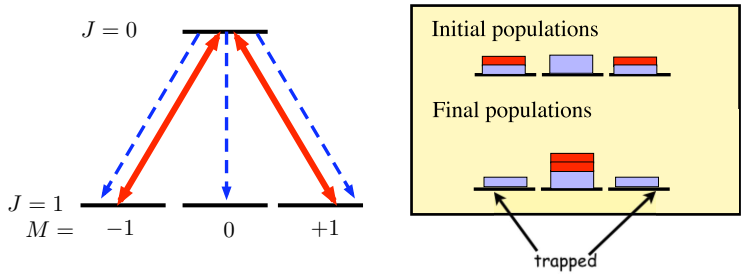

Fig. 40. Optical pumping can produce trapped population. Left frame: As in Fig. 39, linkage patterns for laser radiation (solid line) and spontaneous emission (dashed lines) for linearly polarized light, in a reference system aligned perpendicular to the polarization direction. The linear polarization is expressed as a (coherent) superposition of two circular polarizations. Right frame: As in Fig. 39, population distributions before (above) and after (below) many cycles of optical pumping. Dark red fill marks the portion affected by laser radiation, light blue fill marks the portion unaffected by laser radiation. After optical pumping (below) population is only partially removed from sublevels $M = \pm 1$, leaving a trapped coherent superposition of quantum states. Section 10.6 offers further insight into population trapping states.

population distribution, in $M = \pm 1$, is not a coherent superposition; it is an incoherent *mixture* of two quantum states.

The redistribution of population from optical pumping appears differently if we choose the quantization axis differently. Figure 40 shows the linkages when the polarization is linear but the quantization axis is chosen to be perpendicular to the polarization direction, say in the direction of propagation. It is then necessary to express linear polarization as a superposition of right-

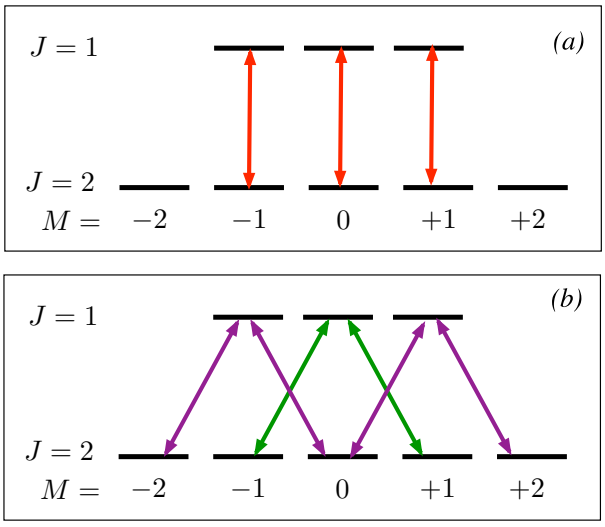

Fig. 41. Linkage patterns for $J = 2 \leftrightarrow J = 1$, in the absence of spontaneous emission. (a) Linear polarization, in direction of quantization axis. Excitation occurs through three independent linkages; two (dark) states are unaffected. (b) Linear polarization, in helicity basis. There are two independent excitation linkages: a five-state "letter-M" and a three-state lambda.

and left-circularly polarized light, for which the excitation selection rules are $\Delta M = \pm 1$. It might appear that, with this coordinate system, population will accumulate entirely in the $M = 0$ sublevel. This is not correct, as will be explained in Sec. 11.8 and Appendix M: Owing to coherence, only a portion of the initial population is affected by the laser radiation. The remainder is unaffected by the radiation; it remains in a *population trapping* state that does not become excited and therefore does not fluoresce – a *dark state* coherent superposition of $M = \pm 1$. The portion affected by the radiation, indicated by dark red fill in Fig. 39, becomes an incoherent mixture of two quantum states after optical pumping.

The preceding examples illustrate situations in which radiative excitation produces measurable changes of quantum-state probabilities. However, because these rely on spontaneous emission, they do not exhibit the phase coherence that is of central concern in the present article. For such purposes it is necessary to rely solely upon laser-induced transitions, and to deal with coherent excitation.

8.4 General angular momentum

As angular momentum J increases, so too do the number of linkages possible between sublevels. A simple example will illustrate some of the considerations that occur. Figure 41 illustrates linkage patterns for a $J = 2 \leftrightarrow J = 1$ transition (in the absence of spontaneous emission), as viewed with two choices of coordinates.

Frame (a), appropriate to linear polarization aligned with the quantization axis, shows that

there are three independent two-state transitions, associated with states $M = 0, \pm 1$. The states with $M = \pm 2$ are unlinked, and do not undergo excitation; they are dark states, or population-trapping states, meaning that they are unaffected by the laser radiation that would otherwise produce excitation and subsequent fluorescence.

Frame (b) shows the same system but with an helicity basis for the polarizations, i.e. a combination of right- and left-circular polarization. The linkages now appear as two independent systems: a 5-state letter-M linkage pattern (starting with $J, M = 2, -2$) and a three-state lambda linkage (starting with $J, M = 2, -1$). All magnetic sublevels have linkages to excited states. This appearance is deceiving; the number of dark states cannot depend on the (arbitrary) choice of coordinate alignment. As discussed in Appendix M, each of the independent linkage patterns of frame (b) has a single dark state. Thus, as in the portrayal of frame (a), the full 7-state system has two dark states.

9 Refinements

The simple two-state quantum system has found many applications. Many other situations require only small modifications of the elementary model. Here I mention a few of these.

9.1 Statistical averages

When dealing with laser-excitation of atomic beams or with other aggregates of single atoms it is essential to recognize that observed properties, such as excitation probabilities, originate in an ensemble of systems, each of which differs in some parameter that affects the excitation. Each individual system within the ensemble evolves subject to a distinct RWA Hamiltonian, say $\mathsf{W}(t;e)$, that depends upon a set of environmental parameters, here denoted e. The systems evolve independently, and thus the observable probabilities are averages over probabilities obtained from considering separate time evolutions. The required algorithm, for a discrete set of environmental parameters e_j, is

$$\bar{P}_n(t) = \Sigma_j p(e_j)\,|C_n(t;e_j)|^2, \tag{227}$$

where $C_n(t;e)$ is the solution to the TDSE with RWA Hamiltonian $\mathsf{W}(t;e)$ and $p(e)$ is the probability of finding the parameters e.

An important example of such environmental averages occurs for impurity atoms embedded in a solid matrix. Each impurity atom may have a different set of near neighbors, and hence will be subject to a different set of static interactions. Each such environment produces a different shift of the basic energy levels E_n, and hence a different value of the detuning. The observed properties of an ensemble of impurity atoms must average over the detuning distribution. Appendix F provides other useful examples.

It is important to recognize that there usually is no single "average" RWA Hamiltonian $\bar{\mathsf{W}}(t)$ that will reproduce the averaging of eqn. (227); one cannot write

$$\bar{P}_n(t) = |\bar{C}_n(t)|^2, \quad \text{with} \quad \frac{d}{dt}\bar{\mathbf{C}}(t) = -\mathrm{i}\bar{\mathsf{W}}(t)\bar{\mathbf{C}}(t). \tag{228}$$

9.2 Beyond the RWA

The RWA provides a mechanism to average over rapid variations at the carrier frequency and thereby place emphasis upon slower transition changes. The validity of this approximation improves as the carrier frequency ω becomes much larger than the Rabi frequency Ω. However, situations arise in which this condition fails. An alternative approach is then needed [93].

A particularly fruitful approach begins from an idealization of the interaction Hamiltonian as perfectly periodic, with period equal to $\tau = 2\pi/\omega$ for carrier frequency ω. That is, the Hamiltonian $\mathsf{H}(t)$ that appears in the equation

$$\frac{d}{dt}\mathbf{c}(t) = -\frac{\mathrm{i}}{\hbar}\mathsf{H}(t)\mathbf{c}(t) \tag{229}$$

has periodicity $\mathsf{H}(t+\tau) = \mathsf{H}(t)$. Such situations were widely studied during the 19th century, and their solution is now generally called *Floquet theory* [94] [2, § 10.2]. Appendix L discusses this approach. The extension from perfect periodicity to pulses involves *adiabatic Floquet theory*,

cf. Appendix L.6 [95]. Basically these approaches increase the dimensions of the Hamiltonian matrix; they can be viewed as enlarging the Hilbert space by introducing an additional degree of freedom, one that has an infinite number of states, each associated with a Fourier harmonic.

9.3 The nonessential states; Effective Hamiltonian

Although the Bohr resonance condition may restrict appreciable population to only two "essential" states, this does not mean that the remaining "nonessential" states have no effect on the dynamics. Even with miniscule excitation probability these nonessential states can have two important effects, each based on regarding them as nonresonant intermediate states in a chain of transitions that is overall resonant. Both effects can be treated by means of an "effective" Hamiltonian H^{eff} [2, § 14.8]. Section 10.3.1 discusses how such an effective two-state Hamiltonian arises from a three-state system when detuning is large. In general the elements of H^{eff} have the following interpretation.

The off-diagonal elements of H^{eff} describe multiphoton transitions, the simplest of which are two-photon transitions, such as occur with stimulated Raman scattering when the excited state is nonresonant. Much effort dealt with calculations of these multiphoton transition rates during the early decades of laser usage [96].

The diagonal elements of H^{eff} can be regarded as transitions from an initial state into an excited state and back again. From a version of the energy-time uncertainty principle,

$$\Delta \times \tau > \hbar, \tag{230}$$

one expects that, as the detuning Δ grows large (in units of Rabi frequency), the duration of excitation τ must become small (in units of Rabi cycles). These processes, though producing negligible excitation, produce an induced dipole moment. In turn, this induced moment, parameterized as a *polarizability* of the atom, interacts with the laser electric field to produce an energy shift – a *dynamic Stark effect* [80].

10 Three states

The next logical step beyond the two-state system is the three-state system excited by two distinct radiative transitions. As with the previous discussion, I shall take the interaction to be that of electric-dipole transitions, here with two laser fields, identified by letters P and S. The carrier frequencies of the two fields, ω_P and ω_S respectively, are each assumed to be close to resonance with one, and only one, of the transitions, so that each field can be uniquely identified with a particular transition [97]. I shall assume that the P field is (near) resonance only with the 1-2 transition, while the S field is (near) resonant only with the 2-3 transition. Thus the nonzero interactions, for linearly polarized fields, are

$$V_P(t) = -d_{12}\mathcal{E}_P(t)\cos(\omega_P t + \varphi_P), \tag{231}$$

$$V_S(t) = -d_{23}\mathcal{E}_S(t)\cos(\omega_S t + \varphi_S). \tag{232}$$

Within the coherence time of the laser fields the phases φ_P and φ_S remain constant at a fixed position, unless specifically modulated by an experimenter. Their constant absolute value is uncontrollable, and so one of them can usually be taken as zero at some convenient initial time. The second phase cannot be similarly chosen unless the two fields have the same frequency and derive from the same laser field (i.e. states 1 and 3 are degenerate), through the use of beam splitters and manipulation of differing optical paths; then a controllable phase difference can be specified. The phases affect comparisons of successive experiments on a single atom or simultaneous observation of several atoms. Such situations call for an average over the phases; see Sec. 9.1.

This system has three possible linkage patterns, shown in Fig. 42. In free atoms the selection rules for electric-dipole radiation require that linked states should have opposite parity. Thus it is not possible to have a closed loop of excitation linkages with only electric dipole radiation in a free atom. However, there exist alternative interactions, and alternative systems, for which closed loops are possible; cf. Sec. 11.6.

Each of the linkage patterns shown Fig. 42 leads to a similar RWA Hamiltonian; the only difference is in the definition of the diagonal elements – the detunings. For the ladder system the third detuning is the *sum* of two single-step detunings, while for the lambda and vee linkages it is the *difference* of two detunings.

The vee linkage is distinguishable from the other linkages only by the initial conditions [63]: Whereas the initial population of the lambda and ladder systems resides in one end of the linkage chain, for the vee system population initially resides in the *middle* level of a chain. When the interaction occurs, population proceeds towards the ends of the chain, from which it returns with constructive or destructive interference of amplitudes.

Numerous papers have described coherent excitation of three-state systems [98]. Making an obvious extension of the two-state system we write the statevector for the three-state system as

$$\Psi(t) = C_1(t)\psi_1'(t) + C_2(t)\psi_2'(t) + C_3(t)\psi_3'(t), \tag{233}$$

[63] This distinction fails for a system that has already been subjected to coherent excitation, thereby producing a distribution of population amongst the three states.

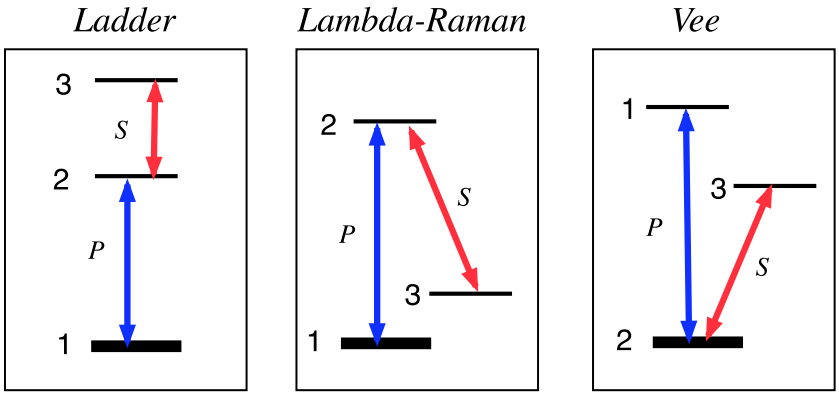

Fig. 42. Types of three-state excitation: from left to right these are the ladder, lambda and vee linkages. The ground state is the initial state of the three-state chain for the ladder and lambda, but is the middle state of the vee.

where, anticipating the removal of Hamiltonian matrix elements that vary at the carrier frequencies, we choose the rotating coordinates to be

$$\psi_1'(t) = \exp[-\mathrm{i}(E_0/\hbar)t]\ \psi_1, \tag{234}$$
$$\psi_2'(t) = \exp[-\mathrm{i}(E_0/\hbar+\omega_1)t]\ \psi_2, \tag{235}$$
$$\psi_3'(t) = \exp[-\mathrm{i}(E_0/\hbar+\omega_1\pm\omega_2)t]\ \psi_3. \tag{236}$$

In the definition of $\psi_3'(t)$ the plus sign is used with the ladder system, the minus sign is used with the lambda system. The energy E_0 is a reference energy; it establishes an overall phase to the statevector but is not observable. It can be chosen to simplify the appearance of the RWA Hamiltonian.

10.1 The three-state RWA

The conversion of the Schrödinger equation into a set of ordinary differential equations for the RWA amplitudes $C_n(t)$, produces the matrix equation (108). The RWA Hamiltonian matrix for a ladder linkage is (explicit time variation of elements are not shown)

$$\mathsf{W}(t) = -\begin{bmatrix} \Delta_1 & \frac{1}{2}\Omega_P\exp(-\mathrm{i}\varphi_P) & 0 \\ \frac{1}{2}\Omega_P\exp(+\mathrm{i}\varphi_P) & \Delta_2 & \frac{1}{2}\Omega_S\exp(-\mathrm{i}\varphi_S) \\ 0 & \frac{1}{2}\Omega_S\exp(+\mathrm{i}\varphi_S) & \Delta_3 \end{bmatrix}. \tag{237}$$

The off-diagonal elements of this matrix are half the Rabi frequencies,

$$\Omega_P = -d_{12}\mathcal{E}_P/\hbar, \qquad \Omega_S = -d_{23}\mathcal{E}_S/\hbar, \tag{238}$$

appropriately phased. In general the amplitudes $\mathcal{E}_P$ and $\mathcal{E}_S$ are slowly varying, though not explicitly indicated here.

No direct coupling between states 1 and 3 occurs in this description – the linkage pattern does not form a closed loop. This constraint usually follows from parity selection rules, but there are situations where such couplings must be considered; cf. Sec. 11.6. Furthermore, field P is assumed to make no contribution to the 2-3 coupling, nor does field S contribute to the 1-2 coupling. Such couplings are, in fact, present, but they are assumed here to have the sort of rapid time variation that has already been neglected with the use of the rotating wave approximation.

The diagonal elements of the RWA Hamiltonian matrix are detunings – combinations of differences between Bohr transition frequencies and carrier frequencies. The basic single-field detunings are defined by the relationships

$$\hbar\Delta_P \equiv |E_2 - E_1| - \hbar\omega_P, \qquad \hbar\Delta_S \equiv |E_3 - E_2| - \hbar\omega_S. \tag{239}$$

From these, with further choice of the energy zero point E_0, we fix the detunings of the RWA Hamiltonian. A common choice, useful when we consider a chain of excitations involving Rabi frequencies of comparable magnitude and all population resides initially in state 1, is

$$\Delta_1 = 0, \tag{240}$$

$$\Delta_2 = \Delta_P, \tag{241}$$

$$\Delta_3 = \Delta_P \pm \Delta_S, \tag{242}$$

where the plus sign is used for the ladder linkage and the minus sign for the lambda linkage.

10.2 Resonance with equal Rabi frequencies

A simple theoretical situation occurs when both Rabi frequencies are constant and equal, and the two transitions are each resonant. The RWA Hamiltonian then reads [64]

$$\mathsf{W} = -\frac{1}{2}\begin{bmatrix} 0 & \Omega & 0 \\ \Omega & 0 & \Omega \\ 0 & \Omega & 0 \end{bmatrix}. \tag{243}$$

Figure 43 illustrates the histories of excited-state populations (states 2 and 3) for a ladder linkage in which population starts in state 1. The solutions are periodic. Starting from state 1 population flows into state 2 and then arrives, completely, in state 3. From there it returns to the initial state for further periodic cycling. Population arrives in state 2 both in transit to state 3 and on returning. Thus the population oscillations of this state are twice as fast as those for states 1 and 3.

These solutions readily apply to resonant pulsed excitation, so long as all Rabi frequencies share the same time dependence, say $\Omega(t) = f(t)\Omega_0$. The RWA Hamiltonian then factors as $\mathsf{W}(t) = f(t)\mathsf{W}$. By introducing the time scale (cf. Appendix E.1)

$$\tau(t) = \int_{-\infty}^{t} dt'\ f(t') \tag{244}$$

we obtain the equation

$$\frac{d}{d\tau}\mathbf{C}(\tau) = -\mathrm{i}\mathsf{W}\mathbf{C}(\tau), \tag{245}$$

[64] This matrix is a multiple of the spin-one matrix S_x of Appendix C.2. The solutions are therefore special cases of those described in Sec. 11.3.

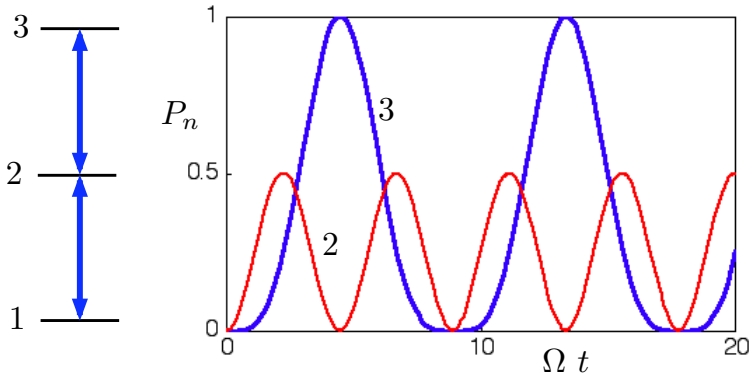

Fig. 43. Population histories of intermediate state 2 and final state 3 for resonant excitation, $\Delta_1 = \Delta_2 = \Delta_3$ and equal Rabi frequencies, $\Omega +_= \Omega_S \equiv \Omega$.

in which the RWA Hamiltonian W is constant. The solutions are those discussed above, but with the scaled time variable $\tau(t)$. This rescaling technique allows the solution to any resonant equations in terms of solutions for a constant RWA Hamiltonian.

10.3 Large intermediate detuning

When intermediate-state detuning is present, the excitation dynamics can exhibit a variety of characteristics, depending on how the detuning compares with the Rabi frequencies. A particularly simple, and useful, example occurs when the detuning is much larger than the Rabi frequencies.

Consider the three-state Hamiltonian for a ladder linkage induced by simultaneous P and S fields (here, for typograhical simplicity, the Rabi frequencies are taken as complex (denoted $\hat{\Omega}$), incorporating the phases of the fields)

$$\begin{aligned}
\frac{d}{dt}C_1 &= -\mathrm{i}\Delta_1 C_1 - \frac{\mathrm{i}}{2}\hat{\Omega}_P^* C_2, \\
\frac{d}{dt}C_2 &= -\mathrm{i}\Delta_2 C_2 - \frac{\mathrm{i}}{2}\hat{\Omega}_P C_1 - \frac{\mathrm{i}}{2}\hat{\Omega}_S^* C_3, \\
\frac{d}{dt}C_3 &= -\mathrm{i}\Delta_3 C_3 - \frac{\mathrm{i}}{2}\hat{\Omega}_S C_2.
\end{aligned} \tag{246}$$

When the excitation is completely resonant at each step then $\Delta_1 = \Delta_2 = \Delta_3$, and the two Rabi frequencies have equal magnitudes, $\hat{\Omega}_P = \hat{\Omega}_S \equiv \hat{\Omega}$, then there occurs periodic excitation from state 1, through state 2, to an complete transfer into state 3, followed by a return. Figure 43 illustrates this periodic behavior. When the intermediate-state detuning Δ_2 becomes large, less population reaches state 2. However, as long as there is two-photon resonance, meaning $\Delta_1 = \Delta_3$ with the present description, population will continue to reach state 3. Figure 44 illustrates the population histories that result when intermediate-state detuning is large but two-photon resonance prevails.

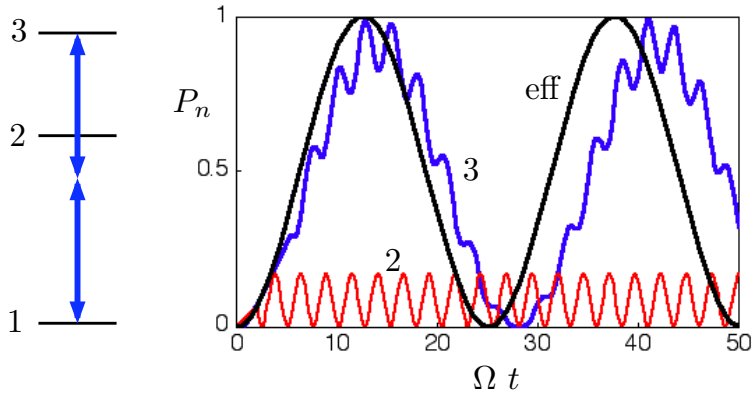

Fig. 44. Population histories of intermediate state 2 and final state 3 for large detuning ($\Delta = 20 \times \Omega$). The smooth black curve shows prediction of effective two-state system, an approximation that becomes increasingly accurate as the detuning grows larger and the population reaching state 2 diminishes.

In the limit of very large intermediated detuning Δ_2, negligible population occurs in state 2. However, there occurs a periodic population transfer – Rabi oscillation – between states 1 and 3. The description of this phenomena involves the reduction of the three-state system to an effective two-state system using adiabatic elimination of state 2.

10.3.1 Adiabatic elimination

When the detuning Δ_2 of the intermediate state 2 is very large, meaning $\Delta_2| \gg |\Omega|$ as we shall now assume, then the derivative of C_2 varies rapidly. We are not concerned with such rapid variations, and we average them out by taking an average over many cycles. The average of the derivative vanishes, and we can solve the resulting equation for the average amplitude $\bar{C}_2$,

$$\bar{C}_2 = -\frac{1}{2\Delta_2}\Big[\hat{\Omega}_P C_1 + \hat{\Omega}_S^* C_3\Big], \tag{247}$$

which thereby becomes linked (adiabatically) to states 1 and 2. Using this result we can *adiabatically eliminate* the occurrence of state 2 in the equations of motion [2, §4.3]. The result is

$$\frac{d}{dt}C_1 = -\mathrm{i}\Delta_1 C_1 + \mathrm{i}\frac{|\hat{\Omega}_P|^2}{4\Delta_2}C_1 + \mathrm{i}\frac{\hat{\Omega}_P^*\hat{\Omega}_S^*}{4\Delta_2}C_3, \tag{248}$$

$$\frac{d}{dt}C_3 = -\mathrm{i}\Delta_3 C_3 + \mathrm{i}\frac{\hat{\Omega}_S\hat{\Omega}_P}{4\Delta_2}C_1 + \mathrm{i}\frac{|\hat{\Omega}_S|^2}{4\Delta_2}C_3. \tag{249}$$

The result is expressible as an effective two-state RWA Hamiltonian

$$\mathsf{W}^{\text{eff}} = \begin{bmatrix} \Delta_1 + M_{11} & M_{12} \\ M_{12}^* & \Delta_3 + M_{22} \end{bmatrix}, \tag{250}$$

involving a two-photon interaction M, i.e. an interaction involving the product of two electric-field amplitudes, expressed here as the product of two Rabi frequencies.

10.3.2 The effective Hamiltonian

The elements of M presented above have the form

$$M_{11} = |\mathcal{E}_P|^2 \, \alpha_{11}(\omega_P), \tag{251}$$
$$M_{22} = |\mathcal{E}_S|^2 \, \alpha_{22}(\omega_S), \tag{252}$$
$$M_{12} = \mathcal{E}_P \mathcal{E}_S \, \alpha_{12}(\omega_P). \tag{253}$$

The coefficients α_{nm} are elements of the *polarizability tensor* [65] [99].

In any real atom there are many nonresonant states, and each of them can be regarded as an appropriate intermediate state in the three-state chain considered here. Thus the effective Hamiltonian should sum over all possible intermediate states. A further alteration of the formula is needed to account properly for the counter-rotating tems that the RWA neglects. With these two corrections one obtains the following expression for the polarizability

$$\alpha_{nm}(\omega) = \Sigma_k \frac{d_{nk} d_{km}}{4\hbar} \Big[\frac{1}{E_k - E_n - \hbar\omega} + \frac{1}{E_k - E_n + \hbar\omega} \Big]. \tag{254}$$

The first of the bracketed fractions dominates for a frequency near a resonance; the second term originates in the counter-rotating terms of the Hamiltonian.

The diagonal elements of M are energy shifts induced by the electric field of the laser, commonly termed dynamic Stark shifts, by contrast to the *static* shifts produced by slowly varying (DC) electric fields.. The magnitude of this shift is proportional to the laser intensity and to the frequency-dependent polarizability, This polarizability produces also an off-diagonal element, a two-photon interaction

$$M_{12} = \mathcal{E}_P \mathcal{E}_S \, \alpha_{12}(\omega_P). \tag{255}$$

This appears, in the ladder linkage as a two-photon Rabi frequency, while for the lambda linkage it is the stimulated Raman Hamiltonian. These situations require the two-photon resonance condition

$$E_3 - E_1 = \hbar(\omega_P \pm \omega_S), \tag{256}$$

where the positive sign accompanies the ladder linkage, the negative sign the lambda linkage.

The off-diagonal elements of M bear interpretation as *multiphoton* transitions, in the present example two-photon (between states of common parity). More generally the effective Hamiltonian produces N-photon transitions, e.g. three-photon (between states of opposite parity). These elements of the effective Hamiltonian replace the Rabi frequency used in all of the preceding discussions. It is important to recognize that any interaction that produces a multiphoton transition will also produce a dynamic Stark shift.

10.4 Weak probe field: Autler-Townes splitting

Laser-induced excitation from the ground state to an excited state can always be followed by fluorescence, because both the Rabi frequency and the Einstein A coefficient involve the same

[65] This tensor usually is shown with subscripts that identify the Cartesian components of the two electric fields that appear in its construction.

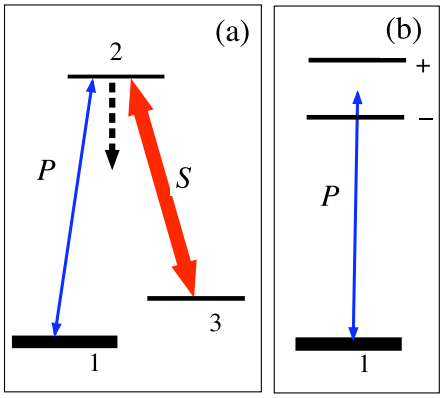

Fig. 45. (a) A weak probe field P couples the initially populated state 1 with an excited state 2, which in turn is coupled by a strong transition to state 3. The linkages are shown as resonant. (b) The couplings in the adiabatic (dressed) basis of the two strongly coupled states. The strong S field acts to split the resonance transition for the weak P field, thereby preventing population transfer from state 1 to the excited state 2 without revision of the P-field detuning.

dipole-transition moment. This fluorescence is strongest when the laser frequency is tuned to the Bohr transition frequency of the two state system: as a function of this frequency the fluorescence signal of an isolated atom traces out a Lorentzian profile, whose width is the lifetime of the excited state and whose central peak coincides with the Bohr frequency; cf. Sec. 7.3.

When laser-induced excitation from the ground state (via P field) occurs in the presence of a second laser-induced excitation (the S field) we must enlarge our mathematical description from a two-state system to a three-state system. The fluorescence from the first excited state now can be modified by the S field, as a result of population flow within a three state system. When the S field is sufficiently strong (i.e. with Rabi frequency much larger than that of the first-step P transition) then the excitation dynamics changes dramatically: once the system is in an excited state, it undergoes many S-field induced Rabi oscillations between the two strongly coupled states 2 and 3 before returning to the ground state via the P-field coupling. These Rabi oscillations affect the fluorescence signal: instead of observing the single Lorentz profile of the two-state system, one observes a splitting of the peak into two components, the *Autler-Townes doublet* [100]. The following paragraphs explain the origin of this effect. [66]

Consider the situation when the population initially resides in state 1, the ground state, which couples via P field to excited state 2, which in turn has linkage via S field to low-lying state 3. Our interest here is in situations where the S field (a *dressing field*) is much stronger than the P field, which acts as a weak *probe field* to the fluorescing excited state. Figure 45(a) shows the assumed linkage pattern.

[66] Often this effect is explained by introducing a photon-number basis for the fields. But with laser excitation the fields are readily described as classical fields; the granularity of quantized fields is not evident. Thus it is useful to have a description that makes no explicit mention of photon number states. Instead, one uses the tool of adiabatic states (also called dressed states) to replace the original unperturbed basis states (the diabatic states or bare states of Sec 6.6).

We take the detunings to be those appropriate to the lambda linkage,

$$\Delta_1 = 0, \qquad \Delta_2 = \Delta_P, \qquad \Delta_3 = \Delta_P - \Delta_S, \tag{257}$$

so that the RWA Hamiltonian matrix, for the lambda linkage, has the following structure (here the fluorescence loss is neglected)

$$\mathsf{W} = \begin{bmatrix} 0 & \frac{1}{2}\hat{\Omega}_P^* & 0 \\ \frac{1}{2}\hat{\Omega}_P & \Delta_P & \frac{1}{2}\hat{\Omega}_S^* \\ 0 & \frac{1}{2}\hat{\Omega}_S & \Delta_P - \Delta_S \end{bmatrix} \begin{matrix} \psi_1 \\ \psi_2'(t) \\ \psi_3'(t) \end{matrix} . \tag{258}$$

Here the Rabi frequencies $\hat{\Omega}$ are regarded as complex valued.To treat this we regard states 2 and 3 as a single strongly-coupled two-state system and we introduce a change of basis states that describe this strongly coupled pair of states. That is, we introduce eigenstates of the RWA Hamiltonian of the two strongly coupled states (examples of dressed states or, when the RWA Hamiltonian has some slow time dependence, adiabatic states),

$$\mathsf{W}^{(2)} = \frac{1}{2}\begin{bmatrix} 2\Delta_P & \hat{\Omega}_S^* \\ \hat{\Omega}_S & 2\Delta_P - 2\Delta_S \end{bmatrix} \begin{matrix} \psi_2'(t) \\ \psi_3'(t) \end{matrix} . \tag{259}$$

The two eigenvalues are

$$\varepsilon_\pm = \Delta_P + \frac{1}{2}\Delta_S \pm \frac{1}{2}\sqrt{(\Delta_S)^2 + |\hat{\Omega}_S|^2}. \tag{260}$$

The diagonalization of this 2×2 submatrix of the full Hamiltonian is accomplished by a unitary transformation U that produces the result

$$\mathsf{U}^\dagger \mathsf{W}^{(2)} \mathsf{U} = \begin{bmatrix} \varepsilon_- & 0 \\ 0 & \varepsilon_+ \end{bmatrix}. \tag{261}$$

Using this transformation matrix we introduce, in place of the original amplitudes C_2 and C_3 of the strongly coupled states, the pair of dressed-state amplitudes A_+ and A_-,

$$\begin{bmatrix} C_2(t) \\ C_3(t) \end{bmatrix} = \mathsf{U} \begin{bmatrix} A_+(t) \\ A_-(t) \end{bmatrix}. \tag{262}$$

Using these, and assuming that the RWA Hamiltonian varies only slowly [67], we write the equation of motion as

$$\frac{d}{dt}\begin{bmatrix} C_1(t) \\ A_+(t) \\ A_-(t) \end{bmatrix} = -\frac{\mathrm{i}}{2}\begin{bmatrix} 0 & \hat{\Omega}_+^* & \hat{\Omega}_- \\ \hat{\Omega}_+ & 2(\Delta_P + \Delta_S + \delta) & 0 \\ \hat{\Omega}_-^* & 0 & 2(\Delta_P + \Delta_S - \delta) \end{bmatrix}\begin{bmatrix} C_1(t) \\ A_+(t) \\ A_-(t) \end{bmatrix} \tag{263}$$

where δ is the generalized (nonresonant) Rabi frequency of the strongly-coupled transition,

$$\delta \equiv \sqrt{(\Delta_S)^2 + |\hat{\Omega}_S|^2}, \tag{264}$$

[67] Appendix K.2 discusses the nonadiabatic couplings that occur between amplitudes A_k when there is variation of the RWA Hamiltonian.

and there are two new Rabi frequencies, $\hat{\Omega}_\pm$. These are proportional to the original probe-field Rabi frequency and to relevant elements of the matrix that transforms from bare to dressed states,

$$\hat{\Omega}_\pm = \hat{\Omega}_P U_{2,\pm}. \tag{265}$$

The ground state, where population initially resides, is now coupled to two states – the two dressed states that have replaced the original bare states. Each of these dressed states is a linear superposition of the original bare states. In particular, each contains some component of state 2, which has the coupling to the ground state, state 1. Thus each one of the dressed states couples (by an amount that depends on S-field detuning) to the initially populated state, although each one receives population at a different rate (depending on the P-field detuning.)

Figure 45(b) illustrates the couplings in the new, adiabatic, basis. The Hamiltonian in this basis has couplings between state 1 and each of the adiabatic states,

$$\mathsf{W}' = \begin{bmatrix} 0 & \frac{1}{2}\hat{\Omega}_+^* & \frac{1}{2}\hat{\Omega}_- \\ \frac{1}{2}\hat{\Omega}_+ & \boxed{\varepsilon_-} & \boxed{0} \\ \frac{1}{2}\hat{\Omega}_-^* & \boxed{0} & \boxed{\varepsilon_+} \end{bmatrix} \begin{matrix} \psi_1 \\ \Phi_- \\ \Phi_+ \end{matrix}. \tag{266}$$

In general, there will occur resonance transitions whenever a diagonal element of the Hamiltonian is equal to the element associated with the initially populated state. In the present situation, with population starting in state 1, that is the first element on the diagonal. For the matrix of eqn. (258) this resonance condition reads $0 = \Delta_P$, meaning either single-photon resonance between states 1 and 2, or else $0 = \Delta_P - \Delta_S$, corresponding to two-photon resonance between states 1 and 3. For the matrix of eqn. (266) the two possible resonance conditions are $\varepsilon_\pm = 0$, meaning

$$\Delta_P = \mp\frac{1}{2}\delta - \frac{1}{2}\Delta_S. \tag{267}$$

In the absence of the S field the two values coincide, requiring $\Delta_P = 0$. However, when the S field is present there are two distinct possibilities for the resonance condition. Thus what was a single resonance in the absence of the 2-3 coupling will now appear as two resonances, the *Autler-Townes doublet*, separated by δ, the *Autler-Townes (AT) splitting* of eqn. (264) [2, §10.4].

The simplest situation is when the strong (dressing) laser is resonant with the original Bohr frequency of the excited-state transition, so that $\Delta_S = 0$. That is,

$$\hbar\omega_S = E_3 - E_2. \tag{268}$$

The two probe-field detunings for resonance are $2\Delta_P = \pm|\hat{\Omega}_S|$. These occur at probe-field frequencies such that

$$\hbar\omega_P = E_2 - E_1 \pm \tfrac{1}{2}\hbar|\hat{\Omega}_S|. \tag{269}$$

That is, when $\Delta_S = 0$ the two resonances are separated by the strong-field Rabi frequency.

The amplitudes of the two components of the doublet depend on the effective Rabi frequency that couples the resonance to the ground state. For example, when the coupling is into the minus component, then the relevant Rabi frequency is $\hat{\Omega}_-$.

Although I have not included fluorescence loss from either of the excited states, such effects can be included if one uses a density matrix rather than a statevector as the fundamental entity of

interest (cf. Appendix H.1). It will still be so that there are two resonances in the coupling out of the ground state and into excited states. The fluorescence will be strongest when the resonance condition holds. Thus a measurement of fluorescence, as a function of probe-field detuning Δ_P, will reveal an Autler-Townes doublet, separated by the strong-field Rabi frequency $|\hat{\Omega}_S|$. Such measurements offer a means of determining Rabi frequencies. When so doing, the S-field resonance condition $\Delta_S = 0$ is obtained by adjusting the S-field frequency to minimize the AT splitting δ for fixed value of $\hat{\Omega}_S$.

10.5 Raman processes

The traditional Raman process is a three-state sequence of transitions in which radiative excitation (perhaps induced by a *pump* laser) is followed by spontaneous emission to a final state differing from the initial state [101] [2, §17.5]. Typically Raman spectroscopy deals with molecules; the transitions are then between vibrational-rotational states, characterized in part by vibrational quantum number v and rotational angular momentum J, M. From any given excited electronic state there are many fluorescing transitions, corresponding to various vibrational and rotational quantum numbers of the final state.

When the final state of the sequence is more energetic than the initial state the resulting emission line (to the red of the pump wavelength) is known as a *Stokes* spectral line. The difference between the pump frequency and the Stokes frequency, the *Raman frequency*, defines the excitation energy of the final state relative to the initial state. When, instead, the final state has lower energy than the initial state, as can occur when the initial quantum state is already excited, then the emission is an *anti-Stokes* line, at a bluer wavelength than the pump field. The wavelengths of the various Stokes and anti-Stokes lines (i.e. the Raman frequencies) characterize the particular molecular species, and so they have provided a valuable diagnostic tool for spectroscopists.

10.5.1 Population transfer

One of the goals of laser excitation has been to transfer population from an initial state to a chosen final state. Raman processes provide a mechanism for transferring population via two-photon transitions, into final states that cannot be reached by electric dipole radiation at optical frequencies. These include states that are degenerate with the initial state. The simplest use of Raman scattering to produce population transfer, shown in Fig. 46(a), employs a pump field of preselected frequency to produce a first step of excitation, but relies on spontaneous emission to produce the final transition. From the excited state there occur many possible emission routes, each with its own Stokes field. The relative probability of a specific one (the *branching ratio*) depends on wavefunctions of the two states. For molecular transitions between vibrational states these are Franck-Condon factors, and hence the population transfer process is termed *Franck-Condon pumping* (FCP) [102]. Because the process relies on spontaneous emission, it does not allow creation of a coherent superposition. And because there are numerous possible final states, it is not possible to achieve appreciable transfer into any one state.

Rather than rely on nature to produce the Stokes field, one can impose a laser field to select one of the de-excitation choices, via stimulated emission, a process often termed *stimulated Raman scattering* (SRS) [103]. By using a second laser field the two-step Raman process, of excitation and decay, can be made more rapid and more selective. The second field is typically

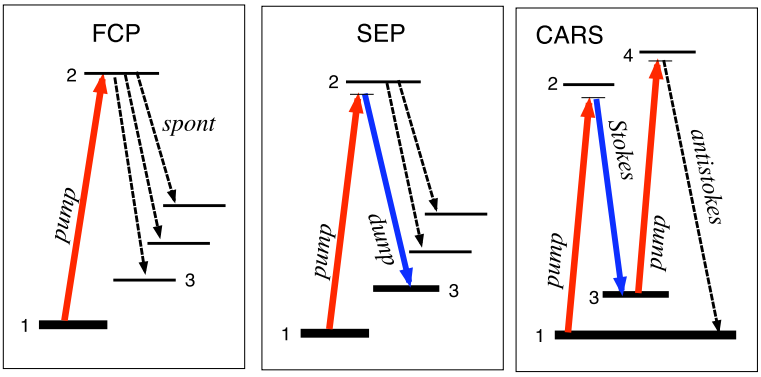

Fig. 46. Raman processes that produce population transfer. (a) Franck-Condon pumping (FCP) converts pump radiation into Stokes radiation via spontaneous emission. (b) Stimulated emission pumping (SEP) selects a particular Stokes transition to stimulate. The pump field need not be resonant, but the pump and dump fields must together satisfy a two-photon resonance condition. (c) Coherent anti-Stokes Raman scattering (CARS) uses a three-photon transition, pump-Stokes-pump, to create a coherent dipole moment (between states 4 and 1) that then produces an anti-Stokes field.

termed the *Stokes field*, independent of its wavelength. Figure 46(b) illustrates this population transfer scheme, often termed *stimulated emission pumping* (SEP) [104]. The use of two simultaneous laser fields, as in SEP, allows selective transfer to a chosen final state, diluted only by any competing spontaneous emission. When used in this way the pump field need not be resonant, but the pump and dump fields must together satisfy a two-photon resonance condition.

Another class of Raman processes, used more for spectroscopic purposes or microscopy than for population transfer, is the coherent anti-Stokes Raman scattering (or spectroscopy) (CARS) sketched in Fig. 46(c) [105]. This is an example of nonlinear optics (*four-wave mixing*) in which a three-photon process, involving pump-Stokes-pump transitions, creates a dipole moment that acts as a source of anti-Stokes radiation; cf. Sec 11.6. As with SEP, the pump and Stokes fields need not be resonant; an overall frequency matching constraint picks out a particular anti-Stokes frequency; cf. Sec. 11.7.

The lambda linkage pattern associated with the Raman process is basically a three-state excitation chain. Conceptually the simplest scheme for transferring population along a chain is to use resonant excitation with equal Rabi frequencies that share the same time dependence. As shown in Sec. 10.2 population then flows from the initial state, 1, to a succession of states along the chain. For the three-state system this can produce Rabi oscillations that will periodically place all population into state 3. Figure 47 illustrates the population flow for such a situation [68].

Such schemes are possible for pulsed excitation, but they require that all Rabi frequencies must rise and fall together, with carefully controlled relative values (typically best results occur when all Rabi frequencies are equal). The technique also suffers from the temporary placement of population in the excited state, from which it may be lost via spontaneous emission to other

[68] Note that although excitation with simultaneous and equal Rabi frequencies can produce complete population transfer, it cannot produce a superposition that does not inclued state 2.

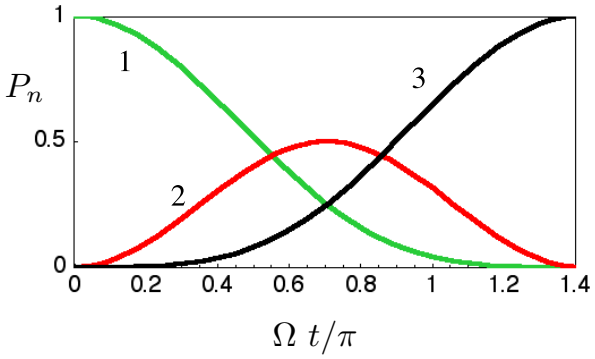

Fig. 47. Population flow for three states, resonant excitation with common Rabi frequency $\Omega_P = \Omega_S = \Omega$. Population flows from state 1 through state 2 into state 3. To obtain complete population transfer the pulse duration must be adjusted to complete only half of a full 3-state Rabi cycle.

states. (This loss can be reduced by using lasers which, while satisfying two-photon resonance conditions, are not not in single-photon resonance.)

One might expect that an effective and robust way to transfer population between state 1 and state 3 would be by placing population first into intermediate state 2 (by means of a π pulse or by RAP) and then transferring this to state 3. This *intuitive* pulse sequence exposes the atom first to the P field and then to the S field. Figure 48 illustrates such a sequence. In the first step, shown in frame (a) the P field induces complete transfer into excited state 2. In the second step, shown in frame (b), the S field transfers this excited-state population to the desired target state 3.

The pulse sequence of Fig. 48, with P preceding S, fits the intuitive understanding of how excitation proceeds when it is described by incoherent rate equations. When such equations apply, only a portion of the population can be transferred at each step (one half at most), because the populations equilibrate under the influence of the excitation.

Sequential pulse transfer via coherent excitation has a major potential drawback: the pulses must place all population into an intermediate state from which spontaneous emission can occur. Thus undesirable population losses occur. It turns out that coherent excitation provides an alternative procedure, one in which (almost) no population resides in state 2, yet (almost) complete population transfer can occur. To understand the possibility we return to an examination of the appropriate TDSE, as following from the Raman Hamiltonian in the RWA.

10.5.2 The Raman Hamiltonian

The coherent dynamics of Raman processes – the coherent flow of population amongst three states – is the same for any three-state chain, whether in lambda or ladder configuration. For definiteness let us consider the lambda linkage pattern, as is appropriate for a stimulated Raman process. Figure 49 shows the energies of the states and the two fields: the pump field P, with frequency ω_P, produces excitation into state 2 from the initially populated state 1. The Stokes field S, with frequency ω_S, produces de-excitation from this intermediate state to the final state 3. The figure shows explicitly the spontaneous emission loss from state 2; the other two states

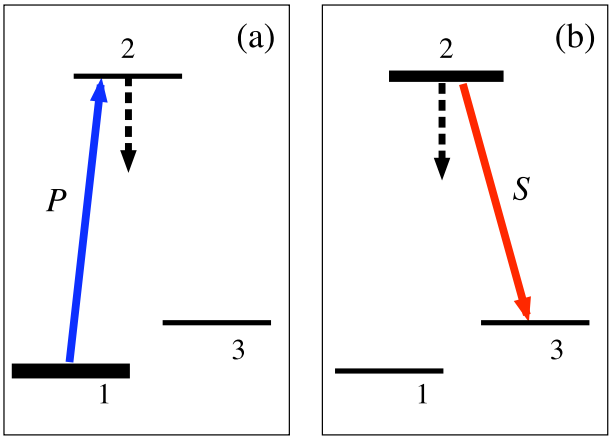

Fig. 48. Population transfer via stimulated Raman transition, intuitive ordering of pulses. (a) The pump pulse places population into the excited state. (b) The Stokes (or dump) pulse moves population into final state. During residence in the excited state some population is lost by spontaneous emission.

are assumed to be stable.

The RWA Hamiltonian for the stimulated Raman processes is basically that of eqn. (237), but with phases suited to the lambda linkage and the allowance for loss from the excited state

$$\mathsf{W}(t) = \begin{bmatrix} 0 & \frac{1}{2}\Omega_P \exp(-\mathrm{i}\varphi_P) & 0 \\ \frac{1}{2}\Omega_P \exp(+\mathrm{i}\varphi_P) & \Delta_P - \mathrm{i}\Gamma & \frac{1}{2}\Omega_S \exp(+\mathrm{i}\varphi_S) \\ 0 & \frac{1}{2}\Omega_S \exp(-\mathrm{i}\varphi_S) & \Delta_P - \Delta_S \end{bmatrix}. \tag{270}$$

Here Γ is the rate at which probability is lost from state 2 and the two detunings are as defined earlier,

$$\hbar\Delta_P = E_2 - E_1 - \hbar\omega_P, \qquad \hbar\Delta_S = E_2 - E_3 - \hbar\omega_S. \tag{271}$$

10.5.3 Stimulated Raman adiabatic passage (STIRAP)

A procedure that does not require either the presence of transient population in state 2, nor the need for careful control of Rabi angles, proceeds via a *counterintuitive* pulse sequence in which the S pulse precedes the P pulse [106]. The procedure is now known as *stimulated Raman adiabatic passage* (STIRAP) [107, 3]. Figure 50 presents several plots that help elucidate the mechanism responsible for the STIRAP technique.

10.6 Explaining STIRAP

The STIRAP dynamics can be understood as a three stage process (first explained to me by K. Bergmann), with time intervals indicated in Fig. 50 as I, II, and III.

I. During the first stage the strong S field acts to produce a dynamic Stark shift such that the weak P field has no effect, see Fig. 45.

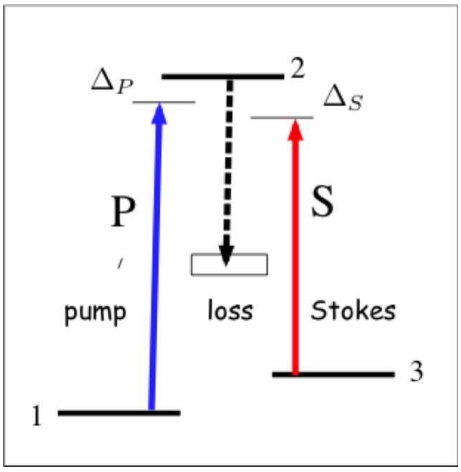

Fig. 49. The stimulated Raman linkage. The P field (pump) links initially populated state 1 with the excited state 2, from which spontaneous emission loss can occur. The S field (Stokes) links the excited state with the metastable state 3. The single-field detunings Δ_P and Δ_S are shown.

II. As the P field becomes stronger, and the S field weaker, the evolution is by means of adiabatic passage. The following paragraphs discuss this regime.

III. In the final stage the the strong P field acts to produce a dynamic Stark shift such that the weak S field has no effect, see Fig. 51.

10.6.1 The dark state

During the intermediate stage of the STIRAP dynamics the time evolution is best described using the three adiabatic states of the RWA Raman Hamiltonian. When the two-photon detuning vanishes ($\Delta_P = \Delta_S$) and the Rabi frequencies are real these eigenstates can be chosen as

$$\Phi_\pm(t) = \frac{1}{\sqrt{2}} \begin{bmatrix} \sin\Theta(t) \\ \pm e^{-\mathrm{i}\alpha} \\ \cos\Theta(t) e^{-\mathrm{i}\beta} \end{bmatrix}, \qquad \varepsilon_\pm = \Delta_P \pm \sqrt{\Delta_P^2 + \Omega_P^2 + \Omega_S^2}, \tag{272}$$

$$\Phi_0(t) = \begin{bmatrix} \cos\Theta(t) \\ 0 \\ -\sin\Theta(t) e^{-\mathrm{i}\beta} \end{bmatrix}, \qquad \varepsilon_0 = 0, \quad \textit{No component of state 2}. \tag{273}$$

Here $\Theta(t)$ is the *mixing angle*, defined through the equation

$$\tan\Theta(t) = \Omega_P(t)/\Omega_S(t), \tag{274}$$

and the phases are those of the fields,

$$\alpha \equiv \varphi_P, \qquad \beta \equiv \varphi_P - \varphi_S. \tag{275}$$

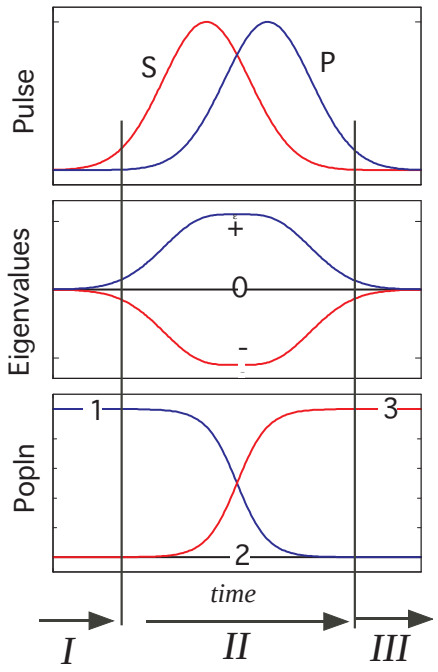

Fig. 50. The STIRAP process. Top frame: the S and P pulse sequence, with S preceding but overlapping with P. Middle frame: the adiabatic eigenvalues vs. time. Bottom frame: population histories. Along the bottom appear labels I, II and III of the three regimes discussed in the following section. [after Fig. 3 of Bergmann et al. Rev. Mod. Phys. **70** 1003 (1998)]

It is generally possible to set $\alpha_S = 0$, because absolute phases are uncontrollable. Only if both pulses derive from the same laser field (i.e. states 1 and 3 are degenerate) through optical elements is the phase difference $\varphi_P - \varphi_S$ controllable.

Notably the null-eigenvalue adiabatic state has no component of the excited state ψ_2. Therefore it cannot fluoresce; it is a *dark* state [108]. It has the construction (in the rotating coordinate basis)

$$\Phi_0(t) = \frac{\Omega_S(t)\psi_1 - \Omega_P(t)e^{-\mathrm{i}\beta}\psi_3(t)}{\sqrt{|\Omega_P|^2 + |\Omega_S|^2}} = \cos\Theta(t)\psi_1 - \sin\Theta(t)e^{-\mathrm{i}\beta}\psi_3(t). \tag{276}$$

For the STIRAP pulse sequence, of Stokes preceding pump, this adiabatic state has the following properties

We see that if we can ensure that the time evolution is adiabatic, then the statevector $\Psi(t)$ follows the adiabatic state $\Phi_0(t)$ and population transfers $1 \to 3$. The final state acquires a phase, $e^{-\mathrm{i}\beta}$, that depends on the difference between P and S field phases. Unless the two fields derive from a common laser field (so $\omega_P = \omega_S$), this is a value fixed by our arbitrary choice of initial phases, and can be taken as zero; any other choice merely implies a redefinition of Hilbert-space coordinates. Figure 52 illustrates the Hilbert-space motion of this time dependence.

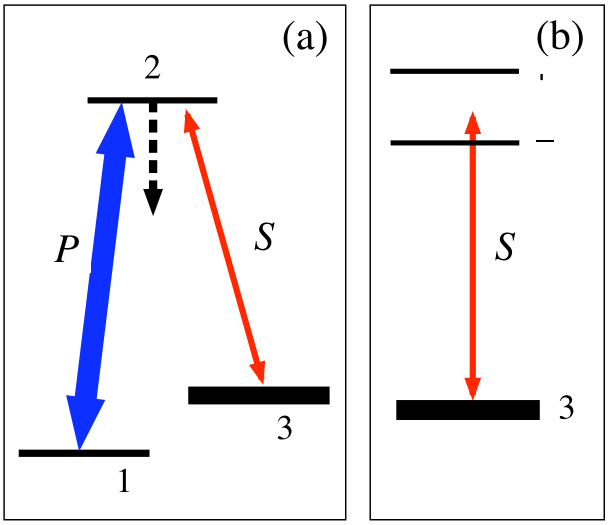

Fig. 51. Final stage of STIRAP. (a) Strong P field, weak S field, after population has been transferred adiabatically to state 3. (b) Dressed-state picture: the P field acts to split the resonance transition for the weak S field, thereby preventing population transfer from state 3 to the excited state 2.

Initially only S field	Finally only P field
$\Omega_P(t) = 0$	$\Omega_S(t) = 0$
$\Phi_0(t) = \psi_1$	$\Phi_0(t) = -e^{-\mathrm{i}\beta}\psi_3$
initial state	*target state*

10.6.2 The adiabatic conditions

Section 6.6 discussed an example of the conditions that must hold for time evolution to be adiabatic in a two-state system. Similar conditions apply for multistate systems. To determine the conditions needed for the adiabatic evolution of the STIRAP process we proceed as in Sec. 6.6 and express the statevector as a superposition of adiabatic states,

$$\Psi(t) = \Sigma_k A_k(t)\Phi_k(t). \tag{277}$$

With the aid of the TDSE we obtain an equation of motion for the amplitudes $A_k(t)$,

$$\frac{d}{dt}\mathbf{A}(t) = -\mathrm{i}\mathsf{W}^A(t)\mathbf{A}(t), \tag{278}$$

where $\mathsf{W}^A($ has as diagonal elements the adiabatic eigenvalues,

$$W^A_{kk}(t) = \varepsilon_k(t), \tag{279}$$

and has as off-diagonal elements the *nonadiabatic couplings*,

$$W^A_{km}(t) = \langle\Phi_k(t)|\dot{\Phi}_m(t)\rangle. \tag{280}$$

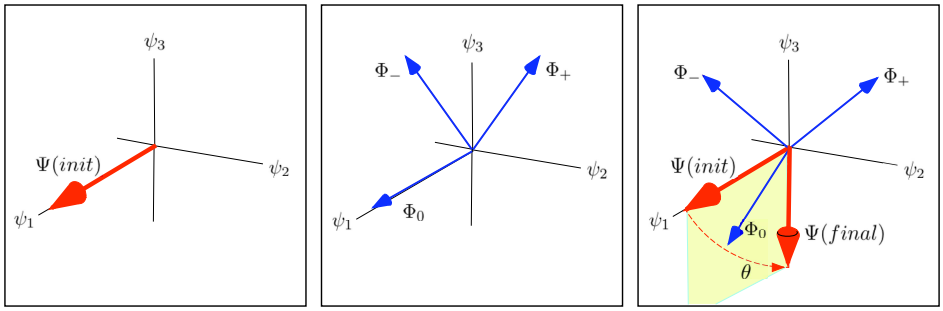

Fig. 52. Three-state system. Left: Initial statevector. Center: Initial adiabatic states. Right: Motion of adiabatic states and statevector.

To assure adiabatic following we require that these off-diagonal elements be much smaller than the separation of diagonal elements. (Note that this criterion cannot be fulfilled when the eigenvalues are degenerate.)

The important nonadiabatic coupling term for STIRAP is

$$\langle \Phi_\pm(t)|\dot{\Phi}_0(t)\rangle = \dot{\Theta}/\sqrt{2}. \tag{281}$$

This must be compared with the eigenvalue separation

$$|\varepsilon_\pm - \varepsilon_0| = \sqrt{\Omega_P^2 + \Omega_S^2} \equiv \widetilde{\Omega}. \tag{282}$$

From these expressions we deduce the *local* requirement

$$\left|\dot{\Omega}_P\Omega_S - \Omega_P\dot{\Omega}_S\right| \ll \widetilde{\Omega}^2. \tag{283}$$

A *global* requirement, derived by requiring that the overall nonadiabatic coupling remain small, is that the time integral of $\widetilde{\Omega}$ should be large – typically more than 10π.

10.7 Demonstrating STIRAP

Several types of experiments demonstrate the STIRAP mechanism [109]. These rely on observing some indicator of population transfer while varying such parameters as the time delay between S and P pulse, or the detuning of one of the fields.

10.7.1 Vary pulse delay

A particularly clear demonstration makes use of controlled temporal separation of the P and S pulses while holding fixed the frequencies such that the two-photon resonance condition holds. Figure 53 presents results obtained with a molecular beam; the needed temporal delay was obtained by altering the physical position of the S and P laser beams through which the molecular beam passed at a right angle. In this experiment a subsidiary laser field servers to probe the final population transfer. When the S field precedes the P field, as occurs toward the left-hand side of the figure, it has no effect on the dynamics. Population transfer occurs via excitation followed by

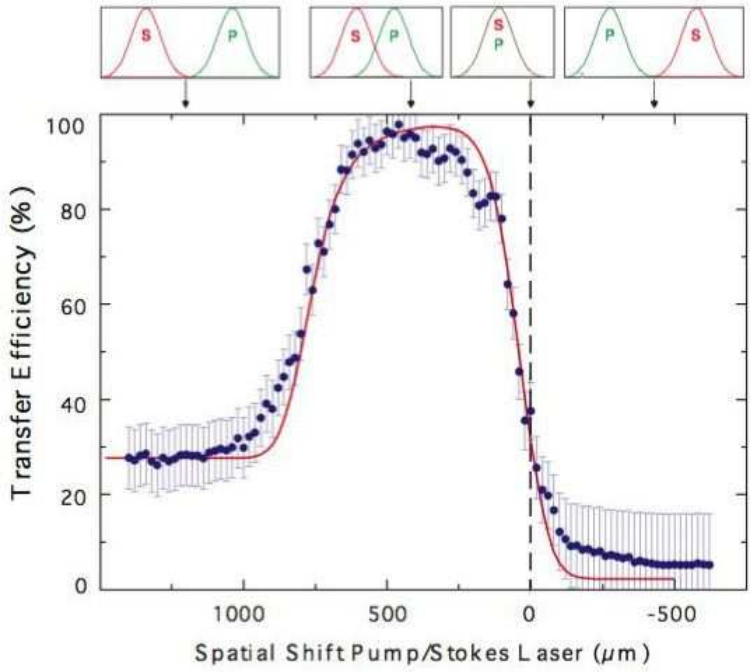

Fig. 53. Population transfer via stimulated Raman process, as a function of spatial separation between S and P laser beams (and hence delay between S and P pulses, as indicated with small inserts along the top). Positive values of separation correspond to S preceding P. [after Fig. 9 of Bergmann et al. Rev. Mod. Phys. **70** 1003 (1998)]

spontaneous emission (an example of FCP). When the P field precedes the S, as at the right-hand side, then any population transfer produced by the P field is reversed by the S field. The maximum transfer occurs, not when the pulses coincide, but when the S field precedes, and overlaps, the P field. This type of plot is a clear indicator of $STIRAP$.

10.7.2 Vary P detuning: The dark resonance

By monitoring the fluorescence from the excited state 2 we obtain a direct measure of population placed there by the P field. In the absence of the S field this fluorescence signal, as a function of P-field detuning, exhibits a Lorentz profile whose width originates with the lifetime of the excited state. When the S field is present and two-photon detuning occurs the population transfer takes place through the dark adiabatic state: no population enters the excited state. The result is a "dark" resonance, as seen in Fig. 54, The spectral width of this narrow feature is the two-photon linewidth.

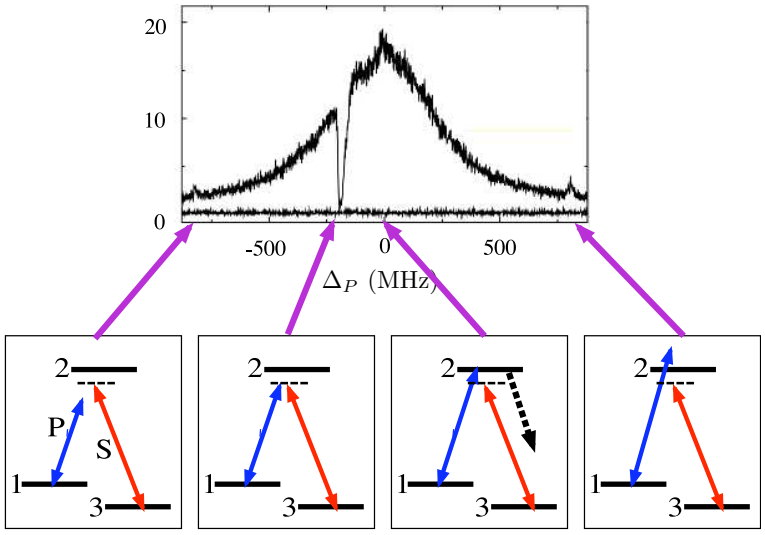

Fig. 54. The STIRAP dark resonance: fluorescence signal from state 2 vs. detuning of P field. The P field takes population into state 2, from which it produces a fluorescence signal. When the P and S fields satisfy the two-photon resonance condition population transfers directly to state 3 without passing through state 2: there is then no fluorescence signal. Frames along the bottom show the changing detuning of the P laser. [after Fig. 8 of Bergmann et al. Rev. Mod. Phys. **70** 1003 (1998)]

10.7.3 Vary P detuning: The bright resonance

The STIRAP process transfers population only when the P and S frequencies satisfy the two-photon resonance condition. One can monitor the success of this transfer by inducing a transition from state 3 (the final state of the STIRAP process) into a fourth state, using a D field, from which fluorescence produces a signal. This signal will be present even in the absence of the S field, because the P field produces excitation whose spontaneous emission populates state 3, and hence leads to a fluorescence signal. However, the population transfer to state 3 is much larger when a stimulated Raman transition assists that transfer, as occurs when there is a two-photon resonance.

Figure 55 illustrates this effect. This demonstration monitored the fluorescence from state 4 of an excitation chain that begins with initially populated state 1, and relies on the sequence of P, S and D fields to produce this fluorescence. In the absence of any resonance with the S field, the P field excites population into state 2, which spontaneously decays to state 3, from which the D field carries the population into state 4, whose fluorescence produces the signal. The dependence of this signal on pump detuning traces out the natural width of the 1-2 transition. Only a portion of the decays place population into state 3, from which the subsequent fluorescence signal derives.

When the S field is present there will occur, when the P and S fields together satisfy the two-photon resonance condition (within the narrow limits of the two-photon linewidth), a more

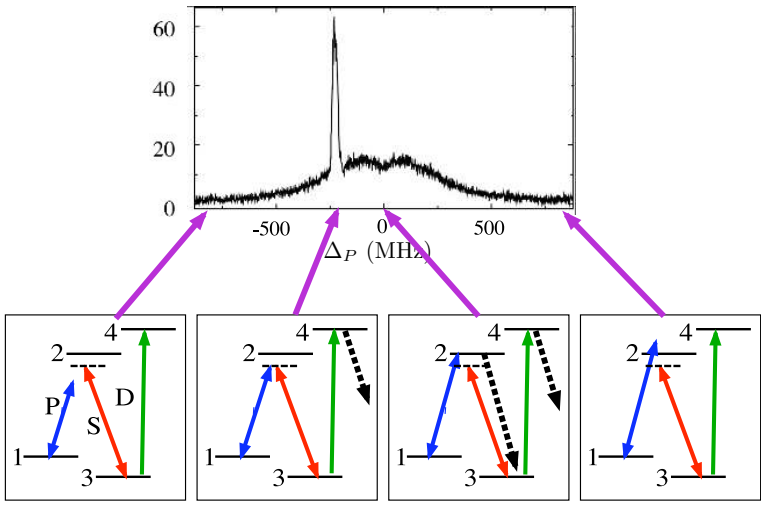

Fig. 55. The STIRAP bright resonance: fluorescence signal from state 4 vs. detuning of P field. A probe field D moves population into state 4 from state 3. Population can arrive into state 3 either when the P and S fields satisfy the two-photon resonance condition, or when the P field places population resonantly into state 2, from which it decays to state 3. Frames along the bottom show the changing detuning of the P laser. [after Fig. 2 of Bergmann et al. Rev. Mod. Phys. **70** 1003 (1998)]

complete transfer of population into state 3. This produces a narrow bright line in the fluorescence signal as a function of P-field frequency.

10.8 STIRAP extensions

The basic three-state STIRAP has been extended in many ways, both theoretically and experimentally, to systems that involve more than three states[3, 107]. In all of these generalizations there occurs a pulse sequence that induces adiabatic transfer. The following sections describe a few of these.

10.8.1 STIRAP with sublevles

The idealization of adiabatic passage in a three-state system readily generalizes in several ways to treat the degeneracy, or near degeneracy, that occurs with magnetic sublevels [110]. Figure 56 shows an example of the most general linkage pattern that occurs with a three-level system in which the linkages begin in a state $J = 0$, proceed via P field into sublevels of $J = 1$, and then by S field to sublevels of $J = 2$. Such linkage patterns have been studied in excitation of metastable neon [111]. When a static magnetic field is present the natural coordinate system is one in which the quantization axies lies along the direction of that field. By suitably choosing the laser propagation axis, and polarization, it is possible to have each of the linkages of Fig. 56 present. The magnetic field produces a Zeeman shift of the sublevels, so that only particular linkages are resonant. Thus with fixed laser polarization it is possible, by altering only the

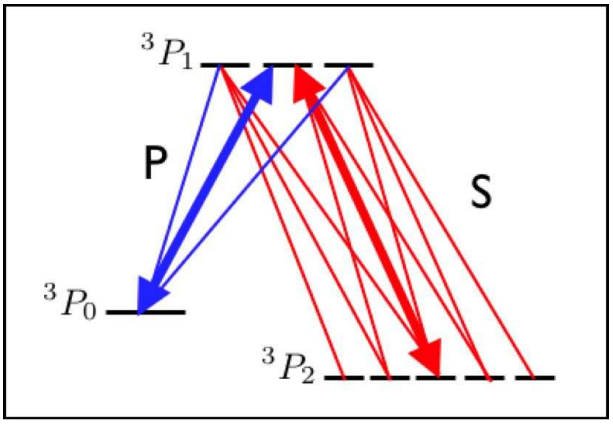

Fig. 56. Linkage patterns available with suitable polarization choices in the $J = 1 \leftrightarrow J = 0 \leftrightarrow J = 1$ of metastable neon. When there is no magnetic field the Zeeman sublevels are degenerate; the choice of polarization then selects the transitions or superpositions of transitions that will be active. When a magnetic field is present the Zeeman sublevels are not degenerate, and the two-photon resonance condition picks out only a single lambda linkage from the array off possibilities shown.

frequencies of the light, to place population into any selected sublevel of $J = 2$ via STIRAP-like adiabatic passage [111].

10.8.2 Degenerate STIRAP

The presence of magnetic sublevels makes possible a number of interesting applications of STIRAP to degenerate Raman transitions. A simple extension is the linkage pattern available with a $J = 1$ to $J = 0$ excitation transition with arbitrary polarization, cf. Fig. 57(a). This has a tripod linkage pattern, discussed in Sec. 10.9.

The transition $J = 2 \leftrightarrow 1$ has, for elliptically polarized light and quantization axis along the propagation direction, cf. Fig, 57(b), two sets of linkages: a three-state lambda (involving $M = \pm 1$ of $J = 2$) and a five-state letter-M pattern (involving $M = 0, \pm 2$ of $J = 2$). When spontaneous emission can be neglected these two sets are independent.

The lambda and letter-M linkages generalize to a linkage pattern in which a single S field alternates with a single P field to produce a chain involving degenerate ground states and degenerate excited states, as shown in Fig. 58. Preliminary optical pumping with circularly polarized light can place all the population into the state at one end of the chain, say the $M = -J$ state. With this as the single initial state, the usual S-P pulse sequence will transfer all population to the other end of the chain. There will never occur population in the excited state, although at intermediate times the population will be distributed amongst the ground sublevels. The underlying theory, for chains of arbitrary length, has been discussed in several papers [112].

Atomic beams of metastable neon atoms have provided many opportunities to demonstrate STIRAP process. Early work [111] demonstrated the use of STIRAP, with appropriately chosen polarizations, to produce complete population transfer into a single selected final magnetic

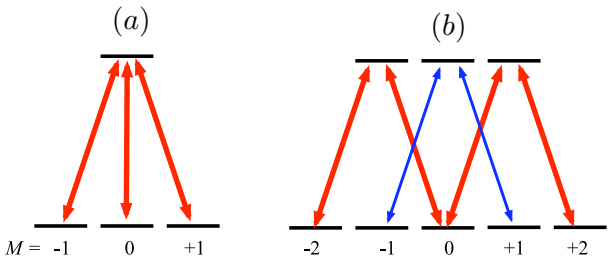

Fig. 57. (a) Linkage pattern for $J = 1$ to $J = 0$ with general polarization – the propagation directions of the three fields cannot all be parallel. The links form a tripod. (b) Linkage pattern for transition $J = 2$ to $J = 1$ available with elliptically polarized light, with quantization axis along propagation direction. There are two independent systems: a three-state lambda (light blue lines) and a five-state letter-M (heavy red lines).

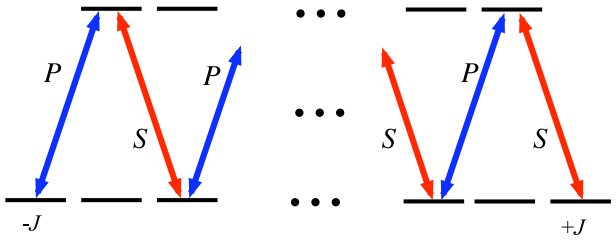

Fig. 58. A chain of P and S linkages in a degenerate system of Zeeman sublevels for integer J, starting from $M = -J$. A STIRAP-like $S - P$ pulse sequence will transfer all population from $M = -J$ to $M = +J$.

sublevel. More recently it has been shown [113] that any degenerate three-level system can be reduced to a set of independent three-state chains, within each of which STIRAP can be implemented.

10.9 The tripod linkage

The inclusion of one additional linkage from the excited state, using a third field, produces a *tripod* linkage pattern. Exact adiabatic eigenstates are known for the tripod system, and its properties have been discussed in several papers [114, 115]. Such a pattern occurs with the $J = 1$ to $J = 0$ excitation transition with arbitrary polarization. Figure 59 shows the labeling of states and fields used in the following; state 1 is the excited state while states 2-4 are low-lying metastable states.

To make the needed RWA we introduce a rotating and phased basis, taking $E_1 = 0$ as the reference energy,

$$\psi_1'(t) \quad = \quad \mathrm{e}^{-\mathrm{i}\varphi_P}\psi_1, \tag{284}$$

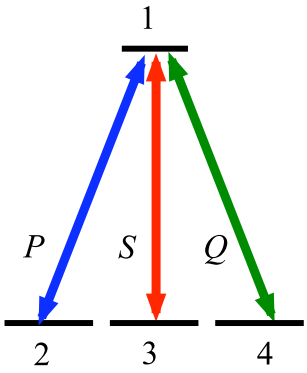

Fig. 59. Linkage pattern for tripod system, showing labeling convention for states and fields. The states 2-4 need not be degenerate, but they are here assumed to be resonant with the linking field.

$$\psi_2'(t) = \mathrm{e}^{+\mathrm{i}\omega_P t}\psi_2, \tag{285}$$
$$\psi_3'(t) = \mathrm{e}^{+\mathrm{i}\omega_S t}\mathrm{e}^{\mathrm{i}(\varphi_P-\varphi_S)}\psi_3, \tag{286}$$
$$\psi_4'(t) = \mathrm{e}^{+\mathrm{i}\omega_Q t}\mathrm{e}^{\mathrm{i}(\varphi_P-\varphi_Q)}\psi_4, \tag{287}$$

where φ_k is the phase of field envelope $\mathcal{E}_k(t)$. This construction makes any superposition of states 2, 3, 4 dependent only on phase differences $\varphi_P - \varphi_S$ and $\varphi_P - \varphi_Q$ [69]. We here assume all fields are resonant, so that $E_2 + \hbar\omega_P = E_3 + \omega_S = E_4 + \omega_Q$, and the Hamiltonian is the *bordered* matrix

$$\mathsf{W}(t) = \frac{1}{2}\begin{bmatrix} 0 & \Omega_P(t) & \Omega_S(t) & \Omega_Q(t) \\ \Omega_P(t) & 0 & 0 & 0 \\ \Omega_S(t) & 0 & 0 & 0 \\ \Omega_Q(t) & 0 & 0 & 0 \end{bmatrix}. \tag{288}$$

This Hamiltonian has four eigenstates. Two of them are dark states (lacking a component in state 1). These can be taken as [114]

$$\Phi_1^D(t) = \begin{bmatrix} 0 \\ \cos\Theta(t) \\ -\sin\Theta(t) \\ 0 \end{bmatrix}, \quad \Phi_2^D(t) = \begin{bmatrix} 0 \\ \sin\phi(t)\,\sin\Theta(t) \\ \sin\phi(t)\cos\Theta(t) \\ \cos\phi(t) \end{bmatrix}, \tag{289}$$

where

$$\tan\Theta(t) = \frac{\Omega_P(t)}{\Omega_S(t)}, \quad \tan\phi(t) = \frac{\Omega_Q(t)}{\sqrt{\Omega_P(t)^2 + \Omega_S(t)^2}}. \tag{290}$$

[69] Unless the several fields derive, via coherent optical manipulations, from a single laser field, these phases are uncontrollable and can be taken to be zero, a choice associated with the arbitrary choice of the moment of zero crossing of each electric field.

Each of these has a null eigenvalue. Because these states are degenerate one must consider the general dark state

$$\Phi(t) = D_1(t)\Phi_1^D(t) + D_2(t)\Phi_2^D(t). \tag{291}$$

When such a state describes the initial condition, and the motion is adiabatic, then only these two states contribute to $\Psi(t)$, but they are resonantly coupled. Let us assume the initial population resides in state 2, and that this initially coincides with state $\Phi_1(t)$. We further suppose the identification after the pulse sequence of $\Phi_1(t) = \psi_2(t)$ and $\Phi_2(t) = \psi_3(t)$. Then the result of adiabatic passage is the superposition

$$\Psi(t) = \cos\Theta_\infty \psi_2(t) + \sin\Theta_\infty \psi_3(t), \tag{292}$$

where the asymptotic mixing angle is

$$\Theta_\infty = \int_{-\infty}^{+\infty} dt\ \sin\phi(t)\frac{d}{dt}\Theta(t) = -\int_{-\infty}^{+\infty} dt\,\Theta(t)\frac{d}{dt}\sin\phi(t). \tag{293}$$

Note that, from the definition of $\psi_3(t)$, the superposition depends on the phase difference $\varphi_P - \varphi_S$ between the S and P fields. When $\omega_P = \omega_S \equiv \omega$ the superposition reads, in the nonrotating basis,

$$\Psi(t) = \mathrm{e}^{-\mathrm{i}\omega t}\left[\cos\Theta_\infty\psi_2 + \sin\Theta_\infty \mathrm{e}^{\mathrm{i}(\varphi_P-\varphi_S)}\psi_3\right]. \tag{294}$$

Thus the superposition is stationary.

11 Multilevel excitation

A variety of extensions and generalizations of two- and three-state excitation hold interest, either theoretically or for applications. As the number of quantum states increases, so too do the variety of linkage patterns. In many of these cases it is possible to introduce a generalization of the RWA such that the Hamiltonian has detunings as diagonal elements and slowly varying Rabi frequencies as the off-diagonal elements [116] [2, §14.2]. The slow variation allows procedures based on either Rabi oscillations (e.g. generalizations of π pulses) or adiabatic evolution (generalizations of RAP or STIRAP). The following sections provides an overview of several multi-state coherent excitation models, treated with a generalized RWA [2, Chap. 14].

11.1 Chains

The simplest extensions of two- and three-state RWA equations are those for a single chain of interactions, in which each state links to no more than two other states (nearest neighbors) and no loops occur [2, Chap. 15]. In the RWA the relative ordering of the bare energies is irrelevant; the ladder and the "letter-N" linkage of Fig. 60 are equivalent [70].

The general rotating-wave coordinate system for the ladder system is

$$\psi_1'(t) = \psi_1, \tag{295}$$
$$\psi_2'(t) = \exp(-\mathrm{i}\,\omega_P t)\psi_2, \tag{296}$$
$$\psi_3'(t) = \exp(-\mathrm{i}\,\omega_P t - \mathrm{i}\,\omega_S t)\psi_3, \tag{297}$$
$$\psi_4'(t) = \exp(-\mathrm{i}\,\omega_P t - \mathrm{i}\,\omega_S t - \mathrm{i}\,\omega_Q t)\psi_4. \tag{298}$$

The letter-N linkage pattern uses similar rotating coordinates, but with opposite sign for ω_S. For a general chain, the rotating coordinates take the form

$$\psi_n'(t) = \exp(-\mathrm{i}\,\omega_1 t - \cdots - \mathrm{i}\,\omega_{n-1} t)\psi_n. \tag{299}$$

[70] What matters, in addition to the values of the RWA Hamiltonian elements, is the *graph* structure; cf. Appendix B.8.

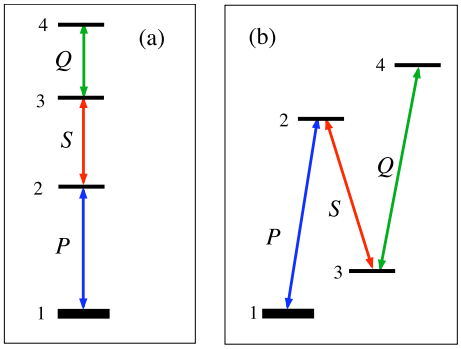

Fig. 60. Equivalent linkages for four-state chains with three interaction P, S and Q: (a) a ladder (b) and "letter-N" linkage.

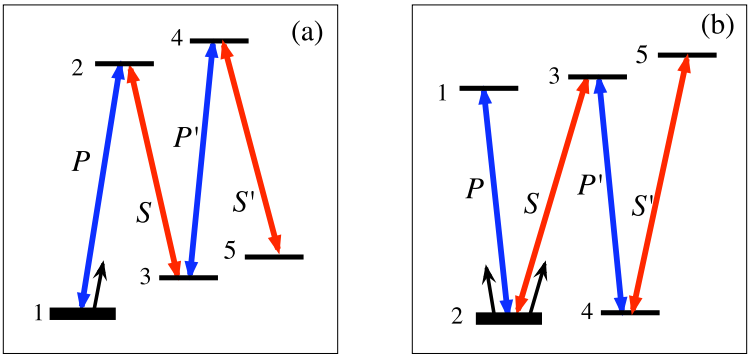

Fig. 61. Five-state chain. (a) Arranged in letter-M pattern, showing links from fields P, P', S and S'. (b) The letter-W linkage. Here population initially resides in one of the intermediate states, and proceeds initially toward two states, as indicated by short arrows; subsequently interference occurs. In both cases the vertical positions of the energy levels in the diagram is irrelevant for the RWA linkage.

The condition required for the general N-state RWA is that the sum and frequency differences $\omega_n \pm \omega_m$ all be either zero or large compared with the inverse of a characteristic time scale for statevector evolution (i.e. the Rabi frequencies). When these conditions hold, one can employ a generalized RWA and obtain the equations

$$\frac{d}{dt}C_n(t) = -\mathrm{i}\Delta_n C_n(t) - \frac{\mathrm{i}}{2}\Omega_n(t)C_{n-1} - \frac{\mathrm{i}}{2}\Omega_{n+1}(t)C_{n+1}. \tag{300}$$

That is, the RWA Hamiltonian matrix for a simple chain (involving nearest-neighbor couplings) is *tri-diagonal*.

Interesting differences occur between chains having an even number of states, e.g. the $N = 4$ linkages shown in Fig. 60, and those with an odd number of states, e.g. the $N = 5$ linkage of the letter-M pattern of Fig. 61(a). In these odd-N systems it is possible to implement a variant of the STIRAP procedure to produce complete population transfer between terminal states of the chain [112].

Although the RWA Hamiltonian has the same tridiagonal structure for any four-state chain, the dynamics will differ significantly if the population starts in one of the intermediate states of the chain (states 2 or 3) rather than a terminal state (1 or 4). As an example, the letter-W linkage of Fig. 61(b) places initial population into one of the intermediate states of the chain, from which it departs along two distinct paths; subsequent interference occurs when population returns.

When the RWA Hamiltonian is constant there exist known analytic solutions for a number of Rabi-frequency sequences, even with detuning [117]. The connection with conventional special functions and classical polynomials [118] occurs through the three-term recurrence relationship which follows from the tri-diagonal form of the RWA Hamiltonian when one seeks the eigenstates and eigenvalues [2, §15.3]. Table 1 lists some of these soluble cases.

. .

Plots of the population histories resemble fluid flow along the chain[2, §15.5]. However, the time varying population distribution along a chain does not always appear as a localized

Tab. 1. Some multistate chains for which solutions are expressible in terms of well-known polynomials

	Δ_n	Ω_n	Polynomial
Uniform	$n\Delta_0$	Ω_0	
Linear	$(2n+1)\Delta_0$	$n\,\Omega_0$	Chebyshev
Harm. Osc.	0	$\sqrt{n}\,\Omega_0$	Hermite
Psueudospin	$\Delta_0 + n\Delta_1$	$\sqrt{n(N-n)}\,\Omega_0$	Trig power
Makarov	0	$\Omega_0 \,/\, \sqrt{n+1}$	Charlier
Decreasing	0	$\Omega_0 \,/\, \sqrt{4-(1/n^2)}$	Legendre

wavepacket. The precise behavior depends upon the sequences of Rabi frequencies. For some choices the wavepacket may undergo such severe alteration as to be unrecognizable after a short time. Other sequences of Rabi frequencies produce exactly periodic behavior, in which the initial state repeatedly receives all the population, albeit with a phase change; cf. Sec. 11.3.

When the detunings are all resonant, population flows from the initial state 1 along the chain to the end of the chain, whereupon it returns (but only with specific choices for Rabi frequencies will this be complete and hence periodic). Figure 62 presents examples of such resonant behavior, for excitation in which all Rabi frequencies are equal.

As mentioned above, when population starts in an intermediate state of the chain it can flow initially in two directions. Figure 63 illustrates an example, for the letter-W system of Fig. 61(b). Note that, as in the right-hand frame of Fig. 62, the population in state 3 varies sinusoidally. In general the N-state solutions (with constant RWA Hamiltonian) are not periodic; Sec. 11.3 discusses an exception.

11.1.1 Harmonic oscillator

The harmonic oscillator, driven by dipole coupling of arbitrary time dependence, is one of the soluble quantum systems widely studied [119][2, § 15.1]. It has an infinite number of evenly spaced nondegenerate energy levels, and so a single laser field will have an RWA Hamiltonian with detunings

$$\Delta_n = n\Delta_1. \tag{301}$$

The linkage pattern is tri-diagonal (i.e. nearest-neighbor couplings), with Rabi frequencies that increase monotonically,

$$\Omega_n(t) = \sqrt{n}\,\Omega_1(t). \tag{302}$$

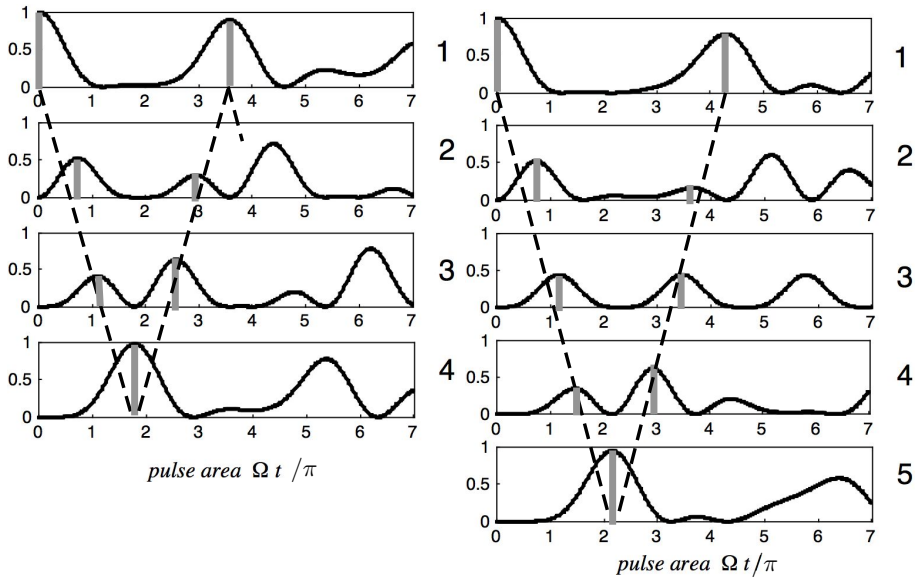

Fig. 62. Resonant population flow, starting from state 1, with equal and constant Rabi frequencies, for chains with length $N = 4$ (left) and $N = 5$ (right). Dashed lines, connecting vertical bars, show time variation of peak populations; these increase nearly linearly with time to the end of the chain, whereupon they reverse. Note that population does not return completely to the initial state 1; the population changes are not periodic (except for state $n = 3$ of $N = 5$).

When the field is steady, population placed into state 1 will pass successively toward states of higher excitation. Eventually the detuning, if present, will become so large that the next-step Rabi frequency will not produce further excitation; states that are further along the chain will receive small or negligible excitation. The turning point for the excitation occurs when the cumulative detuning Δ_n exceeds the Rabi frequency Ω_n [2, § 15.10]. The population return to the initial state is not complete; the behavior is not periodic.

When the excitation is resonant in the first step, it will be resonant for all subsequent steps, and population will pass toward ever higher excitation. This progress must eventually end for any real system. Typically this occurs because the model system has anharmonicity, so that the energy levels become closer together with increasing excitation. Then the cumulative detuning will eventually overcome the Rabi frequency, and excitation will progress no further. Alternatively, the excitation will lead to dissociation and consequent probability loss from the discrete states.

11.1.2 Two-state behavior in an N-state chain

Some N-state chain systems, describable by a constant tri-diagonal RWA Hamiltonian, exhibit dynamics of a simple two-state system, characterized by Rabi oscillations between states 1 and N, with negligible excitation present in other states [120].

One such case occurs when the intermediate cumulative detunings are all much larger than

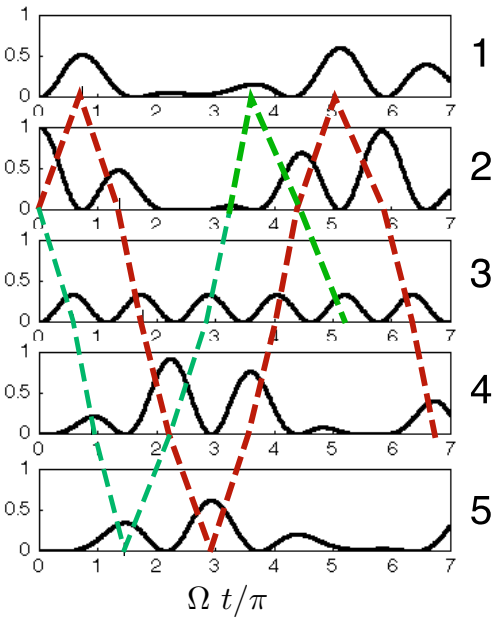

Fig. 63. Population flow in the 5-state W system. Population starts in state 2, and flows in two directions, as marked by the red and green dashed lines. Only state 3 has periodic population history.

the various Rabi frequencies or the final-step cumulative detuning δ [2, §18.7]:

$$\Delta_n = \{0, \Delta_2, \Delta_3, \ldots, \Delta_{N-1}, \delta\}, \quad \Omega_n = \{\Omega_1, \Omega_2, \ldots, \Omega_{N-1}\}. \tag{303}$$

The system then behaves, for initial population in either state 1 or N, as a two state system, with effective detuning and Rabi frequency given as the constructions

$$\widetilde{\Delta} = \delta + \frac{|\Omega_{N-1}|^2}{4\Delta_{N-1}} - \frac{|\Omega_1|^2}{4\Delta_1}, \qquad \widetilde{\Omega} = \frac{1}{2^{N-2}} \frac{\Omega_1 \Omega_2 \cdots \Omega_{N-1}}{\Delta_2 \Delta_3 \cdots \Delta_{N-1}}. \tag{304}$$

The two-state system undergoes an $(N-1)$-photon excitation, subject to dynamic Stark shifts.

A second example occurs when each step of the chain is resonant, except possibly the last, and the two chain-terminating Rabi frequencies are much smaller than all others [2, §18.7]. The detunings and Rabi frequencies fit the pattern

$$\Delta_n = \{0, 0, 0, \ldots, 0, \delta\}, \qquad \Omega_n = \{S_1, L_1, L_2, \ldots, L_{N-2}, S_{N-1}\}. \tag{305}$$

When the number of states is an even integer and the large elements are much larger than the small elements, $|L_n| \gg |S_k|$, the dynamics is that of a two state system that has the original N-state detuning δ and has an effective Rabi frequency which is the ratio of products of odd numbered Rabi frequencies to even-numbered frequencies,

$$\widetilde{\Delta} = \delta, \qquad \widetilde{\Omega} = \frac{S_1 L_3 L_5 \cdots L_{N-3} S_{N-1}}{L_2 L_4 \cdots L_{N-2}}. \tag{306}$$

11.2 Time averaged populations

Observations which take place during many Rabi cycles, yet still within a time interval that allows little loss of probability or coherence, sample time-averaged populations. Such a situation also occurs when we have an ensemble of atoms, each of which undergoes many Rabi cycles, but with an appreciable variation in the Rabi angle. We calculate the appropriate probabilities from the averaging integral

$$\bar{P}_n(T) = \frac{1}{T}\int_0^T dt|C_n(t)|^2 \tag{307}$$

as the limit, over many Rabi cycles,

$$\bar{P}_n = \mathrm{Lim}_{T\to\infty}\bar{P}_n(T). \tag{308}$$

When the illumination is steady the desired values can be obtained from the eigenvalues and eigenvectors of the RWA Hamiltonian that governs the time evolution [2, §15.9]. When plotted as a function of detuning, such averages reveal the presence of multiphoton resonances [2, §15.11].

A simple case is a fully resonant chain (a tridiagonal RWA Hamiltonian with null diagonal elements) in which all the Rabi frequencies are constant and equal. When the initial state is m the average probability for state n is [2, §15.9]

$$\bar{P}_n = \frac{1}{N+1}\left[1 + \frac{1}{2}\delta_{n,m} + \frac{1}{2}\delta_{n,N+1-m}\right]. \tag{309}$$

The probability is uniformly distributed amongst all states, as befits chaotic behavior, apart from an enhancement (by a factor $3/2$) of the initial state m and its "mirror image" $N+1-m$. When the system is initially at one end of the excitation chain, then it is the upper end of the chain that has this enhancement.

11.3 The pseudospin model

An interesting multistate excitation chain occurs when there are N states, coupled only between adjacent states so that the RWA Hamiltonian is tridiagonal, and with elements [121][2, §18.6]

$$W_{nn} = n\Delta_1 + \Delta_0, \tag{310}$$

$$W_{n+1,n} = \tfrac{1}{2}\Omega_0\sqrt{n(N-n)}. \tag{311}$$

Here Ω_0 is allowed to be complex valued. The sequences of Rabi frequencies are slightly larger at the center of the chain than at the ends, for example

$$\begin{aligned}
N = 2: &\qquad \Omega_0\{1\},\\
N = 3: &\qquad \Omega_0\{\sqrt{2},\ \sqrt{2}\},\\
N = 4: &\qquad \Omega_0\{\sqrt{3},\ \sqrt{4},\ \sqrt{3}\},\\
N = 5: &\qquad \Omega_0\{\sqrt{4},\ \sqrt{6},\ \sqrt{6}\,\sqrt{4}\}.
\end{aligned}$$

The structure of these matrix elements is identical to what occurs when expressing the interaction of a magnetic moment (proportional to angular momentum $\mathbf{S}$) with a steady magnetic field $\mathbf{B}$. That is, the interaction is expressible in the form of a scalar product,

$$\mathsf{W} = \widetilde{\Omega}_x \mathsf{S}_x + \widetilde{\Omega}_y \mathsf{S}_y + \widetilde{\Omega}_z \mathsf{S}_z \equiv \widetilde{\mathbf{\Omega}} \cdot \mathbf{S}. \tag{312}$$

The Cartesian components S_k are three $N \times N$ matrix representations of the group $SU(N)$, i.e. spin matrices in N dimensions, cf. Appendix C.2. The part of the magnetic vector is here taken by the vector $\widetilde{\mathbf{\Omega}}$, defined by the Cartesian components

$$\widetilde{\Omega}_x = \text{Re}\,(\Omega_0) \equiv \Omega_R, \quad \widetilde{\Omega}_y = \text{Im}\,(\Omega_0) \equiv \Omega_I, \quad \widetilde{\Omega}_z \equiv \Delta_1, \tag{313}$$

in an abstract three-dimensional space. This form of interaction produces a rotation of the statevector, an N-dimensional analog of the rotation of the Bloch vector. The magnitude of the angular velocity vector,

$$|\widetilde{\mathbf{\Omega}}| = \sqrt{\Delta_1^2 + |\Omega_0|^2}, \tag{314}$$

defines a rotation rate: it is the *rms* value of the detuning Δ_1 and the Rabi frequency Ω_0. That is, the system is equivalent to a spin angular momentum, S, such that the number of states is $N = (2S + 1)$. We identify the *n* th state (with $n = 1, 2, \ldots, N$) as being a particular magnetic substate, labelled by the eigenvalue M (with $M = -S, \ldots, +S$) of the matrix S_z. The correspondence is

$$N = 2S + 1, \qquad S = \tfrac{1}{2}(N - 1), \tag{315}$$

$$n = M + I + 1, \qquad M = n - \tfrac{1}{2}(N + 1). \tag{316}$$

The RWA Hamiltonian can be diagonalized by rotating the vector $\widetilde{\mathbf{\Omega}}$ onto the vertical axis, using the two Euler angles α and β

$$\tan(\alpha) = \text{Im}\,(\Omega_0)/\,\text{Re}\,(\Omega_0), \qquad \tan(\beta) = |\Omega_0|/\Delta_1. \tag{317}$$

In this coordinate system the Hamiltonian appears as a constant multiple of the angular momentum operator $\mathsf{S}_{z'}$

$$\mathsf{W}' = |\tilde{\mathbf{\Omega}}| J_z \equiv Z_0 \mathsf{S}_{z'}. \tag{318}$$

It follows that the eigenvalues of W have the form

$$Z_M = M|\widetilde{\mathbf{\Omega}}| \equiv M Z_0, \tag{319}$$

where M takes integer (or half-integer) values ranging from -S to +S in unit steps. Thus all the eigenvalues of W are multiples of the basic frequency unit $Z_0 \equiv |\widetilde{\mathbf{\Omega}}|$, and so the eigenstates are completely periodic.

The eigenstates of W are angular momentum states in the rotated coordinate system. Referred back to the original basis they are

$$|\hat{\mathbf{\Omega}}; S, M\rangle = \Sigma_{M'} |S, M'\rangle \mathcal{D}^{(S)}_{M'M}(\alpha, \beta, 0). \tag{320}$$

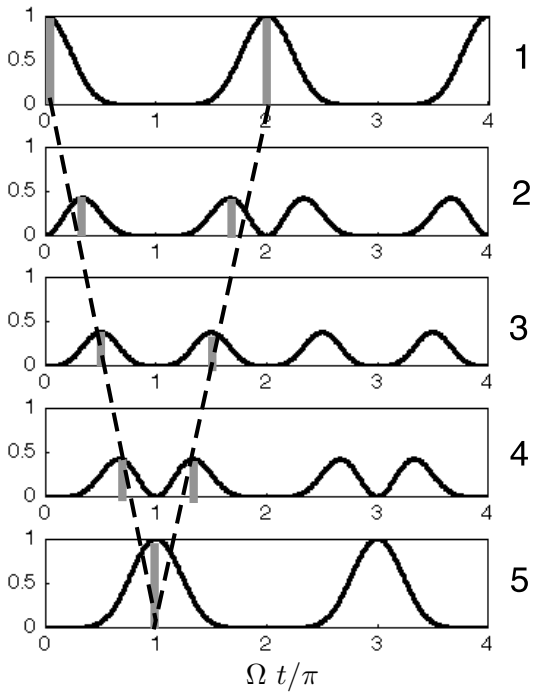

Fig. 64. Resonant population flow, starting from state 1, for 5-state pseudospin model. Population histories are periodic.

The time evolution is evaluated by expressing the state in rotated coordinates. The result is

$$C_n(t) = \Sigma_{M''n'} \mathcal{D}^{(S)}_{MM''}(\alpha, \beta, Z_0 t)\ \mathcal{D}^{(S)}_{M'M''}(\alpha, \beta, 0)^* C_{n'}(0), \tag{321}$$

where

$$M \equiv n - \tfrac{1}{2}(N+1), \qquad M' \equiv n' - \tfrac{1}{2}(N+1). \tag{322}$$

This equation presents an exact analytic expression for the time dependence of the probability amplitude $C_n(t)$ for fixed parameters Ω_0 (Rabi frequencies) and Δ_1 (detunings). It involves a rotation operator $\mathcal{D}^{(S)}(\alpha, \beta, Z_0 t)$ descriptive of a coordinate system turning steadily at the rate $Z_0 = \sqrt{\Delta_1^2 + |\Omega_0|^2}$. When detuning is absent, the vector $\tilde{\mathbf{\Omega}}$ lies in the $x - y$ plane. When the Rabi frequency Ω_0 is real, the vector lies in the $x - z$ plane. In particular, when Ω_0 is real and there is no detuning, the vector lies along the x axis, and time evolution amounts to rotation about this axis at the Rabi frequency. In all cases the behavior is periodic – as can be recognized from the fact that the eigenvalues are all multiples of a common frequency.

Figure 64 illustrates an example of the perfect periodicity observed with the pseudospin model, for $N = 5$ and no detuning.

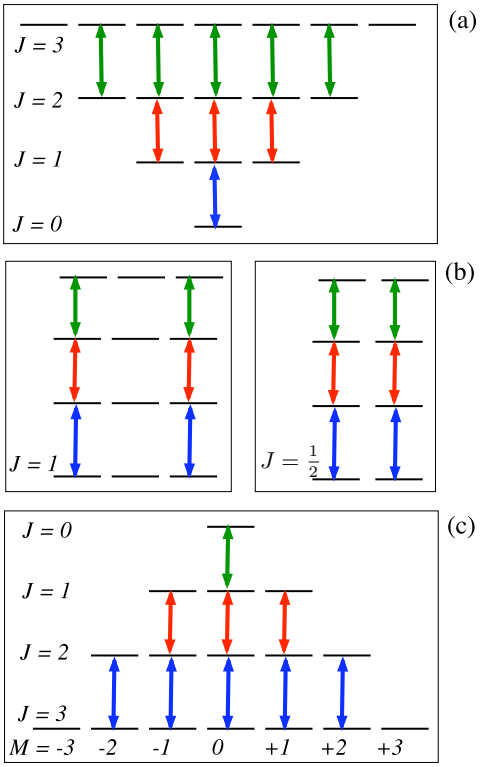

Fig. 65. Parallel angular momentum chains, linear polarization. (a) Increasing J, (b) uniform J, (c) decreasing J. (after Fig. 20.12-1 of [2])

11.4 Parallel chains

Using the angular-momentum selection rules for a single pair of degenerate sublevels it is straightforward to evaluate selection rules for a chain of excitations between degenerate levels. Figures 65 and 66 illustrate examples, for particular simple choices of the polarization at each step [2, §20.12]. These display the linkages as they would occur in a ladder, from least to greatest excitation, but the conclusions apply to any resonant sequence, regardless of the relative energies.

As will be discussed, the linkages appear as independent chains, and the overall excitation probability is the sum of probabilities for the separate chains (i.e. one must sum probabilities, not probability amplitudes). Thus if J_0 denotes the angular momentum of the initial level, and the sublevels sublevels have equal initial probability, then the population in level J at time t is the sum

$$P_J(t) = \frac{1}{2J_0+1}\Sigma_M |C_{JM}(t)|^2, \tag{323}$$

where $C_{JM}(t)$ is the solution for an RWA Hamiltonian appropriate to a particular set of M

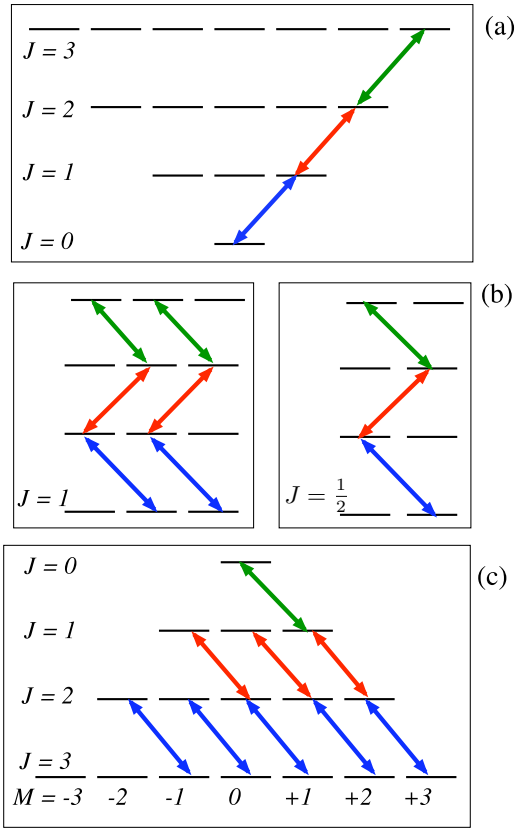

Fig. 66. Parallel angular momentum chains, circular polarization. (a) Increasing J, (b) uniform J, alternating left- and right-circular polarization, (c) decreasing J. (after Figs. 20.12-2 and 20.12-3 of [2])

values. The average over magnetic sublevels, each with a distinct orientation and hence a distinct Rabi frequency, acts to diminish the amplitude of population oscillations.

It is important to recognize that this sum of individual probabilities cannot, in general, be reproduced as the square of any single probability amplitude for an averaged interaction – there is no "average atom" that will exhibit the averaged dynamics.

Figures 65 presents examples of linear polarization at each excitation step. Frame (a) shows a three-step sequence in which each step involves a larger value of J, starting from $J = 0$. The single initial state has a complete linkage path to a state of highest excitation. Frame (b) shows two examples in which angular momentum remains constant along the chain, either $J = 1$ (left hand) or $J = 1/2$ (right hand). For integer J there occurs no transitions $M = 0 \leftrightarrow M = 0$, and so one set of sublevels are unlinked. With half-integer J there are complete linkages between lowest and highest excitation states. Frame (c) shows an example in which angular momentum decreases with excitation. At each step there are two fewer sublevels linked to lower excitation.

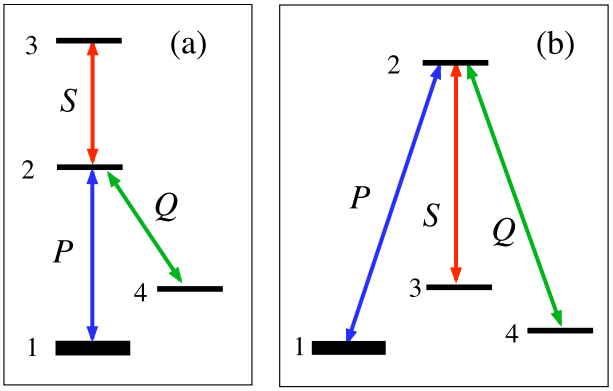

Fig. 67. Equivalent four-state tripod linkages: three states (1, 3, 4) each are linked to a single common state, 2 by the three interactions P, S and Q

Thus with the three excitation stages shown there are 6 ground-state sublevels (of $J = 3$) that have no link to the most excited sublevel ($J = 0$).

Figure 66 illustrates the same sets of J sequences, but with circular polarizations. Frame (a) shows that, as with linear polarization, there exists a linkage between the ground state ($J = 0$) and a fully excited state ($J = 3$). In this illustration each excitation step has the same circular polarization; a comparable connection occurs with alternating right- and left-circular polarization. Frame (b) illustrates two sequences that provide complete linkages between initial states and states of highest excitation, when all levels have the same J. In these cases it is necessary to employ alternating right- and left-circular polarizations in order to have a complete path between ground sublevels and those at the end of the chain. Frame (c) shows circular polarizations linkages in a sequence in which J decreases at each step. As with linear polarization, at each step two sublevels are unlinked to higher excitation.

11.5 Branched chains

For four or more states the RWA Hamiltonian may describe not only simple chains but branched linkages, in which more than two states connect with a particular state [71] [2, §21.4]. Figure 67 illustrates equivalent examples of a four-state tripod linkage, in which three quantum states are linked by independent radiative transitions to a single excited state, but not amongst themselves[72].

Section 10.9 discussed the tripod system in some detail. This system has two degenerate dark states; during adiabatic passage these can become superposed.

The properties of branched chains have consequences that seem quite surprising when first seen. The tripod system exhibits these properties quite directly. Consider a three-state ladder linkage, as in Fig. 42, with loss (say photoionization) from the uppermost state, 3, at rate Γ. Let the two Rabi frequencies be constant and equal, as in Fig. 43. Then population flows along the

[71] The corresponding graphs are *trees*

[72] As with other RWA linkages, the vertical placement of the several energies is irrelevant.

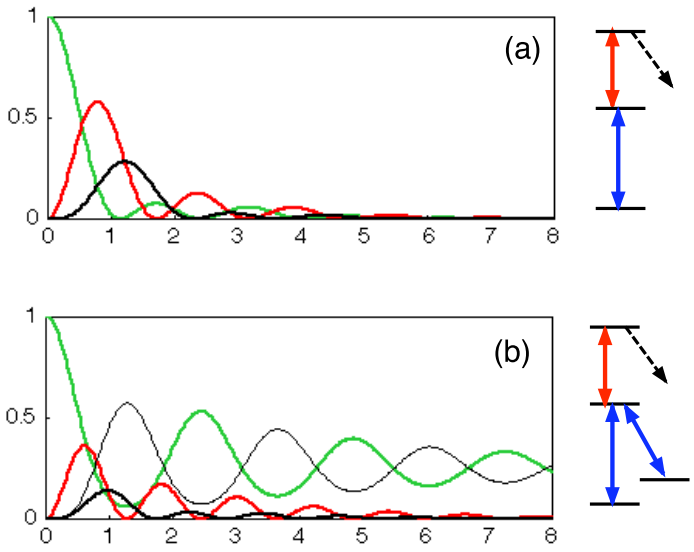

Fig. 68. (a) Population histories for 3 state system, unit Rabi frequencies, with loss $\Gamma = 0.5$ from uppermost state 3. (b) Population histories when there is an additional linkage, unit Rabi frequency, from state 2 to state 4. Population loss is now incomplete; the laser fields create a dark state that remains unaffected by the light. This behavior only occurs when there is a two-photon resonance between states 1 and 4; otherwise population will eventually all be lost.

ladder from initial state 1 to final state 3 with loss during each cycle. If the loss is comparable to the Rabi frequencies, then only a few cycles will be completed before all of the population is lost. Figure 68(a) shows an example of the population histories for such a situation. The addition of a second ground state, state 4 linked to state 2, makes the linkage pattern that of the tripod system. Now only a portion of the population is lost; the remainder is in a dark state; it cycles between states 1 and 4. Figure 68(b) illustrates this history.

More generally, one may deal with systems in which a central chain is interrupted by one or more branches, each of which comprises one or more links. Interestingly, the effect of such a branch on the main chain depends dramatically on whether the branch has an even or an odd number of elements: an odd-element branch will act to sever a resonant chain [122].

11.6 Loops

Although the RWA imposes constraints on the frequencies of any looped linkage, allowable loops can occur in a number of simple situations [123]. The following figures illustrate an example of a loop system obtained by treating linearly polarized light in an helicity basis.

Figure 69 shows the linkages for a pair of resonant transitions involving linear polarized light and the excitation sequence $J = 0 \leftrightarrow 1 \leftrightarrow 0$. The coordinates for quantization appear in frame (c). Frame (a) shows the linkages when both fields have the same polarization direction, and this is taken as the quantization axis, z. There occurs a direct connection between the ground state g

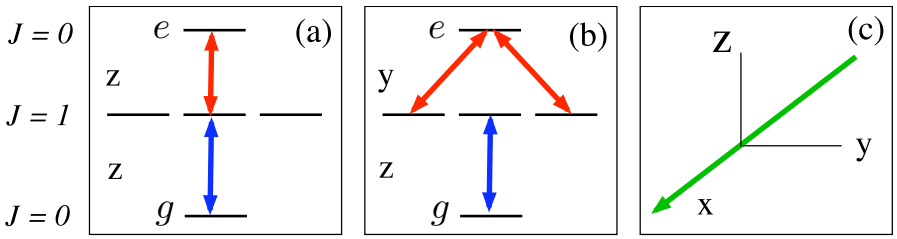

Fig. 69. Examples of three-level linkage patterns for $J = 0 \leftrightarrow 1 \leftrightarrow 0$ sequence. (a) Parallel linear polarization, z, z. (b) Crossed linear polarization, z, y. No exitation can occur to state e (c) The geometry: the propagation axis is y.

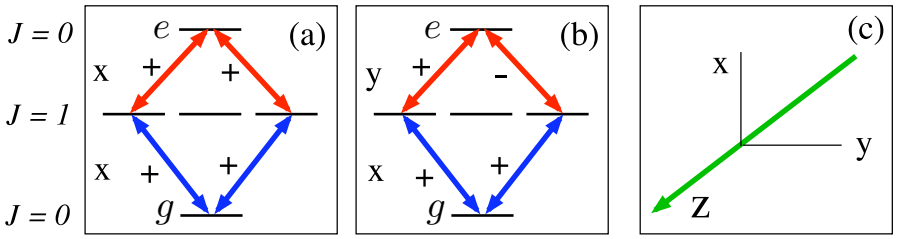

Fig. 70. Examples of three-level linkage patterns for $J = 0 \leftrightarrow 1 \leftrightarrow 0$ sequence. (a) Parallel linear polarization, x, x, in helicity basis (b) Crossed linear polarization, x, y, in helicity basis. (c) The geometry: the propagation axis is the quantization axis z.

and the most excited state e, a simple three-state ladder.

Frame (b) shows the linkage pattern when the first-step polarization is along the z axis, and the second-step polarization is x, i.e. the two fields are *cross polarized*. As can be seen, there is no connection between state g and the most excited state e; population undergoes two-state Rabi oscillations, with never any population in the uppermost level, but no population can reach excited state et.

Figure 70 presents these same systems using a different choice of quantization axis relative to the polarization, one in which each interaction is shown in an helicity basis. Now the links form a closed loop; they differ only in the relative phases of the paths. The possibility of excitation cannot depend upon our choice of coordinates; the result is easiest to recognize with the choice of Fig. 69.

Frame 70(a) shows the phases that occur when the polarizations are parallel, say both being along the x axis. This is equivalent to Fig. 69(a); excitation proceeds from state g to state e via two constructively interfering paths that permits excitation to reach state e.

Frame 70(b) shows the phases that occur when the polarizations are along different axes, x and y. This system is equivalent to Fig. 69(b); there occurs destructive interference in the second step that prevents excitation from reaching the uppermost state e.

The association of destructive interference with crossed polarization is specific to the partic-

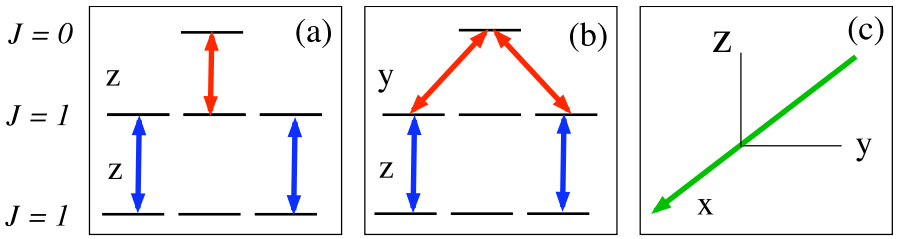

Fig. 71. Examples of three-level linkage patterns for $J = 1 \leftrightarrow 1 \leftrightarrow 0$ sequence. (a) Parallel linear polarization, z, z. No exitation can occur to state e because a selection rule prevents the first step transition $M = 0 \rightarrow M = 0$. (b) Crossed linear polarization, z, y. (c) The geometry: the propagation axis is y.

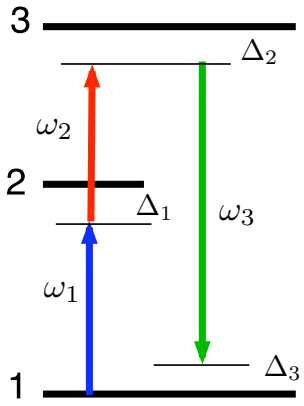

Fig. 72. A three state loop, involving frequencies ω_1, ω_2 and ω_3, showing the three detunings Δ_k.

ular sequence of angular momentum states. Figure 71 depicts the linkage pattern, as expressed in the coordinates of Fig. 69, for the sequence $J = 1 \leftrightarrow 1 \leftrightarrow 0$. In this situation the destructive interference of a loop portrayal of the interaction will occur with parallel polarizations.

11.7 Loops and the RWA; Nonlinear optics

The introduction of the RWA accompanies the use of rotating coordinates in Hilbert space and the neglect of various exponentials, such as $\exp(\pm i2\omega t)$. When linkage loops occur it is generally not possible to eliminate entirely the exponential time variations, except when the frequencies satisfy specific resonance conditions. To illustrate these requirements, consider a three-state loop, as suggested by Fig. 72. Such a linkage pattern will not occur when the interactions are all via electric dipole transitions and the system has a center of symmetry, because then each transition must occur between states of opposite parity. However, in the absence of a center of symmetry such a linkage loop becomes possible.

Let us write the statevector as

$$\Psi(t) = \exp(-\mathrm{i}E_1 t/\hbar)\left[C_1(t)\psi_1 + C_2(t)\mathrm{e}^{-\mathrm{i}\omega_1 t}\psi_2 + C_3(t)\mathrm{e}^{-\mathrm{i}\omega_1 t - \mathrm{i}\omega_2 t}\psi_3\right], \tag{324}$$

and take the Rabi frequencies asociated with carriers ω_k to be Ω_k, for $k = 1, 2, 3$, in keeping with the Hilbert-space rotations appropriate to the three-state ladder. Define the following detunings:

$$\hbar\Delta_1 = E_2 - E_1 - \hbar\omega_1, \tag{325}$$

$$\hbar\Delta_2 = E_3 - E_1 - \hbar\omega_1 - \hbar\omega_2, \tag{326}$$

$$\Delta_3 = \omega_1 + \omega_2 - \omega_3. \tag{327}$$

With the neglect of terms $\exp(\pm\mathrm{i}2\omega_n t)$ compared with unity the Schrödinger equation translates into the following equations:

$$\frac{d}{dt}C_1 = -\frac{\mathrm{i}}{2}\,\Omega_1^* C_2 - \,\mathrm{e}^{-\mathrm{i}\Delta_3 t}\Omega_3^* C_3, \tag{328}$$

$$\frac{d}{dt}C_2 = -\mathrm{i}\Delta_1 C_2 - \frac{\mathrm{i}}{2}\,\Omega_1 C_1 - \frac{\mathrm{i}}{2}\,\Omega_2^* C_3, \tag{329}$$

$$\frac{d}{dt}C_3 = -\mathrm{i}\Delta_2 C_3 - \frac{\mathrm{i}}{2}\,\Omega_2 C_2 - \frac{\mathrm{i}}{2}\mathrm{e}^{\mathrm{i}\Delta_3 t}\Omega_3 C_1. \tag{330}$$

Unless the frequencies obey the resonance condition $\omega_3 = \omega_1 + \omega_2$ there will occur exponential variations at the detuning Δ_3, and the Hamiltonian, in the rotating basis, will not appear slowly varying. Under such situations it is not possible to assume slow variation, as is required for adiabatic passage.

In this system the coherence $C_1 C_3^*$ is associated with a dipole moment at frequency $\omega_1 + \omega_2$. As indicated in Appendix A.5, this dipole moment serves as a source for growth of radiation at this frequency, thereby converting a photon of energy $\hbar\omega_1$ and another of energy $\hbar\omega_2$ into a single photon of energy $\hbar\omega_3 = \hbar\omega_1 + \hbar\omega_2$. By maximizing the relevant coherence one maximizes the frequency conversion.

A straightforward extension of this discussion to a chain of four states, as in Fig. 46(c) allows treatment of CARS and other four-wave mixing examples of nonlinear optics. For CARS the coherence $C_1 C_4^*$ is responsible for producing a field of frequency $\omega_4 = 2\omega_P - \omega_S$. For a three-state ladder linkage, with $E_1 < E_2 < E_3$ the coherence $C_1 C_4^*$ produces a field of frequency $\omega_4 = \omega_1 + \omega_2 + \omega_3$. In either case the frequency conversion can be optimized by maximizing the relevant coherence [124].

11.8 Bright and dark states

As we have seen, a simple rotation of the physical coordinates used for labeling directions can produce different linkage patterns in the Hamiltonian matrix. When we deal with two degenerate levels in an angular momentum basis and the polarization is linear, the choice of quantization (z) axis presents a simple picture of two-state linkages, rather than the more elaborate ones of, say, Fig 57, that occur when the polarization is elliptical or is linear but not along the quantization axis. Similarly, right- or left-circular polarization appears, when expressed in a coordinate frame parallel to the propagation direction, as linkages between pairs of states; cf. Figs. 65 and 66.

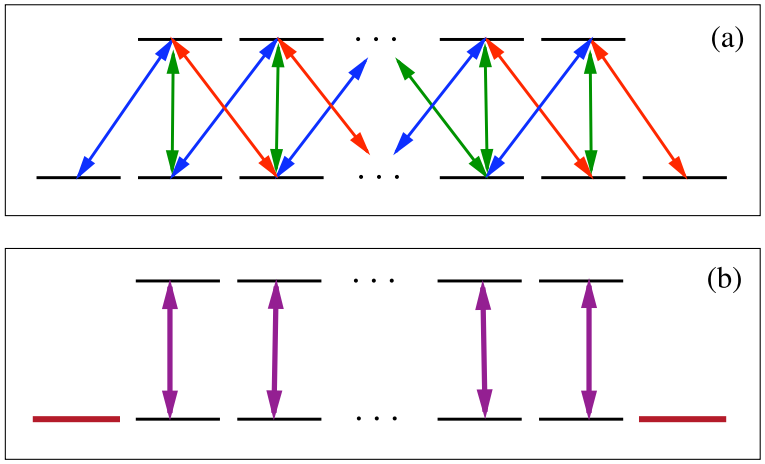

Fig. 73. (a) Angular momentum linkage pattern for general elliptic polarization at arbitrary angle to quantization axis, $J \leftrightarrow J-1$. (b) Equivalent linkage after Morris-Shore transformation. There are $J-1$ independent pairs of coupled states and two dark states.

That is, for particular polarizations it is possible to choose a quantization axis such that the tripod linkage appears as a two-state linkage.

Such simplification is not possible for general elliptical polarization, as represented by an arbitrary point on the Poincaré sphere (see Sec. 8.1.2) and parametrized by two angles, θ describing the relative magnitudes of the two spherical components and ϕ describing the phase between them; cf. Fewell (1993) [67]. Only specific points on the Poincaré sphere permit the linkage simplification. Although such simplification does not occur through choice of quantization axis, one may ask if it is possible to transform the Hilbert space to produce such two-state simplifications, as shown in Fig. 73, for arbitrary polarization.

We have seen that, in the lambda linkage pattern with two-photon resonance, it was possible to introduce a combination of states 1 and 3 such that one of them (the dark state) had no linkage with the excited state 2, while the other (the bright state) had all of the oscillator strength of the transition into state 2. One may ask if it is possible to find other linkage patterns, in systems with more than 3 states, for which a similar simplification to two state dynamics is possible.

The answer, first drawn to my attention by Jim Morris, is that indeed there are many situations in which it is possible to introduce a Hilbert-space basis in which complicated linkages appear as independent two-state linkages, together with unlinked *spectator states*. The transformation is now known as the Morris-Shore transformation [125]. It can be applied whenever the relevant Hamiltonian matrix has the following properties:

I. The complete set of states can be separated into two sets, say N_A of set A (ground, including the initial state), and N_B of set B (excited). There are no couplings within A set or B set; only couplings between A and B [73]. These may be of any form, not necessarily link-

[73] The graph corresponding to this linkage pattern is said to be *bipartite*.

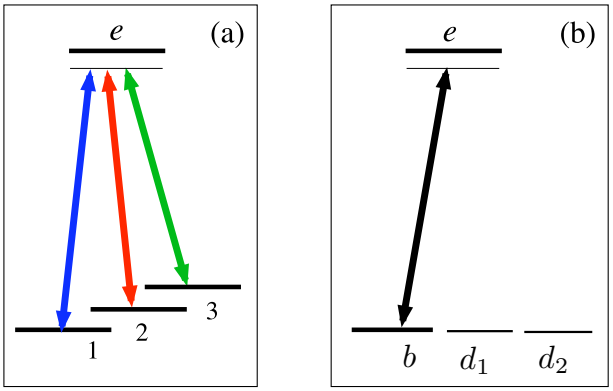

Fig. 74. (a) The four-state tripod linkage. (b) Equivalent linkage after transformation into a single bright state b and two dark states d_1 and d_2 using the MS transformation. (Vertical locations of the energy levels are irrelevant.)

ing only a single state with at most 3 other states, as occurs with electric-dipole radiation between angular momentum states.

II. The states within each set are degenerate. In the RWA this means that the states of each set share a single common detuning; overall there are only two detunings, Δ_A and Δ_B. Either or both of these may be zero.

When these conditions hold, it is possible to introduce a new set of basis states, superpositions within the A set and within the B set, such that the original Hamiltonian appears in block diagonal form: it consists of a set of two-state submatrices, plus additional unlinked portions that describe spectator states. Appendix M discusses the transformation.

When there are equal numbers of A and B states, $N_A = N_B$, then the resulting transformation produces N_A pairs of two-state interactions, each with a unique Rabi frequency but all sharing the same detunings. When there are more states in set A (the unexcited states), then there are N_B bright states and $N_A - N_B$ dark states.

Figure 74 illustrates this transformation for the four-state tripod linkage induced by three independent fields. After the transformation all the dynamics is concentrated in a two-state system, between the excited state e and a bright combination b of states 1, 2 and 3. There are two degenerate dark states d_1 and d_2 that are not directly affected by the field, although their composition does depend on the three fields.

12 Preparing superpositions

The first interests in coherent excitation with laser pulses focused on producing complete population transfer – typically inversion of a two-state system, starting from the ground state. In recent years attention has shifted towards more general quantum-state manipulation, such as the preparation of a specified coherent superpositions of two or more quantum states [126]. Theorists have long been interested in coherent superpositions [127], particularly of quantum states whose extent is macroscopic – the so-called "Schrödinger cat" states [128]. As with the procedures for producing population transfer by means of coherent excitation, the techniques for more general quantum-state manipulation are of two classes: the impulsive change, in which a resonant pulse induces a controlled partial Rabi oscillation, and adiabatic changes [129]. I will concentrate on the latter technique, and will discuss only superpositions of atomic states, as contrasted with field states.

In considering superpositions it is essential to distinguish between superpositions of *degenerate* states (those that share a common unperturbed energy $E_1 = E_2 = \ldots,$) from superpositions of *nondegenerate* states. The distinction becomes clear when we write the statevector, in the absence of any laser interaction, as

$$\Psi(t) = \Sigma_n \exp(-\mathrm{i}E_n t/\hbar)\, c_n\, \psi_n. \tag{331}$$

This is the most general form for the statevector of the undisturbed atom: a fixed superposition of bare states ψ_n, each multiplied by a periodic phase factor $\exp(-\mathrm{i}E_n t/\hbar)$. Although the probabilities determined from this superposition are constant,

$$P_n(t) = |c_n|^2, \tag{332}$$

other properties are not. In particular, the coherences (cf. Appendix H.2), undergo oscillations at Bohr frequencies. For example, the two-state coherence is

$$\rho_{12}(t) = \mathrm{Re}\left[c_1 c_2^* \exp[\mathrm{i}(E_2 - E_1)t/\hbar]\right]. \tag{333}$$

Between nondegenerate pairs of states there generally exists some nonzero radiative transition probability and hence some nonzero probability of population loss via spontaneous emission. However, this need not be that of an electric-dipole interaction; the spontaneous emission rate may be that of a "forbidden" transition, e.g. electric quadrupole or octopole, or magnetic dipole. Thus it may well be that the excited state is sufficiently long lived that laser-induced excitation (via electric-quadrupole or magnetic-dipole interaction) can be regarded as coherent excitation. Under such situations one may take interest in creating a two-state superposition

$$\Psi(t) = \exp[-\mathrm{i}E_1 t/\hbar]\,[c_1\psi_1 + c_2\psi_2'(t)]\,, \qquad \psi_2'(t) \equiv \exp[-\mathrm{i}(E_2 - E_1)t/\hbar]\psi_2, \tag{334}$$

in which, apart from an overall phase, the structure appears constant in a reference frame that rotates at the Bohr frequency for the transition. However, during one Bohr period the actual superposition will, for example, cycle between $\psi_1 + \psi_2$ and $\psi_1 - \psi_2$.

The energies occurring in this equation are eigenvalues of the Hamiltonian in the absence of laser radiation. Therefore they include Zeeman shifts produced (deliberately or randomly) by magnetic fields, and Stark shifts produced by electric fields. Even though these may be small, they will in due time alter the phase of the superposition.

12.1 Nondegenerate states: wavepackets

The construction of nondegenerate superpositions has been particularly useful in studies of vibrational excitation of molecules. There one uses a single laser pulse to excite a single vibrational state into a set of closely spaced vibrational states of an excited electronic state. The relevant RWA Hamiltonian has a bordered structure,

$$\mathsf{W} = \tfrac{1}{2}\begin{bmatrix} 0 & 0 & 0 & \cdots & \Omega_1 \\ 0 & 2\Delta_2 & 0 & \cdots & \Omega_2 \\ \vdots & \vdots & \vdots & \vdots & \vdots \\ \Omega_1 & \Omega_2 & \cdots & \Omega_N & 2\Delta_N \end{bmatrix}. \tag{335}$$

where the magnitude of the detunings Δ_n increase steadily with increasing n. After pulsed excitation with constant detunings [74] the wavefunction for vibrational coordinate x then has the form

$$\Psi(t,x) = \Sigma_n \exp(-\mathrm{i}E_n t/\hbar) c_n\, \psi_n(x) \tag{336}$$

and the probability of observing the value x is

$$P(x) = \left|\Sigma_n \exp(-\mathrm{i}E_n t/\hbar) c_n\right|^2. \tag{337}$$

This distribution offers the opportunity to construct *wavepackets* – localized spatial distributions that move with time [130]. In a typical application one creates an initial wavepacket constructed from electronically excited vibrations, allows this to evolve undisturbed, and then at an appropriate time, induces a second set of transitions, this time back to low-lying electronic states. Such procedures allow, in principle, the coherent control of unimolecular chemical reactions, such as dissociation.

12.2 Degenerate discrete states

When the superposed quantum states are degenerate, then the time variation of the statevector, in the absence of laser radiation, is a single overall oscillatory phase. Expressed in terms of a wavefunction, the construction reads

$$\Psi(t,x) = \exp(-\mathrm{i}E_1 t/\hbar)\, \Sigma_n\, c_n \psi'_n(x). \tag{338}$$

Not only the probabilities but also the coherences are static; one has a stationary superposition.

Such a stationary situation cannot occur in the simple two-state system excited via interaction by laser pulses, although such superpositions can be produced by a pulsed DC electric field (i.e. one with null carrier frequency). The simplest linkage that allows creation of a degenerate two-state superposition using laser fields is that of the lambda linkage, as exhibited with the stimulated Raman RWA Hamiltonian. With this system we can create superpositions of degenerate Zeeman sublevels of an atom characterized by angular momentum quantum numbers J and M.

[74] Excitation with swept detunings can produce complete population transfer from the initial state into a single final state.

There are several possibilities for constructing a superposition of Zeeman sublevels via two-stage lambda-like linkages and STIRAP-like pulses [131]. To illustrate these, consider in a system having $J = 1$ for the ground level (with states 1 and 3 having, respectively, $M = \mp 1$) and $J = 0$ for the excited state (state 2, with $M = 0$). We excite the system using a single carrier frequency but various choices of elliptical polarizations. Suppose we wish to construct a superposition of states 1 and 3, starting from state 1. We require two polarizations, σ_+ linking states 1 and 2 (the P field), and σ_1 linking states 2 and 3 (the S field).

One possibility is to have large single-photon detuning Δ_P but resonant two-photon detuning, so that state 2 can be adiabatically eliminated. The result is a simple two-state system, with transitions between states 1 and 3 driven by the two-photon Raman Rabi frequency [75]

$$\hat{\Omega}_R(t) = \frac{\hat{\Omega}_P(t)\hat{\Omega}_S(t)^*}{2\Delta_P}. \tag{339}$$

We can apply the two pulses simultaneously, with individual Rabi angles adjusted such that the two-photon Raman Rabi angle

$$A_R = \int_{-\infty}^{+\infty} dt\, \Omega_R(t) \tag{340}$$

produces the desired superposition upon completion of the pulse.

Another possibility is to employ a STIRAP-type pulse sequence, with the S pulse preceding the P pulse. However, unlike STIRAP, here we proceed with the adiabatic evolution only until the mixing angle has reached the value needed for the predeterminded superposition. From that moment on, we force the two fields to maintain a constant ratio, so as to maintain this mixing angle, as they diminish. In this way we produce a *fractional STIRAP* [132]. It is also possible to use SCRAP to produce superpositions [133].

The full STIRAP procedure can be used to produce specified superpositions of degenerate Zeeman sublevels. Consider a linkage between sublevels of $J = 1$, through a single excited state having $J = 0$ via P field, and continuing to via S field to metastable sublevels of $J = 1$, as shown in Fig. 56. By choosing polarizations of the two fields appropriately, the STIRAP procedure can produce a variety of sublevel superpositions.

12.3 Transferring superpositions

Once a two-state superposition has been created, various pulse sequences can alter its composition; the vector model of Sec. 7 offers a simple prescription for selecting an angular velocity vector, and pulse duration, that will produce any desired rotation of the Bloch vector, i.e. will convert any initial superposition state into a prescribed final superposition.

Often it proves useful to consider the set of states within which superpositions are to be prepared or transferred (the *target states* or *working states*) as a subspace of a larger Hilbert space, obtained by including a set of *ancillary* states which, though not populated initially or finally, participate in the statevector transformation [76].

[75] The two-photon interaction generally has a phase factor $\exp(-\mathrm{i}\varphi_P + \mathrm{i}\varphi_S)$ multiplying the Rabi frequency

[76] The ancillary states must be *essential* states – their linkages to the working states must be part of the full Hamiltonian – though initially and finally they hold no probability.

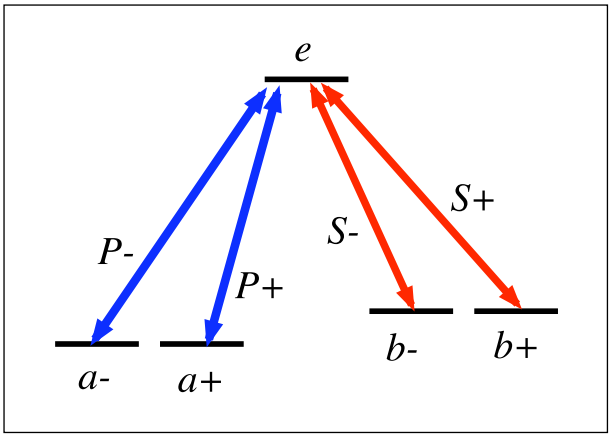

Fig. 75. Adjustment of P and S pulses can transfer a superposition from amplitudes a to amplitudes b through ancillary excited state e.

The simplest example is that of the lambda system: we can use a fractional-STIRAP technique to create a specified superposition of the two ground states with the aid of an ancillary excited state. More generally, we partition the full Hilbert space into two sets of states, with links only between them, not within them; cf. Sec. 11.8. Although we are interested only in manipulating states of the target set, we do so by means of unitary transformations that involve the ancillary states.

Such procedures allow us, for example, to transfer a superposition from one pair of states to a second pair of states, with the aid of a single ancillary state [134], as depicted in the five-state fan linkage of Fig. 75. This linkage pattern permits manipulation by means of a degenerate STIRAP-like adiabatic passage involving two simultaneous S-field components and two delayed P-field components. With suitable adjustment of the two pairs of amplitudes, transfer takes place between amplitudes $a_{\pm}$ and amplitudes $b_{\pm}$.

13 Measuring superpositions

Numerous papers have examined issues connected with measuring coherent superpositions – an aspect of the more encompassing concerns of quantum measurement theory [135] or quantum tomography [136]. Many of these articles suggested techniques based on adiabatic evolution [137]. The next sections describe some of these.

To completely characterize a superposition of N states we require the magnitude and phase of N probability amplitudes. Out of these parameters the overall phase of the statevector is usually not of interest. It is relatively straightforward to obtain values for the relative amplitudes of the several states, either by observing the relative strength of a fluorescence signal or by measuring the relative photoionization signal, as shown in Fig 76. Such signals can come directly from the state of interest, as indicated in Fig 76 (a), or they can be observed following a probe interaction (a *transfer field*) as in Fig 76 (b). They can also be evaluated after a sequence of events that include spontaneous emission, as in Fig 76 (c).

By suitably choosing the frequency and polarization of the probe field or the transfer field, it is possible to obtain signals directly proportional to the population in a specified constituent of a superposition. However, such measurements give no information about the phase. To obtain that information it is necessary to map the phase onto a population.

13.1 Two-state superpositions

A two-state system provides an instructive example of possible techniques for obtaining the required information concerning the superposition amplitudes. We parametrize the initial statevector with two angles θ, ϕ

$$\Psi(0) = \cos(\theta/2)\ \psi_1 + \sin(\theta/2)\mathrm{e}^{\mathrm{i}\phi}\ \psi_2. \tag{341}$$

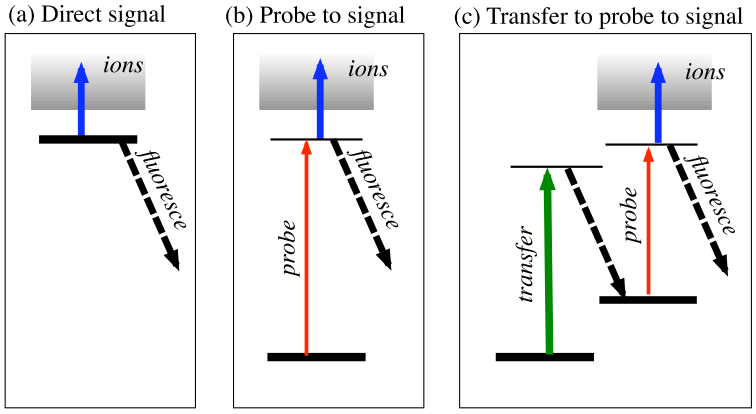

Fig. 76. Various methods for observing populations. (a) Direct observation of fluorescence or photoionization (b) Produce controlled exctitation by a probe field, followed by observation of ionization or fluorescence (c) Allow population transfer by spontaneous emission prior to probe step.

Our objective is to devise a set of measurements from which to deduce these two parameters.

13.1.1 Direct excitation to signal

A straightforward procedure, suggested by Vitanov [137], is available when the two (working) states are degenerate and each has an excitation linkage to a single nondegenrate excited state, forming a lambda linkage pattern discussed earlier. The decay of the nondegenerate excited state – the decay rate and the angular distribution of radiation – does not depend on how it was excited, and hence any measurement of fluorescence intensity provides a measure of the population transferred and, in turn, the original population in the linked state. The links, labeled P and S, are uniquely fixed, either by polarization or, if the states are not degenerate, by frequency; we assume that these have the same time dependence, as will happen if they are elliptical polarization components.

We excite the system using either a single pulse or two simultaneous pulses, as described by the RWA Hamiltonian

$$\mathsf{W} = \tfrac{1}{2}\begin{bmatrix} 0 & 0 & \Omega_P \mathrm{e}^{-\mathrm{i}\varphi_P} \\ 0 & 0 & \Omega_S \mathrm{e}^{+\mathrm{i}\varphi_S} \\ \Omega_P \mathrm{e}^{+\mathrm{i}\varphi_P} & \Omega_S \mathrm{e}^{-\mathrm{i}\varphi_S} & 2\Delta \end{bmatrix} \begin{matrix} 1 \\ 2 \\ e \end{matrix} \tag{342}$$

and parametrized by the two constant angles

$$\tan\Theta = \Omega_P(t)/\Omega_S(t), \qquad \beta = \varphi_P - \varphi_S. \tag{343}$$

We measure the fluorescence signal $\mathcal{S}(\Theta, \beta)$ produce from such excitation, for several choices of the parameters Θ and β. One possible sequence is shown in Fig. 77. From the resulting signals we obtain the desired amplitude and phase of the superposition:

$$\tan(\theta/2) = \frac{\sqrt{\mathcal{S}(0,0)}}{\sqrt{\mathcal{S}(\pi/2,0)}}, \tag{344}$$

$$\cos\phi = \frac{2\mathcal{S}(\pi/4,0) - \mathcal{S}(0,0) - \mathcal{S}(\pi/2,0)}{2\sqrt{\mathcal{S}(0,0)\mathcal{S}(\pi/2,0)}}, \tag{345}$$

$$\sin\phi = \frac{2\mathcal{S}(\pi/4,\pi/2) - \mathcal{S}(0,0) - \mathcal{S}(\pi/2,0)}{2\sqrt{\mathcal{S}(0,0)\mathcal{S}(\pi/2,0)}}. \tag{346}$$

The procedure can also be applied to measurements of more general superpositions that include an incoherent component and which therefore require a density matrix for description, and to treat an arbitrary number of degenerate sublevels [137]. Again the method uses direct transitions into a single fluorescing excited state, with a set of different linkages patterns, to analyze a Zeeman coherence.

In more complicated situations than the simple case considered here, when excitation occurs to a degenerate excited state, the resulting fluorescence will have an angular distribution that depends upon the specific excited-state superposition, and hence upon the initial superposition. Under such conditions other procedures must be used.

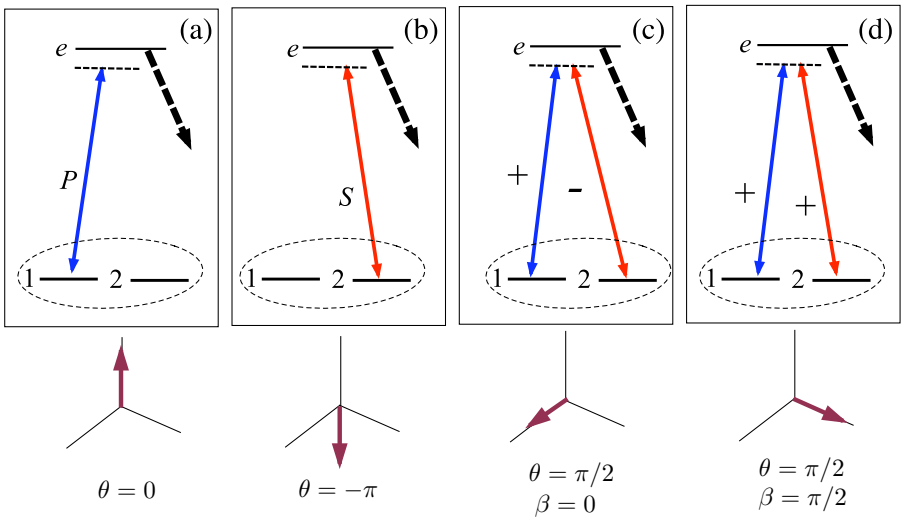

Fig. 77. Set of pulsed interactions used to obtain fluorescence signal $\mathcal{S}(\Theta, \beta)$ for determination of superposition parameters.

13.1.2 Indirect excitation to signal

Rather than map the superposition directly into a signal-producing excited state we can instead use STIRAP to map it into a fixed lower-lying state whose population can subsequently be probed, either by fluorescence, by photoionization, or by laser-induced fluorescence. Figure 78 indicates the linkages involved: two simultaneous P fields, distinguished by polarization (magnitude and phase), and a single S field.

The analysis of a pair of states involves a sequence of STIRAP-like transitions that produce complete population transfers from initial states to a single analysis state. The concept relies on constructing a sequence of population transfers in which the P pulse has two components, thereby connecting two working states with the excited state. In turn a single S linkage connects this state to a single final-analysis state. The overall linkage pattern is that of the tripod system

13.2 Analyzing three -state superpositions

As the number of states increases, so too does the complexity of the measurement scheme needed to specify completely the characteristics of an unknown quantum state. With three states it is still possible to use polarization characteristics to provide the needed distinct probes. The simplest arrangement of linkages for this purpose is the tripod [114, 115]. Figure 79 illustrates a tripod-linkage example with which to probe a degenerate three-state superposition through transitions to an excited state e followed by fluorescence.

As with the two-state direct-excitation probe, the fluorescence from the nondegenerate excited state does not depend on how it was prepared. It therefore serves as a signal probe proportional to the population transferred.

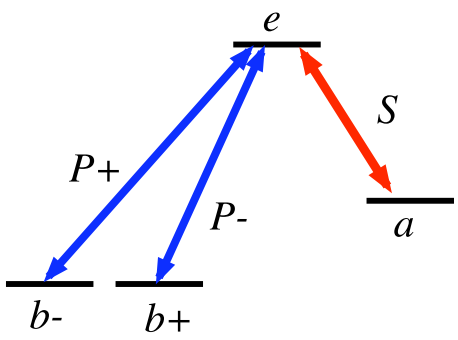

Fig. 78. Linkage pattern for mapping a superposition of states b_- and b_+ into population of a single state a by STIRAP with a two-component pump field $P_\pm$. Subsequent excitation and fluorescence from state a produces the signal.

We consider the unknown superposition

$$\Psi = c_-\psi_{-1} + c_0\psi_0 + c_+\psi_{+1}, \tag{347}$$

labeled by integers appropriate to magnetic quantum number M of $J = 1$.The RWA Hamiltonian for the set of linkages shown in Fig. 79 is a bordered matrix

$$\mathsf{W}(t) = \tfrac{1}{2}\begin{bmatrix} 0 & 0 & 0 & \hat\Omega_+(t)^* \\ 0 & 0 & 0 & \hat\Omega_0(t^*) \\ 0 & 0 & 0 & \hat\Omega_-(t)^* \\ \hat\Omega_+(t) & \hat\Omega_0(t) & \hat\Omega_-(t) & 2\Delta \end{bmatrix} \begin{matrix} -1 \\ 0 \\ +1 \\ e \end{matrix}. \tag{348}$$

The three Rabi frequencies appearing here are complex numbers, but we shall require that *they all have common time dependence*; we introduce amplitudes A_k and phases β_k, the control parameters, by writing

$$\hat\Omega_k(t) = A_k \exp(-\mathrm{i}\beta_k) f(t/T). \tag{349}$$

The procedure is to measure the fluorescence signal from state e for various choices of the control parameters, and from these to deduce the unknown superposition parameters.

The first step toward the theoretical description comes from recognizing that all of the transition strength of the three separate linkages can be combined into a transition into the excited state from a single "bright-state" superposition,

$$\Phi_b = \tfrac{1}{2}\sqrt{(1-\eta)(1+\varepsilon)}\,\mathrm{e}^{\mathrm{i}\beta_+}\psi_{-1} + \tfrac{1}{\sqrt{2}}\sqrt{1+\eta}\,\mathrm{e}^{\mathrm{i}\beta_0}\psi_0 \tag{350}$$

$$+\tfrac{1}{2}\sqrt{(1-\eta)(1-\varepsilon)}\,\mathrm{e}^{\mathrm{i}\beta_-}\psi_+. \tag{351}$$

The defining parameters here are the phases β_{0+}, β_{0-}, β_{-+} and the amplitudes

$$\varepsilon = \frac{A_+^2 - A_-^2}{A_+^2 + A_-^2}, \qquad \eta = \frac{A_0^2 - A_+^2 - A_-^2}{A_0^2 + A_+^2 + A_-^2}. \tag{352}$$

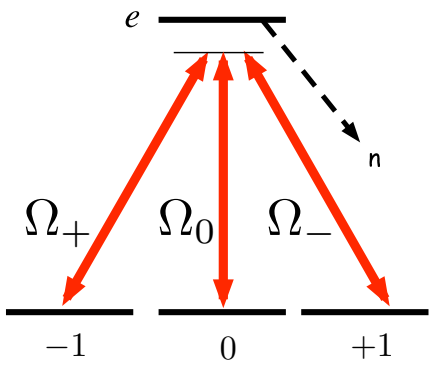

Fig. 79. Mapping population in three degenerate Zeeman sublevels, $M = -1, 0, +1$, onto excitation followed by fluorescence signal.

This bright state and the excited state are linked, with detuning Δ, by the effective Rabi frequency $\Omega(t) = \sqrt{A_0^2 + A_+^2 + A_-^2}\, f(t/T)$.

The population in this bright state, expressed in terms of density matrices, is

$$\begin{aligned} P_b(\varepsilon, \eta, \beta_{0+}, \beta_{0-}) &= R_{-1-1}(\varepsilon,\eta)\rho_{-1-1} + R_{00}(\varepsilon,\eta)\rho_{00} + R_{11}(\varepsilon,\eta)\rho_{11} \\ &+ R_{-10}(\varepsilon,\eta)\,|\rho_{-10}|\,\cos(\varphi_{-10} + \beta_{0+}) \\ &+ R_{01}(\varepsilon,\eta)\,|\rho_{01}|\,\cos(\varphi_{10} + \beta_{0-}) \\ &+ R_{-11}(\varepsilon,\eta)\,|\rho_{-11}|\,\cos(\varphi_{-11} + \beta_{-+}). \end{aligned}$$

Here the $R_{ij}(\varepsilon, \eta)$ are known functions.

The three probe fields act on this population to produce transitions into the excited state; the resulting population is proportional to the initial bright-state population and to a transition rate,

$$P_e(t) = p_{b\to e}(t, t_i) P_b. \tag{353}$$

The fluorescence signal $\mathcal{S}$ is proportional to this population (and to the probability η_b that this excited state will produce a fluorescence signal.) Thus the signal can be related to the initial bright-state population as

$$\mathcal{S} = \eta_b P_b \times \mathcal{P}_{b\to e}, \tag{354}$$

where $\mathcal{P}_{b\to e}$ is an appropriate time-integrated transition rate. For a short pulse the signal is

$$\mathcal{S} = \eta_b P_e(t_f) = \eta_b P_b \times\ p_{b\to e}(t, t_i). \tag{355}$$

where η is the probability that the population will produce a signal. For a long pulse, producing optical pumping, the signal is

$$\mathcal{S} = \eta_b\, \Gamma_e \int_0^\infty dt\ P_e(t) = \eta_b P_b \times \Gamma_e \int_0^\infty dt\ p_{b\to e}(t, t_i). \tag{356}$$

We conduct a series of measurements, each with a different setting of the excitation parameters. There results a set of linear equations relating the observed signal to combinations of the original density matrix elements,

$$\begin{aligned}\mathcal{S}(\varepsilon,\eta,\beta_{0+},\beta_{0-}) &= \eta\mathcal{P}_{b\to e}\,[R_{-1-1}\rho_{-1-1}+R_{00}\rho_{00}+R_{11}\rho_{11}\\ &+ R_{-10}\,|\rho_{-10}|\,\cos(\varphi_{-10}+\beta_{0+})\\ &+ R_{01}\,|\rho_{01}|\,\cos(\varphi_{10}+\beta_{0-})\\ &+ R_{-11}\,|\rho_{-11}|\,\cos(\varphi_{-11}+\beta_{-+})]\,.\end{aligned}$$

Here the quantities $R_{ij}(\varepsilon,\eta)$ are known; the unknowns to be determined are ρ_{ij}, ϕ_{ij} and η_b. In principle, one can evaluate the unknown parameters from a set of nine independent measurements of $\mathcal{S}$; cf. Vitanov et al. in [137].

13.3 Alternative schemes

A number of schemes for mapping degenerate superpositions onto fluorescence signals have been discussed for use with atomic beams [138]. Conceptually the simplest procedure for measuring a superposition that has been constructed with the aid of crafted laser pulses starting from a single state, is to attempt to reverse the process using a second set of adjustable laser pulses. When these precisely mimic the preparation-laser set in reversed time ordering, then the system will return to the initial state. By noting the conditions of the reversing-laser pulses that maximize the population in the single state, one can deduce the nature of the superposition.

When the superposition is produced in an atomic beam by a STIRAP transition into a set of magnetic sublevels, then in principle it is possible to reverse the procedure by passing the beam through a second pair of S and P beams but with the P pulse preceding the S pulse. If the polarizations of the second set of fields are identical to those of the first set, then all of the population will be returned to the single original state. When any other polarizations occur in the second set, then the population transfer will be incomplete. Thus a measurement of the population that returns to the original state, for various choices of polarizations in the second pair, will reveal the polarizations of the first pair of beams, and hence will reveal the parameters of the superposition; cf. Unanyan et al. [137].

Rather than employ a fixed set of measurements, as described here, one can instead proceed by a sequence of measurements that depend, at each step, upon the information gained from previous measurements [139]. Such a procedure allows progressive improvement in estimates.

14 Summary

Coherent excitation of a few-state quantum system, as induced by pulses of laser radiation, can produce a variety of predetermined changes. These range from distortion of the internal structure of an atom to the creation of stationary coherent superpositions.

This review has discussed some ways of inducing and picturing these changes. Although wavefunction displays serve well for depicting single orbitals, coherent changes in multi-electron atoms or molecules are exhibited most simply by presenting changes in Hilbert-space coordinates – either in a system of fixed coordinates or in a basis of steadily rotating coordinates. This review presents numerous examples. For any two-state system the Bloch sphere, and the Bloch vector, provide a useful depiction of the laser-induced changes. The evolution of an N-state system can be exhibited as multiple points on a single Bloch sphere or as a multidimensional coherence vector.

The relevant equation of motion governing coherent excitation is the time-dependent Schrödinger equation (TDSE), typically used in the rotating wave approximation (RWA). This review describes the use of rotating coordinates in Hilbert space to simplify both the numerical solution and the interpretation of the TDSE.

Two broad categories of coherent excitation have proven useful, and were here discussed: an interaction that, following sudden (impulsive) initiation, remains constant; and an interaction that changes slowly (adiabatically). Each of these idealizations allows simplified interpretations, based on eigenstates of the Hamiltonian as alternative coordinates in Hilbert space.

The goal of complete population transfer between quantum states, made possible with several pulsed excitation procedures, is a special case of the more general objective of creating predetermined coherent superpositions of quantum states. It corresponds to placement of the statevector along a predetermined direction in Hilbert space. For impulsive excitation this corresponds to a fraction of a Rabi cycle;

To verify the resulting superposition, or to analyze an unknown superposition, it is necessary to devise procedures that measure not only populations but relative phases of the constituent quantum states. Various schemes offer techniques for mapping the phases onto populations and thence onto various signals. Some of them have been discussed here. It is important to be mindful of the situations in which phase cannot be controlled.

The models and mathematics presented in this review, though originally developed to treat simple goals of optimizing excitation, continue to have relevance as interests shift toward very detailed manipulation of quantum states – often termed quantum-state engineering. Ongoing development of experimental techniques, combined with recognition of new applications of quantum theory, continue to make this theory relevant to contemporary research.

15 Acknowledgments

This review builds upon work begun decades ago, when the study of laser-induced changes to atomic structure was comparatively new. The theory underlying the resulting coherent excitation of atoms was relatively novel, and came together in a two-volume textbook published in 1990 [2]. That work owed much to collaborations with Mike Johnson, Dick Cook, Joe Eberly [140] and Peter Knight [141]. The subject has since expanded in many directions. I have continued to work on some of these and to give review talks. I am indebted to many colleagues for opportunities to expand my own understanding, reflected in the present review, notably Klaas Bergmann, Leonid Yatsenko, Razmik Unanyan, Nikolay Vitanov, Michael Fleischhauer and Thomas Halfmann, to all of whom I am grateful for stimulating discussions and some support. I am grateful to Vlado Buzek for encouraging the present manuscript.

16 Appendices

The following appendices provide a number of definitions and mathematical properties used in formulating descriptions of coherent excitation. They also present additional examples and clarifications of some aspects of the theory.

A Radiation parameters

Throughout this review the effect of radiation has been presented as an interaction between an atomic moment (specifically the electric dipole moment) and a nearly periodic electromagnetic field (specifically an electric field). Several useful possibilities exist for characterizing quantitatively the electric field and, in turn, the strength of the interaction between radiation and an atom. These rely on characteristics of the radiation, including intensity (typically expressed in W / cm^2), and of the atom, including a dipole transition moment or an equivalent parameter. The following paragraphs present basic equations descriptive of the radiation field, with particular emphasis on the fields appropriate to coherent excitation and quantum-state manipulation.

A.1 Radiation propagation

When the atoms form macroscopic aggregates, through which the laser radiation must pass, the laser-induced alteration of atomic states produces new fields that subtract from or add to the original field [2, Chap. 12]. As a result, pulses propagating through mtter are altered. The pulse amplitude will, at first, decreass (through absorption), but more dramatic effects can occur that drastically alter the shape of the pulse as it travels through greater thicknesses of matter. Furthermore, new frequencies may be generated.

Prior to the advent of laser radiation there was little interest in short pulses, and the equations describing radiation dealt with the flow of energy through matter that could absorb or divert the radiation [63, 142]. The matter was characterized by a static complex-valued index of refraction, whose imaginary part produced absorption while the real (dispersive) part altered the propagation velocity [143]. But as it became possible to create pulses whose duration was comparable to, or shorter than, the response time of the material (i.e. the Rabi frequency for two-state excitation), it was necessary to treat in more detail the coupling between matter and radiation [144].

The starting point for a description of the field changes is the set of Maxwell field equations [43, 145][2, §9.1]. The basic dynamical Maxwell equations for the fields $\mathbf{E}$ and $\mathbf{B}$ in matter are, using SI units

$$\nabla \times \mathbf{E} + \frac{\partial}{\partial t}\mathbf{B} = 0, \tag{357}$$

$$\nabla\times(\mathbf{B} - \mu_0\mathbf{M}) - \frac{1}{c^2}\frac{\partial}{\partial t}(\mathbf{E} + \epsilon_0\mathbf{P}) = \mu_0\mathbf{j}'. \tag{358}$$

The universal constants ϵ_0 (the permittivity of free space) and $\mu_0 = 1/c^2\epsilon_0$ occur as a consequence of using SI units To these we add the Maxwell equations of constraint

$$\nabla \cdot \mathbf{B} = 0, \qquad \nabla\cdot(\epsilon_0\mathbf{E} + \mathbf{P}) = \rho'. \tag{359}$$

The field $\mathbf{j}'$ expresses any currents of free charge; the field ρ' is the density of free charge. Both of these fields are absent in the treatment of radiation propagating through neutral matter. The fields $\mathbf{P}$ and $\mathbf{M}$ express, respectively, the polarization and magnetization density (Amperian currents).

The two dynamical equations combine to produce the single inhomogeneous *wave equation*

$$\nabla \times \nabla \times \mathbf{E} + \frac{1}{c^2}\frac{\partial^2}{\partial t^2}\mathbf{E} = -\mu_0 \frac{\partial^2}{\partial t^2}\mathbf{P} - \mu_0 \frac{\partial}{\partial t}\nabla \times \mathbf{M} - \mu_0 \frac{\partial}{\partial t}\mathbf{j}'. \tag{360}$$

Given a solution to the wave equation for $\mathbf{E}$, we can determine the companion magnetic field $\mathbf{B}$ by integrating eqn. (357). In the absence of free-charge currents ($\mathbf{j}' = 0$), as is the case for neutral matter assumed in the following , the time and spatial variations of the polarization field $\mathbf{P}$ and magnetization field $\mathbf{M}$ act as the sole sources for the electric and magnetic fields $\mathbf{E}$ and $\mathbf{B}$.

Several approximations are commonly made when using the wave equation for quantum optics. The first of these treats the electric and magnetic fields near the atom as transverse plane waves. Any vector field $\mathbf{F}$ can be expressed as the sum of a lamellar (longitudinal) part $\mathbf{F}^L$ whose curl vanishes and a solenoidal (transverse) part $\mathbf{F}^T$ whose divergence vanishes [77]

$$\nabla \times \mathbf{F}^L = 0, \qquad \nabla \cdot \mathbf{F}^T = 0. \tag{361}$$

By applying this decomposition to the electric field $\mathbf{E}$ and polarization field $\mathbf{P}$ we obtain, n the absence of free currents and magnetization, the *wave equation*

$$\left[\nabla^2 - \frac{1}{c^2}\frac{\partial^2}{\partial t^2}\right]\mathbf{E}^T = \mu_0 \frac{\partial^2}{\partial t^2}\mathbf{P}^T. \tag{362}$$

It is the solenoidal part of the electric field, $\mathbf{E}^T$, that constitutes the propagating radiation, and it is this field that is to be determined here. However, the field acting on the atom, and parametrized as the Rabi frequency, is the total field. For typographical simplicity I shall omit the label T upon this field; the field $\mathbf{E}$ and its source field $\mathbf{P}$ are to be understood as transverse.

It is customary, in quantum optics, to idealize the matter as a homogeneous distribution of identical atoms, each having electric dipole moment $\langle \mathbf{d} \rangle$ and magnetic moment $\langle \mathbf{m} \rangle$. With this approximation the polarization and magnetization fields are the expectation values,

$$\mathbf{P} = \mathcal{N}\langle \mathbf{d} \rangle, \qquad \mathbf{M} = \mathcal{N}\langle \mathbf{m} \rangle, \tag{363}$$

where $\mathcal{N}$ is the number density of atoms. It is through these macroscopic fields that the effects of atomic excitation alter the radiation.

For weak steady-state monochromatic radiation (as contrasted with transient pulsed radiation), or for steady nonresonant radiation, the atomic dipole moment expectation value $\langle \mathbf{d} \rangle$ is an induced moment directly proportional to the electric field $\mathbf{E}$. (This proportionality is readily understood from the Lorentz model of Appendix I.) Under these conditions the macroscopic polarization field $\mathbf{P}$ is linearly proportional to the electric field. When coherent excitation occurs, this proportionality fails. In particular, it fails for the first few cycles of an incident electric field,

[77] For plane waves the solenoidal (divergenceless) fields are transverse to the propagation direction whereas the lamellar fields are directed longitudinally, along the propagation axis. Because we usually deal with plane waves it is customary to refer to radiation fields as transverse.

before the atom has been able to equilibrate with the altered environment. Nonetheless it is useful to retain a description of the incoherent effects by writing the polarization field as comprising two parts, one linear and the remainder nonlinear

$$\mathbf{P} = {}^{lin}\mathbf{P} + {}^{nl}\mathbf{P}. \tag{364}$$

The mathematics of radiation description simplifies by expressing the real fields $\mathbf{E}$ and $\mathbf{P}$ as sums of two complex fields, corresponding to positive and negative frequency parts, e.g.

$$\mathbf{E} = \mathbf{E}^{(+)} + \mathbf{E}^{(-)} = 2\mathrm{Re}\mathbf{E}^{(+)}. \tag{365}$$

We then write the linear contribution to the positive frequency part of the polarization field as

$${}^{lin}\mathbf{P}^{(+)} = \chi\mathbf{E}^{(+)} = (\epsilon_b - \epsilon_0)\mathbf{E}^{(+)} = \mathcal{N}\alpha\mathbf{E}^{(+)}. \tag{366}$$

In general both χ (the electric susceptibility) and ϵ_b (the dielectric constant) as well as the single-atom polarizability α, will be complex-valued time-dependent (or frequency-dependent) tensors (cf. Sec. 10.3.2).

As may be surmised, the separation of $\mathbf{P}$ into these parts is, to some extent, arbitrary. The simplest procedure is to regard the contribution to the nonlinear part as arising in the dynamics of the near-resonant quantum states, i.e. the essential states. The remaining, linear, portion is attributed to the virtual levels that are treated by means of an effective Hamiltonian, cf. Sec. 10.3.2.

We use the linear portion of the polarization field, as parametrized by ϵ_b, to define a refractive index (possibly complex)

$$\eta_b = c\sqrt{\mu_b\epsilon_b}. \tag{367}$$

The resulting inhomogeneous wave equation for the E field reads, in the absence of magnetization and free currents,

$$\left[\nabla^2 - \frac{(\eta_b)^2}{c^2}\frac{\partial^2}{\partial t^2}\right]\mathbf{E}^{(+)} = \frac{\partial^2}{\partial t^2}\mu_b\,{}^{nl}\mathbf{P}^{(+)}. \tag{368}$$

This equation applies quite generally. For application to excitation by laser pulses several further approximations prove useful.

A.2 Radiation intensity

In the absence of the polarization field ${}^{nl}\mathbf{P}^{(+)}$, e.g. in vacuum (so $\eta_b = 1$) , the wave equation for $\mathbf{E}^{(+)}$, eqn. (368), is homogeneous. It then has such solutions as the plane wave $\exp(\mathrm{i}\mathbf{k}\cdot\mathbf{r} - \mathrm{i}\omega t)$, where the propagation vector $\mathbf{k}$ has Cartesian components k_x, k_y, k_z and is constrained in magnitude by the frequency, $|\mathbf{k}| = \eta_b\omega/c$. A simple example is the form assumed throughout this review for the linearly polarized radiation, at fixed position $\mathbf{r}$,

$$\mathbf{E}(t) = \hat{\mathbf{e}}\,\mathcal{E}(t)\,\cos(\omega - \varphi), \tag{369}$$

where $\hat{\mathbf{e}}$ is a unit vector descriptive of the electric field direction (transverse to the propagation direction) and $\mathcal{E}(T)$ is a real-valued pulse envelope. The phase φ appearing here is expressible, for given Cartesian coordinates x, y, z, as

$$\varphi = k_x x + k_y y + k_z z, \qquad k_x^2 + k_y^2 + k_z^2 = (\eta_b\omega/c)^2. \tag{370}$$

This plane wave is accompanied by a magnetic field; in SI units it is

$$\mathbf{B}(t) = \frac{1}{c}\hat{\mathbf{k}}\times\mathbf{E}(t), \tag{371}$$

where $\hat{\mathbf{k}}$ is a unit vector in the direction of propagation and $\times$ indicates the vector, or cross, product. The momentum flow of this wave, expressed by the *Poynting vector* $\mathbf{S}(t)$, is proportional to the cycle-averaged vector product of the E and B fields,

$$\mathbf{S}(t) = c^2\epsilon_0\{\mathbf{E}(t)\times\mathbf{B}(t)\}_{av}. \tag{372}$$

The intensity of this beam (power per unit area) $I(t)$, defined as the magnitude of the Poynting vector, is proportional to the cycle-averaged square of the electric field; in SI units the relationship is

$$I(t) = c\epsilon_0\{|\mathbf{E}(t)|^2\}_{av} = \tfrac{1}{2}c\epsilon_0\{|\mathcal{E}(t)|^2\}_{av}. \tag{373}$$

The numerical connection between the field amplitude $\mathcal{E}(t)$ of eqn. (369) and the intensity $I(t)$ is

$$|\mathcal{E}(t)[\text{V / cm}]| = 27.4\sqrt{I(t)[\text{W/cm}^2]}. \tag{374}$$

A.3 Spatial modes

Traveling waves can be coherently superposed to create standing waves, associated with a rectangular reflecting enclosure. Traveling-wave solutions also include cylindrical waves and the focused Gaussian beams that characterize the output of many laser devices [11].

To categorize the various solutions to the homogeneous wave equation it is often helpful to consider monochromatic fields, for which the positive-frequency field $\mathbf{E}^{(+)}$ has the time dependence $\exp(-\mathrm{i}\omega t)$. Upon extracting this factor as

$$\mathbf{E}^{(+)}(\mathbf{r},t) = \mathbf{U}_\lambda(\mathbf{r})\exp(-\mathrm{i}\omega t), \tag{375}$$

(with λ an identifier to be further defined) the homogeneous field equation becomes the *Helmholtz equation*

$$\nabla^2\mathbf{U}_\lambda(\mathbf{r}) = k^2\mathbf{U}_\lambda(\mathbf{r}), \qquad k \equiv \eta_b\omega/c. \tag{376}$$

That is, the E field is an eigenfunction of the differential operator ∇^2, with eigenvalue k^2. The field $\mathbf{U}_\lambda(\mathbf{r})$ is a *spatial mode*. The label λ distinguishes amongst the functions sharing a common eigenvalue.

There are many possible ways of obtaining solutions to the Helmholtz equation, and the sets of mode fields [2, §9.6]. The equation is separable in a number of coordinate systems, and each of these provides boundary surfaces over which the field has constant value. Cartesian coordinates, with plane parallel surfaces, offer a simple example, as do spherical coordinates, where spheres and angular planes provide the surfaces. Each separable coordinate system leads to analytic functions with which to describe the mode fields, and to boundary surfaces on which the field can be fixed, say with null value. Such fields can be labeled, in part, by the number of nodes in each coordinate.

Another way to characterize the solutions, and to specify λ, is to supplement the differential operator ∇^2 with additional operators whose eigenvalues provide the desired labels. One such operator is the spin operator $\mathbf{S}$: electromagnetic fields are vector fields in three dimensions, and so they are examples of spin-one fields; cf. Appendix C.2. For them the operator $\mathbf{S}^2$ has the value $S(S+1) = 2$.

Propagating plane-wave laser fields, with spatial variation $\exp(\mathrm{i}\mathbf{k}\cdot\mathbf{r})$, have well defined *linear* momentum, meaning they are eigenstates of $\hbar\nabla$ with eigenvalue $\mathbf{k}$. Fields radiated by an atom in free space carry *angular* momentum; their angular variation is characterized by vector spherical harmonics $\mathbf{Y}_{\ell JM}(\hat{\mathbf{r}})$ [2, §19.5].

Modes bearing different labels can be constructed to be orthogonal, and can be normalized such that

$$\int d\mathbf{r}\; \mathbf{U}_\lambda(\mathbf{r})^* \cdot \mathbf{U}_{\lambda'}(\mathbf{r}) = \delta_{\lambda,\lambda'}. \tag{377}$$

They typically provide a complete set of vector fields with which to describe any radiation field. The following table provides some examples of useful ways of characterising the fields.

λ	Eigenstates of	$\mathbf{U}_\lambda(\mathbf{r})$
Linearly polarized plane waves $(j = X, Y, Z)$		
$\mathbf{k}j$	$\mathbf{S}^2$, ∇^2, ∇	$\frac{1}{\sqrt{(2\pi)^3}}\mathbf{e}(j,\hat{\mathbf{k}})\exp(\mathrm{i}\mathbf{k}\cdot\mathbf{r})$
Helicity plane waves $(q = +1, 0, -1)$		
$\mathbf{k}q$	$\mathbf{S}^2$, ∇^2, ∇, $\mathbf{S}\cdot\nabla$	$\frac{1}{\sqrt{(2\pi)^3}}\mathbf{e}(q,\hat{\mathbf{k}})\exp(\mathrm{i}\mathbf{k}\cdot\mathbf{r})$
Vector harmonic spherical waves $(\ell \geq 0, J \geq 1)$		
$k\ell JM$	$\mathbf{S}^2,\ \nabla^2,\ \mathbf{L}^2,\ \mathbf{J}^2,\ J_z$	$\sqrt{\frac{2k^2}{\pi}}j_\ell(kr)\mathbf{Y}_{\ell JM}(\hat{\mathbf{r}})$

A.4 Photons

By expressing the electric field in terms of mode fields,

$$\mathbf{E}^{(+)}(\mathbf{r},t) = \Sigma_\lambda a_\lambda(t)\mathbf{U}_\lambda(\mathbf{r}), \tag{378}$$

one finds that the homogeneous wave equation leads to a dynamical equation for the amplitude $a_\lambda(t)$ that is recognizable as the equation of motion for an harmonic oscillator,

$$\frac{d^2}{dt^2}a_\lambda(t) = -\omega^2 a_\lambda(t). \tag{379}$$

To treat the electromagnetic field as a dynamical entity, governed by quantum theory, we need only treat these amplitudes as quantum variables. Quantization takes place by requiring that they become noncommuting operators,

$$[\hat{a}_\lambda(t)\ ,\ \hat{a}^\dagger_\lambda(t)] = \delta_{\lambda,\lambda'}. \tag{380}$$

and to introduce, as basis states upon which they act, eigenstates of the *number operator*

$$\hat{n}_\lambda(t) = \hat{a}^\dagger_\lambda(t)\, \hat{a}_\lambda(t). \tag{381}$$

The operator $a^\dagger_\lambda(t)$ acts to increase by one the eigenvalue of the number operator for the field in mode λ: It increments the field in this mode. One defines a *photon* of type λ as an increment of the electromagnetic field. Thus the operator $a^\dagger_\lambda(t)$ creates a photon (of type λ). The operator $a_\lambda(t)$ removes one field increment, i.e. annihilates one photon. Because there are many useful ways of choosing the mode fields, there are a corresponding multitude of photon types: traveling waves or standing waves, plane waves or spherical waves, etc. Each type of solution to the Helmholtz equation produces a corresponding type of photon. Often we deal with a single mode, and omit the classifying label λ.

The traditional basis states for treating quantized radiation are the single-mode photon-number states ϕ_n, defined by the requirements that

$$\hat{a}^\dagger \hat{a}\ \phi_n = n\ \phi_n \qquad \text{and} \quad \langle \phi_n | \phi_{n'} \rangle = \delta_{n,n'}. \tag{382}$$

The totality of such states, for a single mode, form a *Fock space*. The photon creation and annihilation operators have the following effects upon these number states

$$\hat{a}^\dagger \phi_n = \sqrt{n+1}\ \phi_{n+1}, \qquad \hat{a}\phi_n = \sqrt{n}\ \phi_{n-1}. \tag{383}$$

Using photon operators we write the electric field, for a single mode, as

$$\mathbf{E} = \tfrac{1}{2}[\hat{\mathbf{e}}\mathcal{E}_1 \hat{a} + \hat{\mathbf{e}}^* \mathcal{E}_1^* \hat{a}^\dagger]. \tag{384}$$

In the traditional case of modes defined within a box of volume $\mathcal{V}$ (e.g., a cube of side L, or $\mathcal{V} = L^3$) the single-photon electric field $\mathcal{E}_1$ is

$$\mathcal{E}_1 = \sqrt{2\hbar\omega/\epsilon_0 \mathcal{V}} e^{\mathrm{i}\varphi}. \tag{385}$$

Although photon number states ϕ_n have long provided a convenient basis for calculations, they are by no means the only useful field states. A particularly useful set of basis states, the Glauber *coherent states* [146], are defined, for complex-valued parameter α, as

$$|\alpha\rangle = \Sigma_{n=0}^{\infty} \phi_n \frac{\alpha^n}{\sqrt{n!}} \exp\left(-\tfrac{1}{2}|\alpha|^2\right). \tag{386}$$

The absolute value of α is the mean photon number, $\bar{n}$, while its phase is that of the field. Such a basis provides the most classical description of a single-mode field, although they are not orthogonal; their overlap is

$$\langle \alpha | \beta \rangle = \exp[\alpha^* \beta - \tfrac{1}{2}|\alpha|^2 - \tfrac{1}{2}|\beta|^2]. \tag{387}$$

To describe a single-mode thermal field at temperature T one requires a density matrix,

$$\rho = \Sigma_{n=0}^{\infty} |\phi_n\rangle p_n(T) \langle \phi_n|, \qquad p_n(T) = [1 + \exp(-\hbar\omega/k_B T)] \exp(-n\hbar\omega/k_B T), \tag{388}$$

where k_B is the Boltzmann constant. The mean photon number for this distribution is

$$\bar{n} = [\exp(\hbar\omega/k_B T) - 1]^{-1}. \tag{389}$$

At high temperatures this approaches the value $\bar{n} \approx \hbar\omega/k_B T$ and the distribution has the probability function

$$p_n(T) = (1/\bar{n}) \exp(-n/\bar{n}). \tag{390}$$

A.5 Pulse propagation

Following conventions of quantum optics we next assume that the refractive index varies slowly, so that there are no reflections from surfaces, and we neglect transverse variation (i.e. we treat the field, at least locally, as a plane wave). We therefore need only deal with forward propatting waves, each of which varies only with the propagation distance z. We therefore write the field as a plane wave, propagating along the z direction, writing [78]

$$\mathbf{E}^{(+)} = \tfrac{1}{2}\hat{\mathbf{e}}\,\mathcal{E}(z,t)\exp(\mathrm{i}kz - \mathrm{i}\omega t). \tag{391}$$

We similarly treat the polarization field as having a single carrier frequency [79],

$${}^{nl}\mathbf{P}^{(+)} = \tfrac{1}{2}\hat{\mathbf{e}}\,\mathcal{P}(z,t)\exp(\mathrm{i}kz - \mathrm{i}\omega t). \tag{392}$$

Then the inhomogeneous wave equation reads

$$\left[\frac{\partial^2}{\partial z^2} - \frac{(\eta_b)^2}{c^2}\frac{\partial^2}{\partial t^2}\right]\mathcal{E}(z,t) = \frac{\partial^2}{\partial t^2}\mu_b\mathcal{P}(z,t). \tag{393}$$

As a final step in the series of traditional idealizations we assume that the envelopes vary only slightly during one cycle of the field,

$$|\frac{\partial}{\partial z}\mathcal{F}| \ll |k\mathcal{F}|, \qquad \frac{\partial}{\partial t}\mathcal{F}| \ll |\omega\mathcal{F}|, \tag{394}$$

where $\mathcal{F}$ is either $\mathcal{E}$ or $\mathcal{P}$. With this approximation we obtain the traditional *slowly-varying envelope approximation* (SVEA),

$$\left[\frac{\partial}{\partial z} + \frac{\eta_b}{c}\frac{\partial}{\partial t}\right]\mathcal{E}(z,t) = \frac{2\pi\omega}{c\epsilon_0\eta_b}\mathrm{i}\mathcal{P}(z,t). \tag{395}$$

The presence of the imaginary unit i on the right-hand side of this equation means that the electric field envelope $\mathcal{E}$ is affected by the polarization envelope that is out of phase with $\mathcal{E}$, when referred to the phase of the carrier $\exp[\mathrm{i}(kz - \omega t)]$.

The equation simplifies when we take, as the time variable for the envelope functions $\mathcal{E}$ and $\mathcal{P}$, a time fixed in a coordinate system that moves with the pulse envelope,

$$\tau = t - \frac{z}{c}\eta_b. \tag{396}$$

In this coordinate system the pulse envelope obeys the simple equation

$$\frac{\partial}{\partial z}\mathcal{E}(z,\tau) = \frac{\omega}{2\eta_b}\sqrt{\epsilon_0}\,\mathrm{i}\mathcal{P}(z,\tau). \tag{397}$$

This is the equation that is customarily used (usually with $\eta_b = 1$) to describe coherent pulse propagation, in the plane-wave SVEA[2, § 12.4]. It represents half of a set of radiation-matter equations. The other half describes the time variation of the polarization, given the electric field,

[78] More generally one should allow multiple carrier frequencies.

[79] We thereby neglect all forms of nonlinear optics in which new frequencies occur, e.g. four-wave mixing.

that is, the time-dependent Schrödinger equation. To make this connection for a two-state atom we introduce the coherence field [2, §12.6]

$$Q(t) = \tfrac{1}{2}\left[r_2(t) + \mathrm{i}r_1(t)\right], \tag{398}$$

constructed from two components of the Bloch vector (cf. Sec. 7.1). The equation for the E field then reads

$$\frac{\partial}{\partial z}\mathcal{E}(z,\tau) = \mathcal{N}(z)\frac{\omega}{c\epsilon_0}\mathbf{d}_{12}\cdot\hat{\mathbf{e}}^* Q(z,\tau). \tag{399}$$

We see that it is the *coherence* (the off-diagonal element of the density matrix), rather than the population inversion, that produces change in a pulse envelope. Depending on the phase of the coherence the result will either be growth of the electric field (i.e. *gain*), as energy transfers from atomic excitation into the field, or diminution of electric field (i.e. absorption and loss), as energy passes from the field to the atoms.

A consistent treatment of pulse propagation requires simultaneous consideration of both the Maxwell equations for the fields and either the Schrödinger equation or density-matrix equations for the atoms, as in the coupled Maxwell-Bloch equations [1, 10, 11, 147]. Treatments of multilevel atoms requires straightforward extension of the two-state atomic equations [148].

When several fields occur, as happens with Raman processes (involving P and S fields), each obeys eqn. (397) with an appropriate source field $\mathcal{P}$. The $\mathcal{P}$ field (i.e. the coherence) may either alter a pre-existing pulse envelope $\mathcal{E}$ or it may serve as the source of a new field, at a frequency set by the frequency of the coherence. The TDSE couples these several coherences, under the influence of the fields, and causes, for example, the growth of the coherence responsible for creating the S field, while adjusting the P-field coherence to produce a diminution of the P field.

As these remarks show, it is the single-atom dipole moment $\langle\mathbf{d}\rangle$ that is responsible, through contribution to the macroscopic polarization field $\mathbf{P}$, for the absorption coefficient and the refractive index of traditional optics [40, 11]. The behavior of time-varying dipole moments, or coherences, also underly the variety of nonlinear optics processes [149] in which several fields combine to produce a coherence which, in turn, serves as the source of a new field, as in CARS [105].

A.6 Spectroscopic parameters

From traditional spectroscopic studies come several parameters with which to describe the resonant interaction between light and an atom – one that exists, ideally, in free space and which therefore has degenerate energy levels. The statistical weight ϖ_n of level n is the angular momentum degeneracy $\varpi_n = (2J_n + 1)$.

The simplest connection between spectral propertis and atomic structure is through the dimensionless *transition strength* $S(1,2)$, the square of the absolute value of the electric dipole transition moment $\mathbf{d}_{12} \equiv \langle 1|\mathbf{d}|2\rangle$ expressed in atomic units [2, §2.9], i.e. the electron charge e times the Bohr radius a_0,

$$S(1,2) = S(2,1) = |\mathbf{d}_{12}|^2/\left(ea_0\right)^2, \tag{400}$$

$$a_0 \equiv (\hbar^2/me^2) \simeq 0.529\times10^{-10}\ \mathrm{m}, \qquad |ea_0| \simeq 2.542\ \text{debye}\ . \tag{401}$$

For transitions between states of angular momentum this is proportional to the reduced matrix element of the dipole moment,

$$S(J, J') = \frac{|(J||d||J')|^2}{(ea_0)^2}. \tag{402}$$

The Einstein A coefficient is expressible using the transition strength as

$$A_{21} = \frac{1}{\tau_{AU}} \frac{4}{3} \left(\frac{2\pi a_0}{\lambda} \right)^3 \frac{S(1,2)}{\varpi_2}, \tag{403}$$

where $\tau_{AU} = a_0/\alpha c \approx 2.42 \times 10^{-17}$ sec is the atomic unit of time and $\lambda_0 = 2\pi c/\omega_0$ is the wavelength corresponding to the Bohr frequency ω_0. The dimensionless absorption oscillator strength (see Appendix. I), for a transition of wavelength λ_0 between degenerate levels having statistical weights ϖ_n, is

$$f_{12} = \frac{4\pi}{3\alpha} \frac{a_0}{\lambda} \frac{S(1,2)}{\varpi_1}. \tag{404}$$

B Mathematics

The following paragraphs review some elementary properties of some of the formal mathematical structures that find use in modeling coherent excitation.

B.1 Vectors and vector spaces

The concept of abstract vector spaces underlies much of mathematical physics [59]. A *vector* is an ordered set of numbers, say $\{a, b, c, \ldots\}$. The number of elements (the number of components) is the *dimension* of the vector. With the requirement that the individual components obey rules of addition, subtraction, multiplication and division by scalars, the set of all vectors of a given dimension N form an abstract *vector space* of dimension N. With the addition of measures of length the space is a *metric space*; the further addition of measures of angle makes the space an *inner product space*.

A simple example occurs when when we specify the three Cartesian coordinates of a mass point or the three angles needed to specify the orientation of a stationary rigid body; these three real numbers are coordinates in a vector space. With the addition of three coordinates descriptive of the rates of change in these coordinates, i.e. velocities, we have a *system space*. A vector space defined by position and momentum coordinates is a *phase space*. In quantum mechanics phase spaces occur with field variables, e.g. phase and amplitude. More generally we might deal with an assembly of parts, each of which requires definition by position and orientation together with their rates of change. A point in this higher dimensional space, a *system point*, provides a complete description of the system when the parts are macroscopic objects (i.e. not noticeably affected by the Heisenberg position-momentum uncertainty relationship that affects microscopic objects).

B.2 Hilbert space

When the elements of the vectors comprising a vector space are complex numbers and finite in number, amongst which both lengths and angles are defined (i.e. a vector space with inner products), the abstract space is a *Hilbert space* [80].

As with other vector spaces, a vector in a Hilbert space, often denoted using the Dirac ket notation $|\cdots\rangle$, is defined by its coordinates. We can regard these as elements of a column vector, say

$$|A\rangle = \begin{bmatrix} A_1 \\ A_2 \\ \vdots \\ A_N \end{bmatrix}, \tag{405}$$

in which the (complex-valued) number A_n is the component along the nth coordinate. The scalar (or *inner*) product of two Hilbert-space vectors, denoted $\langle A|B\rangle$, is defined as the number (possibly complex)

$$\langle A|B\rangle = \Sigma_n A_n^* B_n, \tag{406}$$

where the symbol $\langle A|$ denotes the row vector obtained by transposing columns of A into rows and taking complex conjugates of each element. When the scalar product vanishes, the two vectors are *orthogonal*, a generalization of perpendicular lines of Euclidean geometry. The length of a vector is the square root of the sum of the separate components squared,

$$|A| = \sqrt{\langle A|A\rangle} = \sqrt{\Sigma_n |A_n|^2}, \tag{407}$$

a generalization of the Pythagorean theorem for evaluating the hypotenuse of a right triangle. Vectors whose length is unity are *unit vectors*.

To identify an arbitrary vector in an N-dimensional Hilbert space it is sufficient to specify components along N independent vectors. These need not be orthogonal, but they must provide a complete set, meaning that they suffice to express any vector. Mathematicians refer to such a set as a set of *basis vectors*. In the use of Hilbert space for treating statevectors it is customary to use only sets of orthogonal unit vectors – an *orthonormal set* – as basis vectors.

The connection between Hilbert space and experimental physics takes place through the identification of the basis vectors with quantum states, i.e. with physical states of motion whose properties are amenable to experimental discovery, cf. eqn. 29. Such quantum states are eigenstates of some "unperturbed" Hamiltonian, whose eigenvalues provide the discrete observable energies E_n. In this context the terms "quantum state" and "basis state" or "basis vector" are used interchangeably.

To label the several coordinate axes in this abstract space we use the same integer labels as for the catalog of quantum states. Several notations are useful for Hilbert-space unit vectors,

[80] Hilbert spaces may have denumerably many dimensions. Then they must possess the additional property that any Cauchy sequence is an element of the space.

such as ψ_n and $|n\rangle$. They can also be written as column vectors,

$$\psi_1 = |\psi_1\rangle = |1\rangle = \begin{bmatrix} 1 \\ 0 \\ 0 \\ \vdots \end{bmatrix}, \quad \psi_2 = |\psi_2\rangle = |2\rangle = \begin{bmatrix} 0 \\ 1 \\ 0 \\ \vdots \end{bmatrix}, \cdots . \tag{408}$$

These unit vectors (or the quantum states they represent) have been given various names, such as "bare states" and "diabatic states". Because they are associated with the physically observable quantum states they might well be called "physical states".

When degeneracy is present (see Sec. 8) there is some flexibility in the choice of the unit vectors (or basis states), but always they must include all relevant observable quantum states of the system: they must be independent and complete. Because the associated quantum states are (presumably) distinct, the set of unit vectors can be taken as orthogonal as well as having unit length (i.e. they are *orthonormal*), as expressed by the equation

$$\langle \psi_n | \psi_m \rangle \equiv \langle n | m | \rangle = \delta_{n,m}, \tag{409}$$

where $\delta_{n,m}$ is the Kronecker delta: it is 1 if $n = m$ and 0 otherwise. These N orthogonal unit vectors represent the observable physical quantum states in the absence of laser fields.

B.3 Matrices

Matrices, used extensively here, have been important in applied mathematics and a wide variety of applications [150]. A matrix is a rectangular (or square) array of numbers (possibly complex) labeled by two integer subscript indices; e.g. the numbers M_{nm} with integer n, m, form the matrix M, with n labelling the column and m labeling the row. If there are N rows and M columns the dimension is $N \times M$. A matrix is *square* when it has the same number of rows and columns. A *column vector* is a special case of a rectangular matrix, consisting of just a single column. The transpose of a column vector is a row vector.

From a given matrix one obtains a number of related matrices. The notation M^T denotes the *transpose* of matrix M, obtained by interchanging rows and columns. The *complex congugate* of matrix M, denoted M^*, is obtained by replacing i with $-$i in each each element. The *Hermitian adjoint*, denoted $\mathsf{M}^\dagger$, is the transpose of the complex conjugate (or the complex conjugate of the transpose).

Amongst the types of matrices finding application for quantum-state manipulation are *symmetric*, for which $\mathsf{M}^T = \mathsf{M}$ or $M_{nm} = M_{mn}$; *Hermitian*, for which $\mathsf{M}^\dagger = \mathsf{M}$ or $M_{nm} = M^*_{mn}$; *diagonal*, in which the only nonzero elements are on the diagonal, M_{nn}; *bordered*, for which only one column and one row have nonzero elements; and *banded*, in which the nonzero elements run parallel to the diagonal elements (*tridiagonal* is a special case, in which the bands $M_{n,n\pm1}$ are nonzero and the diagonal elements are arbitrary.).

The *unit matrix*, denoted $\mathbf{1}$, has only nonzero elements along the diagonal; these are all 1. The *trace* of a matrix, Tr M, is the sum of the diagonal elements:

$$\text{Tr } \mathsf{M} = \Sigma_n M_{nn}. \tag{410}$$

The *determinant* of a (square) matrix of dimension N, denoted variously as Det (M) or $|\mathsf{M}|$, is defined as a series of $N!$ terms, each of which contains N factors. The formula reads

$$\text{Det}\,(\mathsf{M}) = |\mathsf{M}| = \Sigma_{jkm\ldots}(-1)^{\phi} M_{1j} M_{2k} M_{3m} \ldots, \tag{411}$$

where the sum goes over all subscripts $j, k, m, \ldots$ such that none of these indices repeat and ϕ is 0 or 1 depending on the permutation of the subscript sequence. For example, for $N = 2$ the determinant is

$$|\mathsf{M}| = M_{11}M_{22} - M_{12}M_{21}. \tag{412}$$

The determinant of higher order reduces to the evaluation of lower-order determinants, generalizing the algorithm shown here for $N = 3$:

$$|\mathsf{M}| = M_{11}\begin{vmatrix} M_{22} & M_{23} \\ M_{32} & M_{33} \end{vmatrix} - M_{12}\begin{vmatrix} M_{21} & M_{33} \\ M_{31} & M_{32} \end{vmatrix} + M_{13}\begin{vmatrix} M_{21} & M_{22} \\ M_{31} & M_{32} \end{vmatrix}. \tag{413}$$

The determinant is antisymmetric with respect to the interchange of any two columns or any two rows. The eigenvalues of the $N \times N$ matrix M are the roots λ of the determinantal equation

$$\text{Det}\,(\mathsf{M} - \lambda \mathbf{1}) = 0. \tag{414}$$

The eigenvalues of any Hermitian matrix are real numbers.

Multiplication of two matrices obeys the following construction:

$$\text{if } \mathsf{AB} = \mathsf{C} \text{ then } C_{nm} = \Sigma_k A_{nk} B_{km}. \tag{415}$$

For example, the product of a 2×2 matrix with a two-element column matrix is another two-element column matrix,

$$\begin{bmatrix} a & b \\ c & d \end{bmatrix}\begin{bmatrix} A \\ B \end{bmatrix} = \begin{bmatrix} aA + bB \\ cA + dB \end{bmatrix}. \tag{416}$$

Matrix multiplication is, in general, noncommutative, i.e. $\mathsf{AB} \neq \mathsf{BA}$. The *commutator* of two matrices is denoted by a square bracket, $[\mathsf{A}, \mathsf{B}] \equiv \mathsf{AB} - \mathsf{BA}$. The multiplication of a column vector $\mathbf{V}$ with a square matrix M, is a column vector $\mathbf{V}' = \mathsf{M}\mathbf{V}$ having elements

$$V'_n = \Sigma_m M_{nm} V_m. \tag{417}$$

The inverse of matrix M is denoted M^{-1}; if it exists it is defined by the equation

$$\mathsf{M}^{-1}\mathsf{M} = \mathsf{M}\mathsf{M}^{-1} = \mathbf{1}. \tag{418}$$

A matrix is *orthogonal* if the inverse is equal to the transpose, i.e

$$\mathsf{M}^{T}\mathsf{M} = \mathsf{M}\mathsf{M}^{T} = \mathbf{1}. \tag{419}$$

Any orthogonal matrix has the property Det $(\mathsf{M}) = \pm 1$. A matrix is *unitary* if the inverse is equal to the Hermitian adjoint i.e

$$\mathsf{M}^{\dagger}\mathsf{M} = \mathsf{M}\mathsf{M}^{\dagger} = \mathbf{1}. \tag{420}$$

Any unitary matrix has the property $|\mathrm{Det}\ (\mathsf{M})| = 1$ Elements of orthogonal and unitary matrices are related by the equations

$$\text{Orthogonal:} \quad \Sigma_j M_{ij} M_{kj} = \delta_{i,k}, \tag{421}$$

$$\text{Unitary:} \quad \Sigma_j M_{ij} M^*_{kj} = \delta_{i,k}. \tag{422}$$

Functions of matrices receive definition based on power series, replacing a scalar variable by a matrix. An important example is the exponential function of a matrix. This is a matrix, defined by the same power series used to define the traditional exponential,

$$\exp(\mathsf{M}) = \Sigma_{n=0}^{\infty} \frac{(\mathsf{M})^n}{n!}. \tag{423}$$

Other scalar functions, defined by convergent power series (e.g. Taylor, Maclaurin, Laurent, etc.) similarly generalize to define functions of matrices.

B.4 Operators

The term *operator* refers to the symbol used for presenting a mapping of elements from one set to another, $\{x\} \rightarrow \{x'\}$ according to some rule; it symbolizes an *operation* or transformation, in which the operator *acts on* set elements. Often the set undergoing the change is the set of values for a function, say $f(x)$; the operator may then be the derivative or the integral or may stand for some other alteration of function values, e.g. a shift $f(x) \rightarrow f(x + a)$. Matrices, when multiplying (acting on) a column vector, are other examples of operators.

In quantum theory the Hamiltonian operator incorporates partial derivatives when acting on a wavefunction, and behaves as a matrix when acting on a statevector. Angular momentum operators, when acting on functions, such as spherical harmonics, involve partial derivatives; they are then examples of *orbital angular momentum*. When acting on components of a vector they are represened by matrices, and are examples of *intrinsic spin*.

B.5 Unitary transformations

Changes to an N-dimensional statevector Ψ can be regarded as the result of some $N \times N$ matrix U to produce a revised statevector Ψ,

$$\Psi' = \mathsf{U}\Psi. \tag{424}$$

Because the statevector should maintain unit length, meaning

$$|\Psi'|^2 \equiv \langle \Psi' | \Psi' \rangle = \langle \Psi | \mathsf{U}^\dagger \mathsf{U} | \Psi \rangle = \langle \Psi | \Psi \rangle = 1, \tag{425}$$

any allowable changes (e.g. time evolution) must have the property that the Hermitian conjugate $\mathsf{U}^\dagger$ is equal to the inverse,

$$\mathsf{U}^\dagger = \mathsf{U}^{-1}, \tag{426}$$

i.e. the matrix U is *unitary*. When the determinant of U is ± 1 the matrix is orthogonal; if the determinant is $+1$ it can be regarded as a rotation.

A unitary matrix can be expressed in exponential form as

$$\mathsf{U} = \exp(\mathrm{i}\mathsf{M}), \tag{427}$$

where the matrix M is Hermitian, $\mathsf{M}^\dagger = \mathsf{M}$. The exponential appearing here receives definition from eqn. (423) as a power series, allowing interpretation as processes of various orders.

The product of two unitary transformations must be unitary. This means that it is possible to find an M such that

$$\exp(\mathrm{i}\,\mathsf{m}_1)\ \exp(\mathrm{i}\,\mathsf{m}_2) = \exp(\mathrm{i}\mathsf{M}). \tag{428}$$

That is, a sequence of changes, such as those caused by laser pulses, produces an overall allowed change. Conversely, any single change can be expressed as a sequence of smaller changes. However, the matrix M is generally not simply the sum $\mathsf{m}_1 + \mathsf{m}_2$. It is possible to evaluate M from m_1 and m_2 using the Campbell-Baker-Hausdorff formula [151],

$$\exp(\mathsf{X})\exp(\mathsf{Y}) = \exp(\mathsf{Z}), \tag{429}$$

where the matrix Z is expressed as a sequence of commutators,

$$\begin{aligned}\mathsf{Z} \;=\; & \mathsf{X}+\mathsf{Y}+\frac{1}{2}[\mathsf{X},\mathsf{Y}] \\ & +\frac{1}{12}[\mathsf{X},[\mathsf{X},\mathsf{Y}]]-\frac{1}{12}[\mathsf{Y},[\mathsf{X},\mathsf{Y}]]-\frac{1}{24}[\mathsf{Y},[\mathsf{X},[\mathsf{X},\mathsf{Y}]]]+\cdots .\end{aligned} \tag{430}$$

Although this formula has proven useful for expressing the overall effect of two pulses, the inverse problem, of designing pulse sequences, usually requires numerical simulation [83]. An exception occurs when the operators are expressible as spin matrices of Appendix C.2, for which commutator relationships permit direct evaluation of eqn. (430).

B.6 Groups

Analysis of the symmetry of the Hamiltonian matrix is often treated using the theory of groups [152]. For this purpose a *group* G is a set of elements a, b, c, . . ., and a binary operation $\star$, which together satisfy the following four conditions:

I. The operation $a \star b$ between any two elements produces an element of G (the elements are *complete*):

$$a \star b = c \quad \text{for all } a, b \text{ and some } c. \tag{431}$$

II. The operation is *associative:*

$$a \star (b \star c) = (a \star b) \star c \quad \text{for all } a, b, c. \tag{432}$$

III. The group contains an *identity* element e such that

$$a \star e = e \star a = a \quad \text{for all } a. \tag{433}$$

IV. Each element a of G has an *inverse* a^{-1} such that

$$a \star a^{-1} = a^{-1} \star a = e \quad \text{for all } a \text{ and some } a^{-1}. \tag{434}$$

The number of elements comprising the group (the *order* of the group) may be finite or infinite (and, if infinite in number, may be nondenumerably infinite – i.e., they may form a continuum). A subset of G which itself forms a group is termed a *subgroup*. If the operation $\star$ is commutative,

$$a \star b = b \star a, \tag{435}$$

the group is *Abelian*.

Two groups whose elements and operation can be put into one-to-one correspondence are said to be *isomorphic*. Every finite group (and some infinite groups) are isomorphic to a set of nonsingular square matrices with the operation of matrix multiplication. Such a matrix set is termed a *representation* of the group.

The rotation and reflection operations which transform solid geometric figures into themselves form elements of *point* groups. Representations of these finite groups are used in classifying (and labelling) electronic states of molecules and of atoms in the presence of static fields (e.g., an atom embedded in a glass or crystal). These groups are discussed in texts on quantum chemistry (e.g., [153]).

The $N!$ possible permutations of N different symbols provide a realization of the *symmetric group* $S(N)$. A theorem of Cayley states that *Every group of order N is isomorphic with a subgroup of* $S(N)$. Representations of this finite group are used in classifying the interchange symmetry of multielectron wavefunctions and in labelling electronic states of molecules and multielectron atoms.

The most common examples of groups with nondenumerable sets of elements are those whose elements are square matrices, taken with the group operation of matrix multiplication. (These are examples of *dynamical groups*, in distinction to symmetry groups). The set of all nonsingular $N \times N$ square matrices form a representation of the *general linear group*, $GL(N)$. Amongst the subgroups of this group are the set of $N \times N$ unitary matrices; these represent the *unitary group* $U(N)$. The unitary matrices with determinant +1 represent the *special unitary group* $SU(N)$. The set of $N \times N$ orthogonal matrices serve as representations of the *orthogonal group* $O(N)$. The subset of orthogonal matrices with determinant +1 form the *special orthogonal group* $SO(N)$.

B.7 Lie groups

Continuous groups (topological groups) are those whose elements can be labelled by a set of continuously variable parameters. *Lie groups* [154] are special examples in which each group element can be identified using a finite number of continuously varying parameters, say α_1, α_2, $\ldots \alpha_N$. The dimension of the group is number of needed parameters, N. Let $M(\alpha_1, \alpha_2, \ldots \alpha_N)$ be a group element. Then the requirement for continuity means that, for small increments of the parameters, we can write

$$M(0, \ldots \delta\alpha_j \ldots 0) = M(0, \ldots 0 \ldots 0) + \mathrm{i}\delta\alpha_j \mathsf{X}_j M(0, \ldots 0 \ldots 0). \tag{436}$$

where $M(0,\ldots 0\ldots 0)$ is the unit element of the group. In the limit of infinitisimal increments this leads to the differential equation

$$\frac{\partial}{\partial\alpha_j}M(0,\ldots 0\ldots 0) = \mathrm{i}\mathsf{X}_j M(0,\ldots 0\ldots 0). \tag{437}$$

A Lie group may be regarded as the set of solutions to these differential equations. The operator X_j associated with parameter α_j is the (infinitesimal) *generator* of displacements. For a one-dimensional group it has the structure

$$M(\alpha) = \exp(\mathrm{i}\alpha\mathsf{X})M(0). \tag{438}$$

For example, the RWA Hamiltonian is the generator of time displacements of the solutions to the TDSE, i.e. the time evolution matrix $\mathsf{U}(t)$. The generators of rotations parametrized by the three Euler angles are the three angular momentum operators; their matrix representations are spin matrices: spin S is associated with matrices of dimension $N = 2S + 1$.

B.8 Graphs

Within the generalized RWA the Hamiltonian matrix has slowly varying (or constant) elements. These form a pattern that can be classified using the mathematics of graph theory [155]. A graph, in this sense, is a set of points (or *nodes* or *vertices*) and a set of lines (or *edges*) that join (or connect) pairs of points. Only the association of lines and points matters, not the position of these on a page. The pattern of linkages between vertices provided by the lines constitutes the *graph*. For application to analysis of a RWA Hamiltonian matrix the points correspond to quantum states and the edges correspond to interaction linkages between states.

The number of vertices is the *order* of the graph. Two vertices are *adjacent* (or *neighbors*) if they are joined by an edge. The *degree* of a vertex is the number of edges joined to the vertex.

A *path* is a set of connected vertices. A path that returns to a vertex is a *cycle* (a *loop* in the terminology of coherent excitation). A graph is said to be *complete* if all the vertices are pairwise adjacent, i.e. if the linkage pattern is a single closed loop. A *tree* is a set of connected vertices in which there is no cycle.

An *r-partite* graph is one in which there are r classes of vertices such that vertices in the same class are not adjacent. A *bipartite* graph is one in which vertices can be separated into two sets, with linkages only between the sets, not within a set.

C The Hamiltonian

In presenting the Hamiltonian operator as a matrix the elements depend very much on the coordinate system used, i.e. upon the choice of quantum states to use as Hilbert-space coordinates. Given such a set one can write the Hamiltonian as

$$\mathsf{H}(t) = \Sigma_{m,n}|\psi_n\rangle H_{nm}(t)\langle\psi_m| \equiv \Sigma_{m,n}|n\rangle H_{nm}(t)\langle m|, \tag{439}$$

where the matrix elements are evaluated as projections back onto the basis vectors,

$$H_{nm}(t) = \langle\psi_n|\mathsf{H}(t)|\psi_m\rangle. \tag{440}$$

One has, for example, the matrix representation

$$\mathsf{H}(t) = \begin{bmatrix} H_{11}(t) & H_{12}(t) & \cdots \\ H_{21}(t) & H_{22}(t) & \cdots \\ \vdots & \vdots & \ddots \end{bmatrix}. \tag{441}$$

C.1 Basis matrices

It often proves useful to present the elements of the instantaneous Hamiltonian as arising from elementary matrices (or transition operators). One such set is

$$\hat{\pi}_{nm} \equiv |\psi_n\rangle\langle\psi_m| \equiv |n\rangle\langle m|. \tag{442}$$

These transition matrices link only pairs of quantum states.They have the property

$$\hat{\pi}_{nk}\hat{\pi}_{km} = \hat{\pi}_{nm}. \tag{443}$$

When acting on a statevector that is expressed as a superposition of basis states, $\Psi = \Sigma_m c_m|m\rangle$ the operator $\hat{\pi}_{nm}$ replaces the state m with the state n: it can be said to *annihilate* state m and *create* state n. The matrices $\hat{P}_n \equiv \hat{\pi}_{nn}$ are *projection operators*, with the property $\hat{P}_n\hat{P}_n = \hat{P}_n$, i.e. they are *idempotent*.

Using these matrices as a basis we obtain the presentation (decomposition) of the Hamiltonian as

$$\mathsf{H}(t) = \Sigma_n E_n\hat{\pi}_{nn} + \Sigma_{m\neq n}V_{nm}(t)\hat{\pi}_{nm}. \tag{444}$$

The elementary matrices $\hat{\pi}$ form a complete set, meaning that any matrix can be expressed as a sum of these. They are but one possible complete set of matrices that can serve to express the RWA Hamiltonian matrix. Appendix C.2 presents one alternative, Appendix H.4 discusses another.

A similar expansion can be used for the RWA Hamiltonian, but with the use of rotating basis states,

$$\hat{\pi}_{nm}(t) \equiv |\psi'_n(t)\rangle\langle\psi'_m(t)|. \tag{445}$$

Note that the diagonal matrix $\hat{\pi}_{nn}(t)$ is independent of t When the linkage pattern is a chain, with connections only between adjacent states of the chain, the resulting expression is

$$\mathsf{W}(t) = \Sigma_n\Delta_n\hat{\pi}_{nn} + \tfrac{1}{2}\Sigma_{n\neq m}\Omega_n(t)\hat{\pi}_{n,n+1}(t) + \tfrac{1}{2}\Sigma_{n\neq m}\Omega_n(t)^*\hat{\pi}_{n,n-1}(t). \tag{446}$$

C.2 Spin Matrices

Various other sets of matrices, characterized by symmetries, prove useful for expressing the Hamiltonian. The theory of angular momentum, regarded as offering generators of Lie groups, offers a simple approach. Whenever three operators satisfy the cyclic commutation relations

$$\left[\hat{J}_1, \hat{J}_2\right] = \mathrm{i}\hat{J}_3, \qquad \left[\hat{J}_2, \hat{J}_3\right] = \mathrm{i}\hat{J}_1, \qquad \left[\hat{J}_3, \hat{J}_1\right] = \mathrm{i}\hat{J}_2, \tag{447}$$

then these serve as components of a three dimensional angular momentum vector [81] . It is customary to regard these operators as components of a Cartesian vector and to use the axis labels x, y, z in place of the labels 1,2,3. However, the properties of angular momentum do not require that the operators refer to variables in ordinary (Euclidean) space. The operator

$$\hat{\mathbf{J}}^2 \equiv (\hat{J}_1)^2 + (\hat{J}_2)^2 + (\hat{J}_2)^2 = (\hat{J}_x)^2 + (\hat{J}_y)^2 + (\hat{J}_z)^2 \tag{448}$$

commutes with each of the three angular momentum operators J_k, and so it is possible to obtain eigenstates of $\hat{\mathbf{J}}^2$ and any single $\hat{J}_k$. Conventionally this is chosen to be $\hat{J}_3 = \hat{J}_z$. The operator $\hat{\mathbf{J}}^2$ has as eigenvalues the numbers $j(j+1)$ where $2j$ is a non-negative integer. For given j the eigenvalues m of $\hat{J}_z$ differ by unity, ranging from $-j$ to $+j$. Denoting the angular momentum states by $|j, m\rangle$, the operators have the following effect

$$\hat{\mathbf{J}}^2|j, m\rangle = j(j+1)|j, m\rangle, \qquad \hat{J}_z|j, m\rangle = m|j, m\rangle. \tag{449}$$

The eigenstates of $\hat{J}_z$ are orthonormal,

$$\langle j, m|j, m'\rangle = \delta_{m,m'}. \tag{450}$$

From the remaining two angular momentum operators we can construct the combinations

$$\hat{J}_{\pm 1} = \mp\frac{1}{\sqrt{2}}(\hat{J}_x \pm \mathrm{i}\hat{J}_y). \tag{451}$$

The operator $\hat{J}_{+1}$ is a *raising* operator, acting to increase the eigenvalue m by unity, while $\hat{J}_{-1}$ is a *lowering operator*, acting to decrease m by one. Specifically they have the effect

$$\sqrt{2}\hat{J}_{\pm 1}\,|j, m\rangle = \mp\sqrt{j(j+1) - m(m \pm 1)}\,|j, m \pm 1\rangle. \tag{452}$$

Thus by starting with the "stretched" state $|j, j\rangle$ we can construct any desired state by successing actions of a lowering operator:

$$|j, m\rangle = \sqrt{\frac{(j+m)!}{(2j)!(j-m)!}}\,(\hat{J}_x - \mathrm{i}\hat{J}_y)^{j-m}\,|j, j\rangle. \tag{453}$$

These operators properties can be represented using square matrices for each $\hat{J}_k$. These are the (three) *spin matrices* $\hat{J}_k = \mathsf{S}_k$. Any one of the matrices, conventionally chosen to be $\mathsf{S}_3 \equiv \mathsf{S}_z$, can be brought to diagonal form by unitary transformation; these elements are the $2S + 1$ eigenvalues of $J_z = \mathsf{S}_z$. A matrix representing spin S has dimension $N = 2S + 1$. Conversely, matrices of dimension N are associated with spin $S = (N-1)/2$. The eigenvectors of the spin matrices, $|S, M\rangle$, are column vectors, of dimension $2S + 1$. These have the property

$$\mathsf{S}^2|S, M\rangle = S(S+1)|S, M\rangle, \qquad \mathsf{S}_z|S, M\rangle = M|S, M\rangle, \tag{454}$$

for $M = -S, -S+1, \ldots, +S$.

[81] In atomic physics the total angular momentum $\hat{\mathbf{J}}$ is the sum of a part $\hat{\mathbf{L}}$ that acts to generate displacements of function values (i.e. *orbital angular momentum* represented by partial derivatives) and a part S that alters the components of vectors (i.e. *intrinsic spin*). The essential properties of any angular momentum operator are those of the commutation relations presented here.

For dimension $N = 2$ the spin matrices are those for $S = 1/2$:

$$\mathsf{S}_x = \tfrac{1}{2}\begin{bmatrix} 0 & 1 \\ 1 & 0 \end{bmatrix}, \qquad \mathsf{S}_y = \tfrac{1}{2}\begin{bmatrix} 0 & -\mathrm{i} \\ \mathrm{i} & 0 \end{bmatrix}, \qquad \mathsf{S}_z = \tfrac{1}{2}\begin{bmatrix} 1 & 0 \\ 0 & -1 \end{bmatrix}. \tag{455}$$

These are half the Pauli spin matrices, $\mathsf{S}_k = \frac{1}{2}\sigma_k$. These three matrices, together with the two-dimensional unit matrix $\mathbf{1}$, provide a complete set of four two-dimensional basis matrices: any square two-dimensional matrix can be expressed as a linear combination of these four matrices. This implies that the dynamics of any two-state system can be cast into the form of a spin-half particle. The eigenstates of S_z, associated with eigenvalues $\pm 1/2$, are just the basis vectors representing the two quantum states,

$$\psi_1 = \begin{bmatrix} 1 \\ 0 \end{bmatrix}, \qquad \psi_2 = \begin{bmatrix} 0 \\ 1 \end{bmatrix}. \tag{456}$$

For dimension $N = 3$ the spin matrices are those for $S = 1$. In a basis in which S_z is diagonal the three matrices are

$$\mathsf{S}_x = \frac{1}{\sqrt{2}}\begin{bmatrix} 0 & 1 & 0 \\ 1 & 0 & 1 \\ 0 & 1 & 0 \end{bmatrix}, \qquad \mathsf{S}_y = \frac{1}{\sqrt{2}}\begin{bmatrix} 0 & -\mathrm{i} & 0 \\ \mathrm{i} & 0 & -\mathrm{i} \\ 0 & \mathrm{i} & 0 \end{bmatrix}, \qquad \mathsf{S}_z = \begin{bmatrix} 1 & 0 & 0 \\ 0 & 0 & 0 \\ 0 & 0 & -1 \end{bmatrix}. \tag{457}$$

The eigenstates of S_z, associated with eigenvalues $-1, 0, +1$, are just the three-state basis vectors

$$\psi_1 = \begin{bmatrix} 1 \\ 0 \\ 0 \end{bmatrix}, \qquad \psi_2 = \begin{bmatrix} 0 \\ 1 \\ 0 \end{bmatrix}, \qquad \psi_3 = \begin{bmatrix} 0 \\ 0 \\ 1 \end{bmatrix}. \tag{458}$$

These states need not have any association with any atomic angular momentum; it is only necessary that there be three of them.

For dimension $N = 3$ the spin matrices by themselves are not sufficient to express the nine elements of any arbitrary matrix; we require another six independent matrices. A simple procedure is to take products of pairs of the three basic matrices, say $\mathsf{T}_{ij} = \mathsf{S}_i\mathsf{S}_j$. However, other possibilities, characterized by symmetries, also prove useful, such as the combinations $\mathsf{S}_i\mathsf{S}_j \pm \mathsf{S}_j\mathsf{S}_i$. Appendix H.4 discusses examples.

C.3 Angular momentum coupling

In systems having several degrees of freedom, perhaps involving several particles, there occur independent sets of operators whose commutation properties mark them as examples of angular momentum. A common example is the intrinsic spin and orbital angular momentum of an atomic electron, or the vector nature and spatial dependence of a vector field. Such situations, involving two sets of angular momentum operators $\mathbf{J}(A)$ and $\mathbf{J}(B)$, permit complete description by product states

$$|J_1M_1, J_2M_2\rangle_{AB} \equiv |J_1M_1\rangle_A |J_2M_2\rangle_B, \tag{459}$$

where

$$\mathbf{J}(a)^2|JM\rangle_a = J(J+1)|JM\rangle_a, \qquad J_z(a)|JM\rangle_a = M|JM\rangle_a, \quad a = A, B. \tag{460}$$

It often proves useful to introduce, in place of these *uncoupled* basis states, superpositions that are eigenstates of the total angular momentum [2, §19.1]

$$\mathbf{J} = \mathbf{J}(A) + \mathbf{J}(B), \quad \text{meaning} \quad J_i = J_i(A) + J_i(B), \quad i = x, y, z. \tag{461}$$

Such *coupled* basis states are constructed with the aid of Clebsch-Gordan (CG) coefficients [91],

$$|J_1 J_2 J M\rangle_{AB} = \Sigma_{M_1 M_2} |J_1 M_1\rangle_A |J_2 M_2\rangle_B (J_1 M_1, J_2 M_2 | J M), \tag{462}$$

or three-j symbols,

$$|J_1 J_2 J M\rangle_{AB} = \Sigma_{M_1 M_2} |J_1 M_1\rangle_A |J_2 M_2\rangle_B (-1)^{J_1 - J_2 + M} \sqrt{2J+1} \begin{pmatrix} J_1 & J_2 & J \\ M_1 & M_2 & -M \end{pmatrix}. \tag{463}$$

The inverse relationship expresses an uncoupled state as a superposition of coupled states,

$$|J_1 M_1\rangle_A |J_2 M_2\rangle_B = \Sigma_{JM} |J_1 J_2 J M\rangle_{AB} (-1)^{J_1 - J_2 + M} \sqrt{2J+1} \begin{pmatrix} J_1 & J_2 & J \\ M_1 & M_2 & -M \end{pmatrix}. \tag{464}$$

The coupling coefficients incorporate the following constraints:

$$|J_1 - J_2| \leq J \leq J_1 + J_2, \qquad M = M_1 + M_2. \tag{465}$$

This coupling procedure has use for any pair of eigenstates of angular momentum operators, e.g. for combinations of spherical unit vectors with spherical harmonics to form spherical vector fields, for combinations of spin matrices to construct symmetry adapted basis matrices, and for multiple two-state systems.

C.4 Alternative basis vectors

The physical states (as here defined) provide a convenient basis in which to present the Hamiltonian matrix. Apart from arbitrary constant phases they are define by the requirement that they are eigenstates of the unperturbed (free atom) Hamiltonian,

$$\mathsf{H}^{at} \psi_n = E_n \psi_n, \tag{466}$$

having unit length. In the absence of interaction, the statevector can always be written as

$$\Psi(t) = c_1 \exp[-\mathrm{i} E_1 t/\hbar] \psi_1 + c_2 \exp[-\mathrm{i} E_2 t/\hbar] \psi_2 + \cdots. \tag{467}$$

where c_n is a constant complex number, fixed by the initial conditions; the probabilities remain constant as $P_n = |c_n|^2$. The time varying phase factors produce the result

$$\frac{d}{dt}\Psi(t) = -\frac{\mathrm{i}}{\hbar} \left[E_1 c_1 \exp(-\mathrm{i} E_1 t/\hbar) \psi_1 + E_2 c_2 \exp(-\mathrm{i} E_2 t/\hbar) \psi_2 + \cdots \right], \tag{468}$$

as is needed for the time dependent Schrödinger equation.

However, one could choose any other coordinate system, even one that is time dependent, and write the matrix representation of the operator H as

$$\mathsf{H}(t) = \Sigma_{m,n} |\psi'_n(t)\rangle H'_{n,m}(t) \langle \psi'_m(t)|, \tag{469}$$

where $\psi'_n(t)$ is a unit vector, perhaps time dependent when expressed in the original basis, but part of a complete set of orthonormal unit vectors at each fixed time,

$$\langle\psi'_n(t)|\psi'_m(t)\rangle = \delta_{n,m}. \tag{470}$$

The matrix elements of the operator $\mathsf{H}(t)$, expressed in the primed basis, read

$$H'_{n,m}(t) = \langle\psi'_n(t)|\mathsf{H}(t)|\psi'_m(t)\rangle. \tag{471}$$

That is, we have many ways of writing the Hamiltonian matrix; they differ by the choice of Hilbert-space basis vectors in which the matrix is expressed – they differ by the choice of coordinate unit vectors.

In the primed reference frame the unit vectors appear to be fixed (by definition) and are, as with any unit vectors, expressible as column vectors with unity in one place. For example, in the primed coordinate system we can write

$$\psi'_1 = \begin{bmatrix} 1 \\ 0 \\ 0 \\ \vdots \end{bmatrix}, \quad \psi'_2 = \begin{bmatrix} 0 \\ 1 \\ 0 \\ \vdots \end{bmatrix}, \cdots. \tag{472}$$

However, one must recognize that the unit vectors in the primed system are not the same as those of the fixed unprimed system, though their column-vector representation is identical. The connection between two choices of basis is obtained by using the expansion of eqn. (439) in eqn. (471):

$$H'_{i,j}(t) = \Sigma_{n,m}\langle\psi'_i(t)|\psi_n\rangle H_{n,m}\langle\psi_m|\psi'_j(t)\rangle. \tag{473}$$

This aspect of column-vector displays is not confined to Hilbert space. When we describe positions of a particle in ordinary three-dimensional Euclidean space we use unit vectors that, with any choice of coordinates (Cartesian, cylindrical, spherical, spheroidal, etc.) appear the same in any coordinate system, namely

$$\begin{bmatrix} 1 \\ 0 \\ 0 \end{bmatrix}, \quad \begin{bmatrix} 0 \\ 1 \\ 0 \end{bmatrix}, \quad \begin{bmatrix} 0 \\ 0 \\ 1 \end{bmatrix}. \tag{474}$$

We can write this coordinate transformation as the result of a unitary transformation

$$H'_{i,j}(t) = \Sigma_{n,m}U^\dagger_{i,n}(t)H_{n,m}U_{m,j}(t), \tag{475}$$

where the transformation matrix

$$U_{m,j}(t) = \langle\psi_m|\psi'_j(t)\rangle \tag{476}$$

is the Hilbert-space rotation that produces the unprimed coordinate system from the primed one. This connection can be written as

$$\mathsf{H}'(t) = \mathsf{U}^\dagger(t)\mathsf{H}(t)\mathsf{U}(t), \tag{477}$$

but in doing so it must be understood that this matrix equation implies a change of basis vectors: the matrix $\mathsf{H}'(t)$ does not use the same coordinate system (associated with the physical states) as does $\mathsf{H}(t)$.

D Systems with parts

Any actual implementation of a discrete quantum state has more than a single degree of freedom, meaning its dynamics involves more than a single coordinate. Each degree of freedom leads to a set of quantum states, identified by quantum numbers or simply by a running index. For example, within the nonrelativistic model of the hydrogen atom the electron has orbital energy as specified by the principle quantum number n, orbital angular momentum ℓ and orbital orientation, as specified by the magnetic quantum number m. The overall description of the atom requires specification of each of these quantum numbers. Another example occurs when there are two or more particles within the system, each of which has its set of quantum numbers, as occurs with ions in a magneto-optical trap.

Each degree of freedom has an associated Hilbert space whose basis vectors describe the possible states of that degree of freedom. To describe M degrees of freedom we require M independent Hilbert spaces. Any quantum state must specifiy attributes from each of these. A possible quantum state of the system might therefore have the form of a product, written variously as

$$\Psi = \psi_n^A \psi_m^B \psi_k^C \cdots \equiv |n\rangle_A |m\rangle_B |k\rangle_C \cdots, \equiv |n, m, k, \cdots\rangle_{ABC\ldots} \tag{478}$$

where the labels $A, B, C, \ldots$ identify the various degrees of freedom (or the various particles). More generally the state will be some superposition of such products, say

$$\Psi = \Sigma_{n,m,k,\ldots} C_{nmk\ldots} \mathcal{S} |n, m, k, \cdots\rangle_{ABC\ldots} \tag{479}$$

Here $\mathcal{S}$ denotes any neccessary symmetrizing operator, such as would be needed if the degrees of freedom are those associated with indistinguishable partices (e.g. electrons within an atom). For example, with two identical particles the needed symmetry is

$$\mathcal{S}|n, m\rangle_{AB} = \frac{1}{\sqrt{2}}[|n, m\rangle_{AB} \pm |m, n\rangle_{AB}], \tag{480}$$

where the plus sign occurs with Bosons and the minus sign with Fermions. The system quantum state is *separable* if we can write the statevector as a simple product, as in eqn. (478).

D.1 Correlation and entanglement

Under appropriate conditions the degrees of freedom can become *correlated*. That is, if by learning that the A degree of freedom is definitely in state n, then it may follow that the B portion of the system must be in state m [82]. When one of the following conditions holds such correlation is known as *entanglement* [156]

I. One degree of freedom represents internal structure while another represents center of mass motion (e.g. of a trapped particle).

II. The degrees of freedom are associated with distinct particles (or photons) which, though initially together, are observed physically separated.

[82] We do not regard subsystems to be correlated if it is known *a priori* that they must be, respectively in states n and m; they must be in a state for which different possible measurement outcomes are possible.

D.2 Two parts

The simplest illustration is that of a quantum system that has two parts, two degrees of freedom, say A and B. Examples include those of the following table: . .

A	B	$A + B$
electron orbit L, M_L	electron spin S, M_S	total ang. mom. J, M
electron J, M	nuclear spin I, M_I	hyperfine F, M_F
atom internal	CM motion	trapped atom
atom	quantized field	dressed states
atom	environment	

Each subsystem has a set of basis states, say ψ_n^A for set A and ψ_n^B for set B. The statevector can always be written as a sum of products, in the form

$$\Psi(t) = \Sigma_{nm}\, C_{nm}(t)\, \psi_n^A\, \psi_m^B. \tag{481}$$

That is, we use a direct-product Hilbert space $\mathcal{H}(A) \otimes \mathcal{H}(B)$ to describe the full system. An example occurs when we treat the electromagnetic field as quantized. Then for a single-mode field the full Hilbert space can be taken as the product of a space having atomic unit vectors ψ_m and a Fock space having photon-number states ϕ_n as a basis; we write

$$\Psi(t) = \Sigma_{nm}\, C_{nm}(t)\, \psi_m\, \phi_n. \tag{482}$$

For a system having two parts a separable state has the form

$$\Psi(t) = \Phi^A(t)\, \Phi^B(t), \tag{483}$$

where the individual factors are expressible as vectors within the respective subspaces.

$$\Phi^A(t) = \Sigma_n\, C_n^A(t)\, \psi_n^A, \qquad \Phi^B(t) = \Sigma_m\, C_m^B(t)\, \psi_m^B. \tag{484}$$

For any such state both A and B have definite properties; separate measurements give no additional information.

The quantum state is *not* separable if such a factoring is not possible,

$$\Psi(t) \neq \Phi^A(t)\, \Phi^B(t). \tag{485}$$

Under such conditions a measurement of either A or B provides new information: we can deduce properties of B from measurements of A and so the subsystem parts are correlated. If the above conditions hold they are entangled.

The eigenstates of a Hamiltonian that links two subsystems can be classified by their correlation properties. Let the full Hamiltonian for a two-part system be the sum of the following parts,

$$\begin{array}{lll} \mathsf{H}(t) & = \mathsf{H}^A & \textit{part A, eigenstates } \psi^A_n \\ & +\mathsf{H}^B & \textit{part B, eigenstates } \psi^B_m \ . \\ & +\mathsf{V}^A(t) + \mathsf{V}^B(t) + \mathsf{H}^{AB} & \textit{interaction} \end{array} \tag{486}$$

For further simplification, suppose that each part – each subsystem – has just two quantum states.

$$\psi^A_\pm \quad \text{and} \quad \psi^B_\pm \quad \text{(e.g. spin one half or two-state atoms).} \tag{487}$$

When the interaction has the form $\mathbf{V}^A \cdot \mathbf{V}^B$,

$$\mathsf{H}^{AB} = -V^A_- V^B_+ + V^A_0 V^B_0 - V^A_+ V^B_- \quad \text{where} \quad V_j \psi_k = v_{j,k} \psi_{j+k}, \tag{488}$$

then the eigenstates of H^{AB} are a triplet (threefold degenerate)

$$\Phi^T_{+1} = \psi^A_+ \psi^B_+, \tag{489}$$

$$\Phi^T_0 = [\psi^A_+ \psi^B_- + \psi^A_- \psi^B_+]/\sqrt{2} \quad \textit{correlated}, \tag{490}$$

$$\Phi^T_{-1} = \psi^A_- \psi^B_-, \tag{491}$$

and a singlet

$$\Phi^S_0 = [\psi^A_+ \psi^B_- - \psi^A_- \psi^B_+]/\sqrt{2} \quad \textit{correlated}. \tag{492}$$

The correlated states are entangled if either of the above conditions hold.

D.3 Multiple parts

When the system has many parts, either from several degrees of freedom or from multiple particle composition, there can occur two classes of interactions. Within each part there may occur interactions of the sort described within this article: there is a Hamiltonian that connects the various states associated with this part, and which can induce changes in the constituent quantum states. But there may also occur interactions between the parts – between particles or between degrees of freedom. The Hamiltonian for the full system has a block structure, in which matrices replace the elements that elsewhere appear as the numbers W_{nm}. When the interactions are between nearest-neighbors, then the block structure is a generalization of the tri-diagonal matrices which occur in the chain linkage. When all the parts interact with a common part, as occurs when trapped particles interact with a common common collective mode (a "bus"), then the block structure is a generalization of the bordered matrix. In all these cases the linkage patterns between parts generalize the linkage patterns between states, and similar techniques can be used to express the effect of a Hamiltonian, e.g. the use of spin matrices.

E Analytically soluble two-state models

Although numerical solutions to the TDSE provide useful simulations for arbitrary excitation conditions, and permit the construction of plots that provide important insight into the system behavior, it is also useful to have available analytic solutions. These are available for a variety of pulses [157] [2, Chap. 5]. They offer, in particular, analytic expressions for the *pulse aftermath* $P_n(\infty)$,

$$P_2(\infty) = \text{population transfer}, \tag{493}$$

$$P_1(\infty) = \text{coherent population return}. \tag{494}$$

The following paragraphs discuss several useful examples.

E.1 Resonant excitation

For resonant excitation, $\Delta(t) = 0$, with pulse $\Omega(t) = \Omega_0 f(t)$ the two-state RWA equation reads

$$\frac{d}{dt}\begin{bmatrix} C_1(t) \\ C_2(t) \end{bmatrix} = -\frac{\mathrm{i}f(t)}{2}\begin{bmatrix} 0 & \mathrm{e}^{\mathrm{i}\varphi}\Omega_0 \\ \mathrm{e}^{-\mathrm{i}\varphi}\Omega_0 & 0 \end{bmatrix}\begin{bmatrix} C_1(t) \\ C_2(t) \end{bmatrix}. \tag{495}$$

For any pulse shape $f(t)$ we can introduce a time scale

$$\tau(t) = \int_{-\infty}^{t} dt' f(t'). \tag{496}$$

Then the equation of motion becomes that of a constant Hamiltonian

$$\frac{d}{d\tau}\begin{bmatrix} C_1(t) \\ C_2(t) \end{bmatrix} = -\frac{\mathrm{i}}{2}\begin{bmatrix} 0 & \mathrm{e}^{\mathrm{i}\varphi}\Omega_0 \\ \mathrm{e}^{-\mathrm{i}\varphi}\Omega_0 & 0 \end{bmatrix}\begin{bmatrix} C_1(t) \\ C_2(t) \end{bmatrix}. \tag{497}$$

The general solution, expressible in terms of trigonometric functions and initial amplitudes, depends only on the pulse area $A(t) \equiv \Omega_0\tau(t)$.

$$\begin{bmatrix} C_1(t) \\ C_2(t) \end{bmatrix} = \begin{bmatrix} \cos(\Omega_0\tau/2) & -\mathrm{i}\mathrm{e}^{\mathrm{i}\varphi}\sin(\Omega_0\tau/2) \\ +\mathrm{i}\mathrm{e}^{-\mathrm{i}\varphi}\sin(\Omega_0\tau/2) & \cos(\Omega_0\tau/2) \end{bmatrix}\begin{bmatrix} C_1(-\infty) \\ C_2(-\infty) \end{bmatrix}. \tag{498}$$

By adjusting the duration of the pulse, and the peak Rabi frequency Ω_0, one can produce any desired excitation, from none at all to complete population transfer; one can transform any initial superposition into a specified final superposition.

E.2 Constant with detuning

The general construction of solutions for constant RWA Hamiltonian can be accomplished in several ways. One can use LaPlace transforms [158][2, § 14.6] to replace the coupled ordinary differential equations by a set of simultaneous algebraic equations. From the solution to these equations, and the consequent inverse transform, one obtains the general solution, for arbitrary initial conditions.

Alternatively, one can convert from the bare-state basis into the dressed-state basis, where the time evolution involves only the factors $\exp(\pm\mathrm{i}\widetilde{\Omega}t)$. The desired solution is obtained by returning

to the original basis. The results are best expressed in terms of a time-evolution operator $\mathsf{U}(t)$ such that

$$\mathbf{C}(t) = \mathsf{U}(t)\mathbf{C}(0). \tag{499}$$

The time evolution matrix can be written

$$\mathsf{U}(t) = \frac{1}{\sqrt{\Delta^2 + |\Omega|^2}} \begin{bmatrix} \widetilde{\Omega}\cos(\widetilde{\Omega}t/2) + \mathrm{i}\Delta\sin(\widetilde{\Omega}t/2) & -\mathrm{i}e^{\mathrm{i}\varphi}|\Omega|\sin(\widetilde{\Omega}t/2) \\ +\mathrm{i}e^{-\mathrm{i}\varphi}|\Omega|\sin(\widetilde{\Omega}t/2) & \widetilde{\Omega}\cos(\widetilde{\Omega}t/2) - \mathrm{i}\Delta\sin(\widetilde{\Omega}t/2) \end{bmatrix}, \tag{500}$$

where $\widetilde{\Omega} \equiv \sqrt{\Delta^2 + |\Omega|^2}$. This reduces, for resonant excitation, to the time evolution matrix implied by eqn. (498). In the limit of large detuning, $|\Delta| \gg |\Omega|$, there is little population change; if the population resides initially in state 1 then the population of state 2 is

$$P_2(t) = |\Omega/\Delta|^2 \sin^2(\widetilde{\Omega}t/2). \tag{501}$$

Appreciable excitation occurs only if the detuning is less than the Rabi frequency. Conversely, an increase of Rabi frequency allows excitation over a greater range of detunings. Equation (198) quantifies these properties.

E.3 Chirped detuning

The model of chirped RAP finds application in many physical systems. An idealization, the Landau-Zener (or Landau-Zener-Stückelberg) model [79], provides an analytic solution. In this model the Rabi frequency is a constant, Ω_0, and the detuning varies linearly with time, at rate $r = \beta^2$,

$$\Delta(t) = \Delta_0 + \beta^2 t. \tag{502}$$

The solutions to the TDSE for this RWA Hamiltonian is expressible in terms of parabolic cylinder functions. One follows the time evolution from $t \to -\infty$, when the population is entirely in state 1, to a conclusion as $t \to +\infty$. The populations then are

$$P_1(\infty) = \exp(-\pi y), \qquad P_2(\infty) = 1 - \exp(-\pi y), \tag{503}$$

where

$$y = (\Omega_0/\beta)^2. \tag{504}$$

When y is very large, meaning $(\Omega_0)^2 \gg |\dot{\Delta}|$, the time evolution is *adiabatic*, and population transfers entirely from state 1 to state 2. For smaller values of y the transfer is incomplete, and the final state is a coherent superposition of states 1 and 2. In the limit of weak interaction or rapid chirp, $(\Omega_0)^2 \ll |\dot{\Delta}|$, the time evolution is *diabatic* and the system remains in the initial state 1. This simple model has been extended to allow variation of the Rabi frequency, as is needed for modeling chirped RAP [159].

E.4 Pulsed with detuning

A set of N coupled first-order equations are equivalent to a single Nth-order equation. For the two-state system

$$\frac{d}{dt}\begin{bmatrix} C_1(t) \\ C_2(t) \end{bmatrix} = -\frac{\mathrm{i}}{2}\begin{bmatrix} 0 & \Omega(t) \\ \Omega(t) & 2\Delta(t) \end{bmatrix}\begin{bmatrix} C_1(t) \\ C_2(t) \end{bmatrix} \tag{505}$$

the resulting equation is

$$\frac{d^2}{dt^2}C_n(t) + \mathrm{i}\Delta\frac{d}{dt}C_n(t) + [(\Omega/2)^2 - \mathrm{i}(\dot{\Omega}/2)]C_n(t) = 0. \tag{506}$$

The usual initial conditions are that population resides in state 1

$$C_1(0) = 1, \qquad \dot{C}_1(0) = 0, \tag{507}$$

$$C_2(0) = 0, \qquad \dot{C}_2(0) = -\mathrm{i}(\Omega/2). \tag{508}$$

This second-order ODE has much in common with those studied by mathematicians during the 19th century. Their solutions define what are commonly called the *special functions* of mathematical physics. A perusal of textbooks will provide numerous applicable examples involving such special functions as trigonometric (from constant), Bessel (from exp), hypergeometric (from sech), and parabolic cylinder (from chirp). Numerous examples have been discussed [157][2, Chap. 5]. Amongst the pulses that have been studied for application to coherent excitation are those in table 2.

. .

The final probability amplitudes can be expressed in terms of Cayley-Klein parameters α, β as

$$\begin{bmatrix} C_1(+\infty) \\ C_2(+\infty) \end{bmatrix} = \begin{bmatrix} \alpha & \beta \\ -\beta^* & \alpha^* \end{bmatrix}\begin{bmatrix} C_1(-\infty) \\ C_2(-\infty) \end{bmatrix}. \tag{509}$$

These can be evaluated analytically for some pulses, including the following (from Kyoseva and Vitanov, [157]).

$$\text{Rosen-Zener [160]}: \qquad \alpha = \frac{\Gamma(\frac{1}{2} + \mathrm{i}\delta)^2}{\Gamma(\frac{1}{2} + a + \mathrm{i}\delta)\Gamma(\frac{1}{2} - a + \mathrm{i}\delta)}, \tag{510}$$

$$\text{Allen-Eberly [10, 161]}: \qquad \alpha = \frac{\cos(\pi\sqrt{a^2 - b^2})}{\cosh(\pi b)}, \tag{511}$$

$$\text{Demkov-Kunike [162]}: \qquad \alpha = \frac{\Gamma(\frac{1}{2} + \mathrm{i}\delta + ib)\Gamma(\frac{1}{2} + \mathrm{i}\delta - \mathrm{i}b)}{\Gamma(\frac{1}{2} + \sqrt{a^2 + b^2} + \mathrm{i}\delta)\Gamma(\frac{1}{2} - \sqrt{a^2 + b^2} + \mathrm{i}\delta)}. \tag{512}$$

Here

$$a = \Omega_0 T/2, \qquad b = BT/2, \qquad \delta = \Delta_0 T/2. \tag{513}$$

Such formulas allow one to design pulses that will produce an arbitrary time-evolution matrix, thereby producing an arbitrary predetermined transformation of one statevector into another.

Tab. 2. Examples of soluble pulsed interactions

Pulse shape	$\Omega(t)$	$\Delta(t)$
Constant	Ω_0	Δ_0
Piecewise constant	$\Omega_1, \Omega_2, \ldots, \Omega_{N-1}$	$t_0, t_1, \ldots t_N$
Exponential $(t > 0)$	$\Omega_0\, \mathrm{e}^{-\gamma_p t}$	Δ_0
Landau-Zener (chirp) [79]	Ω_0	$r\, t$
Rosen-Zener [160]	$\Omega_0\, \mathrm{sech}(t/T)$	Δ_0
Allen-Eberly [161]	$\Omega_0 \mathrm{sech}(t/T)$	$B\, \tanh(t/T)$
Demkov-Kunike [162]	$\Omega_0 \mathrm{sech}(t/T)$	$\Delta_0 + B\, \tanh(t/T)$
Bambini-Berman [163]	$\frac{\Omega_0}{2\pi\gamma_p t} \frac{\sqrt{x(1-x)}}{1+\lambda x}$	Δ_0

E.5 Coherent population return (CPR)

Unless the carrier frequency ω is very close to resonance with the Bohr frequency ω_0 (in which case the final population depends only on the temporal pulse area), the pulse-produced excitation, $P_2(\infty)$, depends very significantly upon the temporal shape of the pulse – whether it has abrupt or gradual change. In particular, when the nonresonant pulse is sufficiently smooth (e.g. an atom moving sufficiently slowly through a laser beam) there will occur complete *coherent population return* (CPR): after a transient excursion to the excited state all population will return to the ground state. Under such conditions fluorescence will only occur for small detunings. A typical measure of "small" in this context is the inverse of the Fourier bandwidth of the pulse, typically $\Delta_0 = C/T$, where T is the pulse duration and C is a parameter, of order unity, that depends on the temporal shape of the pulse. Thus as a pulse becomes longer lasting the frequency-time uncertainty narrows the range of detunings for which permanent excitation can occur.

E.6 Bichromatic field

Numerous authors have considered a variety of situations in which two frequencies contribute to the interaction between two states; the field is *bichromatic* [164]. Here we consider a simple version in which the bichromatic field is pulsed. Let the field have two frequency components, ω_a and ω_b, so that the interaction has the form

$$V(t) = -d_{12}[\mathcal{E}_a(t)\cos(\omega_a) + \mathcal{E}_b(t)\cos(\omega_b)]. \tag{514}$$

When the field amplitudes are constant this interaction is exactly periodic. It can be treated using Floquet theory, cf. Appendix L.

Here we consider pulsed excitation. We introduce a reference frame rotating at the mean frequency

$$\bar{\omega} = \tfrac{1}{2}(\omega_a + \omega_b) \tag{515}$$

so that

$$\Psi(t) = C_1(t)\psi_1 + \mathrm{e}^{-\mathrm{i}\bar{\omega}t} C_2(t)\psi_2. \tag{516}$$

Then the Hamiltonian, in this basis, has diagonal elements

$$\hbar W_{11} = E_1, \tag{517}$$

$$\hbar W_{22} = E_1 + \hbar\omega_0 - \hbar\bar{\omega}, \tag{518}$$

where the Bohr frequency is $\omega_0 = (E_2 - E_1)/\hbar$. The off-diagonal element is

$$\hbar W_{12}(t) = \Omega_a(t)\cos(\omega_a t)\mathrm{e}^{-\mathrm{i}\bar{\omega}t} + \Omega_b(t)\cos(\omega_b t)\mathrm{e}^{-\mathrm{i}\bar{\omega}t}. \tag{519}$$

We denenote the carrier frequency difference as $\delta \equiv \omega_a - \omega_b$ and introduce a rotating wave approximation by neglecting terms that vary with frequency $(3\omega_n - \omega_m)/2$. The result is

$$\hbar W_{12} = \tfrac{1}{2}\Omega_a(t)\mathrm{e}^{\mathrm{i}\delta t/2} + \tfrac{1}{2}\Omega_b(t)\mathrm{e}^{-\mathrm{i}\delta t/2}. \tag{520}$$

Suppose that the two Rabi frequencies are each equal to $\Omega(t)$, meaning that the two components of the bichromatic field are equal. Then, with the choice $E_1 = 0$, the RWA Hamiltonian is

$$\mathsf{W}(t) = \begin{bmatrix} 0 & \Omega(t)\cos(\delta t/2) \\ \Omega(t)\cos(\delta t/2) & \Delta \end{bmatrix}, \tag{521}$$

where Δ is the difference between the Bohr frequency and the mean carrier frequency,

$$\Delta = \omega_0 - \bar{\omega}. \tag{522}$$

Resonance, $\Delta = 0$, occurs when the mean frequency $\bar{\omega}$ equals the Bohr frequency. That is, the two carrier frequencies are symmetrically distributed around the Bohr frequency. Under these circumstances the probability amplitude $C_2(t)$, for a system that starts in state 1, is

$$C_2(t) = \sin(A(t)), \qquad A(t) = \int_{-\infty}^{t} dt'\, \Omega(t')\cos(\delta\, t'/2). \tag{523}$$

This generally is nonzero; indeed, $|C_2(t)|$ can equal unity. It is noteworthy that these large values occur even though neither carrier frequency is equal to the Bohr frequency: first-order perturbation theory would predict null permanent population transfer [83].

[83] I am indebted to Andon Rangelov for pointing out this interesting example of excitation despite "missing frequencies".

F Examples of statistical averages

The following paragraphs discuss several examples of the statistical averages mentioned in Sec. 9.1. These have particular relevance for particle beams excited by passage through laser beams.

F.1 Motion across a laser beam

The pulsed excitation of an atom within a particle beam, as it moves across the profile of a laser beam, originates with the spatial variation of the laser beam; in the atom rest frame the laser field appears as a pulse..

Let the y coordinate of a Cartesian system be taken as the axis of a collimated laser beam, whose electric field $\mathcal{F}(x,z)$ therefore has variation only in the x,z plane. Typically this variation has Gaussian form, say

$$\mathcal{F}(x,z) = \mathcal{E}_0 \exp[-(x/w_x)^2] \exp[-(z/w_z)^2], \tag{524}$$

but other forms occur. Consider an atom moving with constant velocity $v_\perp$ parallel to the x axis (and hence perpendicular to the laser-beam axis), at constant height z above the midplane of the laser beam. The x position of the center of mass for this atom is $x = v_\perp t$, with $x = 0$ taken to coincide with the center of the laser beam, and $t = 0$ taken at the moment of maximum field. The electric field at the moving center of mass for this atom is

$$\mathcal{E}(t,z) = \mathcal{E}_0 \exp[-(z/w_z)^2] \exp[-(tv_\perp/w_x)^2], \tag{525}$$

That is, the atom experiences a Gausian-pulse field, centered at time $t = 0$ and of duration $T_v \equiv w_x/v_\perp$, and of peak value $\mathcal{E}_0 \exp[-(z/w_z)^2]$. The interaction strength for such a field is parametrized by a Rabi frequency that depends upon $v_\perp$ and z,

$$\Omega(t;v,z) = \Omega_0 \exp[-(z/w+z)^2] \exp[-(tv_\perp/w_x)^2], \tag{526}$$

and thus the RWA Hamiltonian and the probability amplitudes also carry this same dependence; the TDSE reads

$$\frac{d}{dt}\mathbf{C}(t;v_\perp,z) = -\mathrm{i}\mathsf{W}(t;v_\perp,z)\mathbf{C}(t;v_\perp,z). \tag{527}$$

The various solutions for different velocities differ because faster atoms experience shorter pulse durations, though the peak Rabi frequencies are the same. Thus different velocities lead to different numbers of Rabi cycles. Similarly, atoms moving at different heights z across the beam experience different peak values of the field, and hence different numbers of Rabi cycles.

In practice one deals with a beam of atoms, distributed in z and with differing x velocities. For comparison with experimental results one must therefore average the probabilities over these distributions. (The averaging is of probabilities, not probability amplitudes, because each atom trajectory is independent.) The result has the form

$$\bar{P}_n(t) = \int dz\, p_Z(z) \int dv_\perp\, p_V(v_\perp) |C_n(t;z,v_\perp)|^2, \tag{528}$$

where $p_Z(z)$ is the probability of a trajectory offset by z, and $p_V(v_\perp)$ is the probability distribution of velocities perpendicular to the laser axis. This prescription can only be evaluated for

a discrete set of solutions to the TDSE, obtained with discrete values for the parameters $z, v_\perp$. Thus the practical evaluation of probabilities uses the algorithm

$$\bar{P}_n(t) = \Sigma_j p_Z(z_j)\, p_V(v_j)\, |C_n(t; z_j, v_j)|^2. \tag{529}$$

If the spread of velocities is sufficiently small one can treat all trajectories as though they had the mean velocity $\bar{v}_\perp$. Similarly, if the distribution in z is much smaller than the width w_z of the laser beam then one can consider only the trajectory having $z = 0$. Under this approximation the required probabilities are obtained from a single solution to the TDSE,

$$\bar{P}_n(t) = |C_n(t; 0, \bar{v}_\perp)|^2, \tag{530}$$

involving the Rabi frequency

$$\Omega(t) = \Omega_0 \exp[-(t\bar{v}_\perp/w_x)^2]. \tag{531}$$

The use of a single average velocity requires that the spread in times $\delta t = w_x/\delta v_\perp$ resulting from the spread in velocities $\delta v_\perp$ should be much less than a mean Rabi period, $1/\Omega_0$.

F.2 Motion along a laser beam: Doppler effect

An atom moving nonrelativistically with velocity $v_{||}$ along the axis of a laser beam experiences the carrier frequency Doppler shifted to the value $[1 + v_{||}/c]\omega$. This appears in the RWA Hamiltonian $\mathsf{W}(t; v_{||})$ as an altered detuning,

$$\Delta = \omega_0 - [1 + v_{||}/c]\omega. \tag{532}$$

Exact resonance requires that, for given carrier frequency ω, the velocity $v_{||}$ should have the value

$$v_{||} = \frac{c}{\omega}[\omega_0 - \omega]. \tag{533}$$

A distribution of velocities around this value will produce probability amplitudes that are not resonant, and population oscillations that differ in frequency and magnitude [2, § 22.2]. The observable probabilities obtain from the algorithm

$$\bar{P}_n(t) = \Sigma_j p_V(v_j) |C_n(t; v_j)|^2. \tag{534}$$

F.3 Orientations

Any atom that has nonzero angular momentum J has $2J + 1$ possible discrete orientations with respect to any arbitrary direction (see Sec. 8), for example, the direction of the electric field of linearly polarized light. Each distinct orientation of the atom corresponds to a distinct projection of the dipole moment upon the electric field, i.e. a distinct value of $\mathbf{d} \cdot \mathbf{E}$. Unless special preparation techniques are used, each of these orientations will be present in the initial ensemble of quantum states, and predictions of atomic behavior must include an average over all possible orientations, i.e. an average over a set of different Rabi frequencies [2, § 22.4]. Section 11.4 discusses some examples of these averages; see eqn. (323).

F.4 Collisions

An atom in a vapor is affected by random encounters with other particles of the vapor, charged and neutral. Each encounter with a single projectile produces a time-varying interaction $V(t)$ characterised by the distance of closest approach (impact parameter) b as well as the orientation of the plane of projectile motion. When the projectile is charged, and remains beyond the extent of the atom wavefunction, its effect can be regarded as an electric field directed along the changing interparticle distance. The effect of such a field, for a single encounter, can be modeled using the TDSE. An average over all possible trajectories (i.e. velocities and distance of closest approach) is needed to describe the vapor environment.

G Hyperfine linkages

A quantum state that has electronic angular momentum J has $2J+1$ magnetic sublevels, distinguished by quantum number M_J. In the absence of an external field these are degenerate. When the atom nucleus has also angular momentum, customarily denoted I, this adds an additional degree of freedom, with $2I+1$ nuclear orientations, distinguished by a projection quantum number M_F. The interaction energy of the nuclear electric and magnetic moments with the electric and magnetic fields of the electrons produces hyperfine structure in the spectra [89].

The magnetic moments associated with the angular momenta $\mathbf{I}$ and $\mathbf{J}$ produce a spin-spin interaction observable as a hyperfine splitting of the energy levels. When $I > 1$ the nucleus has an electric quadrupole moment, and this can interact with the local electric-field gradient to produce additional hyperfine splitting. The Hamiltonian responsible for the hyperfine interaction, [2, §21.1]

$$\mathsf{H}^{HF} = \mathsf{H}^{NM1} + \mathsf{H}^{NE2}, \tag{535}$$

has therefore two contributions, often written as

$$\mathsf{H}^{NM1} = hA\,\mathsf{T}^{(1)}(\mathbf{1})\cdot\mathsf{T}^{(1)}(\mathbf{J}), \quad \text{magnetic dipole}, \tag{536}$$

$$\mathsf{H}^{NE2} = hB\,\mathsf{T}^{(2)}(\mathbf{1})\cdot\mathsf{T}^{(2)}(\mathbf{J}), \quad \text{electric quadrupole}. \tag{537}$$

Here A and B are parameters derived from the structure of the specific atom and $\mathsf{T}^{(k)}(\mathbf{J})$ is an irreducible tensor of order k constructed from angular momentum $\mathbf{J}$. As examples, the 0 component of the first and second rank tensors are

$$T_0^{(1)}(\mathbf{J}) = J_z, \qquad T_0^{(2)}(\mathbf{J}) = \frac{1}{\sqrt{6}}\left[2(J_z)^2 - (J_x)^2 - (J_y)^2\right]. \tag{538}$$

To express a quantum state involving the separate nuclear and atomic degrees of freedom we can use product states $|I, M_I\rangle|J, M_J\rangle$. The hyperfine interactions have linkages between such different different states; they are not diagonal. However, each of these is a scalar, and so the total angular momentum of the system, combining electronic and nuclear angular momenta, customarily denoted F, is not altered by hyperfine interactions. The quantized orientations of this vector are labeled by quantum number M_F. The overall quantum state, in the presence of hyperfine interaction, carries the labels J, I, F, M_F.

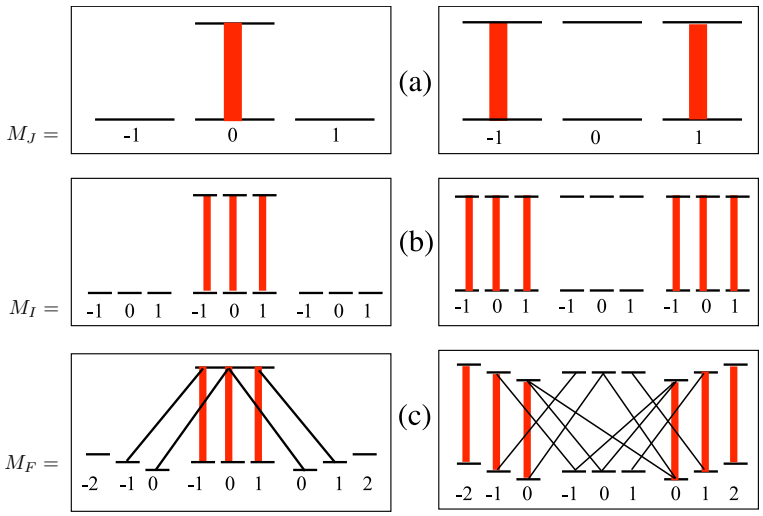

Fig. 80. Linkage pattern for $J = 1 \rightarrow 0$ (left columns) and $J = 1 \rightarrow 1$ (right columns) with linear polarization. (a) Without nuclear spin (b) with nuclear spin $I = 1$ but negligible hyperfine interaction (c) with nuclear spin $I = 1$ and hyperfine interaction. (after Figs. 1 and 2 of Shore et al. [165])

Electric dipole transitions between hyperfine sublevels obey similar selection rules as do transitions in the absence of nuclear spin (cf. Sec. 8.1): F can change by at most one unit, and M_F obeys the same selection rules as does M_J. That is, F may change by 0 or ± 1 (but $0 \leftrightarrow 0$ transitions do not occur) as may M_F.

Figure 80 illustrates some linkage patterns that occur for linear polarization when hyperfine interactions are present [165]. In the left column are examples for excitation $J = 1 \rightarrow 0$, while the right column shows examples for excitation $J = 1 \rightarrow 1$. In the top row (a) there is no nuclear spin; sublevels bear labels M_j. The middle row (b) shows the effect of including the additional degeneracy of nuclear spin $I = 1$, but without including the hyperfine interaction. Here each sublevel of given M_J is associated with three possible orientations of the nuclear spin. This does not change during an electric-dipole radiative interaction. The bottom row shows the quantum labels needed in the presence of hyperfine interaction. The hyperfine interaction shifts the energies and mixes the quantum states. Strong lines show linkages allowed in the limit of zero hyperfine interaction. Weak lines show transitions that are allowed by first-order perturbation theory.

In the uncoupled basis the matrix elements of the dipole moment are an application of the Wigner-Ekert theorem, eqn. (200)

$$\begin{aligned} &\langle IM_I, JM_J | d_q | I'M_I', JM_J' \rangle \\ &\quad = \delta(I, I')\, \delta(M_I, M_I')\, (-1)^{J-M} \begin{pmatrix} J & 1 & J' \\ -M_J & q & M_{J'} \end{pmatrix} (J||d||J'), \end{aligned} \tag{539}$$

where $\delta(n, m)$ is the Kronecker delta and $(J||d||J')$ is the reduced matrix element of the dipole transition moment, cf. Appendix A.6. The radiative interaction involves electrons, not nuclear

spins, and so the quantum numbers I, M_i do not change. With this choice of basis one can treat separately each M_I value, so that the matrices do not involve all $(2I+1)(2J+1)$ sublevels simultaneously. Alternatively, in the coupled basis the required expression is [91] [2, §21.1]

$$\langle IJFM|d_q|I'J'F'M'\rangle = \delta(I,I')\,(-1)^{F-M}\begin{pmatrix} F & 1 & F' \\ -M & q & M' \end{pmatrix}$$
$$\times(-1)^{I+J+F+1}\sqrt{(2F+1)(2F'+1)}\begin{Bmatrix} J & 1 & J' \\ F' & I & F \end{Bmatrix}(J||d||J'), \tag{540}$$

where $\{:::\}$ is a six-j symbol. The atomic Hamiltonian must, in either case, include the hyperfine interaction, H^{HF}. The choice of coupling scheme does not affect the final results, although the computations differ: if one chooses the *coupled* scheme, then H^{HF} is already diagonal, whereas the diagonalization of H^{HF} in the *uncoupled* scheme produces the coupled states as eigenstates.

H Alternative descriptions of coherent dynamics

Rather than deal with statevectors, several alternatives offer tools for describing coherent excitation. The following subsections mention some of these.

H.1 The density matrix

When incoherent processes such as spontaneous emission occur, the Schrödinger equation no longer provides a description of the dynamics. To treat such situations it is necessary to introduce a statistical average of bilinear combinations of probability amplitudes, a *density matrix* [166] [2, Chap. 6].

In the simplest situations the system can be described by a single statevector (it is then in a *pure* state), and the density matrix has for elements the values

$$\rho_{nm}(t) = \langle n|\Psi(t)\rangle\,\langle\Psi(t)|m\rangle. \tag{541}$$

We can regard these as matrix elements of the operator

$$\rho(t) = |\Psi(t)\rangle\,\langle\Psi(t)|, \qquad \text{pure state.} \tag{542}$$

More generally the system is in a *mixed* state, describable by probabilities p_k,

$$\rho(t) = \Sigma_k|\Psi_k(t)\rangle\,p_k\,\langle\Psi_k(t)|, \qquad \text{mixed state.} \tag{543}$$

When the statevector expansion involves rotating coordinates, with preset time-dependent phases of the form

$$\Psi(t) = \Sigma_n C_n(t)\exp[-\mathrm{i}\zeta_n(t)]\psi_n \equiv \Sigma_n C_n(t)\psi'_n(t), \tag{544}$$

then elements of the density matrix, expressed in terms of the rotating-coordinate probability amplitudes $C_n(t)$, are

$$\rho_{nm}(t) = \{C_n(t)C_m(t)^*\}_{av}\,\exp[-\mathrm{i}\zeta_n(t)+\mathrm{i}\zeta_m(t)]. \tag{545}$$

It often proves useful to regard the density matrix itself in the rotating coordinates of eqn. (97), writing

$$\tilde{\rho}_{nm}(t) = \{C_n(t)C_m(t)^*\}_{av}\,. \tag{546}$$

H.2 Interpretation

The elements of the density matrix have the following interpretation. The diagonal elements of the density matrix (for either pure or mixed states) are populations:

$$P_n(t) = \rho_{nn}(t) = \tilde{\rho}_{nn}(t). \tag{547}$$

These are independent of the (rotating) phases of the Hilbert-space coordinates. The off-diagonal elements are *coherences*. They are needed, for example, in the calculation of the expectation value of the dipole moment,

$$\begin{aligned} \langle d(t) \rangle &\equiv \{ \langle \Psi(t) | d | \Psi(t) \rangle \}_{av} & (548) \\ &= \Sigma_{nm}\, \rho_{nm}(t)\, d_{mn}. & (549) \end{aligned}$$

When expressed in rotating coordinates this reads

$$\begin{aligned} \langle d(t) \rangle &= \Sigma_{nm}\, \tilde{\rho}_{nm}(t)\, d_{mn}\, \exp[-\mathrm{i}\zeta_n(t) + \mathrm{i}\zeta_m(t)] & (550) \\ &= \Sigma_{nm}\, \{ C_n(t) C_m(t)^* \}_{av}\, d_{mn}\, \exp[-\mathrm{i}\zeta_n(t) + \mathrm{i}\zeta_m(t)], & (551) \end{aligned}$$

and there are time-varying phases [84].

Because probabilities must sum to unity [85] , any density matrix has unit trace:

$$\mathrm{Tr}\,[\rho] \equiv \Sigma_n \rho_{nn} = 1. \tag{552}$$

The density matrix for a pure state has the property

$$\rho \times \rho = \rho. \tag{553}$$

Thus any pure state has the property than the trace of any power of the density matrix is unity,

$$\mathrm{Tr}\,[\rho^n] = 1, \qquad \textit{pure state}. \tag{554}$$

A mixed state has the property, for $n > 1$,

$$\mathrm{Tr}\,[\rho^n] \leq 1, \qquad \textit{mixed state}. \tag{555}$$

For example, for $n = 2$ this inequality,

$$\mathrm{Tr}\,[\rho^2] \leq \mathrm{Tr}\,[\rho], \tag{556}$$

provides the constraint

$$\Sigma_{ij} \rho_{ij} \rho_{ji} \leq \Sigma_k \rho_{kk}. \tag{557}$$

For a two -dimensional density matrix the most general form in which no off-diagonal elements appear is

$$\rho = \frac{1}{a+b} \begin{bmatrix} a & 0 \\ 0 & b \end{bmatrix}. \tag{558}$$

[84] The differences between these phases appear as frequencies that determine which field envelope will be associated with a particular coherence; cf. Appendix A.5.

[85] Here we assume a lossless system.

This has unit trace, as required. However, the square of this matrix has trace

$$\text{Tr}\,[\rho^2] = \frac{a^2+b^2}{(a+b)^2}. \tag{559}$$

This can only be a pure state, describable by a single statevector, if one of the diagonal elements vanishes. That is, a pure state whose density matrix has more than one diagonal element must also have off-diagonal elements.

H.3 The equations of motion

The time evolution of the density matrix is governed by the RWA Hamiltonian $\mathsf{W}(t)$ plus terms that describe incoherent processes, i.e. relaxation processes. The simplest examples occur when spontaneous emission is included. The relevant equations then read

$$\begin{aligned}\frac{d}{dt}\tilde{\rho}_{mn}(t) &= -\mathrm{i}\Sigma_k\,[W_{mk}(t)\tilde{\rho}_{kn}(t) - \tilde{\rho}_{mk}(t)W_{kn}(t)] \\ &\quad -\tilde{\rho}_{mn}(t)\Sigma_k\tfrac{1}{2}(A_{mk}+A_{nk}) + \delta_{mn}\Sigma_k\tilde{\rho}_{kk}(t)A_{km}.\end{aligned} \tag{560}$$

The spontaneous emission rates A_{mk} are unidirectional: $A_{mk} = 0$ unless $E_m > E_k$. For two states these equations read

$$\frac{d}{dt}\tilde{\rho}_{11} = -\mathrm{i}W_{12}\tilde{\rho}_{21} + \mathrm{i}W_{21}\tilde{\rho}_{12} + A_{21}\tilde{\rho}_{22}, \tag{561}$$

$$\frac{d}{dt}\tilde{\rho}_{22} = -\mathrm{i}W_{21}\tilde{\rho}_{12} + \mathrm{i}W_{12}\tilde{\rho}_{21} - A_{21}\tilde{\rho}_{22}, \tag{562}$$

$$\frac{d}{dt}\tilde{\rho}_{12} = +\mathrm{i}[W_{22}-W_{11}]\tilde{\rho}_{12} - \mathrm{i}W_{12}[\tilde{\rho}_{22}-\tilde{\rho}_{11}] - \tfrac{1}{2}A_{21}\tilde{\rho}_{12},. \tag{563}$$

$$\frac{d}{dt}\tilde{\rho}_{21} = -\mathrm{i}[W_{22}-W_{11}]\tilde{\rho}_{21} + \mathrm{i}W_{21}[\tilde{\rho}_{22}-\tilde{\rho}_{11}] - \tfrac{1}{2}A_{21}\tilde{\rho}_{21}. \tag{564}$$

The first two equations have the form of eqn. (18),

$$\frac{d}{dt}P_1 = A_{21}P_2 - \frac{\mathrm{i}}{2}\Omega[\tilde{\rho}_{21}-\tilde{\rho}_{12}], \tag{565}$$

$$\frac{d}{dt}P_2 = -A_{21}P_2 + \frac{\mathrm{i}}{2}\Omega[\tilde{\rho}_{21}-\tilde{\rho}_{12}], \tag{566}$$

but with the appearance of additional quantities, the coherences $\tilde{\rho}_{12}$ and $\tilde{\rho}_{21} = \tilde{\rho}_{12}^*$. These obey the equations

$$\frac{d}{dt}\tilde{\rho}_{12} = \mathrm{i}\Delta\tilde{\rho}_{12} - \frac{\mathrm{i}}{2}\Omega[P_2-P_1] - \tfrac{1}{2}A_{21}\tilde{\rho}_{12}, \tag{567}$$

$$\frac{d}{dt}\tilde{\rho}_{21} = -\mathrm{i}\Delta\tilde{\rho}_{21} - \frac{\mathrm{i}}{2}\Omega[P_2-P_1] - \tfrac{1}{2}A_{21}\tilde{\rho}_{21}. \tag{568}$$

There occur no Milne-Einstein B coefficient here, only the Einstein A coefficient, because absorption and stimulated emission originate with the coherent interaction, as parametrized by the Rabi frequency Ω.

More generally one can include other processes that are suitably random, i.e. without memory. The general form of the equation is then

$$\frac{d}{dt}\tilde{\rho}_{mn}(t) = -\mathrm{i}\Sigma_j\,[W_{mj}(t)\tilde{\rho}_{jn}(t) - \tilde{\rho}_{mj}(t)W_{jn}(t)] + \Sigma_{jk}\mathcal{R}_{mnjk}(t)\tilde{\rho}(t)_{jk}. \tag{569}$$

Here $\mathsf{W}(t)$ describes the effects of coherent interactions, such as laser pulses, and $\mathcal{R}(t)$ describes random (Markov) processes, such as spontaneous emission, collisions and other random interruptions. We can neglect $\mathcal{R}(t)$ for time intervals shorter than relaxation times. The equation is then equivalent to the Schrödinger equation. Note that although the variables of this equation are matricies, the elements of the density matrix can be ordered into one-dimensional arrays, and so the equations can be written, akin to the Schrödinger equation, as a set of coupled ODEs,

$$\frac{d}{dt}\tilde{\rho}(t) = -\mathrm{i}\mathsf{L}(t)\tilde{\rho}(t). \tag{570}$$

The array $\mathsf{L}(t)$ combines the RWA Hamiltonian and relaxation terms.

H.4 The coherence vector

The presentation of coherent excitation dynamics as motion of a vector in an abstract space offers opportunities for gaining insight into the response of the system to various pulses or pulse sequences. Such pictures need not be limited to the two-state vector model of motion of a point on the Bloch sphere. One higher dimensional model that offers a simple pictorial description of excitation dynamics is the pseudospin model of Sec. 11.3. Other authors have generalized the notion of the Bloch vector, descriptive of two-state behavior, to obtain in N-dimensions a vector (termed by Hioe and Eberly the *coherence vector*) that obeys a generalization of the torqued motion of the Bloch vector [167].

The starting point for this generalization is the set of elementary operators $\hat{\pi}_{nm} \equiv |n\rangle\langle m|$ used to present the Hamiltonian in the form

$$\mathsf{H}(t) = \Sigma_n E_n\hat{\pi}_{nn} + \Sigma_{n\neq m}V_{nm}(t)\hat{\pi}_{nm}, \tag{571}$$

and to express elements of the density matrix,

$$\rho_{nm}(t) = \mathrm{Tr}\,[\hat{\pi}_{nm}\rho(t)]. \tag{572}$$

We combine these to form new operators, for $n, m \leq N$ and $L < N$,

$$\hat{u}_{nm} \equiv [\hat{\pi}_{nm} + \hat{\pi}_{mn}], \tag{573}$$

$$\hat{v}_{nm} \equiv -\mathrm{i}[\hat{\pi}_{nm} - \hat{\pi}_{mn}], \tag{574}$$

$$\hat{w}_n \equiv= \sqrt{\frac{2}{L(L+1)}}[\hat{\pi}_{11} + \hat{\pi}_{22} + \cdots + \hat{\pi}_{LL} - L\hat{\pi}_{L+1,L+1}]. \tag{575}$$

In the special case of two dimensions these are the three Pauli matrices, i.e. twice the spin-half matrices of Appendix C.2. They provide links between every pair of states. We then form an ordered array from these N^2-1 operators,

$$\hat{\mathsf{s}} = [\hat{u}_{12}, \cdots, \hat{v}_{12}, \cdots, \hat{w}_1, \cdots, \hat{w}_{N-1}]^T. \tag{576}$$

These operators have the commutation property

$$[\hat{s}_n, \hat{s}_m] = 2\mathrm{i}\Sigma_k \epsilon_{nmk} \hat{s}_k, \tag{577}$$

where ϵ_{nmk} is the completly antisymmetric structure constant of the $SU(N)$ group. Using these operators we have the constructions

$$\rho(t) = \frac{1}{N}\mathbf{1} + \tfrac{1}{2}\Sigma_{n=1}^{N^2-1} S_n(t)\hat{s}_n, \qquad \text{where } S_n(t) = \mathrm{Tr}\,[\rho(t)\hat{s}_n], \tag{578}$$

$$\mathsf{H}(t) = \frac{\hbar}{2}\Sigma_{n=1}^{N^2-1} \Gamma_n(t)\hat{s}_n, \qquad \text{where } \Gamma_n(t) = \mathrm{Tr}\,[\mathsf{H}(t)\hat{s}_n]. \tag{579}$$

The equation of motion for the functions $S_n(t)$ is

$$\frac{d}{dt}S_n(t) = \Sigma_{mk}\, \epsilon_{nmk}\, \Gamma_m(t)\, S_k(t). \tag{580}$$

This is a generalization of the torque equation satisfied by the Bloch vector (to which it reduces when $N=2$). The quantities $S_n(t)$ are elements of a coherence vector $\mathbf{S}(t)$ in N^2-1 dimensions, for which we can write the equation of motion as a torque equation,

$$\frac{d}{dt}\mathbf{S}(t) = \mathbf{\Gamma}(t)\times\mathbf{S}(t). \tag{581}$$

The set of N^2-1 elements of the coherence vector are not all independent. As pointed out by Hioe and Eberly, the motion of this vector is constrained by a set of conserved quantities

$$c(N,m) \equiv \mathrm{Tr}[\rho(t)^m], \quad n \le N, \tag{582}$$

where N is the dimensionality of the Hamiltonian. The first of these, $c(N,1)$ simply states that probability is conserved.

An alternative form for the coherence vector was proposed by Oreg and Goshen [167]. It is based on using state labels that run, not from 1 to N, but from $-S$ to $+S$ for $N = 2S+1$, as in the pseudospin model [121]. Using three-j symbols we construct, for $k = 0, \ldots, 2S$ and $q = -k, \ldots + k$, the N^2 matrices

$$\hat{s}_q^{(k)} = \Sigma_{mm'}(-1)^{S-m}\sqrt{2k+1}\begin{pmatrix} S & k & S \\ m & q & m' \end{pmatrix}|m\rangle\langle m'|. \tag{583}$$

These are infinitisimal generators of the unitary group $U(N)$; those for $k \neq 0$ are infinitisimal generators of $SU(N)$ With this basis the coherence vector takes the form of *irreducible tensors* (k labels the order, q labels the the component)

$$S_q^{(k)}(t) = (-1)^q \mathrm{Tr}\,[\rho(t)\hat{s}_{-q}^{(k)}], \tag{584}$$

and the RWA Hamiltonian has the construction

$$\mathsf{W}(t) = \Sigma_{kq}\Gamma_q^{(k)}(t)\hat{s}_q^{(k)}, \qquad \Gamma_q^{(k)}(t) = (-1)^q \mathrm{Tr}\,[\mathsf{W}(t)\hat{s}_{-q}^{(k)}]. \tag{585}$$

The equation of motion for the coherence vector, in the RWA, has the form

$$\frac{d}{dt}S_q^{(k)}(t) = \Sigma_{k'q'k''q''} f_{q'q''q}^{k'k''k}\ \Gamma_{q'}^{(k')}(t) S_{q''}^{(k'')}(t), \tag{586}$$

where the structure constants $f_{q'q''q}^{k'k''k}$ are expressible in terms of three-j and six-j symbols. When the Hamiltonian is restricted by suitable symmetry properties, the equation of motion breaks into independent blocks.

I The Lorentz atom

Prior to the development of quantum theory H. A. Lorentz developed a model of atomic structure that provided a quantitative description of the response of to weak monochromatic light [16]. In this model atoms comprised an infinite number of "Lorentz electrons", each of charge e and mass m_e, held by a restoring force to an equilibrium position but responding to the Lorentz force exerted by the radiation [86]. We can recover this model as a limiting case of a quantum description of two-state excitation.

The relevant equations follow from the equation of motion for the density matrix of a two-state atom driven by a monochromatic field and subject to spontaneous emission. Specifically we require the equations for the real and imaginary components of the coherence, because these provide the expectation value of the dipole moment. Expressed in terms of Bloch variables these equations read

$$\begin{aligned}
\frac{d}{dt}r_1(t) &= -\omega_{12}r_2(t) - \frac{A}{2}r_1(t), \\
\frac{d}{dt}r_2(t) &= +\omega_{12}r_1(t) - 2V(t)r_3(t) - \frac{A}{2}r_2(t),
\end{aligned} \tag{587}$$

where the interaction is

$$V(t) = -d_{12}\mathcal{E}\cos(\omega t) = \tfrac{1}{2}\hbar\Omega\cos(\omega t). \tag{588}$$

To derive an equation descriptive of harmonic motion we take the second derivative of r_1, obtaining the acceleration

$$\frac{d^2}{dt^2}r_1(t) \quad = \quad -\omega_{12}\frac{d}{dt}r_2(t) - \frac{A}{2}\frac{d}{dt}r_1(t). \tag{589}$$

[86] There are obvious difficulties in considering an infinite number of real particles, each of finite mass, within an atom that also has finite mass. Thus the "Lorentz electron" is not the same entity as the electron that we treat as a particle bound to an atomic nucleus. Nevertheless, the Lorentz model provides a remarkably good description of the spectroscopic properties of atoms, and their effect upon the radiation propagation as parametrized by the complex index of refraction.

Taken with the first-order equations this produces the result

$$\begin{aligned}\frac{d^2}{dt^2}r_1(t) &= -[\omega_{12}-(A/2)^2]r_1(t)+2\omega_{12}V(t)r_3(t)+A\omega_{12}r_2(t)\\ &= -[\omega_{12}^2+(A/2)^2]r_1(t)-A\frac{d}{dt}r_1(t)+2\omega_{12}V(t)r_3(t).\end{aligned} \tag{590}$$

This is the equation of motion for a driven and damped harmonic oscillator: it has a harmonic restoring force expressed by the frequency ω_{12} (altered slightly by spontaneous emission), a frictional force proportional to velocity and to A, and a driving force expressed by the final term. To make the connection with a Lorentz oscillator we define the oscillator coordinate to be $x = x_{12}r_1$ where the dipole transition moment is $d_{12} = ex_{12}$. Then the equation reads

$$\frac{d^2}{dt^2}x(t) = -\omega_c^2 x(t) - A\frac{d}{dt}x(t) + f_{12}\frac{F(t)}{m_e}r_3(t), \tag{591}$$

where the classical oscillator frequency is

$$\omega_c = \sqrt{\omega_{12}^2+(A/2)^2}, \tag{592}$$

the electron mass is m_e and the force $F(t)$ acting on the electron, of charge e, is

$$F(t) = e\mathcal{E}(t)\cos(\omega t). \tag{593}$$

The dimensionless factor f_{12} is the *oscillator strength*,

$$f_{12} = 2m_e|x_{12}|^2/\hbar. \tag{594}$$

This can be written, using atomic units of length $a_0 = \hbar^2/me^2$ and energy $E_{AU} = \mathrm{e}^2/a_0$, as

$$f_{12} = \frac{2}{3}\frac{\hbar\omega_{12}}{E_{AU}}S(1,2), \tag{595}$$

where $S(1,2) = 3|x_{12}/a_0|^2$ is the spectroscopic transition strength.

In the absence of the interaction V the oscillator has a natural frequency ω_c differing (slightly) from the Bohr transition frequency ω_{12} by the square of the damping rate $A/2$. This damping originates with the loss of coherence due to spontaneous emission; it acts like a frictional force upon the oscillator, eventually bringing it to rest at the equilibrium position.

The forcing term here differs from the classical force assumed by Lorentz: it depends upon the population inversion r_3. When the excitation is weak, the population remains in the ground state, and so $r_3 = -1$. This is the regime of the Lorentz oscillator.

J Center of mass motion

The center of mass motion of a nonrelativistic free particle, of mass m and velocity v, has wave-like properties characterized by the de Broglie wavelength $\lambda_d = 2\pi\hbar/mv$. The possibility of producing particle beams whose de Broglie wavelength is of macroscopic size makes possible the duplication of effects equivalent to those of classical optics but using matter waves , i.e. atom optics [168].

The absorption of a traveling-wave photon of frequency ω brings with it not only the addition of excitation energy $\hbar\omega$ but also an increment in linear momentum $\hbar k = \hbar\omega/c$ in the direction of beam propagation. Resonant radiation therefore exerts a force on an atom [169]. This force, induced by a single photon, deflects an atom of mass M by the angle

$$\theta = \arctan[\hbar\omega/Mvc]. \tag{596}$$

Subsequent de-excitation by *stimulated* emission will remove this momentum increment, thereby leaving the atom velocity as it was prior to excitation. However, *spontaneous* emission produces a radiation field which is distributed in angle, and hence the associated momentum change is disributed over a range of angles. When spontaneous emission events are important, as is the case with excitation over a sufficiently long time, then the combination of laser excitation followed by spontaneous emission produces radiation pressure [41]. The combination of absorption and spontaneous emission can serve as a cooling mechanism [42].

When two laser beams are present, propagating in opposite directions, then atoms can absorb radiation from one beam and return it to the other. A sequence of such events, appearing as Rabi oscillations of the internal excitation energy, will be accompanied by a coherent alteration of the center of mass motion of each atom. Multiple absorption and emission events induced by counter propagating laser beams can induce a momentum change of $\Delta p = n\hbar k$. To describe fully the effect of radiation upon moving atoms it is therefore necessary to suplement the internal degrees of freedom (two or three excitation states, for example) with a continuum of linear momentum states for the center of mass coordinate $\mathbf{r}$. We write the wavefuntion for this coordinate as the superposition

$$\Psi(\mathbf{r},t) = \int d\mathbf{p}\Sigma_n C_{n,\mathbf{p}}(t)\psi_n(t)\phi_{\mathbf{p}}(\mathbf{r}), \tag{597}$$

where for center-of-mass motion we use the free-particle wavefunctions

$$\phi_{\mathbf{p}}(\mathbf{r}) = \exp(\mathrm{i}\mathbf{p}\cdot\mathbf{r})/\sqrt{(2\pi)^3}. \tag{598}$$

The relevant Hamiltonian, for center of mass motion affected by coherent excitation, has been presented in several works [170][2, §15.12].

A simple example will illustrate the basic principles. Because momentum changes occur in discrete increments it is useful to consider photons as the increments, and to deal with photon states. To treat the interaction of an atom with quantized radiation we require a Hamiltonian comprising three parts,

$$\mathsf{H} = \mathsf{H}^{fld} + \mathsf{H}^{at} + \mathsf{H}^{int}, \tag{599}$$

describing, respectively, the field, the atom and the interaction.

Consider a two-state atom of mass M traveling in the x,z plane axis and passing through monochromatic counterpropagating plane-wave laser beams, directed along the x axis. These have mode fields $\exp(\pm\mathrm{i}kx)$. Quantization leads to two sets of photon states, $\phi_{n_\pm}^{(\pm)}$, for these two fields. The field Hamiltonian for this system is the energy of the two fields,

$$\mathsf{H}^{fld} = \hbar\omega[\hat{a}_+^\dagger\hat{a}_+ + \hat{a}_-^\dagger\hat{a}_-]. \tag{600}$$

Let us assume that the atom is only slightly deflected from its initial direction, and so only the changing motion in the x direction need be evaluated; the original momentum maintains a constant value, say $\hbar K$. Changes of x momentum can only occur in discrete increments, of value $\hbar k$ added to an initial value $\hbar k_0$, and so the center-of-mass momentum state, for x motion, can be chosen to be defined (apart from normalization) through the property

$$\hat{p}_x \Phi_\nu = \hbar(k_0 + \nu k)\Phi_\nu. \tag{601}$$

To describe the combined state of the internal atomic structure, the center of mass motion, and the state of the two fields we express the statevector as

$$\Psi(t) = \Sigma_{a,\nu,n_+,n_-} \exp[-\mathrm{i}(n_+ + n_-)\omega t]\, C_{a,\nu,n_+,n_-}(t)\, \psi'_a(t)\, \Phi_\nu\, \phi^{(+)}_{n_+} \phi^{(-)}_{n_-}, \tag{602}$$

where the internal-excitation states are taken as

$$\psi'_1(t) = \psi_1\ \exp(\mathrm{i}\omega t/2), \qquad \psi'_2(t) = \psi_2\ \exp(-\mathrm{i}\omega t/2). \tag{603}$$

The Hamiltonian for the atom can, with suitable basis and in the RWA, be taken as

$$\mathsf{H}^{at} = \frac{1}{2M}\left[\hat{p}_x - \hbar k(\hat{a}^\dagger_+ \hat{a}_+ - \hat{a}^\dagger_- \hat{a}_-)\right]^2 + E_1 \hat{\pi}_{11} + E_2 \hat{\pi}_{22}. \tag{604}$$

This accompanies an interaction

$$\mathsf{H}^{int} = \frac{\hbar\Omega_0}{\sqrt{8}} \hat{\pi}_{21}\left[\hat{a}_+ + \hat{a}_-\right] + \frac{\hbar\Omega_0}{\sqrt{8}} \hat{\pi}_{12}\left[\hat{a}^\dagger_+ + \hat{a}^\dagger_-\right]. \tag{605}$$

That is, each excitation of the atom requires loss of a photon; a change of photon number alters the momentum of the atom. From this Hamiltonian, and the statevector expansion of eqn. (602), we obtain a set of coupled equations for the probability amplitudes. Their solution describes the progressive increase of transverse momentum $\hat{p}_x$ with Rabi cycling of the field-induced excitation and de-excitation [170].

Interesting effects occur when a three-state atom undergoes stimulated Raman transitions effected by collinear but counterpropagating pump and Stokes beams. Complete population transfer will then alter the center of mass motion, in the direction of the laser beams, by one increment from each beam. Typically the atoms move perpendicular to the laser beams, and so the result will be observable as an alteration of the atomic beam direction. This action, of complete beam deflection, is an atomic mirror, albeit for atoms at grazing incidence [171].

When the excitation produces a superposition of internal energy states, then it also will produce a superposition of center-of-mass linear momentum states. This action is an atomic beam splitter [172]. For small deflection angles, when longitudinal momentum is much larger than photon recoil, the problem can be modeled as a one dimensional Schrödinger eqn for the transverse motion of the atoms.

K Adiabatic states

The idealization of a constant pulse amplitude readily extends to pulse amplitudes that vary slowly with time. In place of the constant eigenstates of the RWA Hamiltonian discussed in

section 6.4 one employs slowly varying *adiabatic states*. By definition these are instantaneous eigenvectors of the RWA Hamiltonian. For the two-state system they obey the equation

$$\mathsf{W}(t)\Phi_{\pm}(t) = \varepsilon_{\pm}(t)\Phi_{\pm}(t). \tag{606}$$

The eigenvalues of the two-state RWA Hamiltonian matrix are

$$\varepsilon_{\pm}(t) = \tfrac{1}{2}[\Delta(t) \pm \tilde{\Omega}(t)], \qquad \tilde{\Omega}(t) \equiv \sqrt{\Delta(t)^2 + |\Omega(t)|^2}. \tag{607}$$

Using the abbreviations

$$s(t) \equiv \sin\Theta(t), \qquad c(t) \equiv \cos\Theta(t), \tag{608}$$

we write these adiabatic states as an orthogonal rotation of the original bare diabatic states (which are already in a rotating reference frame),

$$\Phi_{+}(t) = s(t)\psi_1 + c(t)\psi_2(t), \tag{609}$$
$$\Phi_{-}(t) = c(t)\psi_1 - s(t)\psi_2(t). \tag{610}$$

It is easy to verify with the aid of trigonometric identities that this construction provides eigenvectors of a matrix that has the form

$$\mathsf{W}(t) = \tilde{\Omega}(t) \begin{bmatrix} 0 & s(t)c(t) \\ s(t)c(t) & c(t)^2 - s(t)^2 \end{bmatrix}, \tag{611}$$

and that the eigenvalues are

$$\varepsilon_{-}(t) = -s(t)^2\,\tilde{\Omega}(t), \qquad \varepsilon_{+}(t) = +c(t)^2\,\tilde{\Omega}(t). \tag{612}$$

To identify the mixing angle $\Theta(t)$ we use trigonometric identities to rewrite eqn(611) as

$$\mathsf{W}(t) = \tilde{\Omega}(t) \begin{bmatrix} 0 & \frac{1}{2}\sin 2\Theta(t) \\ \frac{1}{2}\sin 2\Theta(t) & \cos 2\Theta(t) \end{bmatrix}. \tag{613}$$

Thereby we identify the mixing angle as obtained from the equation

$$\cot 2\Theta(t) = \Delta(t)/\Omega(t). \tag{614}$$

The construction of the adiabatic states, expressed with the framework of diabatic states, is completely determined by the mixing angle. In turn, this is controllable by prescribing the pulsed changes of Rabi frequency and detuning. Thus the adiabatic states can be considered known. What remains to be done is to associate the unknown statevector $\Psi(t)$ with the adiabatic states, and to understand the conditions under which that connection can remain constant while the adiabatic states change.

K.1 Terminology

The terminology of "adiabatic" and "diabatic" dates from early work on the theory of reactive scattering [173]: *diabatic* states refer to colliding atoms that move toward each other along potential energy surfaces that do not allow excitation, whereas the *adiabatic* states incorporate the full interaction energy. The dependence of the interatomic potential energy on separation distance translates to a time dependence for moving particles, and hence the adiabatic states are time dependent.

An alternative terminology originated for the treatment of atoms interacting with quantized radio-frequency fields [74] and subsequently used for various calculations with CW laser radiation. The atom-field interaction is then constant. The eigenstates of the resulting full Hamiltonian (involving states of free atoms and free photons) were termed "dressed states", contrasting with the "bare states" of the non-interacting atoms and fields In that case the Hamiltonian was independent of time, and the relationship between dressed and bare states was constant.

The verbal similarity between the words *adiabatic* and *diabatic* is a potential source of unfortunate confusion, and therefore many speakers and authors prefer the terms *bare state* for the diabatic basis states $\psi_n(t)$ that are eigenstates of an unperturbed Hamiltonian, and use the term *dressed state* to describe an eigenstate of the full Hamiltonian; when the Hamiltonian changes with time these are the adiabatic states.

K.2 Adiabatic evolution

Considerable literature deals with adiabatic evolution [174]. Some articles are specific for two-state systems [175] while others treat the three-state lambda system [176]. Adiabatic evolution of the statevector occurs when it is expressible as a fixed, time-independent, superposition of adiabatic states. For a two-state system we can write the statevector in the adiabatic basis as

$$\Psi(t) = A_+(t)\Phi_+(t) + A_-(t)\Phi_-(t) \equiv \Sigma_k A_k(t)\Phi_k(t). \tag{615}$$

Evolution will be adiabatic if the coefficients A_k are time independent. The following paragraphs discuss the conditions needed for that result.

The time derivative of the construction (615) is

$$\frac{d}{dt}\Psi(t) = \Sigma_k \dot{A}_k(t)\Phi_k(t) + \Sigma_k A_k(t)\dot{\Phi}_k(t). \tag{616}$$

From the TDSE we obtain the requirement that this derivative should be

$$\frac{d}{dt}\Psi(t) - \mathrm{i}\mathsf{W}(t)\Sigma_k A_k(t)\Phi_k(t) = -\mathrm{i}\Sigma_k \varepsilon_k(t) A_k(t)\Phi_k(t). \tag{617}$$

The time derivatives of the adiabatic states are

$$\frac{d}{dt}\Phi_\pm(t) = \pm\dot{\Theta}(t)\Phi_\mp(t), \tag{618}$$

so these undergo interchange at a rate dependent on the time derivative of the mixing angle. From eqn. (616) we obtain the following equation, basically the RWA Schrödinger equation in an adiabatic basis,

$$\frac{d}{dt}\mathbf{A}(t) = -\mathrm{i}\mathsf{W}^A(t)\mathbf{A}(t), \tag{619}$$

where $\mathbf{A}(t) = [A_-(t),\ A_+(t)]^T$ is a column vector of the adiabatic coefficients and the RWA Hamiltonian, in the adiabatic basis, is

$$\mathsf{W}^A(t) = \begin{bmatrix} \varepsilon_-(t) & \mathrm{i}\dot{\Theta}(t) \\ -\mathrm{i}\dot{\Theta}(t) & \varepsilon_+(t) \end{bmatrix}. \tag{620}$$

K.3 Adiabatic conditions

The statevector will remain in a fixed superposition of adiabatic states, i.e. the coefficients $A_k(t)$ will remain constant, if the off-diagonal terms of $\mathsf{W}^A(t)$ are smaller than the difference of the diagonal terms,

$$\dot{\Theta}(t) \ll \varepsilon_+(t) - \varepsilon_-(t) = \tilde{\Omega}(t). \tag{621}$$

Such time evolution is adiabatic.

The nonadiabatic coupling term is the derivative of the mixing angle. We write this as

$$\frac{d}{dt}\Theta(t) = \frac{d}{dt}\frac{1}{2}\arctan[\Omega(t)/\Delta(t)]. \tag{622}$$

We use elementary calculus and the chain rule to write

$$\frac{d}{dt}\Theta(t) \quad = \quad \frac{1}{2} \times \frac{1}{1+[\Omega(t)/\Delta(t)]^2} \times \frac{d}{dt}[\Omega(t)/\Delta(t)]. \tag{623}$$

After a bit of algebra this gives the result

$$\frac{d}{dt}\Theta(t) \quad = \quad \frac{\dot{\Omega}\Delta - \Omega\dot{\Delta}}{2\tilde{\Omega}^2}. \tag{624}$$

Thus the adiabatic condition can be written as

$$|\dot{\Omega}\Delta - \Omega\dot{\Delta}| \ll 2|\tilde{\Omega}|^3. \tag{625}$$

When this condition is fulfilled, by suitable construction of the pulses, then the evolution will be adiabatic, and a detuning sweep will induce a transition between bare diabatic states.

K.4 Adiabatic constraints

We can approximate an upper bound to the change in mixing angle during the pulse of duration τ by writing

$$\dot{\Theta} < 2\pi/\tau. \tag{626}$$

This in turn must be much less than the eigenvalue separation, meaning

$$2\pi \ll |\Omega_0|\tau, \tag{627}$$

where Ω_0 is the value of the Rabi frequency when $\Delta = 0$. That is, the time integrated Rabi frequency (the pulse area) must be much larger than 2π.

Near $\Delta = 0$ the adiabatic condition, eqn. (621), becomes

$$\dot{\Delta} \ll (2\Omega_0)^2. \tag{628}$$

That is, the rate of change in detuning must be small compared with $(2\Omega_0)^2$. This condition emerges from the exact analytic results of the Landau-Zener model of diabatic curve crossing (or adiabatic avoided crossings): to be adiabatic, and hence produce a transition, the evolution must be such that the LZ parameter $\chi = (2\Omega_0)/|\dot{\Delta}|$ should be very much larger than 1.

However, the detuning cannot change too slowly. During the course of the pulse, as Δ passes through zero, there must be a change greater than the separation of eigenvalues, or

$$\dot{\Delta}\tau > |\Omega_0|. \tag{629}$$

We therefore find that, in addition to requiring a large Rabi angle, adiabatic passage requires that the detuning change fit within the bounds

$$(2\Omega_0)^2 \gg |\dot{\Delta}| > \Omega_0/\tau. \tag{630}$$

L Near-periodic excitation

For all but the very shortest pulses, the laser field that produces excitation endures for many optical cycles. It is reasonable, therefore, to regard this, to first approximation, as producing a Hamiltonian that is periodic in time[2, § 4.2]. Let the period be $\tau = 2\pi/\omega$. That is, the Hamiltonian has the property $\mathsf{H}(t) = \mathsf{H}(t+\tau)$. Such a periodic function of time is expressible as a Fourier series [87]

$$\mathsf{H}(t) \quad = \quad \mathsf{H}^{(0)} + \mathsf{H}^{(1)} \exp(\mathrm{i}\omega t) + \mathsf{H}^{(-1)} \exp(-\mathrm{i}\omega t) + \cdots \tag{631}$$

where the matrices $\mathsf{H}^{(m)}$ are constant. For the periodic variation $\cos(\omega t)$ discussed in this article only two terms contribute, $m = \pm 1$, but more general situations may occur.

Generally the Hamiltonian of interest is not exactly periodic; the matrices $\mathsf{H}^{(m)}$ vary with time, though they do so more slowly than the basic frequency ω. Equation (631) then becomes

$$\mathsf{H}(t) \quad = \quad \Sigma_{m=-\infty}^{\infty} \mathsf{H}^{(m)}(t) \exp(\mathrm{i}m\omega t). \tag{632}$$

and is then not an exact Fourier series. However, because we have a series decomposition of $\mathsf{H}(t)$ it is natural to look for a similar series for the statevector $\Psi(t)$. Specifically, let us propose the expansion

$$\Psi(t) = \Sigma_a \Sigma_{m=-\infty}^{\infty} C_{a,m}(t)\, \psi_a \exp(\mathrm{i}m\omega t), \tag{633}$$

where the $C_{a,m}(t)$ are expansion coefficients to be determined. The label a specifies the atomic basis state; the sum on m specifies the harmonic.

[87] I have here chosen a single fundamental frequency ω as the basis for the periodicity. In some situations the periodicity results from combinations of multiple commensurable periods. It is possible to introduce multiple periodicities and multiple frequencies $\omega_1, \omega_2, \ldots$ but the notation becomes quite cumbersome.

This construction of the statevector is tantamount to enlarging the Hilbert space by introducing basis vectors [88]

$$\phi_m(t) \equiv \exp(\mathrm{i}m\omega t) \tag{634}$$

and writing the statevector as

$$\Psi(t) = \Sigma_a \Sigma_{m=-\infty}^{\infty} C_{a,m}(t)\, \psi_a \phi_m(t). \tag{635}$$

The enlarged *Floquet space* has an infinite number of dimensions (because it treats an infinite set of harmonics, each requiring a dimension) but, like the original Hilbert space descriptive of the atom, usually only a few of them are needed. When the Hamiltonian is strictly periodic, so that $\mathsf{H}^{(m)}(t)$ is constant, the coefficients $C_{a,m}(t)$ are also constant, and eqn. (636) is a Fourier series. More generally the terms $\mathsf{H}^{(m)}(t)$ vary slowly with time, as do therefore the amplitudes $C_{a,m}(t)$.

From the statevector construction of eqn. (633) it follows that the probability amplitude for state a is a series,

$$C_a(t) \equiv \langle \psi_a | \Psi(t) \rangle = \Sigma_m \phi_m(t)\, C_{a,m}(t) = \Sigma_m \exp(\mathrm{i}m\omega t)\, C_{a,m}(t). \tag{636}$$

The probability of observing the atom in state ψ_a at time t is therefore the square of an infinite sum of harmonically-modulated time-varying amplitudes:

$$P_a(t) = |C_a(t)|^2 = |\Sigma_m \exp(\mathrm{i}m\omega t)\, C_{a,m}(t)|^2. \tag{637}$$

Thus interference can occur between different harmonics.

To obtain equations for the amplitudes $C_{a,m}(t)$ we substitute the expansion (633) into the Schrödinger equation (78) and equate to zero the coefficients of each factor $\psi_a \exp(\mathrm{i}m\omega t)$. This procedure produces an infinite set of coupled equations,

$$\frac{d}{dt} C_{a,m}(t) = -\mathrm{i}m\omega C_{a,m}(t) - (\mathrm{i}/\hbar)\Sigma_b \Sigma_n H_{ab}^{(n)}(t)\, C_{b,m-n}(t). \tag{638}$$

These equations are an exact transcription of the original Schrödinger equation, valid for any number of atomic states and an arbitrary number of harmonics in the interaction. There is, as yet, no RWA approximation, only the assumption that any time variation of $H_{ab}^{(n)}(t)$ be slow compared with the period $2\pi/\omega$.

As with the traditional approach to the TDSE in eqns. (106) - (108), we can express the set of coupled ordinary differential equations in matrix form, as

$$\frac{d}{dt} C_{a,m}(t) = -\mathrm{i}\Sigma_{b,n} K_{ab}^{(n)}(t) C_{b,m-n}(t). \tag{639}$$

The infinite matrix of these coefficients, $K_{ab}^{(n)}(t)$, is sometimes termed the *Floquet Hamiltonian*. It differs from the usual Hamiltonian in having the terms $m\omega$ on the diagonal. When the original Hamiltonian is strictly periodic the Floquet Hamiltonian is constant; more generally it varies slowly with time.

Although the equations are denumerably infinite in number, they are amenable to solution by generalization of any of the techniques that are usable for the two-state case (e.g., Laplace transforms). The following paragraphs comment on some properties of the equations and their solutions.

[88] The functions $\phi_m(t)$ form an infinite dimensional Hilbert space corresponding to a second degree of freedom.

L.1 Two states

A simple illustration of the preceding formalism occurs for a two-state atom, acted on by a linearly polarized sinusoidal interaction of frequency ω [2, §4.2]. There are two basis states in the atomic Hilbert space, ψ_1 and ψ_2, and so the statevector construction of eqn. (633) reads

$$\begin{aligned} \Psi(t) &= \psi_1 \, \Sigma_{m=-\infty}^{\infty} \exp(\mathrm{i}m\omega t) \, C_{1,m}(t) \\ &+ \psi_2 \, \Sigma_{m=-\infty}^{\infty} \exp(\mathrm{i}m\omega t) \, C_{2,m}(t). \end{aligned} \tag{640}$$

To clarify this construction let us use the notation $A_m(t)$ for harmonic components of state 1, and $B_m(t)$ for components of state 2,

$$C_{1,m}(t) = A_m(t), \qquad C_{2,m}(t) = B_m(t). \tag{641}$$

The only contributions to the Hamiltonian are

$$H_{11}^{(0)} = E_1 = 0, \qquad H_{22}^{(0)} = E_2 = \hbar\omega_0, \tag{642}$$

$$H_{21}^{(1)} = H_{21}^{(-1)} = \tfrac{1}{2}\hbar\Omega. \tag{643}$$

The equations of motion derived from eqn. (638) are the infinite sets

$$\begin{aligned} \frac{d}{dt}A_m(t) &= -\mathrm{i}\left[m\omega\right] A_m(t) - \mathrm{i}\frac{\Omega}{2}\left[B_{m-1}(t) + B_{m+1}(t)\right], \\ \frac{d}{dt}B_{m+1}(t) &= -\mathrm{i}\left[(m+1)\omega - \omega_0\right] B_{m+1}(t) - \mathrm{i}\frac{\Omega}{2}\left[A_m(t) + A_{m+2}(t)\right]. \end{aligned} \tag{644}$$

The matrix of coefficients appearing here form the elements of the Floquet Hamiltonian. It has as diagonal elements the frequencies $m\omega$ and the detunings $m\omega - \omega_0$ and as off-diagonal elements half the Rabi frequency Ω.

These equations separate into two independent sets of coupled equations. One set applies to the sequence $\ldots A_{-2}, B_{-1}, A_0, B_1, A_2, \ldots$, while the other set applies to the sequence $\ldots B_{-2}, A_{-1}, B_0, A_1, B_2, \ldots$. For each set the Floquet Hamiltonian has the matrix representation

$$\begin{bmatrix} \ddots & \vdots & \vdots & \vdots & \vdots & \vdots & \\ \ldots & (m+2)\omega & \frac{1}{2}\Omega & 0 & 0 & 0 & \ldots \\ \ldots & \frac{1}{2}\Omega & (m+1)\omega + \omega_0 & \frac{1}{2}\Omega & 0 & 0 & \ldots \\ \ldots & 0 & \frac{1}{2}\Omega & m\omega & \frac{1}{2}\Omega & 0 & \ldots \\ \ldots & 0 & 0 & \frac{1}{2}\Omega & (m-1)\omega + \omega_0 & \frac{1}{2}\Omega & \ldots \\ \ldots & 0 & 0 & 0 & \frac{1}{2}\Omega & (m-2)\omega & \ldots \\ & \vdots & \vdots & \vdots & \vdots & \vdots & \ddots \end{bmatrix}.$$

In particular, a small portion of the set of coupled equations, for even-integer A_n, has the coefficient matrix

$$\begin{bmatrix} \boxed{\begin{matrix} 2\omega & \frac{1}{2}\Omega \\ \frac{1}{2}\Omega & 2\omega+\Delta \end{matrix}} & \begin{matrix} 0 & 0 \\ \frac{1}{2}\Omega & 0 \end{matrix} & \begin{matrix} 0 & 0 \\ 0 & 0 \end{matrix} \\ \begin{matrix} 0 & \frac{1}{2}\Omega \\ 0 & 0 \end{matrix} & \boxed{\begin{matrix} 0 & \frac{1}{2}\Omega \\ \frac{1}{2}\Omega & \Delta \end{matrix}} & \begin{matrix} 0 & 0 \\ \frac{1}{2}\Omega & 0 \end{matrix} \\ \begin{matrix} 0 & 0 \\ 0 & 0 \end{matrix} & \begin{matrix} 0 & \frac{1}{2}\Omega \\ 0 & 0 \end{matrix} & \boxed{\begin{matrix} -2\omega & \frac{1}{2}\Omega \\ \frac{1}{2}\Omega & -2\omega+\Delta \end{matrix}} \end{bmatrix} \begin{matrix} A_{+2} \\ B_{+1} \\ A_0 \\ B_{-1} \\ A_{-2} \\ B_{-3} \end{matrix} .$$

Each 2×2 block is an example of the RWA equations, differing only by the addition of $2m\omega$ to both diagonal elements – a redefinition of the energy zero point (and an overall phase). In turn, the couplings between the different blocks represent counter-rotating terms in the rotating wave picture [89]. When the interaction $\frac{1}{2}\Omega$ is much smaller than 2ω the individual blocks will be nearly independent, and the RWA will apply. The Floquet Hamiltonian can then be approximated by any one of the blocks, for example

$$\frac{d}{dt}\begin{bmatrix} A_m \\ B_{m-1} \end{bmatrix} = -\mathrm{i}\begin{bmatrix} m\omega & \frac{1}{2}\Omega \\ \frac{1}{2}\Omega & m\omega+\Delta \end{bmatrix}\begin{bmatrix} A_m \\ B_{m-1} \end{bmatrix}. \tag{645}$$

These are just the usual RWA equations. Corrections to the RWA obtain by including successively more harmonics, as expressed by enlarging the Floquet Hamiltonian matrix.

This approach, through a truncated Floquet Hamiltonian, can be used when the Hamiltonian elements (i.e. the Rabi frequency and detuning) are slowly varying. At the expense of solving a larger number of coupled equations, one can obtain solutions to the TDSE without restriction upon either the strength of the interaction nor the magnitude of the detuning [90].

L.2 The Jaynes-Cummings model (JCM)

The Floquet treatment of a periodic field, using Fourier exponentials to form a Hilbert space, has much in common with a treatment involving photons, approached with the aid of a Fock space. When the field is quantized the two-state single-mode Hamiltonian operator can be written

$$\begin{aligned} \mathsf{H} = {} & \hbar\omega\hat{a}^\dagger\hat{a} + E_1\hat{\pi}_{11} + E_2\hat{\pi}_{22} \\ & + \frac{\mathrm{i}}{2}d_{12}\hat{\pi}_{12}(t)[\mathcal{E}_1\hat{a}(t) + \mathcal{E}_1^*\hat{a}^\dagger(t)] + \frac{\mathrm{i}}{2}d_{21}\hat{\pi}_{21}(t)[\mathcal{E}_1\hat{a}(t) + \mathcal{E}_1^*\hat{a}^\dagger(t)], \end{aligned} \tag{646}$$

where

$$\hat{a}(t) = \hat{a}\,\mathrm{e}^{-\mathrm{i}\omega t}, \quad \hat{a}^\dagger(t) = \hat{a}^\dagger\,\mathrm{e}^{\mathrm{i}\omega t}, \quad \hat{\pi}_{12}(t) = \hat{\pi}_{12}\,\mathrm{e}^{\mathrm{i}\omega t}, \quad \hat{\pi}_{21}(t) = \hat{\pi}_{21}\,\mathrm{e}^{-\mathrm{i}\omega t}. \tag{647}$$

In the rotating wave approximation this becomes the *Jaynes-Cummings Hamiltonian* [39][2, §10.7],

$$\mathsf{H} = \hbar\omega\hat{a}^\dagger\hat{a} + E_1\hat{\pi}_{11} + E_2\hat{\pi}_{22} + \frac{\mathrm{i}\hbar}{2}\Omega_1^*\hat{\pi}_{12}\hat{a}^\dagger + \frac{\mathrm{i}\hbar}{2}\Omega_1\hat{\pi}_{21}\hat{a}, \tag{648}$$

[89] These couplings are absent when the excitation is by circularly polarized light; the matrix then consists of independent blocks.

[90] However, the assumption of only two essential states fails as the field becomes more intense.

where the single-photon Rabi frequency is derived from the single-photon electric field, $\Omega_1 = d_{12}\mathcal{E}_1/\hbar$. Here each atom transition from higher to lower energy accompanies photon emission, while an energy-increasing transition accompanies the absorption of a photon. This Hamiltonian has two constants of motion, the total atomic probability and the excitation number,

$$\langle\hat{\pi}_{11}\rangle + \langle\hat{\pi}_{22}\rangle = 1, \qquad \langle\hat{a}^\dagger\hat{a}\rangle + \langle\hat{\pi}_{22}\rangle = \text{constant}. \tag{649}$$

The statevector expansion, in atomic states $\psi'_a(t)$ and single-mode photon states ϕ_n, reads

$$\Psi(t) = \Sigma_{n=0}^{\infty} C_{a,n}(t)\psi'_a(t)\phi_n. \tag{650}$$

Akin to the Floquet Hamiltonian with RWA, the use of photon-number basis states produces a set of uncoupled 2×2 blocks, each associated with a different photon number n. The Rabi frequency associated with n photons is $\Omega_n = \sqrt{n}\Omega_1$. Each of these independent two-state systems has an exact analytic solution for probability amplitudes; the JCM allows an exact solution of a system that combines a quantum description of an atom with a fully quantum-mechanical description of the field, albeit in the approximation of single-mode RWA.

To use these solutions it is necessary to average over the initial distribution of photon numbers, using probabilities p_n. For example, when the atom is initially unexcited we require the excitation probability

$$\bar{P}_2(t) = \tfrac{1}{2}\Sigma_{n=0}^{\infty} p_n\,[1 - \cos(\sqrt{n+1}\Omega_1 t)]. \tag{651}$$

The need for averaging required by the JCM introduces a superposition of solutions having different Rabi frequencies. The result is an effective damping of the apparent oscillations.

The JCM is similar to, but not identical with, the Floquet description of monochromatic excitation. The difference between the two approaches is in the succession of Rabi frequencies. For small photon number this becomes significant. In particular, when the mean photon number is very small, as can occur for an atom in a small cavity, and the photon distribution is that of a coherent state, the damped oscillations exhibit a revival, evidence of the discreteness of the photon numbers.

To emphasize the similarity of the two approaches we express the photon number as a deviation from the (large) mean number $\bar{n}$ and write [91]

$$\Psi(t) = \Sigma_{m=-\infty}^{\infty} C_{a,\bar{n},m}(t)\psi_a(t)\phi_{\bar{n}+m}. \tag{652}$$

The counterpart of the Floquet state having harmonic $m = 0$ is the photon state having mean photon number $\bar{n}$; other harmonics are deviations from this mean. The Rabi frequency becomes $\Omega_m = \sqrt{\bar{n} + |m|}\;\Omega_1$. In the limit of large photon number there is little difference between successive blocks of the JCM Hamiltonian, other than the diagonal elements, and both approaches deal with the same equations.

[91] The infinite summation limits merely indicate large positive and negative values of m. In practice, relatively few values of m are needed.

L.3 Floquet's theorem

Sets of coupled ordinary differential equations with exaclty periodic coefficients, of which the two-state Schrödinger equation offers a special example, have properties described by what is sometimes termed *Floquet theory*[94], commemorating *Floquet's theorem*, which asserts that quasiperiodic solutions exist. More specifically, consider a set of N ordinary differential equations involving a vector of unknowns $\mathbf{Y}(t)$, that satisfy the differential equation

$$\frac{d}{dt}\mathbf{Y}(t) = -\mathrm{i}\mathsf{M}(t)\mathbf{Y}(t). \tag{653}$$

When the $N \times N$ matrix $\mathsf{M}(t)$ is periodic, with period $\tau \equiv 2\pi/\omega$, then Floquet's theorem asserts that a vector of solutions $\mathbf{Y}(t)$ can be found with the form

$$\mathbf{Y}(t) = \exp(-\mathrm{i}Zt)\mathbf{y}(t), \tag{654}$$

where the vector $\mathbf{y}(t)$ is periodic, with period τ. This latter periodicity means that $\mathbf{y}(t)$ is expressible as a Fourier series:

$$\mathbf{y}(t) = \Sigma_{m=-\infty}^{\infty}\mathbf{v}(m)\exp(\mathrm{i}m\omega t). \tag{655}$$

Here $\mathbf{v}(m)$ and $\mathbf{y}(t)$, like the original unknown $\mathbf{Y}(t)$, are N-component vectors. Note that although $\mathbf{y}(t)$ is periodic, the construct $\mathbf{Y}(t)$ is instead *quasiperiodic*: the absolute square of $\mathbf{Y}(t)$ is periodic.

The exponent Z is termed variously the *Floquet exponent* or the *quasienergy*. There are as many of these, and as many possible solutions of the form (654), as there are dimensions of the original Hamiltonian, i.e. the number of basis states N. Let us denote by Z_ν one of the N Floquet exponents, associated with a solution

$$\mathbf{Y}(\nu;t) = \exp(-\mathrm{i}Z_\nu t)\mathbf{y}(\nu;t), \tag{656}$$

where

$$\mathbf{y}(\nu;t) = \Sigma_{m=-\infty}^{\infty}\mathbf{v}(\nu,m)\exp(\mathrm{i}m\omega t). \tag{657}$$

The most general solution to eqn. (653) is a linear superposition of these vectors,

$$\mathbf{Y}(t) = \Sigma_\nu c_\nu \mathbf{Y}(\nu;t), \tag{658}$$

with the constants c_ν chosen such that $\mathbf{Y}(t)$ satisfies the required initial conditions, say at $t = 0$: they are solutions to the set of equations

$$\Sigma_\nu c_\nu \mathbf{Y}(\nu;0) = \mathbf{Y}(0). \tag{659}$$

L.4 Two-state Floquet solutions.

From Floquet's theorem we conclude that, for a periodic Hamiltonian, we can write the state vector $\Psi(t)$ in the form

$$\Psi(t) = \Sigma_{\nu=1}^{N}\exp(-\mathrm{i}Z_\nu t)\Sigma_{n=1}^{N}\Sigma_{m=-\infty}^{\infty}c_n(\nu,m)\exp(\mathrm{i}m\omega t)\,\psi_n. \tag{660}$$

For two-state excitation this expression becomes

$$\Psi(t) = c_1(t)\psi_1 + c_2(t)\psi_2, \tag{661}$$

with

$$\begin{aligned} c_1(t) &= \exp(-\mathrm{i}Z_1 t)\Sigma^{\infty}_{even\ n=-\infty} a_n \exp(\mathrm{i}n\omega t), \\ &\quad + \exp(-\mathrm{i}Z_2 t)\Sigma^{\infty}_{odd\ m=-\infty} a_m \exp(\mathrm{i}m\omega t), \end{aligned} \tag{662}$$

$$\begin{aligned} c_2(t) &= \exp(-\mathrm{i}Z_1 t)\Sigma^{\infty}_{odd\ m=-\infty} b_m \exp(\mathrm{i}m\omega t) \\ &\quad + \exp(-\mathrm{i}Z_2 t)\Sigma^{\infty}_{even\ n=-\infty} b_n \exp(\mathrm{i}n\omega t). \end{aligned} \tag{663}$$

When the Hamiltonian is exactly periodic the real-valued exponents Z_1 and Z_2 and the complex-valued amplitudes a_m and b_m are independent of time. These constructions generalizes the RWA expression for $\Psi(t)$. That RWA expression, when written in terms of dressed states $\Phi_{\pm}(t)$, reads

$$\Psi(t) = c_+\Phi_+(t) + c_-\Phi_-(t). \tag{664}$$

Each dressed state has a simple exponential time dependence, through a factor $\exp(-\mathrm{i}Z_{\pm}t)$. In the RWA the formulas read

$$c_1(t) = \exp(-\mathrm{i}Z_+ t)a_0 + \exp(-\mathrm{i}Z_- t)a_1, \tag{665}$$

$$c_2(t) = \exp(-\mathrm{i}Z_+ t)b_1 + \exp(-\mathrm{i}Z_- t)b_0. \tag{666}$$

In the RWA each basis state ψ_n is accompanied by two frequency components, at the eigenvalues Z_+ and Z_- of the 2×2 RWA Hamiltonian matrix. In the more general expression of Eqn. (660) these two eigenvalues become two Floquet exponents Z_1 and Z_2; the values $Z_{\pm}$ are approximations to these. Furthermore, each of the characteristic frequencies Z_1 and Z_2 of the more general expression has an infinite set of associated frequencies $Z_n + m\omega$ differing by integer multiples of the frequency ω: the set of Floquet exponents form a pair of infinite sequences.

Equation (660) presents the general form of a solution to the problem of a two-state atom subject to a periodic off-diagonal interaction. There remains the problem of determining the Floquet exponents Z_1 and Z_2 and the various constant coefficients a_m and b_m, for a given set of parameters that define the Hamiltonian. For the two-state atom these are the Bohr frequency, the field carrier frequency and the Rabi frequency.

L.5 The two-state Floquet exponents; Quasienergies.

To determine the Floquet exponents we return to expansion (633), but this time we place the time dependence of the expansion coefficients entirely into exponentiated phases $\zeta_{a,m}(t)$ by writing, in place of expansion (633), the sum

$$\Psi(t) = \Sigma_a \Sigma_m \psi_a \exp(\mathrm{i}m\omega t) c_{a,m} \exp\left[-i\zeta_{a,m}(t)\right]. \tag{667}$$

The ground-state amplitudes $a_m = c_{1m}$ and excited-state amplitudes $b_m = c_{2,m}$ are now required to be constants. This can be accomplished by taking the phases $\zeta_n(t)$ to be

$$\hbar\zeta_{1,m}(t) = \hbar\zeta_{2,m\pm1}(t) = \begin{cases} (E_1 + \hbar Z)t & \text{for } m \text{ even} \\ (E_1 + \hbar Z)t & \text{for } m \text{ odd.} \end{cases} \tag{668}$$

This approach gives, in place of the differential equations (644) - (645), the set of algebraic equations

$$0 = [m\omega - Z]\, a_m + \tfrac{1}{2}\Omega\,[b_{m-1} + b_{m+1}]\,, \tag{669}$$

$$0 = [\omega_0 + (m+1)\omega - Z]\, b_{m+1} + \tfrac{1}{2}\Omega\,[a_m + a_{m+2}]\,. \tag{670}$$

These homogeneous equations have solutions only for selected values of Z, namely those which produce a null value for the determinant of the coefficients of the unknowns a_m and b_m. We may regard these equations as an eigenvalue equation for the Floquet Hamiltonian, i.e., the infinite matrix implied by Eqns. (668). Thus the Floquet exponents Z_ν are the eigenvalues of the Floquet Hamiltonian.

These equations make no assumption about the excitation frequency ω. It need not be close to resonance and it need not be much larger than the Rabi frequency. The equations as written are, of course, restricted to a two-state atom and to a single-frequency field, but even so they have no simple closed-form analytic solutions.

L.6 Adiabatic Floquet theory

Just as the slowly varying RWA Hamiltonian has slowly varying adiabatic states that can be used to describe the statevector, so too does a slowly varying Floquet Hamiltonian lead to slowly varying generalizations of the basic Floquet states. These, and the Floquet exponents, become slowly varying functions of time. Several papers describe the use of such states [95].

During adiabatic evolution the statevector remains aligned with a fixed superpositiion of these, perhaps with a single one. Just as we identify two-state behavior from plots of the two simple adiabatic energies, so too can we use plots of the more general Floquet eigenvalues for this purpose. Instead of dealing with two curves, one for each of the two adiabatic energies, we have an infinite replication of pairs of curves, each set being offset by frequency ω. To understand the dynamics we consider a system point as it follows one of these curves through possible crossings with other curves.

M Dark states: the Morris-Shore transformation

Under specific conditions it is possible to replace an interaction pattern comprising multiple linkages with a set of independent two-state interactions. The necessary conditions are

I. Two sets of states,

   Set A (ground), with N_A elements.

   Set B (excited), with N_B elements.

II. There are no couplings within A set or B set, only couplings between A and B. [92]

III. The sets share common diagonal elements. In the RWA these are detunings Δ_A and Δ_B.

[92] The graph corresponding to this linkage pattern is therefore bipartite.

The RWA Hamiltonian therefore has the structure

$$\mathsf{W} = \begin{bmatrix} \Delta_A \mathbf{1}_A & \mathsf{V} \\ \mathsf{V}^\dagger & \Delta_B \mathbf{1}_B \end{bmatrix} \begin{matrix} A \\ B \end{matrix} \tag{671}$$

where $\mathbf{1}_A$ and $\mathbf{1}_B$ are unit matrices, of dimension N_A and N_B respectively, and V is a rectangular matrix, of dimension $N_A \times N_B$.

Given this Hamiltonian, we introduce a Hilbert-space transformation

$$\widetilde{C}_j(t) = \Sigma_j U_{jn} C_n(t), \tag{672}$$

such that the resulting equation of motion,

$$\frac{d}{dt}\widetilde{\mathbf{C}}(t) = -\mathrm{i}\widetilde{\mathsf{W}}(t)\widetilde{\mathbf{C}}(t), \tag{673}$$

involves a Hamiltonian that has the structure of uncoupled 2×2 blocks together with a unit matrix $\mathbf{1}_S$ of dimension $N_S = |N_A - N_B|$,

$$\widetilde{\mathsf{W}} = \begin{bmatrix} \mathsf{w}^{(1)} & \mathbf{0} & \mathbf{0} & \cdots & \mathbf{0} \\ \mathbf{0} & \mathsf{w}^{(2)} & \mathbf{0} & \cdots & \mathbf{0} \\ \mathbf{0} & \mathbf{0} & \mathsf{w}^{(3)} & \ddots & \mathbf{0} \\ \vdots & \vdots & \vdots & \ddots & \mathbf{0} \\ \mathbf{0} & \mathbf{0} & \mathbf{0} & \mathbf{0} & \Delta\, \mathbf{1}_S \end{bmatrix}, \tag{674}$$

where the individual $2\times$blocks have the form

$$\mathsf{w}^{(j)} = \begin{bmatrix} \Delta_A & \frac{1}{2}\bar{\Omega}^{(j)} \\ \frac{1}{2}\bar{\Omega}^{(j)} & \Delta_B \end{bmatrix} \tag{675}$$

and Δ is the detuning associated with the larger set of states. The result of this *Morris-Shore* (MS) transformation is a set of independent 2-state systems plus N_S uncoupled spectator states. The number of coupled pairs of states is $N_<$, the lesser of the two dimensions N_A and N_B. Of each pair, one state (a *bright* state) comprises a superposition of states from set A. The other set comprises a superposition of states from set B (excited states). Figure 81 shows the results of the MS transformation.

The transformation to block-diagonal form $\widetilde{\mathsf{W}} = \mathsf{U}\mathsf{W}\mathsf{U}^\dagger$ is by means of a transformation matrix

$$\mathsf{U} = \mathsf{G}\begin{bmatrix} \mathsf{A} & 0 \\ 0 & \mathsf{B} \end{bmatrix}\mathsf{G}^{-1} \qquad \text{where} \qquad \begin{matrix} \mathsf{A} = \text{ acts on } A \text{ states (ground)} \\ \mathsf{B} = \text{ acts on } B \text{ states (excited)} \\ \mathsf{G} = \text{ permutation matrix} \end{matrix} \tag{676}$$

The transformation matrices A and B are defined such that they diagonalize the square matrices $\mathsf{V}\mathsf{V}^\dagger$ and $\mathsf{V}^\dagger\mathsf{V}$, respectively

$$\mathsf{A}\mathsf{V}\mathsf{V}^\dagger\mathsf{A}^\dagger = \text{diagonal}, \qquad \mathsf{B}^\dagger\mathsf{V}^\dagger\mathsf{V}\mathsf{B} = \text{diagonal}.$$

The elements of these matrices are the squares of the rabi frequencies $\Omega^{(j)}$. The signs of eigenvalues are obtained only by evaluating $\mathsf{U}\mathsf{W}\mathsf{U}^\dagger$.

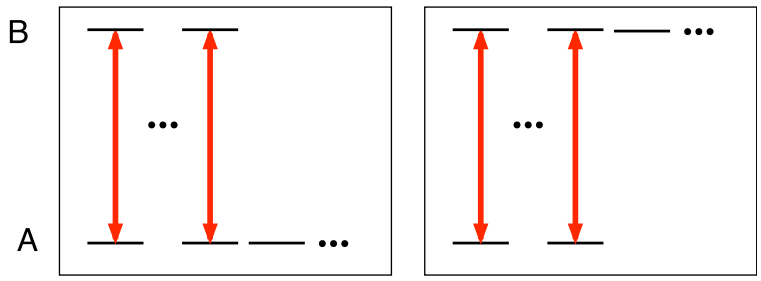

Fig. 81. Results of the MS transformation. Left: More lower states, $N_B < N_A$; Have $N_A - N_B$ dark states. Right: More upper states, $N_B < N_A$; Have $N_B - N_A$ spectator states

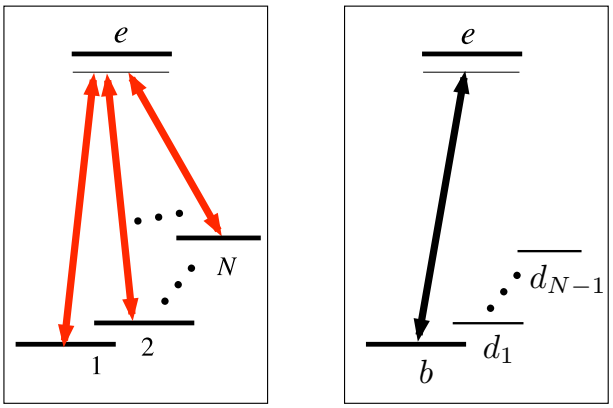

Fig. 82. Equivalent linkages, for a general fan-type linkage pattern. There is one bright state, $N-1$ dark states and one excited state.

The simplest example of a MS transformation occurs with the three-state system. There is one uncoupled state after the MS transformation; it may either be a dark state (if it is in the set that includes the initial state, so that the linkage has the lambda pattern) or a spectator state (as happens when the initial state is the center of the chain, so the linkage forms a vee pattern). A generalization of this occurs when the A set comprises several states, all linked to a single excited state, in a "fan" pattern. The four-state tripod is an example of this. Figure 82 illustrates an N-state generalization: there is a single bright state and $N-1$ dark states.

The MS transformation allows simplification of resonant excitation of any degenerate two-level angular momentum system, by elliptically polarized light for a laser beam oriented at an arbitrary angle to the quantization axis. Such a system has a linkage pattern similar to that shown in Fig. 73(a). The MS transformation simplifies this linkage into $2J_< + 1$ Independent two-state links, as would occur if the excitation had been linearly polarized along the quantization axis; see Fig. 73(b).

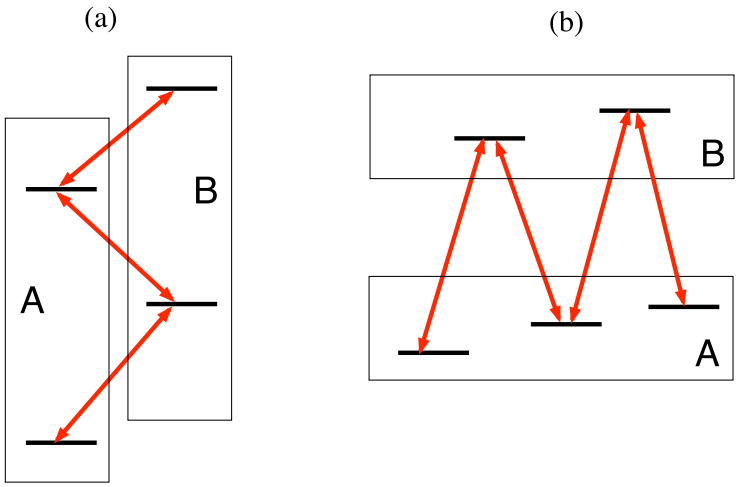

Fig. 83. Examples of chains amenable to Morris-Shore transformation

Numerous other situations allow application of a MS transformation. Figure 83 shows some examples of chain-linkage patterns that are amenable to a MS transformation.

One of the generalizations of the MS transformation makes possible, under certain conditions, a reduction in which the final result includes not only independent single- and two-state blocks of the transformed Hamiltonian, but also three-state blocks: both two-state and three-state excitation chains arise from the set of transformed A states. The conditions for such restructuring have been discussed by Rangelov et al. (2006) [125].

The restructuring of the Hamiltonian discussed here has wider application, whenever one encounters a set of ordinary differential equations in the form

$$\frac{d}{dx}\mathbf{C}(x) = \mathsf{M}\mathbf{C}(x) \tag{677}$$

for variables $C_n(x)$. When the matrix M has the appropriate structure, the Morris-Shore transformation can then reduce the number of variables for which solutions are required, by introducing "dark" combinations that remain fixed. When x denotes time, the dark superpositions represent constants of the motion. Such is the case in treatments of dark-state polaritons [177].

References

[1] **Quantum optics**

P. L. Knight, "Quantum Optics" in *The New Physics*, ed. P. Davies (Cambridge Univ. Press, Cambridge, 1989)

M. O. Scully and M. S. Zubairy, *Quantum Optics*, (Cambridge, Cambridge, U.K., 1997)

P. Meystre and M. Sargent, III, *Elements of Quantum Optics*, (Springer-Verlag, New York, 1999)

T. W. Hänsch and H. Walther, "Laser spectroscopy and quantum optics" Rev. Mod. Phys. **71**, S242 - S252 (1999)

W. P. Schleich, *Quantum Optics in Phase Space*, (Wiley-VCH, Weinheim, 2001)

R. R. Puri, *Mathematical Methods of Quantum Optics*, (Springer, New York, 2001)

V. Vedral, *Modern Foundations of Quantum Optics*, (World Scientific, Singapore, 2001)

S. Barnett, N, and P. M. Radmore, *Methods in Quantum Optics*, (Oxford Univ. Press, Oxford, 2002)

C. Gerry and P. Knight, *Introductory Quantum Optics*, (Cambridge Univ. Press, Cambridge, 2004)

M. Fox, *Quantum Optics: An Introduction*, (Oxford University Press, New York, 2006)

S. Haroche and J.-M. Raimond, *Exploring the Quantum. Atoms, Cavities and Photons*, (Oxford U. Press, New York, 2006)

P. Lambropoulos and D. Petrosyan, *Quantum Optics and Quantum Information: An Introduction*, (Springer, New York, 2006)

F. DellAnno, S. D. Siena and F. Illuminati, "Multiphoton quantum optics and quantum state engineering" Phys. Rep. **428**, 53-168 (2006)

D. F. Walls and G. Milburn, J., *Quantum Optics*, (Springer-Verlag, Berlin, 2007)

[2] **Coherent excitation: Shore book**

B. W. Shore, *The Theory of Coherent Atomic Excitation*, (Wiley, N.Y., 1990)

[3] **Coherent excitation reviews**

N. V. Vitanov, T. Halfmann, B. W. Shore and K. Bergmann, "Laser-induced population transfer by adiabatic passage techniques" Ann. Rev. Phys. Chem. **52**, 763-809 (2001)

N. V. Vitanov, M. Fleischhauer, B. W. Shore and K. Bergmann, "Coherent manipulation of atoms and molecules by sequential laser pulses" Adv. Atomic Mol. Opt. Phys. **46** 55-190 (2001)

B. W. Shore, "Coherent manipulation of atomic excitation" Bulgarian J. Phys. **33**, 052-70 (2006)

[4] **Coherent excitation**

T. Brandes, "Coherent and collective quantum optical effects in mesoscopic systems" Phys. Rep. **408**, 315-474 (2005)

D. J. Tannor, *Introduction to Quantum Mechanics: A Time Dependent Perspective*, (University Science Books, Sausalito, CA, 2005)

V. Letokhov, *Laser Control of Atoms and Molecules*, (Oxford U. Press, New York, 2007)

[5] **Trace element analysis**

Z.-T. Lu and K. D. A. Wendt, "Laser-based methods for ultrasensitive trace-isotope analyses" Rev. Sci. Instrum. **74**, 1169-1179 (2003)

B. W. Shore, "Coherence and transient nonlinearity in laser probing" Spect. Chim, Acta B **58**, 969-998 (2003)

A. Lindinger, C. Lupulescu, M. Plewicki, F. Vetter, A. Merli, S. M. Weber, L. Wöste, "Isotope selective ionization by optimal control using shaped femtosecond laser pulses" Phys. Rev. Lett. **93**, 033001 (2004)

[6] **Coherent control** see also [7]

A. Assion, T. Baumert, J. Helbing, V. Seyfried and G. Gerber, "Coherent control by a single phase shaped femtosecond laser pulse" Chem. Phys. Lett. **259**, 488-494 (1996)

R. J. Gordon and S. A. Rice, "Active control of the dynamics of atoms and molecules" Ann. Rev. Phys. Chem. **48**, 601-641 (1997)

R. J. Gordon, L. C. Zhu and T. Seideman, "Coherent control of chemical reactions" Accounts Chem. Res. **32**, 1007-1016 (1999)

T. C. Weinacht, J. Ahn and P. H. Bucksbaum, "Controlling the shape of a quantum wavefunction" Nature **397**, 233-5 (1999)

H. Rabitz and W. S. Zhu, "Optimal control of molecular motion: Design, implementation, and inversion" Accounts Chem. Res. **33**, 572-578 (2000)

S. A. Rice and M. Zhao, *Optical Control of Molecular Dynamics*, (Wiley, New York, 2000)

T. Brixner, N. H. Damrauer and G. Gerber, "Femtosecond quantum control" Adv. Atomic, Mol. Opt. Phys. **46**, 1-54 (2001)

H. Rabitz, "Optimal control of quantum systems: Origins of inherent robustness to control field fluctuations" Phys. Rev. A **66**, 063405 (2002)

M. Shapiro and P. Brumer, "Coherent control of molecular dynamics" Repts. Prog. Phys. **66**, 859-942 (2003)

M. Shapiro and P. Brumer, *Principles of the Quantum Control of Molecular Processes*, (Wiley, New York, 2003)

M. Shapiro and P. Brumer, "Quantum control of bound and continuum state dynamics" Phys. Repts. **425**, 195-264 (2006)

[7] **Chemical reactions and laser radiation** see also [6]

D. J. Tannor and S. A. Rice, "Coherent pulse sequence control of product formation in chemical reactions" Adv. Chem. Phys. **70**, 441-524 (1988)

R. J. Gordon and S. A. Rice, "Active control of the dynamics of atoms and molecules" Ann. Rev. Phys. Chem. **48**, 601-641 (1997)

H. Rabitz, R. d. Vivie-Riedle, M. Motzkus and K. Kompa, "Whither the future of controlling quantum phenomena?." Science **288**, 824-828 (2000)

M. Dantus, "Coherent nonlinear spectroscopy: From femtosecond dynamics to control" Ann. Rev. Phys. Chem.. **52**, 639-679 (2001)

H. Rabitz, "Shaped laser pulses as reagents" Science **299**, 525 - 527 (2003)

P. Nuernberger, G. Vogt, T. Brixner and G. Gerber, "Femtosecond quantum control of molecular dynamics in the condensed phase" Phys. Chem. Chem. Phys. **9**, 2470 (2007)

[8] **Molecular alignment produced by laser pulses**

H.-G. Rubahn, E. Konz, S. Schiemann and K. Bergmann, "Alignment of electronic angular momentum by stimulated Raman scattering with delayed pulses" Z. Phys. D **22**, 401-06 (1991)

Y. Band and P. S. Julienne, "Complete alignment and orientation of atoms and molecules by stimulated Raman scattering with temporally shifted lasers" J. Chem. Phys. **96**, 3339-41 (1992)

M. Auzinsh and R. Ferber, ed. *Optical Polarization of Molecules*, (Cambridge Univ. Press, Cambridge, 1995)

S. Guérin, L. P. Yatsenko, H. R. Jauslin, O. Faucher and B. Lavorel, "Orientation of polar molecules by laser induced adiabatic passage" Phys. Rev. Lett. **88**, 233601 (2002)

H. Stapelfeldt and T. Seideman, "Colloquium: Aligning molecules with strong laser pulses" Rev. Mod. Phys. **75**, 543 (2003)

A. S. Meijer, Y. Zhang, D. H. Parker, W. J. v. d. Zande, A. Gijsbertsen and M. J. J. Vrakking, "Controlling rotational state distributions using two-pulse stimulated Raman excitation" Phys. Rev. A **76**, 023411 (2007)

V. Kumarappan, S. S. Viftrup, L. Holmegaard, C. Z. Bisgaard and H. Stapelfeldt, "Aligning molecules with long or short laser pulses" Phys. Scr. **76**, C63-C68 (2007)

[9] **Quantum information**

A. Ekert and R. Josza, "Shor's quantum algorithm for factorizing numbers" Rev. Mod. Phys. **68**, 733-753 (1996)

A. Barenco, "Quantum physics and computers" Contemp. Phys. **37**, 375 (1996)

C. P. Williams and S. H. Clearwater, *Explorations in Quantum Computing*, (Springer, Berlin, 1997)

J. Preskill, "Lecture notes for Physics 229: Quantum Information and Computation," available on-line at http://www.theory.caltech.edu/people/preskill/ph229/ (1998)

D. Bouwmeester, A. K. Ekert and A. Zeilinger, ed. *The Physics of Quantum Information: Quantum Cryptography, Quantum Teleportation, Quantum Computation*, (Springer, Berlin, 2000)

M. A. Nielsen and I. L. Chuang, *Quantum Computation and Quantum Information*, (Cambridge U. Press, New York, 2000)

G. Leuchs and T. Beth, *Quantum Information Technology*, (Wiley, New York, 2003)

P. Zoller, T. Beth, D. Binosi, R. Blatt, H. Briege, D. Bruss, T. Calarco, J. I. Cirac, D. Deutsch, J. Eisert, A. Ekert, C. Fabre, N. Gisin, P. Grangiere, M. Grassl, S. Haroche, A. Imamoglu, A. Karlson, J. Kempe, L. Kouwenhoven, S. Krll, G. Leuchs, M. Lewenstein, D. Loss, N. Ltkenhaus, S. Massar, J. E. Mooij, M. B. Plenio, E. Polzik, S. Popescu, G. Rempe, A. Sergienko, D. Suter, J. Twamley, G. Wendin, R. Werner, A. Winter, J. Wrachtrup and A. Zeilinger, "Quantum information processing and communication. Strategic report on current status, visions and goals for research in Europe" Eur. Phys. J. D **36**, 203-228 (2005)

V. Vedral, *Introduction to Quantum Information*, (Oxford U. Press, New York, 2006)

W. P. Schleich and H. Walther, ed. *Elements of Quantum Information*, (Wiley-VCH, Weinheim, 2007)

[10] **Two-level atoms: Allen & Eberly**

L. Allen and J. H. Eberly, *Optical Resonance and Two-Level Atoms*, (Wiley, New York, 1975)

[11] **Laser operation**

A. E. Siegman, *Lasers*, (University Science Books, Mill Valley, Calif., 1986)

P. W. Milonni and J. H. Eberly, *Lasers*, (Wiley, N.Y., 1988)

[12] **Kinetic theory of gases**

A. Einstein, "On the movement of small particles suspended in a stationary liquid demanded by the molecular-kinetic theory of heat" Ann. Physik **17**, 549-560 (1905)

E. H. Kennard, *Kinetic Theory of Gases*, (McGraw-Hill, N.Y., 1938)

J. Jeans, *The Dynamical Theory of Gases*, (Dover, N.Y., 1954)

[13] **Spectra and spectroscopy**

S. Walker and H. Straw, *Spectroscopy*, (Chapman & Hall, London, 1961)

W. R. Hindmarsh, *Atomic Spectra*, (Pergamon, London, 1967)

C. H. Townes and A. L. Schawlow, *Microwave Spectroscopy*, (Dover, New York, 1975)

A. C. Corney, *Atomic and Laser Spectroscopy*, (Clarendon, Oxford, 1977)

E. L. Grove, *Applied Atomic Spectroscopy*, (Plenum, N.Y., 1978)

J. I. Steinfeld, *Molecules and Radiation*, (MIT Press, Cambridge, Mass., 1985)

J. M. Hollas, *Modern Spectroscopy*, (Wiley, N.Y., 1987)

A. I. Burshtein and S. I. Temkin, *Spectroscopy of Molecular Rotation in Gases and Liquids*, (Cambridge University Press, Cambridge, 1994)

A. P. Thorne, U. Litzen and S. Johansson, *Spectrophysics: Principles and Applications*, (Springer, New York, 1999)

W. Demtröder, *Laser Spectroscopy . Basic Concepts and Instrumentation*, (Spriinger, Berlin, 2003)

[14] **Spectral line formation**

J. T. Jefferies, *Spectral Line Formation*, (Blaisdell, Waltham MA, 1968)

R. G. Athay, *Radiative Transfer in Spectral Lines*, (Reidel, Dordrecht, 1972)

J. Cooper, R. J. Ballagh, K. Burnett and D. G. Hummer, "On redistribution and the equations for radiative transfer" Ap. J. **260**, 299-316 (1982)

C. J. Cannon, *The Transfer of Spectral Line Radiation*, (Cambridge Univ. Press, N.Y., 1985)

[15] **Spectral line shapes**

H. V. Regemorter, "Spectral line broadening," in *Atoms and Molecules in Astrophysics*, ed. T. R. Carson and M. J. Roberts (Academic, N.Y., 1972)

A. Ben-Reuven, "Spectral line shapes in gases in the binary-collision approximation" Adv. Chem. Phys. **33**, 235-293 (1975)

R. G. Breene, *Theories of Spectral Line Shapes*, (Wiley, N.Y., 1981)

S. Mukamel, "Collisional broadening of spectral line shapes in two-photon and multiphoton processes" Phys. Rep. **93**, 1-60 (1982)

I. I. Sobel'man, L. A. Vainshtein and E. A. Yukov, *Excitation of Atoms and Broadening of Spectral Lines*, (Springer, N.Y., 1995)

V. I. Romanenko and L. P. Yatsenko, "Adiabatic population transfer in the three-level Lambda-system: Two-photon lineshape" Opt. Comm. **140**, 231-236 (1997)

W. Nörtershäuser, B. A. Bushaw, P. Müller and K. Wendt, "Line Shapes in Triple-Resonance Ionization Spectroscopy" Appl. Opt. **39**, 5590-5600 (2000)

[16] **The Lorentz electron**

H. A. Lorentz, *The Theory of Electrons*, (Dover, N.Y., 1952)

F. L. Friedman and L. Sartori, *The Classical Atom*, (Addison-Wesley, Reading, Mass., 1965)

K. F. Schaffner, "The Lorentz electron theory of relativity" Am. J. Phys. **37**, 498-513 (1969)

J. Z. Buchwald and A. Warwick, *Histories of the Electron: The Birth of Microphysics*, (MIT Press, Cambridge, MA, 2001)

[17] **0scillator strength**

D. R. Bates and A. Damgaard, "The calculation of the absolute strengths of spectral lines" Phil. Trans. Roy. Soc. Lond. A **242**, 101-122 (1949)

M. N. Lewis, *Oscillator Strength of Ionizing Transitions. Data Salculated in the Hydrogen-Lke Approximation.*, (U.S. National Bureau of Standards, Washington, D.C., 1953)

L. C. Green, P. P. Rush and D. D. Chandler, "Oscillator strengths and matrix elements for the electric dipole moment for hydrogen" Ap. J. Suppl. **3**, 37-50 (1957)

U. Fano and J. W. Cooper, "Spectral distribution of atomic oscillator strengths" Rev. Mod. Phys. **40**, 441 (1968)

H. C. Goldwire, Jr. , "Oscillator strengths for electric dipole transitions of hydrogen" Astrophys. J. Suppl. **17**, 445-465 (1968)

W. L. Wiese and A. W. Weiss, "Regularities in atomic oscillator strengths" Phys. Rev. **175**, 50 (1968)

D. Layzer and R. H. Garstang, "Theoretical atomic transition probabilities" Ann. Rev. Astron. Astrophys. **6**, 449-94 (1968)

D. H. Menzel, "Oscillator strengths, f, for high-level transitions in hydrogen" Astrophys. J. Suppl. **18**, 221-246 (1969)

C. M. Penney, "Light scattering in terms of oscillator strengths and refractive indices" J. Opt. Soc. Am. **59**, 34-42 (1969)

A. F. Starace, "Length and velocity fomulas in approximate oxcillator-strength calculations" Phys. Rev. A **3**, 1242-45 (1971)

M. W. Smith and W. L. Wiese, "Graphical presentations of systematic trends of atomic oscillator strengths along isoelectronic sequences and new oscillator strengths derived by interpolation" Ap. J. Supp. **23**, 103-192 (1971)

A. L. Stewart, " Atomic structure and oscillator strengths," in *Atomic Processes and Applications*, ed. (North-Holland, N.Y., 1976)

A. Merts and R. E. H. Clark, "Quantum defect methods applied to oscillator strengths" JQSRT **38**, 287-293 (1987)

[18] **Laser isotope separation**

C. B. Moore, "Application of lasers to isotope separation" Accounts Chem. Res. **6**, 1 (1973)

N. V. Karlov and A. M. Prokhorov, "Laser isotope separation" Sov. Phys. Usp. **19**, 285-300 (1976)

V. S. Letokhov, "Principles of laser isotope separation," in *Frontiers in Laser Spectroscopy*, ed. R. Baliean, S. Haroche and S. Liberman (North-Holland, Amsterdam, 1977)

N. V. Karlov, B. B. Krynetskii, V. A. Mishin and A. M. Prokhorov, "Laser isotope separation of rare earth elements" Appl. Opt. **17**, 856-862 (1978)

N. V. Karlov, B. B. Krynetskii, V. A. Mishin and A. M. Prokhorov, "Selective atomic photoionization and its use in isotope separation and spectroscopy" Sov. Phys. Usp. **22**, 220-234 (1979)

C. P. Robinson and R. J. Jensen, "Laser methods of isotope separation," in *Uranium Enrichment*, ed. S. Villari (Springer, Berlin, 1979)

V. S. Letokhov, "Laser isotope separation" Nature **277**, 605 - 610 (1979)

J. L. Emmett, W. F. Krupke and J. I. Davis, "Laser R & D at the Lawrence Livermore National Laboratory for fusion and isotope separation applications" IEEE J. Quant. Elec. **QE-20**, 591-602 (1984)

J. A. Paisner, "Atomic vapor laser isotope separation" App. Phys. B **46**, 253-260 (1988)

P. T. Greenland, "Laser isotope separation" Contemp. Phys. **31**, 405 - 424 (1990)

O. Atabek, M. Chrysos and R. Lefebvre, "Isotope separation using intense laser fields" Phys. Rev. A **49**, R8-R11 (1994)

A. Lindinger, A. Merli, M. Plewicki, F. Vetter, S. M. Weber, L. Wöste, "Optimal control of isotope selective fragmentation" Chem.Phys. Lett. **413**, 315-320 (2005)

[19] **Lasers in analytic chemistry**

A. Mottana and F. Burragato., ed. *Absorption Spectroscopy in Mineralogy*, (Elsevier, Amsterdam, 1990)

G. Gauglitz and T. Vo-Dinh., ed. *Handbook of Spectroscopy*, (Wiley-VCH, Weinheim 2003)

S. Svanberg, *Atomic and Molecular Spectroscopy: Basic Aspects and Practical Applications*, (Springer-Verlag, Berlin, 2004)

J. R. Lakowicz, *Principles of Fluorescence Spectroscopy*, (Springer, New York, 2006)

[20] **Lasers for forensics**

M. M. Mossaba, *Spectral Methods in Food Analysis: Instrumentation and Applications*, (Marcel Dekker, New York, 1999)

[21] **Lasers in archeology**

H. G. M. Edwards and J. M. Chalmers, ed. *Raman Spectroscopy in Archaeology and Art History*, (Springer, New York, 2005)

[22] **Lasers in industry**

J. M. Chalmers, ed. *Spectroscopy in Process Analysis*, (CRC Press Boca Raton, FL 2000)

I. R. Lewis and H. G. M. Edwards, ed. *Handbook of Raman Spectroscopy. From the Research Laboratory to the Process Line*, (Marcel Dekker, New York, 2001)

K. A. Bakeev, ed. *Process Analytical Technology: Spectroscopic Tools and Implementation Strategies for the Chemical and Pharmaceutical Industries*, (Blackwell, Ames, Iowa, 2005)

[23] **Lasers for environmental monitoring**

C. Elachi, *Introduction to the Physics and Techniques of Remote Sensing*, (Wiley-Interscience, New York, 1987)

M. W. Sigrist, ed. *Air Monitoring by Spectroscopic Techniques*, (Wiley, New York, 1994)

R. J. H. Clark and R. E. Hester, ed. *Spectroscopy in Environmental Science*, (Wiley, New York, 1995)

R. S. Muttiah, ed. *From Laboratory Spectroscopy to Remotely Sensed Spectra of Terrestrial Ecosystems*, (Kluwer, Dordrecht, 2002)

[24] **Astrophysical spectroscopy** see also [63]

A. Dalgarno and D. Layzer, ed. *Spectroscopy of Astrophysical Plasmas*, (Cambridge Univ., N.Y., 1987)

A. V. Filippenko, "Optical spectra of supernovae" Ann. Rev. Astron. Astrophys. **35**, 309-355 (1997)

K. Robinson, *Spectroscopy: The Key to the Stars: Reading the Lines in Stellar Spectra*, (Springer Verlag, London, 2007)

[25] **Xray spectroscopy**

B. K. Agarwal, *X-ray Spectroscopy: An Introduction*, (Springer, Berlin, 1991)

R. Jenkins, R. W. Gould and D. Gedcke., ed. *Quantitative X-ray Spectrometry*, (M. Dekker, New York, 1995)

A. T. Ellis, P. J. Potts, M. Holmes, G. J. Oliver, C. Streli and P. Wobrauschek, "Atomic spectrometry update - x-ray fluorescence spectrometry" J. Analyt. At. Spectrometry **12**, R 461-R 490 (1997)

[26] **Nuclear magnetic resonance (NMR)**

C. P. Slichter, *Principles of Magnetic Resonance*, (Springer, Berlin, 1990)

H. Günther, *NMR Spectroscopy: Basic Principles, Concepts, and Applications in Chemistry*, (Wiley, Ne York, 1995)

E. D. Becker, *High Resolution NMR. Theory and Chemical Applications*, (Academic Press, San Diego, 2000)

J. H. Nelson, *Nuclear Magnetic Resonance Spectroscopy*, (Prentice Hall, Upper Saddle River, NJ, 2003)

B. Blümich, *Essential NMR for Scientists and Engineers*, (Springer Berlin 2005)

N. E. Jacobsen, *NMR Spectroscopy Explained: Simplified Theory, Applications and Examples for Organic Chemistry and Structural Biology*, (Wiley-Interscience, Hoboken, N.J. , 2007)

T. N. Mitchell and B. Costisella., *NMR–From Spectra to Structures: An Experimental Approach*, (Springer, Berlin, 2007)

[27] **Coherent light**

R. J. Glauber, "The quantum theory of optical coherence" Phys. Rev. **130**, 2529-2539 (1963)

L. Mandel and E. Wolf, "Coherence properties of optical fields" Rev. Mod. Phys. **37**, 231-287 (1965)

E. Wolf, "Coherence and radiometry" J. Opt. Soc. Am. **68**, 6-17 (1978)

L. Mandel and E. Wolf, *Optical Coherence and Quantum Optics*, (Cambridge University Press Cambridge, 1995)

[28] **Selectivity improved by coherence**

. P. Conde, L. Brandt and T. Halfmann, "Trace isotope detection enhanced by coherent elimination of power broadening" Phys. Rev. Lett. **97**, 243004 (2006)

[29] **Cavity quantum electrodynamics (cavity QED)** see also [39]

S. Haroche and D. Kleppner, "Cavity QED" Physics Today **42**, 24 (1989)

E. A. Hinds, "Cavity quantum electrodynamics," Adv. At. Mol. Opt. Phys. **28** 237 (1991)

P. Meystre, "Cavity QED," in *Nonlinear Optics in Solids*, ed. O. Keller (Springer-Verlag, Heidelberg, 1990), pp. 26-35

M. J. Shaw and B. W. Shore, "Coherent atomic excitation in a cavity .1. Low density" J. Mod. Opt. **37**, 937-963 (1990)

V. Buzek, G. Drobny, M. S. Kim, G. Adam and P. L. Knight, "Cavity QED with cold trapped ions" Phys. Rev. A **56**, 2352-60 (1997)

S. Haroche and J.-M. Raimond, *Exploring the Quantum. Atoms, Cavities and Photons*, (Oxford U. Press, New York, 2006)

[30] **Atomic and molecular structure**

G. Herzberg, *Molecular Spectra and Molecular Structure I. Spectra of Diatomic Molecules*, (Van Nostrand, N.Y., 1950)

E. U. Condon and G. H. Shortley, *The Theory of Atomic Spectra*, (Cambridge Univ. Press, Cambridge, 1953)

J. C. Slater, *Quantum Theory of Atomic Structure*, (McGraw-Hill, N.Y., 1960)

I. I. Sobel'man, *Introduction to the Theory of Atomic Spectra*, (Pergamon, N.Y., 1972)

W. G. Richards and P. R. Scott, *Structure and Spectra of Atoms*, (Wiley, N.Y., 1976)

I. I. Sobel'man, *Atomic Spectra and Radiative Transitions*, (Springer, Berlin, 1979)

E. U. Condon and H. Odabasi, *Atomic Structure*, (Cambridge Univ. Press, N.Y., 1980)

H. C. Longuet-Higgins, *Molecular Physics*, (Taylor & Francis, London, 1980)

R. D. Cowan, *The Theory of Atomic Structure and Spectra*, (Univ. California Press, Berkeley, 1981)

D. Papousek and M. R. Aliev, *Molecular Vibrational-Rotational Spectra* , (Elsevier, Amsterdam, 1982)

L. Szaz, *The Electronic Structure of Atoms*, (Wiley, New York, 1992)

V. P. Shevelko, *Atoms and Their Spectroscopic Properties*, (Springer, New York, 1997)

Z. Rudzikas, *Theoretical Atomic Spectroscopy*, (University Press, Cambridte, 1997)

B. H. Bransden and C. J. Joachain, *Physics of Atoms and Molecules*, (Longmans, London, 2003) 2nd ed.

D. Budker, D. Kimball and D. DeMille, *Atomic Physics: An Exploration through Problems and Solutions*, (Oxvord, N.Y., 2004)

C. E. Burkhardt and J. J. Leventhal, *Topics in Atomic Physics*, (Springer, New York, 2005)

W. Demtröder, *Molecular Physics: theoretical principles and experimental methods*, (Wiley-VCH, Weinheim, 2005)

W. Demtröder, *Atoms, Molecules, and Photons: An Introduction to Atomic-, Molecular-, and Quantum-Physics*, (Springer, Berlin, 2006)

G. W. F. Drake, ed. *Springer Handbook of Atomic, Molecular, and Optical Physics*, (Springer, New York, 2006)

H. S. Friedrich, *Theoretical Atomic Physics*, (Springer-Verlag, Berlin, 2006)

[31] **Quantum states** see also [34]

P. A. M. Dirac, *The Principles of Quantum Mechanics*, (Clarendon, Oxford, 1958)

K. Vogel, V. M. Akulin and W. P. Schleich, "Quantum state engineering of the radiation field" Phys. Rev. Lett. **71** 1816-1819 (1993)

U. Leonhardt, *Measuring the Quantum State of Light*, (Cambridge Univ. Press, Cambridge, 1997)

D. Vion, A. Aassime, A. Cottet, P. Joyez, H. Pothier, C. Urbina, D. Esteve and M. H. Devoret, "Manipulating the quantum state of an electrical circuit" Science **296**, 886-889 (2002)

R. G. Newton, "What is a state in quantum mechanics?" Am. J. Phys. **72**, 348-350 (2004)

L. F. Wei, Y.-X. Liu and F. Nori, "Engineering quantum pure states of a trapped cold ion beyond the Lamb-Dicke limit" Phys. Rev. A **70**, 063801 (2004)

[32] **Quantum dots**

D. Loss and D. P. DiVincenzo, "Quantum computation with quantum dots" Phys. Rev. A **57**, 120 (1998)

N. H. Bonadeo, J. Erland, D. Gammon, D. Park, D. S. Katzer and D. G. Steel, "Coherent optical control of the quantum state of a single quantum dot" Science **282**, 1473 - 1476 (1998)

A. Imamoglu, D. D. Awschalom, G. Burkard, D. P. DiVincenzo, D. Loss, M. Sherwin and A. Small, "Quantum information processing using quantum dot spins and cavity QED" Phys. Rev. Lett. **83**, 4204 (1999)

D. Bimberg, M. Grundmann and N. N. Ledentsov, *Quantum Dot Heterostructures*, (Wiley, New York, 1999)

T. H. Stievater, X. Li, D. G. Steel, D. Gammon, D. S. Katzer, D. Park, C. Piermarocchi and L. J. Sham, "Rabi oscillations of excitons in single quantum dots" Phys. Rev. Lett. **87**, 133603 (2001)

H. Kamada, H. Gotoh, J. Temmyo, T. Takagahara and H. Ando, "Exciton Rabi oscillation in a single quantum dot" Phys. Rev. Lett. **87**, 246401 (2001)

S. M. Reimann and M. Manninen, "Electronic structure of quantum dots" Rev. Mod. Phys. **74**, 1283 (2002)

[33] **Superconding devices**

D. V. Averin, "Adiabatic quantum computation with Cooper pairs," Solid State Comm. **105**, 659 (1998)

J. Clarke, A. N. Cleland, M. H. Devoret, D. Esteve and J. M. Martinis, "Quantum mechanics of a macroscopic variable: The phase difference of a Josephson junction," Science **239**, 992 (1998)

Y. Makhlin, G. Schön and A. Shnirman, "Quantum-state engineering with Josephson-junction devices" Rev. Mod. Phys. **73**, 357 - 400 (2001)

J. Q. You, J. S. Tsai and F. Nori, "Scalable quantum computing with Josephson junction qubits" Phys. Rev. Lett. **89**, 197902 (2002)

J. Q. You and F. Nori, "Superconducting circuits and quantum information" Physics Today **58**, 42-47 (2005)

L. F. Wei, J. R. Johansson, L. X. Cen, S. Ashhab and F. Nori, "Controllable coherent population transfers in superconducting qubits for quantum computing" Phys. Rev. Lett. **100**, 113601 (2008)

[34] **Quantum mechanics textbooks**

A. Messiah, *Quantum Mechanics*, (Wiley, N.Y., 1962)

L. I. Schiff, *Quantum Mechanics*, (McGraw-Hill, New York, 1968)

C. Cohen-Tannoudji, B. Diu and F. Lalo, *Quantum Mechanics*, (Wiley-Interscience, N.Y., 1977)

L. D. Landau and E. M. Lifshitz, *Quantum Mechanics (Non-Relativistic Theory)*, (Pergamon, N.Y., 1977)

W. Greiner and B. Mller, *Quantum Mechanics: Symmetries*, (Springer, New York, 1989)

[35] **Atomic structure calculations**

C. F. Fischer, "A general multi-configuration Hartree-Fock program" Comp. Phys. Comm. **14**, 145 (1978)

F. Herman and S. Skillman, *Atomic Structure Calculations*, (Prentice-Hall, Englewood Cliffs, N.J., 1963)

C. F. Fischer and W. Guo, "B splines for HF computations" J. Comp. Phys. **90**, 486 (1990)

C. F. Froese-Fischer, T. Brage and P. Jnsson, *Computational Atomic Structure: An MCHF Approach*, (Institute of Physics, Bristol, 1997)

H. F. Schaefer, III, *Quantum Chemistry: The Development of Ab Initio Methods in Molecular Electronic Structure Theory*, (Dover, Mineola, N.Y., 2004)

F. Jensen, *Introduction to Computational Chemistry*, 2nd ed. (Wiley, Hoboken, N.J., 2006)

D. A. McQuarrie, *Quantum Chemistry*, (University Science Books, Sausolito, CA, 2007)

W. R. Johnson, *Atomic Structure Theory: Lectures on Atomic Physics*, (Springer, Berlin, 2007)

I. P. Grant, *Relativistic Quantum Theory of Atoms and Molecules*, (Springer, New York, 2007)

R. J. Bartlett and M. Musia, "Coupled-cluster theory in quantum chemistry" Rev. Mod. Phys. 7 **9**, (2007)

I. N. Levine, *Quantum Chemistry*, (Prentice Hall, Upper Saddle River, NJ, 2008) 6th ed.

[36] **Atomic transition data**

C. H. Corliss, *Experimental Transition Probabilities for Spectral Lines of Seventy Eements Derived from the NBS Tables of Spectralline Intensities; The Wavelength*, (U.S. Govt. Print. Off. Washington, 1962)

W. L. Wiese, M. W. Smith and B. M. Glennon, *Atomic transition probabilities*, (Government Printing Office, Washington, DC, 1969)

W. F. Meggars, C. H. Corliss and B. Scribner, *Tables of Spectral-Line Intensities Part I - Arranged by Elements*, (National Bureau of Standards Washington, 1975)

[37] **Quantized field; Quantum electrodynamics (QED)** see also [39]

W. Heitler, *Quantum Theory of Radiation*, (Clarendon, Oxford, 1954)

J. M. Jauch and F. Rohrlich, *The Theory of Photons and Electrons*, (Addison-Wesley, Reading, Mass., 1955)

A. I. Akhiezer and V. B. Berestetskii, *Quantum Electrodynamics*, (Interscience, N.Y., 1965)

I. Bialynicki-Birula and Z. Bialynicka-Birula, *Quantum Electrodynamics*, (Pergamon, N.Y., 1975)

C. Cohen-Tannoudji, J. Dupont-Roc and G. Grynberg, *Atom-Photon Interactions. Basic Processes and Applications*, (Wiley, New York, 1992)

[38] **Photons** see also [29, 37]

R. Loudon, *The Quantum Theory of Light*, (Clarendon, Oxford, 1973)

E. Goldin, *Waves and Photons*, (Wiley, N.Y., 1982)

R. J. Cook, "Photon dynamics" Phys. Rev. **25**, 2164-67 (1982)

O. R. Frisch, "Take a photon reprinted," in *Concepts of Quantum Optics*, ed. P. L. Knight and L. Allen (Pergamon, N.Y., 1983)

J. Oxenius, *Kinetic Theory of Particles and Photons*, (Springer, N.Y., 1986)

I. Bialynicki-Birula, "Photon wave functions" Prog. Optics **36**, 245-294 (1996)

M. S. Kim, "Recent developments in photon-level operations on travelling light fields" J. Phys. B **41**, 133001 (2008)

[39] **The Jaynes-Cummings model** see also [141]

E. T. Jaynes and F. W. Cummings, "Comparison of quantum and semiclassical radiation theories with application to the beam maser" Proc. IEEE **51**, 89 (1963)

F. W. Cummings, "Stimulated emission of radiation in a single mode" Phys. Rev. **140**, A1051-56 (1965)

J. Gea-Banacloche, "A new look at the Jaynes-Cummings model for large fields: Bloch sphere evolution and detuning effects" Opt. Comm. **88**, 531-50 (1992)

B. W. Shore and P. L. Knight, "Topical Review. The Jaynes-Cummings model" J. Mod. Opt. **40**, 1195-1238 (1993)

[40] **Optics: Born & Wolf**

M. Born and E. Wolf, *Principles of Optics*, (Pergamon, N.Y., 1999) 7th ed.

[41] **Radiation pressure**

A. Ashkin, "Applications of laser radiation pressure" Science **210**, 1081-87 (1980)

V. G. Minogin and V. S. Letokhov, *Laser Light Pressure on Atoms*, (Gordon and Breach, N.Y., 1986)

[42] **Laser cooling and trapping** see also [47]

S. Stenholm, "The semiclassical theory of laser cooling" Rev. Mod. Phys. **58**, 699-740 (1986)

R. Blatt, W. Ertmer, P. Zoller and J. L. Hall, "Atomic-beam cooling: A simulation approach" Phys. Rev. A **34**, 3022-3033 (1986)

S. Chu and C. Wieman, ed. "Special issue on laser cooling and trapping of atoms" J. Opt. Soc. Am. B **6**, No. 11 (1989)

A. P. Kazantsev, G. I. Durdotovich and V. P. Yakovlev, *Mechanical Action of Light on Atoms*, (World Scientific, Singapore, 1990)

C. J. Foot, "Laser cooling and trapping of atoms" Contemp. Phys. **32**, 369-381 (1991)

C. Cohen-Tannoudji, "Laser cooling and trapping of neutral atoms - Theory" Phys. Rep. **219**, 153-164 (1992)

S. Chu, "Laser trapping of neutral particles" Sci. Am. **Feb.**, 71-76 (1992)

H. Metcalf and P. Vanderstraten, "Cooling and trapping of neutral atoms" Phys. Rep. **244**, 204-286 (1994)

W. M. Itano, J. C. Bergquist, J. J. Bollinger and D. J. Wineland, "Cooling methods in ion traps" Physica Scripta **T 59**, 106-20 (1995)

C. Savage, "Introduction to light forces, atom cooling, and atom trapping" Australian J. Phys. **49**, 745-764 (1996)

A. Ashkin, "Optical trapping and manipulation of neutral particles" Proc. Natl. Acad. Sci. **94**, 48534860 (1997)

C. E. Wieman, D. E. Pritchard and D. J. Wineland, "Atom cooling, trapping, and quantum manipulation" Rev. Mod. Phys. **71**, S253-62 (1999)

H. J. Metcalf and P. v. d. Straten, *Laser Cooling and Trapping*, (Springer, New York, 1999)

K. C. Neuman and S. M. Block, "Optical trapping" Rev. Sci. Inst. **75**, 2787-2809 (2004)

[43] **Lorentz force**

J. D. Jackson, *Classical Electrodynamics*, (Wiley, New York, 1999)

[44] **Laser incoherence and noise**

W. H. Louisell, *Radiation and Noise in Quantum Electronics*, (McGraw-Hill, N.Y., 1964)

K. Wodkiewicz, B. W. Shore and J. H. Eberly, "Pre-Gaussian noise in strong laser-atom interactions" J. Opt. Soc. Am. B **1**, 398-405 (1984)

J. H. Eberly, K. Wodkiewicz and B. W. Shore, "Noise in strong laser-atom interactions: Phase telegraph noise" Phys. Rev. A **30**, 2381-2388 (1984)

K. Wodkiewicz, B. W. Shore and J. H. Eberly, "Noise in strong laser-atom interactions: Frequency fluctuations and nonexponential correlations" Phys. Rev. A **30**, 2390-2398 (1984)

C. W. Gardiner and P. Zoller, *Quantum Noise*, (Springer, New York, 1999)

[45] **Free electron in laser field**

L. V. Keldysh, "Ionization in the field of a strong electromagnetic wave" Sov. Phys. JETP **20**, 1307-14 (1965)

J. H. Eberly, "Interaction of very intense light with free electrons" Prog. Optics **7**, 361-415 (1969)

H. R. Reiss, "Complete Keldysh theory and its limiting cases" Phys. Rev. A **42**, 1476-86 (1990)

[46] **Atomic beams**

N. F. Ramsey, *Molecular Beams*, (Oxford Univ. Press, (Lond.) , 1956)

G. Scoles, D. C. Laine and U. Valbusa, ed. *Atomic and Molecular Beam Methods*, (Oxford, Oxford, 1988)

G. Sanna and G. Tomassetti, *Introduction to Molecular Beams Gas Synamics*, (Imperial College Press, London, 2005)

[47] **Trapped ions and atoms** see also [49]

H. Walther, "Single atoms in cavities and traps," in *Current Trends in Optics*, ed. J. C. Dainty (Academic, London, 1994)

R. Blatt, J. I. Cirac and P. Zoller, "Trapping states of motion with cold ions" Phys. Rev. A **52**, 518-524 (1995)

M. Freyberger, "Probing the quantum state of a trapped atom" Phys. Rev. A **55**, 4120 (1997)

G. Z. K. Horvath, R. C. Thompson and P. L. Knight, "Fundamental physics with trapped ions" Contemp. Phys. **38**, 25-48 (1997)

X. S. Xie and J. K. Trautman, "Optical studies of single molecules at room temperature" Ann. Rev. Phys. Chem. **49**, 441-480 (1998)

D. Leibfried, R. Blatt, C. Monroe and D. Wineland, "Quantum dynamics of single trapped ions" Rev. Mod. Phys. **75**, 281-325 (2003)

S. Maniscalco, "Single trapped cold ions: A testing ground for quantum mechanics" J. Opt. B **7**, R1-R17 (2005)

D. Meschede and A. Rauschenbeutel, "Manipulating single atoms" Adv. At. Mol. Opt. Phys., **53**, 75 (2006)

J. Fortagh and C. Zimmermann, "Magnetic microtraps for ultracold atoms" Rev. Mod. Phys. **79**, 235-289 (2007)

[48] **Pulse formation**

A. Assion, T. Baumert, J. Helbing, V. Seyfried and G. Gerber, "Coherent control by a single phase shaped femtosecond laser pulse" Chem. Phys. Lett. **259**, 488-94 (1996)

T. Baumert, T. Brixner, V. Seyfried, M. Strehle and G. Gerber, "Femtosecond pulse shaping by an evolutionary algorithm with feedback" App. Phys. B **65**, 779-82 (1997)

A. Assion, T. Baumert, M. Bergt, T. Brixner, B. Kiefer, V. Seyfried, M. Strehle and G. Gerber, "Control of chemical reactions by feedback-optimized phase-shaped femtosecond laser pulses" Science **282**, 919 (1998)

T. Brixner, M. Strehle and G. Gerber, "Feedback-controlled optimization of amplified femtosecond laser pulses" Appl. Phys. B **68**, 281-4 (1999)

A. M. Weiner, "Femtosecond pulse shaping using spatial light modulators" Rev. Sci. Instrum. **71**, 1929-1960 (2000)

T. Brixner, N. H. Damrauer, P. Niklaus and G. Gerber, "Photoselective adaptive femtosecond quantum control in the liquid phase." Nature **414**, 57-60 (2001)

M. Wollenhaupt, V. Engel and T. Baumert, "Femtosecond laser photoelectron spectroscopy on atoms and small molecules: Prototype studies in quantum control" Ann. Rev. Phys. Chem. **56**, 25 - 56 (2005)

P. Nuernberger, G. Vogt, T. Brixner and G. Gerber, "Femtosecond quantum control of molecular dynamics in the condensed phase." Phys Chem Chem Phys. **9**, 2470-97 (2007)

[49] **Optical lattices**

G. K. Brennen, C. M. Caves, P. S. Jessen and I. H. Deutsch, "Quantum logic gates in optical lattices" Phys. Rev. Lett. **82**, 1060 - 1063 (1999)

O. Morsch and M. Oberthaler, "Dynamics of Bose-Einstein condensates in optical lattices" Rev. Mod. Phys. **78**, 179- (2006)

A. Ashkin, *Optical Trapping and Manipulation of Neutral Particles Using Lasers*, (World Scientific, Hackensack, N.J., 2007)

T. Iida and H. Ishihara, "Theory of resonant radiation force exerted on nanostructures by optical excitation of their quantum states: From microscopic to macroscopic descriptions" Phys. Rev. B **77**, 245319 (2008)

[50] **Adiabatic passage for atom in solid**

J. Klein, F. Beil and T. Halfmann, "Rapid adiabatic passage in a Pr3+:Y2SiO5 crystal" J. Phys. B **40**, S345-S358 (2007)

[51] **Stabilization in intense fields** see also [52]

K. Burnett, P. L. Knight, B. R. M. Piraux and V. C. Reed, "Suppression of ionization in strong laser fields" Phys. Rev. Lett. **66**, 301-4 (1991)

K. C. Kulander, K. J. Schafer and J. L. Krause, "Dynamic stabilization of hydrogen in an intense, high-frequency, pulsed laser field" Phys. Rev. Lett. **66**, 2601-4 (1991)

R. Grobe and C. K. Law, "Stabilization in superintense fields: A classical interpretation" Phys. Rev. A **44**, R4114-17 (1991)

B. Piraux, E. Huens and P. L. Knight, "Atomic stabilization in ultrastrong laser fields" Phys. Rev. A **44**, 721-32 (1991)

A. Scrinzi, N. Elander and B. Piraux, "Stabilization of Rydberg atoms in superintense laser fields" Phys. Rev. A **48**, R2527-30 (1993)

J. H. Eberly and K. C. Kulander, "Atomic Stabilization by Super-Intense Lasers" Science **262**, 1229 - 1233 (1993)

M. Gavrila, "Atomic stabilization in superintense laser fields" J. Phys. B **35**, R147-R193 (2002)

[52] **Ultrastrong fields** see also [53]

M. Crance and M. Aymar, "Dynamics of multiphoton ionisation to multiple continua" J. Phys. B **13**, L421-L426 (1980)

B. W. Shore and P. L. Knight, "Enhancement of high optical harmonics by excess-photon ionisation" J. Phys. B **20**, 413-423 (1987)

A. L'Huillier, K. J. Schafer and K. C. Kulander, "Theoretical aspects of intense field harmonic generation" J. Phys. B. **24**, 3315-41 (1991)

M. H. Mittleman, *Introduction to the Theory of Laser-Atom Interactions*, (Plenum, New York, 1993)

P. B. Corkum, "Plasma perspective on strong field multiphoton ionization" Phys. Rev. Lett. **71**, 1994 - 1997 (1993)

K. Burnett, V. C. Reed and P. L. Knight, "Atoms in ultra-intense laser fields" J. Phys. B **26**, 561-598 (1993)

M. Ivanov, T. Seideman, P. Corkum, F. Ilkov and P. Dietrich, "Explosive ionization of molecules in intense laser fields" Phys. Rev. A **54**, 1541 - 1550 (1996)

M. Protopapas, C. H. Keitel and P. L. Knight, "Atomic physics with super-high intensity lasers" Repts. Prog. Phys. **60**, 389-486 (1997)

T. Brabec and F. Krausz, "Intense few-cycle laser fields: Frontiers of nonlinear optics" Rev. Mod. Phys. **72**, 545 - 591 (2000)

B. Piraux and K. Rzazewski, ed. *Super-Intense Laser-Atom Physics*, (Springer, Berlin, 2001)

J. H. Posthumus, "The dynamics of small molecules in intense laser fields" Repts. Prog. Phys. **67**, 623-665 (2004)

A. Becker and F. H. M. Faisal, "Intense-field many-body S-matrix theory" J. Phys. B: **38**, R1-R56 (2005)

P. B. Corkum and F. Krausz, "Attosecond science" Nature Physics **3**, 381 - 387 (2007)

C. Winterfeldt, C. Spielmann and G. Gerber, "Colloquium: Optimal control of high-harmonic generation" Rev. Mod. Phys. **80**, 117 (2008)

[53] **Calculation of ultrastrong-field wavefunctions**

K. C. Kulander, "Multiphoton ionization of hydrogen: A time-dependent treatment" Phys. Rev. A **35**, 445-7 (1987)

K. C. Kulander, "Time-dependent theory of multiphoton ionization of xenon" Phys. Rev. A **38**, 778-787 (1988)

C. Cerjan, "Variable time-step integrator for intense field dynamics" J. Opt. Soc. Am. B **7**, 680-84 (1990)

C. Cerjan and K. Kulander, "Efficient time propagation for finite-difference representations of the time-dependent Schrödinger equation" Comp. Phys. Comm. **63**, 529-537 (1991)

C. Leforestier, R. H. Bisseling, C. Cerjan, M. D. Feit, R. Friesner, A. Guldberg, A. Hammerich, G. Jolicard, W. Karrlein, H.-D. Meyer, N. L. , O. Roncero and R. Kosloff, "A comparison of different propagation schemes for the time dependent Schrdinger equation" J. Comp. Phys. **94**, 59-80 (1991)

J. L. Krause, K. J. Schafer and K. C. Kulander, "Calculation of photoemission from atoms subject to intense laser fields" Phys. Rev. A **45**, 4998-5010 (1992)

C. Cerjan and R. Kosloff, "Efficient variable time-stepping scheme for intense field-atom interactions" Phys. Rev. A **47**, 1852 - 1860 (1993)

[54] **Undisturbed multi-electron atomic wavefunctions**

M. Klapisch, "A program for atomic wavefunction computations by the parametric potential method" Comp. Phys. Comm. **2**, 239 (1971)

E. Clementi and C. Roetti, "Roothaan-Hartree-Fock atomic wavefunctions: Basis functions and their coefficients for ground and certain excited states of neutral and ionized atoms, Z 54" At. Data and Nucl. Data Tables **14**, 177-478 (1974)

M. W. Schmidt and M. S. Gordon, "The construction and interpretation of MCSF wavefunctions" Ann. Rev. Phys. Chem. **49**, 233-266 (1998)

W. Kohn, "Nobel Lecture: Electronic structure of matterwave functions and density functionals" Rev. Mod. Phys. **71**, 1253 (1999)

J. A. Pople, "Nobel Lecture: Quantum chemical models" Rev. Mod. Phys. **71**, 1267 - 1274 (1999)

P. Fulde, "Wavefunction methods in electronic-structure theory of solids" Advances in Physics **51**, 909 - 948 (2002)

[55] **Atomic orbitals**

C. C. J. Roothaan, "New developments in molecular orbital theory" Rev. Mod. Phys. **23**, 69-89 (1951)

C. K. Jorgensen, *Orbitals in Atoms and Molecules*, (Academic, N.Y., 1962)

R. S. Berry, "Atomic orbitals. Resource paper-V" J. Chem. Ed. **43**, 283-299 (1966)

W. J. Hehre, R. F. Stewart and J. A. Pople, "Self-consistent molecular-orbital methods. I. Use of Gaussian expansions of Slater-type atomic orbitals" J. Chem. Phys. **51**, 2657 (1969)

P. O. D. Offenhartz, *Atomic and Molecular Orbital Theory*, (McGraw-Hill, N.Y., 1970)

B. W. Shore, "Use of the Rayleigh-Ritz-Galerkin method with cubic splines for constructing single-particle bound-state radial wavefunctions; the hydrogen atom and its spectrum" J. Phys. B **6**, 1923-1931 (1973)

K. Wolinski, J. F. Hinton and P. Pulay, "Efficient implementation of the gauge-independent atomic orbital method for NMR chemical shift calculations" J. Am. Chem. Soc. **112**, 8251-8260 (1990)

[56] **Rydberg atoms**

S. A. Edelstein and T. F. Gallagher, "Rydberg atoms" Adv. At. Mol Phys. **14**, 365-392 (1978)

S. Feneuille and P. Jacquinot, "Atomic Rydberg states" Adv. At. Mol. Phys. **17**, 99-166 (1981)

D. Kleppner, " The spectroscopy of highly excited atoms," in *Progress in Atomic Spectroscopy, Part B*, ed. W. H. and H. Kleinpoppen (Plenum, N.Y., 1978)

H. Walther, " Radiation interaction of Rydberg atoms," in *Quantum Electrodynamics and Quantum Optics*, ed. A. O. Barut (Plenum, N.Y., 1984)

S. Haroche and J. M. Raimond, "Radiative properties of Rydberg states and resonant cavities" Adv. At. Mol. Phys. **20**, 350 (1985)

P. L. Knight, " Rydberg atoms and quantum optics," in *Frontiers in Quantum Optics*, ed. E. R. Pike and S. Sarkar (Adam Hilger, 1986)

[57] **Rabi frequency** see also [69]

P. L. Knight and P. W. Milonni, "The Rabi frequency in optical spectra" Phys. Repts. **66**, 21-107 (1980)

[58] **Electron wavepacket in intense field**

P. B. Corkum, "Plasma perspective on strong field multiphoton ionization" Phys. Rev. Lett. **71**, 1994 - 1997 (1993)

M. Lewenstein, P. Balcou, M. Y. Ivanov, A. L'Huillier and P. B. Corkum, "Theory of high-harmonic generation by low-frequency laser fields" Phys. Rev. A **49**, 2117-2132 (1994)

N. Hay, M. Lein, R. Velotta, R. De Nalda, E. Heesel, M. Castillejo, P. L. Knight and J. P. Marangos, "Investigations of electron wave-packet dynamics and high-order harmonic generation in laser-aligned molecules" J. Mod. Opt. **50**, 561-577 (2003)

P. B. Corkum and F. Krausz, "Attosecond science" Nature Physics **3**, 381 - 387 (2007)

[59] **Hilbert space**

G. Birkhoff and S. MacLane, *A Survey of Modern Algebra*, (Macmillan, N.Y., 1953)

D. W. Cohen, *An Introduction to Hilbert Space and Quantum Logic*, (Springer, New York, 1989)

P. Szekeres, *A Course in Modern Mathematical Physics. Groups, Hilbert Space and Differential Geometry*, (Cambridge U. Press, New York, 2004)

A. Vourdas, "Quantum systems with finite Hilbert space" Repts. Prog. Phys. **67**, 267-320 (2004)

L. Debnath and P. Mikusinski, *Introduction to Hilbert Spaces: With Applications*, (Academic, New York, 2005)

[60] **Two-level behavior**

C. A. Coulter, "Atoms in moderately strong electromagnetic fields: General method and its application to the two-level atom" Phys. Rev. A **10**, 1946-1954 (1974)

A. J. Leggett, S. Chakravarty, A. T. Dorsey, M. P. A. Fisher, A. Garg and W. Zwerger, "Dynamics of the dissipative two-state system" Rev. Mod. Phys. **59**, 1-85 (1987)

[61] **The Majorana formula**

E. Majorana, "Atomi orientati in campo magnetico variabile" Nuov. Cim. **9**, 43-50 (1932)

F. Bloch and I. I. Rabi, "Atoms in variable magnetic fields" Rev. Mod. Phys. **17**, 237 (1945)

H. Bacry, "Orbits of the rotation group on spin states" J. Math. Phys. **15**, 1686 (1974)

J. Schwinger, "The Majorana formula" Trans. N.Y. Acad. Sci. [II] **38**, 170-184 (1977)

H. Mäkelä and K.-A. Suominen, "Inert states of spin-S systems" Phys. Rev. Lett. **99**, 190408 (2007)

[62] **Rate equations** see also [63]

T. R. Carson and M. J. Roberts, ed. *Atoms and Molecules in Astrophysics*, (Academic, N.Y., 1972)

W. H. Tucker, *Radiation Processes in Astrophysics*, (MIT Press, Cambridge, Mass., 1975)

V. G. Minogin, "Kinetic equation for atoms interacting with laser radiation" Sov. Phys. JETP **52**, 1032 (1980)

G. B. Rybicki and A. P. Lightman, *Radiative Processes in Astrophysics*, (Wiley, N.Y., 1985)

[63] **Astrophysics and radiative transfer**

V. A. Ambartsumyan, *Theoretical Astrophysics*, (Pergamon, N.Y., 1958)

S. Chandrasekhar, *Radiative Transfer*, (Dover, N.Y., 1960)

D. Mihalas, *Stellar Atmospheres*, (Freeman, San Francisco, 1978)

K. R. Lang, *Astrophysical Formulas*, (Springer, Berlin, 1980)

A. R. Rau, *Astronomy-Inspired Atomic and Molecular Physics*, (Springer, Berlin, 2002)

B. W. Carroll and D. A. Ostlie, *Introduction to Modern Astrophysics*, (Pearson Addison-Wesley, San Francisco 2007)

[64] **Spontaneous emission in a cavity** see also [39]

E. M. Purcell, "Spontaneous emission probabilities at radio frequencies" Phys. Rev. **69**, 681 (1946)

P. Goy, J. M. Raimond, M. Gross and S. Haroche, "Observation of cavity-enhanced single-atom spontaneous emission" Phys. Rev. Lett. **50**, 1903-1906 (1983)

J. J. Sanchez-Mondragon, N. B. Narozhny and J. H. Eberly, "Theory of spontaneous emission lineshape in an ideal cavity" Phys. Rev. Lett. **51**, 550- (1983)

G. S. Agarwal, "Vacuum-field Rabi oscillations of atoms in a cavity" J. Opt. Soc. Am. B **2**, 480-5 (1985)

S. Haroche and J. M. Raimond, "Radiative properties of Rydberg states and resonant cavities" Adv. At. Mol. Phys. **20**, 350 (1985)

H.-B. Lin, J. D. Eversole, C. D. Merritt and A. J. Campillo, "Cavity-modified spontaneous emission rates in liquid microdroplets" Phys. Rev. A **45**, 6756-60 (1992)

[65] **Photonic crystals**

J. D. Joannopoulos, R. D. Meade and J. N. Winn., *Photonic Crystals: Molding the Flow of Light*, (Princeton University Press, Princeton, N.J. , 1995)

D. G. Angelakis, E. Paspalakis and P. L. Knight, "Coherent phenomena in photonic crystals" Phys. Rev. A **64**, 3801 (2001)

F. Zolla, G. Renversez, A. Nicole, B. Kuhlmey, S. Guenneau and D. Felbacq, *Foundations of Photonic Crystal Fibres*, (World Scientific, Singapore, 2005)

S. Selleri, F. Poli and A. Cucinotta, *Photonic Crystal Fibers*, (Springer New York, 2007)

[66] **Electric-dipole interaction**

E. A. Power, *Introductory Quantum Electrodynamics*, (Longmans & Green, London, 1964)

E. A. Power and T. Thirunamachandran, "On the nature of the Hamiltonian for the interaction of radiation with atoms and molecules: (e/mc)p.A, d.E and all that" Am. J. Phys. **46**, 370-378 (1978)

D. P. Craig and T. Thirunamachandran, *Molecular Quantum Electrodynamics: An Introduction to Radiation-Molecule Interactions*, (Academic, N.Y., 1984)

C. Cohen-Tannoudji, J. Dupont-Roc and G. Grynberg, *Photons & Atoms. Introduction to Quantum Electrodynamics*, (Wiley, New York, 1989)

[67] **Selection rules**

L. C. Balling and J. J. Wright, "Use of angular momentum selection rules in laser isotope separation" Appl. Phys. Lett. **29**, 411-413, (1976)

M. P. Fewell, "The absorption of arbitrarily polarized light by atoms and molecules" J. Phys. B **26**, 1957-74 (1993)

N. V. Vitanov, Z. Kis and B. W. Shore, "Coherent excitation of a degenerate two-level system by an elliptically polarized laser pulse" Phys. Rev. A **68**, 3414 (2003)

Y.-X Liu, J. Q. You, L. F. Wei, C. P. Sun and F. Nori, "Optical selection rules and phase-dependent adiabatic state control in a superconducting quantum circuit" Phys. Rev. Lett. **95**, 087001 (2005)

[68] **Solving ordinary differential equations (ODEs)**

E. L. Ince, *Ordinary Differential Equations*, (Dover, N.Y., 1956)

L. Collatz, *The Numerical Treatment of Differential Equations*, (Springer, N.Y., 1966)

C. W. Gear, *Numerical Initial Value Problems in Ordinary Differential Equations*, (Prentice-Hall, Engelwood Cliffs N.J, 1971)

J. C. Butcher, *Numerical Methods for Ordinary Differential Equations*, (Wiley, Chichester, 2003)

[69] **The original introduction of the rotating wave picture**

I. I. Rabi, N. F. Ramsey and J. Schwinger, "Use of rotating coordinates in magnetic resonance problems" Rev. Mod. Phys. **26**, 167-171 (1954)

[70] **Quasicontinuum**

G. C. Stey and R. W. Gibbard, "Decay of quantum states in some exactly soluble models" Physica **60**, 1-26 (1972)

J. H. Eberly, J. J. Yeh and C. M. Bowden, "Interrupted coarse-grained theory of quasi-continuum photoexcitation" Chem. Phys. Letts. **86**, 76-80 (1982)

B. W. Shore, "Coherence in the quasi-continuum model" Chem. Phys. Letts. **99**, 240 (1983)

E. Kyrölä and J. H. Eberly, "Quasicontinuum effects in molecular excitation" J. Chem. **82**, 1841-1854 (1985)

[71] **Open systems**

E. B. Davies, *Quantum Theory of Open Systems*, (Academic, New York, 1976)

H.-P. Breuer and F. Petruccione, *The Theory of Open Quantum Systems*, (Oxford Univ. Press, Oxford, 2002)

[72] **Time dependent perturbation theory** see also [34]

P. W. Langhoff, S. T. Epstein and M. Karplus, "Aspects of time-dependent perturbation theory" Rev. Mod. Phys. **44**, 602-44 (1977)

[73] **Triple integral**

N. V. Vitanov and B. W. Shore, "Quantum transitions driven by missing frequencies" Phys. Rev. A **72**, 052507 (2005)

[74] **Dressed states in RF field**

C. Cohen-Tannoudji and S. Haroche, "Interprtation quantique des diverses rsonances observes lors de la diffusion de photons optiques et de radiofrquence par un atome" J. de Phys. **30**, 125-144 (1969)

C. Cohen-Tannoudji and S. Haroche, "Absorption et diffusion de photons optiques par un atome en interaction avec des photons de radiofrquence" J. de Phys. **30**, 153-168 (1969)

S. Haroche, "L'atome habill: une tude thoriqe et exprimentale des proprits physiques d'atomes en interaction avec des photons de radiofrquence" Annales de Phys. **6**, 189-326 and 327-387 (1971)

[75] **Dressed states**

P. R. Berman and J. Ziegler, "Generalized dressed-atom approach to atom-strong-field interactions – application to the theory of lasers and Bloch-Siegert shifts" Phys. Rev. A **15**, 2042-2052 (1977)

D. Dalibard and C. Cohen-Tannoudji, "Dressed-atom approach to atomic motion in laser light: the dipole force revisited" J. Opt. Soc. Am. **B2**, 1707-1860 (1985)

C. Cohen-Tannoudji, J. Dupont-Roc and G. Grynberg, *Photons and Atoms: Introduction to Quantum Electrodynamics*, (Wiley, N.Y., 1989)

[76] **Rapid adiabatic passage (RAP)** see also [78, 174]

D. Grischkowsky, "Adiabatic following and slow optical pulse propagation in rubidium vapor" Phys. Rev. A **7**, 2096-2101 (1973)

M. M. T. Loy, "Observation of population inversion by optical adiabatic rapid passage" Phys. Rev. Lett. **32**, 814-17 (1974)

D. Grischkowsky and M. M. T. Loy, "Self-induced adiabatic rapid passage" Phys. Rev. A **12**, 1117-20 (1975)

[77] **Adiabatic evolution and adiabatic following** see also [3, 76, 174, 78]

M. D. Crisp, "Adiabatic-following approximation" Phys. Rev. A **8**, 2128 - 2135 (1973)

R. T. Robiscoe, "Quasiadiabatic solution to the two-level problem" Phys. Rev. A **25**, 1178-1180 (1982)

S. Stenholm, *Foundations of Laser Spectroscopy*, (Wiley, N.Y., 1984)

M. V. Berry, "Quantal phase factors accompanying adiabatic changes" Proc. Roy. Soc. (Lond.) A **392**, 45 (1984)

M. V. Berry, "The adiabatic limit and the semiclassical limit" J. Phys. A **17**, 1225-33 (1984)

C. Liedenbaum, S. Stolte and J. Reuss, "Inversion produced and reversed by adiabatic passage" Phys. Rep. **178**, 1-24 (1989)

S. Klarsfeld and J. O. Oteo, "Magnus approximatin in the adiabatic picture" Phys. Rev. A **45**, 3329-32 (1992)

J. H. Eberly, A. Rahman and R. Grobe, "Coherent control and adiabatic photon physics" Laser Physics **6**, 69-73 (1996)

E. E. Nikitin, "Nonadiabatic transitions: What we learned from old masters and how much we owe them" Ann. Rev. Phys. Chem. **50**, 1-21 (1999)

[78] **Adiabatic states**

D. Grischkowsky, "Coherent excitation, incoherent excitation and adiabatic states" Phys. Rev. A **14**, 802-812 (1976)

A. Flusberg and S. R. Hartmann, "Probing adiabatic states" Phys. Rev. A **14**, 813-5 (1976)

M. V. Berry, "Histories of adiabatic quantum transitions" Proc. Roy. Soc. (Lond.) A **429**, 61-72 (1990)

[79] **Landau-Zener-Stueckelberg model**

L. D. Landau, "Zur Theorie der Energieübertragung bei Stössen" Phys. Z. Sowjentunion **1**, 88 (1932)

L. D. Landau, "Zur Theorie der Energieübertragung II" Phys. Z. Sowjentunion **2**, 46-51 (1932)

C. Zener, "Non-adiabatic crossing of energy levels" Proc. Roy. Soc. (Lond.) A **137**, 696-9 (1932)

C. Stueckelberg, "Theory of inelastic collisions between atoms" Helv. Phys. Acta **5**, 369-423 (1932)

D. A. Harmin, "Intramanifold level mixing by time-dependent electric fields: Multilevel Landau-Zener effect" Phys. Rev. A **44**, 433-61 (1991)

N. V. Vitanov and B. M. Garraway, "Landau-Zener model - Effects of finite coupling duration" Phys. Rev. A **53**, 4288-4304 (1996)

N. V. Vitanov and K.-A. Suominen, "Nonlinear level-crossing models" Phys. Rev. A **59**, 4580-4588 (1999)

[80] **Dynamic Stark effect**

S. H. Autler and C. H. Townes, "Stark effect in rapidly varying fields" Phys. Rev. **100**, 703-722 (1955)

A. Kastler, "Displacement of energy levels of atoms by light" J. Opt. Soc. Am. **53**, 902-10 (1963)

L. D. Zusman and A. I. Burshtein, "Stark effect in the field of incoherent radiation" Sov. Phys. JETP **34**, 520-526 (1972)

S. S. Hassan and R. K. Bullough, "Theory of the dynamical Stark effect" J. Phys. B **8**, L147-52 (1975)

B. Renaud, R. M. Whitley and C. R. Stroud, Jr., "Correlation functions and the ac Stark effect" J. Phys. B **9**, L19-24 (1976)

C. Cohen-Tannoudji and S. Reynaud, "Modification of resonance Raman scattering in very intense fields" J. Phys. B **10**, 365 (1977)

J. Wong, J. C. Garrison and T. H. Einwohner, "Dynamic Stark splitting by coupled one- and two-photon resonances" Phys. Rev. **16**, 213-20 (1977)

C. Delsart and J.-C. Keller, "Effects of Zeeman degeneracy on optical dynamic Stark splitting" J. Phys. B **13**, 241-252 (1980)

J. Kourlas, "Resonant fluorescence: Zeeman and ac Stark effects" J. Phys. B. **14**, 1433-1443 (1981)

R. W. Boyd and M. Sargent, III "Population pulsations and the dynamic Stark effect" J. Opt. Soc. Am. B **5**, 99- (1988)

C. A. Nicolaides, C. W. Clark and M. H. Nayfeh, ed. *Atoms in Strong Fields*, (Plenum, N.Y., 1990)

S. Guérin, L. P. Yatsenko, T. Halfmann, B. W. Shore and K. Bergmann, "Stimulated hyper-Raman adiabatic passage. II. Static compensation of dynamic Stark shifts" Phys. Rev. A **58**, 4691-704 (1998)

I. Haque and M. R. Singh, "A study of the ac Stark effect in doped photonic crystals" J. Phys.: Condens. Matter **19**, 156229 (2007)

[81] **SCRAP**

L. P. Yatsenko, A. Vardi, T. Halfmann, B. W. Shore and K. Bergmann, "Source of metastable H(2s) atoms using Stark chirped rapid adiabatic passage" Phys. Rev. A **60**, R4237- R4240 (1999)

T. Rickes, L. P. Yatsenko, S. Steuerwald, T. Halfmann, B. W. Shore, N. V. Vitanov and K. Bergmann, "Efficient adiabatic population transfer by two-photon excitation assisted by a laser-induced Stark shift" J. Chem. Phys. **115**, 534-546 (2000)

A. A. Rangelov, N. V. Vitanov, L. P. Yatsenko, B. W. Shore, T. Halfmann and K. Bergmann, " Stark-shift-chirped rapid-adiabatic-passage technique among three states" Phys. Rev. A **72**, 053403 (2005)

L. P. Yatsenko, V. I. Romanenko, B. W. Shore, T. Halfmann and K. Bergmann, "Two-photon excitation of the metastable 2s state of hydrogen assisted by laser-induced chirped Stark shifts and continuum structure" Phys. Rev. A **71**, 33418-1-10 (2005)

N. Sangouard, L. P. Yatsenko, B. W. Shore and T. Halfmann, "Preparation of nondegenerate coherent superpositions in a three-state ladder system assisted by Stark shifts" Phys. Rev. A **73**, 043415 (2006)

[82] **Pulse trains**

J. H. Eberly, "Optical pulse and pulse-train propagation in a resonant medium" Phys. Rev. Lett. **22**, 760 - 762 (1969)

R. Teets, J. Eckstein and T. W. Hänsch, "Coherent two-photon excitation by multiple lght pulses" Phys. Rev. Lett. **38**, 760 - 764 (1977)

J. Mlynek and W. Lange, "High-resolution coherence spectroscopy using pulse trains" Phys. Rev. A **24**, 1099 - 1102 (1981)

P. W. Milonni and L. E. Thode, "Theory of mesospheric sodium fluorescence excited by pulse trains" Appl. Opt. **31**, 785- (1992)

L. C. Bradley, "Pulse-train excitation of sodium for use as a synthetic beacon" J. Opt. Soc. Am. B **9**, 1931- (1992)

R. J. Temkin, "Excitation of an atom by a train of short pulses" J. Opt. Soc. Am. B **10**, 830- (1993)

N. V. Vitanov and P. L. Knight, "Coherent excitation of a two-state system by a train of short pulses" Phys. Rev. A **52**, 2245-2261 (1995)

B. M. Garraway and N. V. Vitanov, "Population dynamics and phase effects in periodic level crossings" Phys. Rev. A **55**, 4418-4432 (1997)

W. Harshawardhan and G. S. Agarwal, "Multiple Landau-Zener crossings and quantum interference in atoms driven by phase modulated fields" Phys. Rev. A **55**, 2165 - 2171 (1997)

J. M. Supplee, E. A. Whittaker and K. Andrew, "Response of a two-level atom to a frequency-modulated optically coherent pulse train" J. Opt. Soc. Am. B **15**, 1833-1838 (1998)

D. Feliinto, C. A. C. Bosco, L. H. Acioli and S. S. Vianna, "Coherent accumulation in two-level atoms excited by a train of ultrashort pulses" Opt. Comm. **215**, 69-73 (2003)

D. Felinto, L. H. Acioli and S. S. Vianna, "Accumulative effects in the coherence of three-level atoms excited by femtosecond-laser frequency combs" Phys. Rev. A **70**, 043403 (2004)

[83] **Design of pulse train**

R. Scharf, "The Campbell-Baker-Hausdorff expansion for classical and quantum kicked dynamics" J. Phys. A **21**, 2007-2021 (1988)

G. Harel and V. M. Akulin, "Complete control of Hamiltonian quantum systems: Engineering of Floquet evolution" Phys. Rev. Lett. **82**, 1 (1999)

E. A. Shapiro, V. Milner, C. Menzel-Jones and M. Shapiro, "Piecewise adiabatic passage with a series of femtosecond pulses" Phys. Rev. Lett. **99**, 033002 (2007)

[84] **Vector model**

R. P. Feynman, F. L. Vernon, Jr. and R. W. Hellwarth, "Geometrical representation of the Schrdinger equation for solving maser problems" J. Ap. Phys. **28**, 49-52 (1957)

[85] **Power broadening need not occur with pulses** see also [28]

A. Kuhn, S. Steuerwald and K. Bergmann, "Coherent population transfer in NO with pulsed lasers: The consequences of hyperfine structure, Doppler broadening and electromagnetically induced absorption" Eur. Phys. J. B **1**, 57-70 (1998)

N. V. Vitanov, B. W. Shore, L. Yatsenko, K. Böhmer, T. Halfmann, T. Rickes and K. Bergmann, "Power broadening revisited: Theory and experiment" Opt. Comm. **199**, 117-26 (2001)

T. Halfmann, T. Rickes, N. V. Vitanov and K. Bergmann, "Lineshapes in coherent two-photon excitation" Opt. Comm. **220**, 353-359 (2003)

[86] **Mollow triplet spectrum**

B. R. Mollow, "Power spectrum of light scattered by two-level systems" Phys. Rev. **188**, 1969-1975 (1969)

B. R. Mollow, "Absorption and emission line-shape functions for driven atoms" Phys. Rev. A **5**, 1522-1527 (1972)

B. R. Mollow, "Theory of intensity-dependent resonant light scattering and fluorescence" Prog. Optics **18**, 1-43 (1981)

[87] **Zeeman shift** see also [30]

P. Zeeman, "On the influence of magnetism on the nature of light emitted by a substance"' Phil. Mag. **43**, 226 (1897)

[88] **Stark shift**

J. Stark, "The effect of an electric field upon spectral lines" Sitzungsber. Akad. Wiss. Berlin **47**, 932-46 (1913)

A. Lo Surdo, "The electrical analog of the Zeeman effect" Atti R. Accad. Naz. Lincei , part 2 **22**, 664-6 (1913)

A. Lo Surdo, "The electrical analog of the Zeeman effect" Phys. Zs. **15**, 122 (1914)

A. M. Bonch-Bruevich and V. A. Khodovoi, "Current methods for the study of the Stark effect in atoms" Sov. Phys. Usp. **10**, 637-657 (1968)

N. Ryde, *Atoms and Molecules in Electric Fields*, (Almqvist & Wiksells, Stockholm, 1975)

K. J. Kollath and M. C. Standage, "Stark effect," in *Progress in Atomic Spectroscopy, Part B*, ed. W. H. and H. Kleinpoppen (Plenum, N.Y., 1978)

D. A. Harmin, "Theory of the Stark effect" Phys. Rev. A **26**, 2656 (1982)

D. A. Harmin, "Hydrogenic Stark effect: Properties of the wave functions" Phys. Rev. A **24**, 2491-2512 (1986)

C. A. Nicolaides, C. W. Clark and M. H. Nayfeh, ed. *Atoms in Strong Fields*, (Plenum, N.Y., 1990)

C. A. Nicolaides and S. I. Themelis, "Theory of the resonances of the LoSurdo-Stark effect" Phys. Rev. A **45**, 349-57 (1992)

[89] **Hyperfine structure**

H. B. G. Casimir, *On The Interaction Between Atomic Nuclei and Electrons*, (Freeman, San Francisco, 1963)

H. Kopferman, *Nuclear Moments*, (Academic, N.Y., 1958)

A. J. Freeman and R. B. Frankel, ed. *Hyperfine Interactions*, (Academic, N.Y., 1967)

L. Armstrong, Jr., *Theory of the Hyperfine Structure of Free Atoms*, (Wiley, N.Y., 1971)

A. Andreev, *Atomic Spectroscopy : Introduction to the Theory of Hyperfine Structure*, (Springer New York, 2006)

[90] **Chemical shift**

H. Günther, *NMR Spectroscopy: Basic Principles, Concepts, and Applications in Chemistry*, (Wiley, New York, 1995)

E. D. Becker, *High Resolution NMR. Theory and Chemical Applications*, (Academic Press, San Diego, 2000)

[91] **Angular momentum**

A. R. Edmonds, *Angular Momentum in Quantum Mechanics*, (Princeton Univ. Press, Princeton, 1957)

D. M. Brink and G. R. Satchler, *Angular Momentum*, (Clarendon Press, Oxford, 1968)

B. R. Judd, *Angular Momentum Theory for diatomic Molecules*, (Academic, N.Y., 1975)

L. C. Biedenharn and J. D. Louck, *Angular Momentum in Quantum Physics*, (Addison-Wesley, Reading, Mass., 1981)

R. N. Zare, *Angular Momentum: Understanding Spatial Aspects in Chemistry and Physics*, (Wiley, N.Y., 1988)

D. A. Varshalovic, A. N. Moskalev and V. K. Khersonskii, *Quantum Theory of Angular Momentum*, (World Scientific, Singapore, 1988)

[92] **Optical pumping**

C. Cohen-Tannoudji and A. Kastler, "Optical pumping" Prog. Optics **5**, 1-81 (1966)

W. Happer, "Optical pumping" Rev. Mod. Phys. **44**, 169-238 (1972)

A. Omont, "Irreducible components of the density matrix. Application to optical pumping" Prog. Quant. Electron. **5**, 69-138 (1977)

T. G. Walker and W. Happer, "Spin-exchange optical pumping of noble-gas nuclei" Rev. Mod. Phys. **69**, 629 - 642 (1997)

A. Imamogu, E. Knill, L. Tian and P. Zoller, "Optical pumping of quantum-dot nuclear spins" Phys. Rev. Lett. **91**, 017402 (2003)

[93] **Beyond the RWA** see also [69, 94]

J. H. Shirley, "Solution of the Schrödinger equation with a Hamiltonian periodic in time" Phys. Rev. **138 B**, 979-987 (1965)

Y. B. Zel'dovich, "The quasienergy of a quantum-mechanical system subjected to a periodic action" Sov. Phys. JETP **24**, 1006 (1967)

W. R. Salzman, "Time evolution of simple quantum-mechanical systems. II. Two-state system in intense fields" Phys. Rev. Lett. **26**, 220-221 (1971)

D. T. Pegg, "Semi-classical model of magnetic resonance in intense rf fields" J. Phys B **6**, 246-253 (1973)

D. R. Dion and J. O. Hirschfelder, "Time-dependent perturbation of a two-state quantum system in a sinusoidal field" Adv. Chem. Phys. **35**, 265-350 (1976)

G. W. Series, "A semi-classical approach to radiation problems" Phys. Repts. **43**, 1-41 (1978)

K. Zaheer and M. S. Zubairy, "Atom-field interaction without the rotating-wave approximation: A path integral approach" Phys. Rev. A **37**, 1628-33 (1988)

M. D. Crisp, "Jaynes-Cummings model without the rotating-wave approximation" Phys. Rev. A **43**, 2430-35 (1991)

S. J. D. Phoenix, "Counter-rotating contributions in the Jaynes-Cummings model" J. Mod. Opt. **36**, 1163-72 (1989)

[94] **Floquet theory** see also [75]

G. Floquet, "Sur les equations differentielles lineaires a coefficients periodiques" Ann. Ecole. Norm. Suppl. **12**, 47 (1883)

J. H. Poincaré, *Méthodes Nouvelles de la Méchanique Céleste*, Vol. I (Paris, 1892); Vol. II (Paris, 1893); Vol. III (Paris, 1899).

J. H. Shirley, "Solution of the Schrödinger equation with a Hamiltonian periodic in time" Phys. Rev. **138 B**, 979-987 (1965)

V. A. Yakubovich and V. M. Starzhinskii, *Linear Differential equations with Periodic Coefficients*, (Wiley, New York, 1975)

W. R. Salzman, "Quantum mechanics of systems periodic in time" Phys. Rev. A **10**, 461-465 (1974)

S. R. Barone, M. A. Narcowich and F. J. Narcowich, "Floquet theory and applications" Phys. Rev. A **15**, 1109-1125 (1977)

T.-S. Ho, S.-I. Chu and J. V. Tietz, "Semiclassical many-mode Floquet theory" Chem. Phys. Letts. **96**, 464 (1983)

K. F. Milfield and R. E. Wyatt, "Study, extension and application of Floquet theory for quantum molecular systems in an oscillating field" Phys. Rev. A **27**, 72-94 (1983)

S.-I. Chu, "Recent developments in semiclassical Floquet theories for intense field multiphoton processes" Adv. At. Mol Phys. **21**, 197-253 (1985)

M. Pont and R. Shakeshaft, "Analytic structure of the ac quasienergy in the complex field plane" Phys. Rev. A **43**, 3764-84 (1991)

P. Kuchment, *Floquet Theory for Partial Differential Equations*, (Birkhaueser, Basel, 1993)

S. Guérin, F. Monti, J.-M. Dupont and H. R. Jauslin, "On the relation between cavity-dressed states, Floquet states, RWA and semiclassical models" J. Phys. A **30**, 7193-7215 (1997)

A. Jaron, E. Mese and R. M. Potvliege, "Floquet analysis of laser-induced continuum structures" J. Phys. B **33**, 1487-1505 (2000)

A. Keller, C. M. Dion and O. Atabek, "Laser-induced molecular rotational dynamics: A high-frequency Floquet approach" Phys. Rev. A **61**, 023409 (2000)

G. Jolicard, O. Atabek, M. L. Dubernet-Tuckey and N. Balakrishnan, "Nonadiabatic molecular response to short, intense laser pulses: A wave operator generalized Floquet approach" J. Phys. B **36**, 2777 (2003)

[95] **Adiabatic Floquet theory**

S. Guérin and H. R. Jauslin, "Two-laser multiphoton adiabatic passage in the frame of the floquet theory - applications to (1+1) and (2+1) stirap" Eur. Phys. J. D **2**, 99-113 (1998)

K. Drese and M. Holthaus, "Floquet theory for short laser pulses" Eur. Phys. J. D **5**, 119-134 (1999)

S. Guérin and H. R. Jauslin, "Control of quantum dynamics by laser pulses: Adiabatic Floquet theory" Adv. Chem. Phys. **125**, 147 (2003)

N. Sangouard, S. Guérin, L. P. Yatsenko and T. Halfmann, "Preparation of coherent superposition in a three-state system by adiabatic passage" Phys. Rev. A **70**, 013415 (2004)

[96] **Multiphoton processes**

H. B. Bebb and A. Gold, "Multiphoton ionization of hydrogen and rare-gas atoms" Phys. Rev. **143**, 1-24 (1966)

B. A. Zon, N. L. Manakov and L. P. Rapoport, "Perturbation theory for the multiphoton ionization of atoms" Sov. Phys. JETP **34**, 515-519 (1972)

Y. Gontier, N. K. Rahman and M. Trahin, "Exact summation of higher-order terms in multiphoton processes" Phys. Rev. A **14**, 2109-2125 (1976)

S. Mukamel and J. Jortner, "Multiphoton molecular dissociation in intense laser fields" J. Chem. Phys. **65**, 5204-5225 (1976)

L. Rosenberg, "Multiphoton transitions: Approximations for the effective Hamiltonian" Phys. Rev. A **14**, 1137-45 (1976)

J. H. Eberly and P. Lambropoulos, ed. *Multiphoton Processes*, (Wiley, N.Y., 1978)

P. L. Knight, "The role of transients in resonant multiphoton absorption" J. Phys. B. **12**, L449-L452 (1979)

S. Stenholm, "Laser-induced multiphoton transitions" Contemp. Phys. **20**, 37-54 (1979)

Y. Gontier, N. K. Rahman and M. Trahin, "Removal of the intermediate states in an all-order theory of multiphoton processes" Phys. Rev. A **24**, 3102-4 (1981)

M. Crance and L. Armstrong, "Fluorescence induced by resonant multiphoton ionization near an autoionizing state" J. Phys. B **15**, 3199-3210 (1982)

J. Morellec, D. Normand and G. Petite, "Nonresonant multiphoton ionization of atoms" Adv. At. Mol. Phys , **18**, 98-164 (1982)

P. Zoller, "Stark shifts and resonant multiphoton ionization in multimode laser fields" J. Phys. B **15**, 2911-33 (1982)

S. L. Chin and P. Lambropoulos, ed. *Multiphoton Ionization of Atoms*, (Academic, N.Y., 1984)

H. G. Müller and A. Tip, "Multiphoton ionization in strong fields" Phys. Rev. A **30**, 3039-3050 (1984)

R. Shakeshaft, "Theory of multiphoton ionization of atoms by intense laser fields" J. Opt. Soc. Am. B **4**, 705-919 (1987)

F. H. M. Faisal, *Theory of Multiphoton Processes*, (Plenum, N.Y., 1987)

Y. Gontier, N. K. Rahman and M. Trahin, "Resonant multiphoton ionization of atomic hydrogen" Phys. Rev. A **37**, 4694-4701 (1988)

S. J. Smith and P. L. Knight, ed. *Multiphoton Processes*, (Cambridge Univ., New York, 1988)

G. Mainfray and C. Manus, "Multiphoton ionization of atoms" Repts. Prog. Phys. **54**, 1333-72 (1991)

N. B. Delone and V. P. Krainov, *Multiphoton Processes in Atoms*, (Springer, Berlin, 2000)

[97] **Linkage ambiguity**

R. G. Unanyan, S. Guérin, B. W. Shore and K. Bergmann, "Efficient population transfer by delayed pulses despite coupling ambiguity" Euro. Phys. J. D **8**, 443-449 (2000)

[98] **Three states** see also [108]

R. M. Whitley and C. R. Stroud, Jr. , "Double optical resonance" Phys. Rev. A **14**, 1498-1512 (1976)

B. W. Shore and J. Ackerhalt, "Dynamics of multilevel laser excitation: Three-level atoms" Phys. Rev. A **15**, 1640-1646 (1977)

J. N. Elgin, "Semiclassical formalism for the treatment of three-level systems" Phys. Lett. **80A**, 140-142 (1980)

P. M. Radmore and P. L. Knight, "Population trapping and dispersion in a three-level system" J. Phys. B **15**, 561-73 (1982)

H. P. W. Gottlieb, "Linear constants of motion for a three-level atom excited by two modulated electromagnetic waves" Phys. Rev. A **26**, 3713-15 (1982)

F. T. Hioe and J. H. Eberly, "Nonlinear constants of motion for three-level quantum systems" Phys. Rev. A **25**, 2168-2171 (1983)

F. T. Hioe, "Linear and nonlinear constants of motion for two-photon processes in three-level systems" Phys. Rev. A **29**, 3434-36 (1984)

H. P. W. Gottlieb, "Second invariant in an excited three-level system" Phys. Rev. A **32**, 653-4 (1985)

C. E. Carroll and F. T. Hioe, "Three-state model driven by two laser beams" Phys. Rev. A **36**, 724 (1987)

C. E. Carroll and F. T. Hioe, "Driven three-state model and its analytic solutions" J. Math. Phys. **29**, 487 (1988)

C. E. Carroll and F. T. Hioe, "Three-state system driven by resonant optical pulses of different shapes" J. Opt. Soc. Am. B **5**, 1335 (1988)

C. E. Carroll and F. T. Hioe, "Two-photon resonance in three-state model driven by two laser beams" J. Phys. B **22**, 2633-47 (1989)

C. E. Carroll and F. T. Hioe, "Analytic solutions for three state systems with overlapping pulses" Phys. Rev. A **42**, 1522-31 (1990)

V. L. Ermakov and G. Bodenhausen, "Coherence transfer in three-level systems - controlled violation of adiabaticity and antiparallel double resonant irradiation" J. Chem. Phys. **103**, 136-143 (1995)

N. V. Vitanov, "Analytic model of a three-state system driven by two laser pulses on two-photon resonance" J. Phys. B **31**, 709-725 (1998)

T. A. Laine and S. Stenholm, "Adiabatic processes in three-level systems" Phys. Rev. A **53**, 2501-12 (1996)

N. V. Vitanov and S. Stenholm, "Non-adiabatic effects in population transfer in three-level systems" Opt. Comm. **127**, 215-22 (1996)

[99] **Polarizability**

J. H. Van Vleck, *Electric and Magnetic Susceptibilities*, (Clarendon Press, Oxford, 1932)

H. P. Kelly, "Frequency-dependent polarizability of atomic oxygen calculated by many-body theory" Phys. Rev. **182**, 84 - 89 (1969)

G. W. Chantry, "Polarizability theory of the Raman effect," in *The Raman Effect*, ed. A. Anderson, v. 1 and -. ch 2 (Dekker, N.Y., 1971)

J. N. Silverman and J. Hinze, "Calculation of high-order electric polarizabilites via the perturbational-variational Rayleigh-Ritz formalism: Application to the hydrogenic Stark effect" Phys. Rev. A **37**, 1208-1222 (1987)

M. Kutzner, H. P. Kelly, D. J. Larson and Z. Altun, "Calculation of frequency-dependent polarizabilities with application to photodetachment threshold shift in a strong laser field" Phys. Rev. **38**, 5107 (1988)

H. P. Saha, "Ab initio calculation of frequency-dependent atomic dipole polarizability" Phys. Rev. **4**, 2865 - 2870 (1993)

[100] **Autler-Townes effect**

S. H. Autler and C. H. Townes, "Stark effect in rapidly varying fields" Phys. Rev. **100**, 703-722 (1955)

S. Feneuille and M. G. Schweighofer, "Conditions for the observation of the Autler-Townes effect in a two step resonance experiment" J. de Physique **36**, 781-786 (1975)

A. Schabert, R. Keil and P. E. Toschek, "Dependence on light amplitude of the dynamic stark splitting of an optical line" Opt. Comm. **13**, 265-267 (1975)

C. Delsart and J.-C. Keller, "Observation of the optical Autler-Townes splitting in neon gas with a cascade level scheme" J. Phys. B **9**, 2769-2775 (1976)

J. L. Picqué and J. Pinard, "Direct observation of the Autler-Townes effect in the optical range" J. Phys. B **9**, L77-L81 (1976)

H. R. Gray and C. R. Stroud, "Autler-Townes effect in double optical resonance" Opt. Comm. **25**, 359-62 (1978)

G. S. Agarwal and P. A. Naragana, "Effect of probe field strength and the fluctuations of the exciting laser on the asymmetry of Autler & Townes doublet" Opt. Comm. **30**, 364-368 (1979)

M. S. Zubairy, "Quantum state measurement via Autler-Townes spectroscopy" Physics Letters A **222**, 91-96 (1996)

H. S. Freedhoff and Z. Ficek, "Resonance fluorescence and Autler-Townes spectra of a two-level atom driven by two fieldsof equal frequencies" Phys. Rev. **55**, 1234 - 1238 (1997)

A. M. Herkommer, W. P. Schleich and M. S. Zubairy, "Autler-Townes microscopy on a single atom" J. Mod. Opt. **44**, 2507 - 2513 (1997)

M. Wollenhaupt, A. Assion, O. Bazhan, C. Horn, D. Liese, C. Sarpe-Tudoran, M. Winter and T. Baumert, "Control of interferences in an Autler-Townes doublet: Symmetry of control parameters" Phys. Rev. A **68**, 015401 (2003)

R. Garcia-Fernandez, A. Ekers, J. Klavins, L. P. Yatsenko, N. N. Bezuglov, B. W. Shore and K. Bergmann, "Autler-Townes effect in a sodium molecular-ladder scheme" Phys. Rev. **71**, 023401 (2005)

[101] **Raman spectroscopy**

G. Herzberg, *Molecular Spectra and Molecular Structure II. Infrared and Raman Spectra of Polyatomic Molecules*, (Van Nostrand, N.Y., 1950)

A. Anderson, *The Raman Effect I. Principles*, (Dekker, N.Y., 1971)

A. Anderson, *The Raman Effect II. Applications*, (Dekker, N.Y., 1971)

J. A. Konigstein, *Introduction to the Theory of the Raman Effect*, (Reidel, 1972)

D. A. Long, *Raman Spectroscopy*, (McGraw-Hill, N.Y., 1977)

A. Weber, ed. *Raman Spectroscopy of Gases and Liquids*, (Springer, N.Y., 1979)

D. Lee and A. C. Albrecht, "A unified view of Raman, resonance Raman and fluorescence spectroscopy (and their analogues in two-photon absorption)" Adv. Infrared Raman Spect. **12**, 179-213 (1985)

H. Kono, Y. Nomurea and Y. Fujimura, "A theoretical study of origins of resonance Raman and resonance fluorescence using a split-up of the emission correlation function" Adv. Chem. Phys. **80**, 403-462 (1991)

L. D. Ziegler, "On the difference between resonance Raman scattering and resonance fluorescence in molecules - an experimental view" Accounts Chem. Res. **27**, 1-8 (1994)

[102] **Franck-Condon pumping**

H. A. Weaver and M. J. Mumma, "Infrared molecular emissions from comets " Ap. J. **276**, 782-797 (1984)

W. Meier, H. Zacharias and K. H. Welge, "Vibrational excitation of a H2 molecular beam by Franck-Condon pumping" Chem. Phys. Lett. **163**, 88-92 (1989)

[103] **Stimulated Raman processes**

R. W. Hellwarth, "Theory of stimulated Raman scattering" Phys. Rev. **130**, 1850 (1963)

V. A. Zubov, M. M. Sushchinskii and I. K. Shuvalov, "Stimulated Raman scattering of light" Sov. Phys. Usp. **7**, 419-433 (1964)

Y. R. Shen and N. Bloembergen, "Theory of stimulated Brilloun and Raman scattering" Phys. Rev. **137**, A1787-1805 (1965)

N. Bloembergen, "The stimulated Raman effect" Am. J. Phys **35**, 989-1023 (1967)

C.-S. Wang, "Theory of stimulated Raman scattering" Phys. Rev. **182**, 482-494 (1969)

R. L. Carman, F. Shimizu, C. S. Wang and N. Bloembergen, "Theory of Stokes pulse shapes in transient stimulated Raman scattering" Phys. Rev. A **2**, 60-72 (1970)

P. Lallemand, "The Stimulated Raman effect," in *The Raman Effect*, ed. A. Anderson, v. 1, c. 5 and 287-342 (Dekker, 1971)

J. A. Konigstein, *Introduction to the Theory of the Raman Effect*, (Reidel, 1972)

A. Weber, ed. *Raman Spectroscopy of Gases and Liquids*, (Springer, N.Y., 1979)

M. G. Raymer and J. Mostowski, "Stimulated Raman scattering: Unified treatment of spontaneous initiation and spatial propagation" Phys. Rev. A **24**, 1980-93 (1981)

[104] **Stimulated emission pumping (SEP)**

C. Kittrell, E. Abramson, J. L. Kinsey, S. A. McDonald, D. E. Reisner, R. W. Field and D. H. Katayama, "Selective vibrational excitation by stimulated emission pumping" J. Chem. Phys. **75**, 2056 -59 (1981)

H.-L. Dai and R. W. Field, ed. *Molecular dynamics and spectroscopy by stimulated emission pumping*, (World Scientific, Singapore, 1994)

M. Silva, R. Jongma, R. W. Field and A. M. Wodtke, "The dynamics of "stretched molecules": Experimental studies of highly vibraioally excited molecules with stimulated emission pumping" Ann. Rev. Phys. Chem. **52**, 811-52 (2001)

[105] **Coherent anti-Stokes Raman scattering (or spectroscopy) (CARS)**

P. D. Maker and R. W. Terhune, "Study of optical effects due to an induced polarization third order in the electric field strength" Phys. Rev. **137**, A801 - A818 (1965)

M. A. Yuratich and D. C. Hanna, "Coherent anti-Stokes Raman spectroscopy (CARS) selection rules, depolarization ratios and rotational structure" Mol. Phys. **33**, 671-682 (1977)

W. M. Tolles, J. W. Nibler, J. R. McDonald and A. B. Harvey, "A review of the theory and application of coherent anti-Stokes Raman spectroscopy (CARS)" App. Spect. **31**, 253-271 (1977)

M. D. Duncan, J. Reintjes and T. J. Manuccia, "Scanning coherent anti-Stokes Raman microscope" Opt. Lett. **7**, 350 (1982)

M. O. Scully, G. W. Kattawar, R. P. Lucht, T. Opatrn, H. Pilloff, A. Rebane, A. V. Sokolov and M. S. Zubairy, "FAST CARS: Engineering a laser spectroscopic technique for rapid identification of bacterial spores" Proc Natl Acad Sci U S A. 2002 August 20; 99(17): 1099411001. **99**, 17 (2002)

S. Postma, A. C. v. Rhijn, J. P. Korterik, P. Gross, J. L. Herek and H. L. Offerhaus, "Application of spectral phase shaping to high resolution CARS spectroscopy" Opt. Express **16**, 7985-7996 (2008)

[106] **Counterintuitive pulse sequence** see also [140]

B. W. Shore, "Examples of counter-intuitive physics (atomic and molecular excitation)" Contemp. Phys. **36**, 15-28 (1995)

A. A. Rangelov, J. Piilo and N. V. Vitanov, "Counterintuitive transitions between crossing energy levels" Phys. Rev. **72**, 053404 (2005)

[107] **Stimulated Raman adiabatic passage (STIRAP)** see also [3]

J. R. Kuklinski, U. Gaubatz, F. T. Hioe and K. Bergmann, "Adiabatic population transfer in a three-level system driven by delayed laser pulses" Phys. Rev. A **40**, 6741-44 (1989)

G. Z. He, A. Kuhn, S. Schiemann and K. Bergmann, "Population transfer by stimulated Raman scattering with delayed pulses and by the SEP method: A comparative study" J. Opt. Soc. Am. B **7**, 1960-9 (1990)

U. Gaubatz, P. Rudecki, S. Schiemann and K. Bergmann, "Population transfer between molecular vibrational levels. A new concept and experimental results" J. Chem. Phys. **92**, 5363-76 (1990)

B. W. Shore, K. Bergmann, J. Oreg and S. Rosenwaks, "Multilevel adiabatic population transfer" Phys. Rev A **44**, 7442-9 (1991)

G. Coulston and K. Bergmann, "Population transfer by stimulated Raman scattering with delayed pulses: Analytical results for multilevel systems" J. Chem. Phys. **96**, 3467-75 (1992)

A. Kuhn, S. Schiemann, G. Z. He, G. Coulston, W. S. Warren and K. Bergmann, "Population transfer by stimulated Raman scattering with delayed pulses using spectrally broad light" J. Chem. Phys. **96**, 4215-23 (1992)

M. P. Fewell, B. W. Shore and K. Bergmann, "Coherent population transfer among three states: Full algebraic solution and the relevance of diabatic processes in transfer by delayed laser pulses." Australian J. Phys. **50**, 281-304 (1997)

K. Bergmann, H. Theuer and B. W. Shore, "Coherent population transfer among quantum states of atoms and molecules" Rev. Mod. Phys. **70**, 1003-1023 (1998)

[108] **Dark states and population trapping**

H. R. Gray, R. M. Whitley and C. R. Stroud, Jr., "Coherent trapping of atomic populations" Opt. Lett. **3**, 218, (1978)

P. M. Radmore and P. L. Knight, "Population trapping and dispersion in a three-level system" J. Phys. B **15**, 561-73 (1982)

S. Swain, "Conditions for population trapping in a three-level system" J. Phys. B **15**, 3405-3411 (1982)

B. J. Dalton and P. L. Knight, "The effects of laser field fluctuations on coherent population trapping" J. Phys. B **15**, 3997-4015 (1982)

F. T. Hioe and C. E. Carroll, "Coherent population trapping in N-level quantum systems" Phys. Rev. A **37**, 3000-5 (1988)

M. R. Doery, M. T. Widmer, M. J. Bellanca, W. F. Buell, T. H. Bergeman, H. Metcalf and E. J. D. Vredenbregt, "Population accumulation in dark states and subrecoil laser cooling" Phys. Rev. A **52**, 2295-2301 (1995)

E. Arimondo, "Coherent population trapping in laser spectroscopy" Prog. Optics **35**, 259-356 (1996)

V. Milner and Y. Prior, "Multilevel dark states: Coherent population trapping with elliptically polarized incoherent light" Phys. Rev. Lett. **80**, 940-943 (1998)

R. Wynands and A. Nagel, "Precision spectroscopy with coherent dark states" App. Phys. B **68**, 1-25 (1999)

S. Kulin, Y. Castin, M. Ol'shanii, E. Peik, B. Saubamea, M. Leduc and C. Cohen-Tannoudji, "Exotic quantum dark states" Euro. Phys. J. D **7**, 279-84 (1999)

M. Fleischhauer and M. D. Lukin, "Dark-state polaritons in electromagnetically induced transparency" Phys. Rev. Lett. **84**, 5094-5097 (2000)

Z. Kis, W. Vogel, L. Davidovich and N. Zagury, "Dark SU(2) states of the motion of a trapped ion" Phys. Rev. A **63**, 1-7 (2001)

[109] **STIRAP demonstrated**

J. R. Kuklinski, U. Gaubatz, F. T. Hioe and K. Bergmann, "Adiabatic population transfer in a three-level system driven by delayed laser pulses" Phys. Rev. A **40**, 6741-44 (1989)

U. Gaubatz, P. Rudecki, S. Schiemann and K. Bergmann, "Population transfer between molecular vibrational levels. A new concept and experimental results" J. Chem. Phys. **92**, 5363-76 (1990)

G. Z. He, A. Kuhn, S. Schiemann and K. Bergmann, "Population transfer by stimulated Raman scattering with delayed pulses and by the SEP method: A comparative study" J. Opt. Soc. Am. B **7**, 1960-9 (1990)

H.-G. Rubahn and K. Bergmann, "Effect of laser-induced vibrational bond stretching in atom-diatom collisions" Ann. Rev. Phys. Chem. **41**, 735-73 (1990)

G. Coulston and K. Bergmann, "Population transfer by stimulated Raman scattering with delayed pulses: Analytical results for multilevel systems" J. Chem. Phys. **96**, 3467-75 (1992)

A. Kuhn, S. Schiemann, G. Z. He, G. Coulston, W. S. Warren and K. Bergmann, "Population transfer by stimulated Raman scattering with delayed pulses using spectrally broad light" J. Chem. Phys. **96**, 4215-23 (1992)

S. Schiemann, A. Kuhn, S. Steuerwald and K. Bergmann, "Efficient coherent population transfer in the NO molecule using pulsed lasers" Phys. Rev. Lett. **71**, 3637 (1993)

[110] **STIRAP with sublevels**

Z. Kis and S. Stenholm, "Nonadiabatic dynamics in the dark subspace of a multilevel stimulated Raman adiabatic passage process " Phys. Rev. A **64**, 063406 (2001)

Z. Kis, A. Karpati, B. W. Shore and N. V. Vitanov, "Stimulated Raman adiabatic passage among degenerate-level manifolds" Phys. Rev. A **70**, 053405 (2004)

I. Thanopulos, P. Král and M. Shapiro, "Complete control of population transfer between clusters of degenerate states" Phys. Rev. Lett. **92**, 113003 (2004)

Z. Kis, N. V. Vitanov, A. Karpati, C. Barthel and K. Bergmann, "Creation of arbitrary coherent superposition states by stimulated Raman adiabatic passage" Phys. Rev. A **72**, 033403 (2005)

A. D. Boozer, "Stimulated Raman adiabatic passage in a multilevel atom" Phys. Rev. A **77**, 023411 (2008)

[111] **STIRAP in Neon, for transfer**

J. Martin, B. W. Shore and K. Bergmann, "Coherent population transfer in multilevel systems with magnetic sublevels. II. Algebraic analysis" Phys. Rev. A **52**, 583-593 (1995)

J. Martin, B. W. Shore and K. Bergmann, "Coherent population transfer in multilevel systems with magnetic sublevels. III. Experimental results" Phys. Rev. A **54**, 1556-1569 (1996)

B. W. Shore, J. Martin, M. P. Fewell and K. Bergmann, "Coherent population transfer in multilevel systems with magnetic sublevels. I. Numerical studies" Phys. Rev. A **52**, 566-582 (1995)

[112] **STIRAP along a chain**

B. W. Shore, K. Bergmann, J. Oreg and S. Rosenwaks, "Multilevel adiabatic population transfer" Phys. Rev. A **44**, 7442-7447 (1991)

P. Marte, P. Zoller and J. L. Hall, "Coherent atomic mirrors and beam splitters by adiabatic passage in multilevel systems" Phys. Rev. A **44**, R4118-21 (1991)

N. V. Vitanov, B. W. Shore and K. Bergmann, "Adiabatic population transfer in multistate systems via dressed intermediate states" Euro. Phys. J. D **4**, 15-29 (1998)

N. V. Vitanov and S. Stenholm, "Adiabatic population transfer via multiple intermediate states" Phys. Rev. A **60**, 3820-32 (1999)

[113] **STIRAP mechanism in multilevel linkages**

Z. Kis, A. Karpati, B. W. Shore and N. V. Vitanov, "Stimulated Raman adiabatic passage among degenerate-level manifolds" Phys. Rev. A **70**, 053405 (2004)

[114] **Tripod system for superpositions**

R. Unanyan, M. Fleischhauer, B. W. Shore and K. Bergmann, "Robust creation and phase-sensitive probing of superposition states via stimulated Raman adiabatic passage (STIRAP) with degenerate dark states" Opt. Comm **155**, 144-154 (1998)

[115] **Tripod system**

R. G. Unanyan, K. Bergmann and B. W. Shore, "Laser-driven population transfer in four-level atoms: Consequences of non-Abelian geometrical adiabatic phase factors" Phys. Rev. A **59**, 2910-2919 (1999)

R. G. Unanyan, N. V. Vitanov, B. W. Shore and K. Bergmann, "Coherent properties of a tripod system coupled via a continuum" Phys. Rev. A **61**, U402-U410. (2000)

Z. Kis and S. Stenholm, "Nonadiabatic dynamics in the dark subspace of a multilevel stimulated Raman adiabatic passage process" Phys. Rev. A **64**, 063406 (2001)

Z. Kis and F. Renzoni, "Qubit rotation by stimulated Raman adiabatic passage" Phys. Rev. A **65**, 032318 (2002)

E. Paspalakis and Z. Kis, "Pulse propagation in a coherently prepared multilevel medium" Phys. Rev. A **66**, 025802 (2002)

A. Karpati, Z. Kis and P. Adam, "Engineering mixed states in a degenerate four-state system" Phys. Rev. Lett. **93**, 193003 (2004)

R. G. Unanyan and M. Fleischhauer, "Geometric phase gate without dynamical phases" Phys. Rev. A **69**, 050302 (2004)

[116] **General RWA**

J. Wong, J. C. Garrison and T. H. Einwohner, "Multiple-time scale perturbation theory applied to laser excitation of atoms and molecules" Phys. Rev. A **13**, 674-87 (1976)

T. H. Einwohner, J. Wong and J. C. Garrison, "Analytical solutions for laser excitation of multilevel systems in the rotating-wave approximation" Phys. Rev. A **14**, 1452-1456 (1976)

[117] **Analytic solutions for N-state chain** see also [120, 121]

T. H. Einwohner, J. Wong and J. C. Garrison, "Analytical solutions for laser excitation of multilevel systems in the rotating-wave approximation" Phys. Rev. A **14**, 1452-1456 (1976)

A. A. Makarov, "Coherent excitation of equidistant multilevel systems in a resonant monochromatic field" Sov. Phys. JETP **45**, 918-924 (1977)

J. H. Eberly, B. W. Shore, Z. Bialynicka-Birula and I. Bialynicki-Birula, "Coherent dynamics of N-level atoms and molecules I. Numerical experiments" Phys. Rev. A **16**, 2038-47 (1977)

Z. Bialynicka-Birula, I. Bialynicki-Birula, J. H. Eberly and B. W. Shore, "Coherent dynamics of N-Level atoms and molecules. II. Analytic solutions" Phys. Rev. A **16**, 2048-2054 (1977)

B. W. Shore and M. A. Johnson, "Coherence vs. incoherence in stepwise laser excitation" J. Chem. Phys. **68**, 5631 (1978)

R. J. Cook and B. W. Shore, "Coherent dynamics of N-level atoms and molecules III. An analytically soluble periodic case" Phys. Rev. A **20**, 539-44 (1979)

T. H. Einwohner, J. Wong and J. C. Garrison, "Effects of alternative transition sequences on coherent photoexcitation" Phys. Rev. A **20**, 940-947 (1979)

F. T. Hioe and J. H. Eberly, "Multiple-laser excitation of multilevel atoms" Phys. Rev. A **29**, 1164-7 (1984)

M. Kozierowski, "On an exactly solvable N-level system coupled to N-1 field modes" J. Phys. B **19**, L535-L539 (1986)

V. S. Letokhov and A. A. Makarov, "Excitation of multilevel molecular systems by laser ir field" Appl. Phys. B **16**, 47-57 (2005)

[118] **Special functions and classical polynomials**

I. N. Sneddon, *Special Functions of Mathematical Physics and Chemistry*, (Oliver and Boyd, London, 1956)

M. Abramowitz and I. A. Stegun, ed. *Handbook of mathematical functions*, (U. S. Government Printing Office, Washington, D.C., 1964)

W. Magnus, F. Oberhettinger and R. P. Soni, *Formulas and Theorems for the Special Functions of Mathematical Physics*, (Springer, N.Y., 1966)

Y. L. Luke, *The Special Functions and Their Approximations*, (Academic, N.Y., 1969)

N. N. Lebedev, *Special Functions and Their Application*, (Dover, 1972)

A. Erdelyi, W. Magnus, F. Oberhettinger and F. G. Tricomi, ed. *Higher Transcendental Functions*, (Dover, Mineola, N.Y., 2006)

[119] **The Harmonic oscillator**

R. P. Feynman and A. R. Hibbs, *Quantum Mechanics and Path Integrals*, (McGraw-Hill, N.Y., 1965) Chap. 8

P. Carruthers and M. M. Nieto, "Coherent states and the forced harmonic oscillator" Am. J. Phys. **7**, 537 (1965)

M. Moshinsky and O. Novaro, "Harmonic oscillator in atomic and molecular physics" J. Chem. Phys. **48**, 4162-4180 (1968)

H. R. Lewis, Jr. and W. B. Riesenfeld, "An exact quantum theory of the time-dependent harmonic oscillator and of a charged particle in a time-dependent electromagnetic field" J. Math. Phys. **10**, 1458-1473 (1969)

M. Moshinsky, *The Harmonic Oscillator in Modern Physics; from Atoms to Quarks*, (Gordon and Breach, New York, 1969)

S. Carusotto, "Relaxation of a driven harmonic oscillator" Phys. Rev. A **11**, 1407-1413 (1975)

C. E. Wulfman and B. G. Wybourne, "The Lie group of Newton's and Lagrange's equations for the harmonic oscillator" J. Phys. A **9**, 507-18 (1976)

E. G. Harris, "Quantum theory of the damped harmonic oscillator" Phys. Rev. A **42**, 3685-94 (1990)

M. Moshinsky and Y. F. Smirnov, *Harmonic Oscillator in Modern Physics*, (Harwood Academic, Amsterdam, 1996)

S. C. Bloch, *Introduction to Classical and Quantum Harmonic Oscillators*, (Wiley-Interscience, New York, 1997)

C. K. Law, J. H. Eberly and B. Kneer, "Preparation of an arbitrary density matrix of a harmonic oscillator" J. Mod. Opt. **44**, 2149-58 (1997)

[120] **Two-state dynamics in an N-state chain**

B. W. Shore and R. J. Cook, "Coherent dynamics of N-level atoms and molecules IV. Two- and three-level behavior" Phys. Rev. A **20**, 1958 (1979)

B. W. Shore, "Two-level behavior of coherent excitation of multilevel systems" Phys. Rev. A **34**, 1413 (1981)

[121] **The pseudospin model**

R. J. Cook and B. W. Shore, "Coherent dynamics of N-level atoms and molecules III. An analytically soluble periodic case" Phys. Rev. A **20**, 539-44 (1979)

J. Oreg and S. Goshen, "Spherical modes in N-Level systems" Phys. Rev. A **29**, 3205-3207 (1984)

F. T. Hioe, "N-level quantum systems with SU(2) dynamic symmetry" J. Opt. Soc. B **4**, 1327 (1987)

H. Mäkelä and K.-A. Suominen, "Inert states of spin-S systems" Phys. Rev. Lett. **99**, 190408 (2007)

V. Kostak, G. M. Nikolopoulos and I. Jex, "Perfect state transfer in networks of arbitrary topology and coupling configuration" Phys. Rev. A **75**, 042319 (2007)

[122] **Branched chain**

T. H. Einwohner, J. Wong and J. C. Garrison, "Effects of alternative transition sequences on coherent photoexcitation" Phys. Rev. A **20**, 940-947 (1979)

B. W. Shore, "Gating of population flow in resonant multiphoton excitation" Phys. Rev. A **29**, 1578-1582 (1984)

S. P. Krinitzky and D. T. Pegg, "Coherent irradiation of multilevel atoms in branched and cyclic configurations" Phys. Rev. A **33**, 403 - 406 (1986)

B. W. Shore and N. V. Vitanov, "Overdamping in coherently driven quantum systems" Contemp. Phys. **47**, 341-62 (2007)

[123] **Loop linkage**

S. J. Buckle, S. M. Barnett, P.L.Knight, M.A.Lauder and D. T. Pegg, "Atomic interferometers: Phase-dependence in multilevel atomic transitions" Optica Acta **33**, 1129-40 (1986)

W. Maichen, F. Renzoni, I. Mazets, E. Korsunsky and L. Windholz, "Transient coherent population trapping in a closed loop interaction scheme" Phys. Rev. A **53**, 3444-3448 (1996)

R. G. Unanyan, L. P. Yatsenko, K. Bergmann and B. W. Shore, "Population inversion using laser and quasistatic magnetic field pulses" Opt. Comm. **139**, 43-7 (1997)

R. G. Unanyan, L. P. Yatsenko, K. Bergmann and B. W. Shore, "Laser-induced adiabatic atomic reorientation with control of diabatic losses" Opt. Comm. **139**, 48-54 (1997)

A. A. Rangelov, N. V. Vitanov and B. W. Shore, "Population trapping in three-state quantum loops revealed by Householder reflections" Phys. Rev. A **77**, 033404 (2008)

[124] **Coherence-enhanced field creation**

M. Oberst, J. Klein and T. Halfmann, "Enhanced four-wave mixing in mercury isotopes, prepared by stark-chirped rapid adiabatic passage" Optics Comm. **264**, 463-470 (2006)

[125] **Morris-Shore transformation**

J. R. Morris and B. W. Shore, "Reduction of degenerate two-level excitation to independent two-state systems" Phys. Rev. A **27**, 906-912 (1983)

N. V. Vitanov, Z. Kis and B. W. Shore, "Coherent excitation of a degenerate two-level system by an elliptically polarized laser pulse" Phys. Rev. A **68**, 3414 (2003)

Z. Kis, A. Karpati, B. W. Shore and N. V. Vitanov, "Stimulated Raman adiabatic passage among degenerate-level manifolds" Phys. Rev. A **70**, 053405 (2004)

E. S. Kyoseva and N. V. Vitanov, "Coherent pulsed excitation of degenerate multistate systems: Exact analytic solutions" Phys. Rev. A **73**, 023420 (2006)

A. A. Rangelov, N. V. Vitanov and B. W. Shore, "Extension of the Morris-Shore transformation to multilevel ladders" Phys. Rev. A **74**, 053402 (2006); erratum Phys. Rev. A **76** 039901 (2007)

G. S. Vasilev, S. S. Ivanov and N. V. Vitanov, "Degenerate Landau-Zener model: Analytical solution" Phys. Rev. A **75**, 013417 (2007)

E. S. Kyoseva, N. V. Vitanov and B. W. Shore, "Physical realization of coupled Hilbert-space mirrors for quantum-state engineering" J. Mod. Opt. **54**, 2237-2257 (2007)

[126] **Creating an arbitrary atomic state** see also [127]

V. Ramakrishna, R. Ober, X. Sun, O. Steuernagel, J. Botina and H. Rabitz, "Explicit generation of unitary transformations in a single atom or molecule" Phys. Rev. A **61**, 032106 (2000)

V. Ramakrishna, K. L. Flores, H. Rabitz and R. J. Ober, "Quantum control by decompositions of SU(2)" Phys. Rev. A **62**, 053409 (2000)

S. G. Schirmer, H. Fu and A. I. Solomon, "Complete controllability of quantum systems" Phys. Rev. A **63**, 063410 (2001)

S. G. Schirmer, A. I. Solomon and J. V. Leahy, "Criteria for reachability of quantum states" J. Phys. A **35**, 8551-8562 (2002)

C. Altafini, "Controllability of quantum mechanical systems by root space decomposition of SU(N)" J. Math. Phys. **43**, 2051-2062 (2002)

G. Turinici, V. Ramakhrishna, B. Li and H. Rabitz, "Optimal discrimination of multiple quantum systems: Controllability analysis" J. Phys. A **37**, 273-282 (2004)

D. Sugny, A. Keller, O. Atabek, D. Daems, C. M. Dion, S. Gurin and H. R. Jauslin, "Laser control for the optimal evolution of pure quantum states" Phys. Rev. A **71**, 063402 (2005)

R. Cabrera, C. Rangan and W. E. Baylis, "Sufficient condition for the coherent control of n-qubit systems" Phys. Rev. A **76**, 033401 (2007)

J. Werschnik and E. K. U. Gross, "Quantum optimal control theory" J. Phys. B **40**, R175-R211 (2007)

[127] **Quantum atomic-state superpositions**

J. Cohn, "Superpositon and quantum mechanics" Int. J. Theo. Phys. **25**, 829-862 (1986)

M. K. Bennett and D. J. Foulis, "Superposition in quantum and classical mechanics" Found. Phys **20**, 733-744 (1990)

B. M. Garraway and P. L. Knight, "Quantum superpositions, phase distributions and quasi-probabilities" Physica Scripta **48**, 66-76 (1993)

J. I. Cirac and P. Zoller, "Preparation of macroscopic superpositions in many-atom systems" Phys. Rev. A **50**, R2799-R2802 (1994)

B. M. Garraway and P. L. Knight, "Evolution of quantum superpositions in open environments: quantum trajectories, jumps, and localization in phase space" Phys. Rev. A **50**, 2548-63 (1994)

L. K. Grover, "Quantum computing - The advantages of superposition" Science **280**, 228-228 (1998)

J. I. Cirac, M. Lewenstein, K. Molmer and P. Zoller, "Quantum superposition states of Bose-Einstein condensates" Phys. Rev. A **57**, 1208-18 (1998)

Y. Makhlin, G. Schön and A. Shnirman, "Quantum-state engineering with Josephson-junction devices" Rev. Mod. Phys. **73**, 357 - 400 (2001)

M. R. Dowling, S. D. Bartlett, T. Rudolph and R. W. Spekkens, "Observing a coherent superposition of an atom and a molecule" Phys. Rev. **74**, 052113 (2006)

M. P. Silverman, *Quantum Superposition: Counterintuitive Consequences of Coherence, Entanglement, and Interference*, (Springer, Berlin, 2008)

[128] **Schrödinger cat states**

E. Schrödinger, "Present status of quantum mechanics" Naturwiss. **23**, 823-8 (1935)

J. J. Slosser, P. Meystre and E. M. Wright, "Generation of macroscopic superpositions in a micromaser" Opt. Lett. **15**, 233-35 (1990)

V. Buzek, H. Moya-Cessa, P. L. Knight and S. J. D. Phoenix, ""Schrödinger cat" states in the resonant Jaynes-Cummings model: Collapse and revival of oscillations of the photon number distribution" Phys. Rev. **45**, 8190-8203 (1992)

P. Knight, "Practical Schrödinger's cats" Nature **357**, 438-9 (1992)

P. Goetsch, R. Graham and F. Haake, "Schrödinger cat states and single runs for the damped harmonic oscillator" Phys. Rev. A **51**, 136-142 (1995)

C. Monroe, D. M. Meekhof, B. E. King and D. J. Wineland, "A "Schrödinger cat" superposition state of an atom" Science **272**, 1131-6 (1996)

C. C. Gerry and P. L. Knight, "Quantum superpositions and Schrödinger cat states in quantum optics" Am. J. Phys. **65**, 964-74 (1997)

G. S. Agarwal, R. R. Puri and R. P. Singh, "Atomic Schrödinger cat states" Phys. Rev. A **56**, 2249-2254 (1997)

J. R. Friedman, V. Patel, W. Chen, S. K. Tolpygo and J. E. Lukens, "Quantum superposition of distinct macroscopic states" Nature **406**, 43-46 (2000)

[129] **Adiabatic procedures for superpositions**

A. R. Karapetyan and A. D. Gazazyan, "Creation of superposition states in an external magnetic field by using STIRAP" Laser Phys. **11**, 655-657 (2001)

Z. Kis, N. V. Vitanov, A. Karpati, C. Barthel and K. Bergmann, "Creation of arbitrary coherent superposition states by stimulated Raman adiabatic passage" Phys. Rev. A **72**, 33403 (2005)

N. Sangouard, S. Guérin, L. P. Yatsenko and T. Halfmann, "Preparation of coherent superposition in a three-state system by adiabatic passage" Phys. Rev. A **70**, 013415 (2004)

Y. Niu, S. Gong, R. Li and S. Jin, " Creation of atomic coherent superposition states via the technique of stimulated Raman adiabatic passage using a Lambda-type system with a manifold of levels" Phys. Rev. A **70**, 023805 (2004)

[130] **Wavepackets**

D. J. Tannor and S. A. Rice, "Coherent pulse sequence control of product formation in chemical reactions" Adv. Chem. Phys. **70**, 441-524 (1988)

G. Alber and P. Zoller, "Laser excitation of electronic wave packets in Rydberg atoms" Phys. Repts. **199**, 232-280 (1991)

B. M. Garraway and K.-A. Suominen, "Wave-packet dynamics: New physics and chemistry in femto-time" Repts. Prog. Phys. **58**, 365-419 (1995)

D. W. Schumacher, J. H. Hoogenraad, D. Pinkos and P. H. Bucksbaum, "Programmable cesium Rydberg wave packets" Phys. Rev. A **52**, 4719-26 (1995)

J. Cao and K. R. Wilson, "A simple physical picture for quantum control of wave packet localization" J. Chem. Phys. **107**, 1441-1450 (1997)

R. J. Gordon and S. A. Rice, "Active control of the dynamics of atoms and molecules" Ann. Rev. Phys. Chem. **48**, 601-641 (1997)

S. Kulin, B. Saubamea, E. Peik, J. Lawall, T. W. Hijmans, M. Leduc and C. Cohen-Tannoudji, "Coherent manipulation of atomic wave packets by adiabatic transfer" Phys. Rev. Lett. **78**, 4185-8 (1997)

M. W. Noel and C. R. Stroud, Jr., "Shaping an atomic electron wave packet" Opt. Express **1**, 176-185 (1997)

B. M. Garraway and K. A. Suominen, "Adiabatic passage by light-induced potentials in molecules" Phys. Rev. Lett. **80**, 932-935 (1998)

L. E. E. de Araujo, I. A. Walmsley and C. R. Stroud, Jr., "Analytic solution for strong-field quantum control of atomic wave packets" Phys. Rev. Lett. **81**, 955-8 (1998)

A. Assion, T. Baumert, M. Geisler, V. Seyfried and G. Gerber, "Mapping of vibrational wave-packet motion by femtosecond time-resolved kinetic energy time-of-flight mass spectroscopy" Euro. Phys. J. D **4**, 145-9 (1998)

R. M. Koehl, S. Adachi and K. A. Nelson, "Direct visualization of collective wavepacket dynamics" J. Phys. Chem. A **103**, 10260 -10267 (1999)

T. Seideman, "On the dynamics of rotationally broad, spatially aligned wave packets" J. Chem. Phys. **115**, 5965-5973 (2001)

B. M. Garraway and K. A. Suominen, "Wave packet dynamics in molecules" Contemp. Phys. **43**, 97-114 (2002)

[131] **STIRAP for Zeeman coherences**

R. G. Unanyan, B. W. Shore and K. Bergmann, "Preparation of an N-component maximal coherent superposition state using the stimulated Raman adiabatic passage method" Phys. Rev. A **63**, 517-520 (2001)

Z. Kis and S. Stenholm, "Nonadiabatic dynamics in the dark subspace of a multilevel stimulated Raman adiabatic passage process" Phys. Rev. A **64**, 063406 (2001)

Z. Kis and F. Renzoni, "Qubit rotation by stimulated Raman adiabatic passage" Phys. Rev. A **65**, 032318 (2002)

Y. Niu, S. Gong, R. Li and S. Jin, "Creation of atomic coherent superposition states via the technique of stimulated Raman adiabatic passage using a Λ-type system with a manifold of levels" Phys. Rev. A **70**, 023805 (2004)

R. G. Unanyan, M. E. Pietrzyk, B. W. Shore and K. Bergmann, "Adiabatic creation of coherent superposition states in atomic beams" Phys. Rev. A **70**, 053404 (2004)

Z. Kis, A. Karpati, B. W. Shore and N. V. Vitanov, "Stimulated Raman adiabatic passage among degenerate-level manifolds" Phys. Rev. A **70**, 053405 (2004)

A. T. Avelar, L. A. de Souza, T. M. da Rocha Filho and B. Baseia, "Generation of superposed phase states via Raman interaction" J. Opt. B **6**, 383-386 (2004)

E. S. Kyoseva and N. V. Vitanov, "Coherent pulsed excitation of degenerate multistate systems: Exact analytic solutions" Phys. Rev. A **73**, 023420 (2006)

[132] **Fractional STIRAP**

N. V. Vitanov, K.-A. Suominen and B. W. Shore, "Creation of coherent atomic superpositions by fractional stimulated Raman adiabatic passage" J. Phys. B **32**, 4535-4546 (1999)

M. Amniat-Talab, S. Gurin and H.-R. Jauslin, "Decoherence-free creation of atom-atom entanglement in a cavity via fractional adiabatic passage" Phys. Rev. A **72**, 012339 (2005)

[133] **Half SCRAP**

L. P. Yatsenko, N. V. Vitanov, B. W. Shore, T. Rickes and K. Bergmann, "Creation of coherent superpositions using Stark-chirped rapid adiabatic passage" Opt. Comm. **204**, 413-423 (2002)

[134] **Transferring superpositions**

F. Renzoni and S. Stenholm, "Adiabatic transfer of atomic coherence" Opt. Comm. **189**, 69-77 (2001)

I. Thanopulos, P. Král and M. Shapiro, "Complete control of population transfer between clusters of degenerate states" Phys. Rev. Lett. **92**, 113003 (2004)

[135] **Quantum measurement theory**

J. Schwinger, "The algebra of microscopic measurement" Proc. Nat. Acad. Sci. **45**, 1542-53 (1959)

J. A. Wheeler and W. H. Zurek, ed. *Quantum Theory and Measurement*, (Princeton Univ. Press, Princeton, N.J., 1983)

R. J. Glauber, "Amplifiers, attenuators and the quantum theory of measurement," in *Frontiers of Quantum Optics*, ed. E. R. Pike and S. Sarkar Adam (Hilger, London, 1986), pp. 534-82

P. Grangier, "Optical quantum nondemolition measurements – experiments" Phys. Rep. **219**, 121-129 (1992)

P. Meystre, "Cavity quantum optics and the quantum measurement process," in *Prog. Optics*, **XXX**, ed. E. Wolf (Elsevier, New York, 1992), pp. 263-355

V. B. Braginsky and F. Y. Khalili, *Quantum Measurement*, (Cambridge Univ. Press, Cambridge, 1992)

V. P. Belavkin, "Nondemolition principle of quantum measurement theory" Found. Phys. **24**, 685-714 (1994)

P. Kwiat, H. Weinfurter, T. Herzog, A. Zeilinger and M. A. Kasevich, "Interaction-free measurement" Phys. Rev. Lett. **74**, 4763 - 4766 (1995)

D. J. Wineland, J. C. Bergquist, J. J. Bollinger and W. M. Itano, "Quantum effects in measurements on trapped ions" Physica Scripta **T59**, 286-93 (1995)

J. Schwinger and B.-G. Englert, *Quantum Mechanics: Symbolism of Atomic Measurements*, 2003)

[136] **Quantum tomography**

T. J. Dunn, I. A. Walmsley and S. Mukamel, "Experimental determination of the quantum -mechanical state of a molecular vibrational mode using fluorescence tomography" Phys. Rev. Lett. **74**, 884 (1995)

abibitemLeo96 U. Leonhardt, "Discrete Wigner function and quantum -state tomography" Phys. Rev. **53**, 2998 (1996)

G. M. D'Ariano, "Group theoretical quantum tomography" Acta Physica Slovaca **49**, 513-522 (1999)

G. M. D'Ariano and P. L. Presti, "Quantum tomography for measuring experimentally the matrix elements of an arbitrary quantum operation" Phys. Rev. Lett. **86**, 4195 - 4198 (2001)

Y.-x. Liu, L. F. Wei and F. Nori, "Quantum tomography for solid-state qubits" Europhys. Lett. **67**, 874-880 (2004)

[137] **Measuring superpositions**

R. Unanyan, M. Fleischhauer, B. W. Shore and K. Bergmann, "Robust creation and phase-sensitive probing of superposition states via stimulated Raman adiabatic passage (STIRAP) with degenerate dark states" Opt. Comm **155**, 144-154 (1998)

N. V. Vitanov, B. W. Shore, R. G. Unanyan and K. Bergmann, "Measuring a coherent superposition" Opt. Comm. **179**, 73-83 (1999)

A. Lezama, S. Barreiro, A. Lipsich and A. M. Akulshin, "Coherent two-field spectroscopy of degenerate two-level systems" Phys. Rev. A **61**, 013801 (1999)

N. V. Vitanov, "Measuring a coherent superposition of multiple states" J. Phys. B **33**, 2333-2346 (2000)

Z. Kis and S. Stenholm, "Measuring the density matrix by local addressing" Phys. Rev. A **64**, 5401-(2001)

[138] **STIRAP in Neon, for superpositions**

F. Vewinger, M. Heinz, R. G. Fernandez, N. V. Vitanov and K. Bergmann, "Creation and measurement of a coherent superposition of quantum states" Phys. Rev. Lett. **9121**, 3001 (2003)

F. Vewinger, M. Heinz, B. W. Shore and K. Bergmann, "Amplitude and phase control of a coherent superposition of degenerate states. I. Theory" Phys. Rev. A **75**, 043406 (2007)

F. Vewinger, M. Heinz, U. Schneider, C. Barthel and K. Bergmann, "Amplitude and phase control of a coherent superposition of degenerate states. II. Experiment" Phys. Rev. A **75**, 043407 (2007)

[139] **Analysis using conditional measurements**

V. Buzek, G. Drobny, G. Adam, R. Derka and P. L. Knight, "Reconstruction of quantum states of spin systems via the Jaynes principle of maximum entropy" J. Mod. Opt. **44**, 2607-27 (1997)

V. Buzek, R. Derka, G. Adam and P. L. Knight, "Reconstruction of quantum states of spin systems - from quantum Bayesian inference to quantum tomography" Ann. Phys. **266**, 454-496 (1998)

[140] **J. H. Eberly Festschrifts**

B. W. Shore, M. A. Johnson, K. C. Kulander and J. I. Davis, "The Livermore experience: Contributions of J. H. Eberly to laser excitation theory" Optics Express **8**, 28-43 (2001)

B. W. Shore and P. L. Knight, "Surprises in physics: overturning conventional wisdom" Laser Physics **15**, 1-7 (2005)

[141] **Sir Peter Knight Festschrift**

B. W. Shore, "Sir Peter Knight and the Jaynes-Cummings Model" J Mod Opt **54**, 2009 - 2016 (2007)

[142] **Traditional radiative transfer** see also [63]

R. K. Osborn and E. H. Klevans, "Photon transport theory" Ann. Phys. **15**, 105-140 (1961)

F. Kottler, "The elements of radiative transfer" Prog. Optics **3**, 1-28 (1964)

[143] **Refractive index**

G. Breit, "Quantum theory of dispersion" Rev. Mod. Phys. **4**, 504-575 (1932)

J. H. V. Vleck, *The Theory of Electric and Magnetic Susceptibilities*, (Oxford, N.Y., 1932)

S. M. Neamtan, "A quantum-mechanical definition of refractive index" Phys. Rev. **94**, 327 (1954)

C. A. Mead, "Quantum theory of the refractive index" Phys. Rev. **110**, 359-369 (1958)

C. A. Mead, "Theory of the complex refractive index" Phys. Rev. **120**, 854-866 (1960)

E. G. Harris, "Radiative transfer in dispersive media" Phys. Rev. **138**, B479-B485 (1965)

J. V. Kranendonk and J. E. Sipe, "Foundations of the macroscopic electromagnetic theory of dielectric media" Prog. Optics **15**, 245-350 (1977)

[144] **Radiative transfer with coherence**

E. Wolf, "New theory of radiative energy transfer in free electromagnetic fields" Phys. Rev. D **13**, 869-886 (1976)

M. S. Zubairy and E. Wolf, "Exact equations for radiation transfer of energy and momentum in free electromagnetic fields" Opt. Comm. **20**, 321-24 (1977)

E. C. G. Sudarshan, "Quantum theory of radiative transfer" Phys. Rev. A **23**, 2802-9 (1981)

[145] **Maxwell equations**

J. A. Stratton, *Electromagnetic Theory*, (McGraw-Hill, N.Y., 1941)

S. R. D. Groot, *The Maxwell Equations*, (North-Holland, Amsterdam, 1969)

E. A. Power and T. Thirunamachandran, "Maxwell's equations and the multipolar Hamiltonian" Phys. Rev. A **26**, 1800-1801 (1982)

E. A. Power and T. Thirunamachandran, "Quantum electrodynamics with nonrelativistic sources. I. Transformation to the multipolar formalism for second-quantized electron and Maxwell interacting fields" Phys. Rev. A **28**, 2649-2662 (1983)

[146] **Coherent states**

R. J. Glauber, "Coherent and incoherent states of the radiation field" Phys. Rev. **131**, 2766 (1963)

T. W. B. Kibble, " Some applications of coherent states," in *Cargese Lectures in Physics, vol 2*, ed. M. Levy (Gordon and Breach, N.Y., 1968),

F. T. Arecchi, E. Courtens, R. Gilmore and H. Thomas, "Atomic coherent states in quantum optics" Phys. Rev. **A6**, 2211 (1972)

J. R. Klauder and B-S Skagerstam ed. *Coherent States. Applications in Physics and Mathematical Physics*, (World Scientific, Singapore, 1985)

A. Perelomov, *Generalized Coherent States*, (Springer, Heidelberg, 1986)

C. C. Gerry and J. Kiefer, "Radial coherent states for the Coulomb problem" Phys. Rev. **A37**, 665-671 (1988)

V. Buzek, I. Jex and T. Quang, "K-Photon Coherent States" J. Mod. 'Opt. **37**, 159-163 (1990)

V. Buzek, A. D. Wilson-Gordon, P. L. Knight and W. K. Lai, "Coherent states in a finite-dimensional basis - Their phase properties and relationship to coherent states of light" Phys. Rev. A **45**, 8079-8094 (1992)

I. Jex, P. Torma and S. Stenholm, "Multimode Coherent States" J. Mod. 'Opt. **42**, 1377-1386 (1995)

[147] **Maxwell-Schrödinger and Maxwell-Bloch equations** see also [10, 148]

J. H. Eberly, "Optical pulse and pulse-train propagation in a resonant medium" Phys. Rev. Lett. **22**, 760 - 762 (1969)

S. L. McCall and E. L. Hahn, "Self-induced transparency" Phys. Rev. **183**, 457-485 (1969)

A. Icsevgi and W. E. Lamb, Jr., "Propagation of light pulses in a laser amplifier" Phys. Rev. **185**, 517 (1969)

V. S. Letokhov, "Nonlinear amplification of light pulses. III. Ultrashort pulse duration" Sov. Phys. JETP **29**, 221-226 (1969)

D. Dialetis, "Propagation of electromagnetic radiation through a resonant medium" Phys. Rev. A **2**, 1065-1075 (1970)

G. L. Lamb, Jr., "Analytical descriptions of ultrashort optical pulse propagation in a resonant medium" Rev. Mod. Phys. **43**, 99 (1971)

R. E. Slusher, "Self-induced transparency" Prog. Optics **12**, 53-100 (1974)

G. L. Lamb, Jr., "Amplification of coherent optical pulses" Phys. Rev. A **12**, 2052-2059 (1975)

H. Haken and H. Ohno, "Theory of ultra-short laser pulses" Opt. Comm. **16**, 205-208 (1976)

D. J. Kaup, "Coherent pulse propagation: a comparison of the complete solution with the McCall-Hahn theory and others" Phys. Rev. A **16**, 704-719 (1977)

F. P. Mattar, "Transient propagation of optical beams in active media" Appl. Phys. **17**, 53-62 (1978)

M. J. Konipnicki, P. D. Drummond and J. H. Eberly, "Theory of lossless propagation of simultaneous different-wavelength optical pulses" Opt. Comm. **36**, 313-316 (1981)

B. W. Shore, "Extending the definition of optical depth to coherent pulse propagation" Opt. Comm. **37**, 92 (1981)

O. Kocharovskaya, S. Y. Zhu, M. O. Scully, P. Mandel and Y. V. Radeonychev, "Generalization of the Maxwell-Bloch equations to the case of strong atom-field coupling" Phys. Rev. A **49**, 4928-4934 (1994)

Y. Castin, K. Mölmer, "Maxwell-Bloch equations: A unified view of nonlinear optics and nonlinear atom optics" Phys. Rev. **51**, R3426 - R3428 (1995)

K.-J. Boller, A. Imamoglu and S. E. Harris, "Observation of electromagnetically induced transparency" Phys. Rev. Lett. **66**, 2593-96 (1991)

S. E. Harris, "Refractive-index control with strong fields" Opt. Lett. **19**, 2018-20 (1994)

R. W. Ziolkowski, J. M. Arnold and D. M. Gogny, " Ultrafast pulse interactions with two-level atoms" Phys. Rev. **52**, 3082 - 3094 (1995)

J. P. Marangos, "Electromagnetically induced transparency" J. Mod. 'Opt. **45**, 471 - 503 (1998)

M. Fleischhauer, A. Imamoglu and J. P. Marangos, "Electromagnetically induced transparency: Optics in coherent media" Rev. Mod. Phys. **77**, 633 (2005)

[148] **Pulse propagation in multilevel systems**

J. Higginbotham, R. T. Deck and D. G. Ellis, "Distortionless optical pulse propagation in a three-level medium" Phys. Rev. A **16**, 2089-2092 (1977)

J. N. Elgin and Li Fuli, "Propagation effects in three level systems" Opt. Comm. **43**, 355-58 (1982)

A. P. Hickman, J. A. Paisner and W. K. Bischel, "Theory of multiwave propagation and frequency conversion in a Raman medium" Phys. Rev. **33**, 1788-1797 (1986)

V. V. Kozlov, O. Kocharovskaya and M. O. Scully, "Effective two-level Maxwell-Bloch formalism and coherent pulse propagation in a driven three-level medium" Phys. Rev. A **59**, 3986-3997 (1999)

E. Paspalakis and Z. Kis, "Pulse propagation in a coherently prepared multilevel medium" Phys. Rev. A **66**, 025802 (2002)

[149] **Nonlinear optics**

N. Bloembergen, *Nonlinear Optics*, (Benjamin, N.Y., 1965)

Y. R. Shen, "Recent advances in nonlinear optics" Rev. Mod. Phys. **48**, 1-32 (1976)

D. C. Hanna, M. A. Yuratich and D. Cotter, *Nonlinear Optics of Free Atoms and Molecules*, (Springer, Berlin, 1979)

M. S. Feld and V. S. Letokhov, ed. *Coherent Nonlinear Optics. Recent Advances*, (Springer, Berlin, 1980)

Y. R. Shen, *Principles of Nonlinear Optics*, (Wiley, N.Y., 1984)

N. B. Delone and V. P. Krainov, *Fundamentals of Nonlinear Optics of Atomic Gases*, (Wiley, N.Y., 1986)

R. W. Boyd, *Nonlinear Optics*, (Academic, New York, 2003) 2nd ed.

[150] **Matrices**

E. Bodewig, *Matrix Calculus*, (North-Holland, Amsterdam, 1956)

F. R. Gantmacher, *The Theory of Matrices*, (Chelsea, N.Y., 1959)

H. W. Turnbull, *The Theory of Determinants, Matrices and Invariants*, (Dover, N.Y., 1960)

R. A. Frazer, W. J. Duncan and A. R. Collar, *Elementary Matrices and Some Applications to Dynamics and Differential Equations*, (Cambridge Univ. Press, Cambridge, 1965)

J. H. Wilkinson and C. Reinsch, ed. *Linear Algebra*, (Springer, N.Y., 1971)

[151] **Campbell-Baker-Hausdorf formula**

see: http: //en.wikipedia.org/wiki/Baker-Campbell-Hausdorff_formula

[152] **Group theory**

H. Weyl, *The Theory of Groups and Quantum Mechanics*, (Dover, N.Y., 1950)

E. P. Wigner, *Group Theory and Its Application to the Quantum Mechanics of Atomic Spectra*, (Academic, N.Y., 1959)

M. Hamermesh, *Group Theory and its Application to Physical Problems*, (Addison-Wesley, Reading, Mass., 1962)

B. G. Wybourne, *Symmetry Principles and Atomic Spectroscopy*, (Wiley, N.Y., 1970)

A. W. Joshi, *Elements of Group Theory for Physicists*, (Wiley, N.Y., 1982)

[153] **Group theory in chemistry**

H. Eyring, J. Walter and G. E. Kimball, *Quantum Chemistry*, (Wiley, N.Y., 1944)

F. A. Cotton, *Chemical Applications of Group Theory*, (Wiley, N.Y., 1990) 3rd ed.

[154] **Lie groups and dynamical groups**

C. Chevalley, *Theory of Lie Groups*, (Princeton Univ., Princeton, N.J., 1946)

H. J. Lipkin, *Lie Groups for Pedestrians*, (North Holland, Amsterdam, 1965)

M. Bander and C. Itzykson, "Group theory and the hydrogen atom (I)" Rev. Mod. Phys. **38**, 330-345 (1966)

M. Bander and C. Itzykson, "Group theory and the hydrogen atom (II)" Rev. Mod. Phys. **38**, 346-358 (1966)

C. Wulfman, "Dynamical groups in atomic and molecular physics," in *Group Theory and Its Applications*, ed. E. M. Loebl (Academic, N.Y., 1971)

J.-M. Normand, *A Lie Group: Rotations in Quantum Mechanics*, (North-Holland, N.Y., 1980)

[155] **Graph theory**

D. B. West, *Introduction to Graph Theory* , (Prentice Hall, Upper Saddle River, N.J., 2000)

R. Diestel, *Graph Theory*, (Springer, Heidelberg, 2005)

[156] **Entanglement**

J. Schlienz and G. Mahler, "Description of entanglement" Phys. Rev. A **52**, 4396-4404 (1995)

A. Ekert and P. L. Knight, "Entangled quantum systems and the Schmidt decomposition" Am. J. Phys. **63**, 415-423 (1995)

V. Vedral, M. B. Plenio, M. A. Rippin and P. L. Knight, "Quantifying entanglement" Phys. Rev. Lett. **78**, 2275-9 (1997)

V. Vedral, M. B. Plenio, K. Jacobs and P. L. Knight, "Statistical inference, distinguishability of quantum states, and quantum entanglement" Phys. Rev. A **56**, 4452-5 (1997)

S. Hill and W. K. Wootters, "Entanglement of a pair of quantum bits" Phys. Rev. Lett. **78**, 5022 (1997)

G. J. Milburn, *The Feynman Processor: Quantum Entanglement and the Computing Revolution*, (Perseus, Reading, MA, 1998)

A. Rauschenbeutel, G. Nogues, S. Osnaghi, P. Bertet, M. Brune, Jean-Michel Raimond and S. Haroche, "Step-by-step engineered multiparticle entanglement" Science **288**, 2024 - 2028 (2000)

J. M. Raimond, M. Brune and S. Haroche, "Manipulating quantum entanglement with atoms and photons in a cavity" Rev. Mod. Phys. **73**, 565 - 582 (2001)

G. Vidal and R. F. Werner, "Computable measure of entanglement" Phys. Rev. A **65**, 032314 (2002)

M. P. Silverman, *Quantum Superposition: Counterintuitive Consequences of Coherence, Entanglement, and Interference*, (Springer, Berlin, 2008)

[157] **Analytic solutions, two states**

E. E. Nikitin, "The probability of nonadiabatic transitions in the case of nondivergent terms" Opt. Spectrosc. **13**, 431 (1962)

E. E. Nikitin, "Resonance and non-resonance intermolecular energy exchange in molecular collisions" Discuss. Faraday Soc. **33**, 14 -21 (1962)

Y. N. Demkov, "Charge transfer at small resonance defects" Sov. Phys. JETP **18**, 138 (1964)

J. G. Hartley and J. R. Ray, "Solutions to the time-dependent Schrdinger equation" Phys. Rev. A **25**, 2388-2390 (1982)

C. E. Carroll and F. T. Hioe, "A new class of analytic solutions of the two-state problem" J. Phys. A **19**, 3579 (1986)

N. Vitanov and G. Panev, "Generalization of the Demkov formula in near-resonant charge transfer" J. Phys. B **25**, 239-248 (1992)

N. V. Vitanov, "Generalized Demkov model: Strong-coupling approximation" J. Phys. B **26**, L53-L60 (1993) ; addendum *ibid.* 2085 (1993)

N. V. Vitanov, "Generalized Nikitin model: Strong-coupling approximation" J. Phys. B **27**, 1791-1805 (1994)

E. S. Kyoseva and N. V. Vitanov, "Coherent pulsed excitation of degenerate multistate systems: Exact analytic solutions" Phys. Rev. A **73**, 023420 (2006)

[158] **LaPlace transforms**

H. S. Carslaw and J. C. Jaeger, *Operational Methods in Applied Mathematics*, (Oxford Univ Press, London, 1948) 2nd ed.

R. V. Churchill, *Operational Mathematics*, (McGraw-Hill, N.Y., 1958)

E. D. Rainville, *The Laplace Transform: An Introduction*, (Macmillan, N.Y., 1963)

I. N. Sneddon, *The Use of Integral Transforms*, (McGraw-Hill, N.Y., 1972)

W. R. LePage, *Complex Variables and the Laplace Transform for Engineers*, (Dover, N.Y., 1980)

J. L. Schiff, *The Laplace Transform: Ttheory and Applications*, (Springer, New York, 1999)

[159] **Chirped-pulse solutions**

F. T. Hioe and C. E. Carroll, "Analytic solutions to the two-state problem for chirped pulses" J. Opt. Soc. Am. B **B3**, 497-502 (1985)

C. E. Carroll and F. T. Hioe, "Further generalization of Landau-Zener calculation" J. Opt. Soc. Am. B **2**, 1355-60 (1985)

[160] **Rosen-Zener model**

N. Rosen and C. Zener, "Double Stern-Gerlach experiment and related collision phenomena" Phys. Rev. **40**, 502-7 (1932)

[161] **Allen-Eberly model** see also [10]

F. T. Hioe, "Solutions of Bloch equations involving amplitude and frequency modulations" Phys. Rev. A **30**, 2100-2107 (1984)

[162] **Demkov-Kunike model**

Y. N. Demkov and M. Kunike, "Hypergeometric model for two-state approximation in collision theory [in Russian]" Vestn. Leningr. Univ., Ser. 4: Fiz., Khim. **16**, 39 (1969)

F. T. Hioe and C. E. Carroll, "Two-state problems involving arbitrary amplitude and frequency modulations" Phys. Rev. A **32**, 1541 (1985)

J. Zakrzewski, "Analytic solutions of the two-state problem for a class of chirped pulses" Phys. Rev. A **32**, 3748 - 3751 (1985)

K.-A. Suominen and B. M. Garraway, "Population transfer in a level-crossing model with two time scales" Phys. Rev. A **45**, 374 (1992)

[163] **Bambini-Berman model**

A. Bambini and P. R. Berman, "Analytic solutions to the two-state problem for a class of coupling potentials" Phys. Rev. A **23**, 2496-2501 (1981)

E. S. Kyoseva and N. V. Vitanov, "Coherent pulsed excitation of degenerate multistate systems: Exact analytic solutions" Phys. Rev. A **73**, 023420 (2006)

[164] **Bichromatic field**

R. Guccione-Gush and H. P. Gush, "Two-level system in a bichromatic field" Phys. Rev. A **10**, 1474 (1974)

T. S. Ho and S. I. Chu, "Semiclassical many-mode Floquet theory: II. Non-linear multiphoton dynamics of a two-level system in a strong bichromatic field" J. Phys. B **17**, 2101 (1984)

H. Freedhoff and Z. Chen, "Resonance fluorescence of a two-level atom in a strong bichromatic field" Phys. Rev. A **41**, 6013-22 (1990)

F. Ehlotzky, "Atomic phenomena in bichromatic laser fields" Phys. Rep. **345**, 175-264 (1990)

Y. Zhu, Q. Wu, A. Lezama, D. J. Gauthier and T. W. Mossberg, "Resonance fluorescence of two-level atoms under strong bichromatic excitation" Phys. Rev. **41**, 6574 - 6576 (1990)

G. S. Agarwal, Y. F. Zhu, D. J. Gauthier and T. W. Mossberg, "Spectrum of radiation from 2-level atoms under intense bichromatic excitation" J. Opt. Soc. Am. B, **8** 1163-1167 (1991)

G. S. Agarwal, W. Lange and H. Walther, "Cavity-induced decay of Floquet states in a bichromatic driving field" Phys. Rev. A **51**, 721-735 (1995)

R. G. Unanyan, S. Guérin and H. R. Jauslin, "Coherent population trapping under bichromatic fields" Phys. Rev. A **62**, 3407 (2000)

L. P. Yatsenko, B. W. Shore, N. V. Vitanov and K. Bergmann, "Retroreflection-induced bichromatic adiabatic passage" Phys. Rev. A **68**, 3405 (2003)

[165] **Coherent excitation with hyperfine structure**

B. W. Shore and M. A. Johnson, "Effects of hyperfine structure on coherent excitation" Phys. Rev. A **23**, 1608-1610 (1981)

A. Kuhn, S. Steuerwald and K. Bergmann, "Coherent population transfer in NO with pulsed lasers: the consequences of hyperfine structure, Doppler broadening and electromagnetically induced absorption" Eur. Phys. J. D **1**, 57-70 (1998)

[166] **Density matrix**

U. Fano, "Description of states in quantum mechanics by density matrix and operator techniques" Rev. Mod. Phys. **29**, 74 (1957)

R. McWeeny, "Some recent advances in density matrix theory" Rev. Mod. Phys. **32**, 335 (1960)

D. Ter Haar, "Theory and application of the density matrix" Repts. Prog. Phys. **24**, 304 (1961)

A. Omont, "Irreducible components of the density matrix. Application to optical pumping" Prog. Quant. Electron. **5**, 69-138 (1977)

K. Blum, *Density Matrix Theory and Applications*, (Plenum, N.Y., 1981)

B. M. Garraway and P. L. Knight, "Evolution of quantum superpositions in open environments: Quantum trajectories, jumps, and localization in phase space" Phys. Rev. A **50**, 2548-63 (1994)

M. G. A. Paris, "On density matrix reconstruction from measured distributions" Opt. Comm. **124**, 277-282 (1996)

K. L. Pregnell and D. T. Pegg, "Measuring the elements of the optical density matrix" Phys. Rev. A **66**, 013810 (2002)

[167] **Coherence vector**

J. N. Elgin, "Semiclassical formalism for the treatment of three-level systems" Phys. Lett. **80A**, 140-142 (1980)

F. T. Hioe and J. H. Eberly, "N-level coherence vector and higher conservation laws in quantum optics and quantum mechanics" Phys. Rev. Lett. **47**, 838-41 (1981)

J. Oreg, F. T. Hioe and J. H. Eberly, "Adiabatic following in multilevel systems" Phys. Rev. A **29**, 690-7 (1984)

J. Oreg and S. Goshen, "Spherical modes in N-Level systems" Phys. Rev. A **29**, 3205-3207 (1984)

[168] **Atom optics**

M. Kasevich and S. Chu, "Atomic interferometry using stimulated Raman transitions" Phys. Rev. Lett. **67**, 181-184 (1991)

C. S. Adams, "Atom optics" Contemp. Phys. **35**, 1-19 (1994)

C. S. Adams, M. Sigel and J. Mlynek, "Atom optics" Phys. Rep. **240**, 143-210. (1994)

J. Lawall and M. Prentiss, "Demonstration of a novel atomic beam splitter" Phys. Rev. Lett. **72**, 993-996 (1994)

L. S. Goldner, C. Gerz, R. J. Spreeuw, S. L. Rolston, C. I. Westbrook, W. D. Phillips, P. Marte and P. Zoller, "Momentum transfer in laser-cooled cesium by adiabatic passage in a light field" Phys. Rev. Lett. **72**, 997-1000 (1994)

V. I. Balykin and V. S. Letokhov, *Atom Optics with Laser Light*, (Harwood Academic Chur, Switzerland 1995)

P. D. Featonby, G. S. Summy, J. L. Martin, H. Wu, K. P. Zetie, C. J. Foot and K. Burnett, "Adiabatic transfer for atomic interferometry" Phys. Rev. A **53**, 373-380 (1996)

P. R. Berman, ed. *Atom Interferometry*, (Academic, San Diego, 1997)

P. Meystre, *Atom Optics*, (Springer, New York, 2001)

K. Bongs and K. Sengstock, "Physics with coherent matter waves" Repts. Prog. Phys. **67**, 907 (2004)

[169] **Laser force** see also [168, 41]

H. Friedmann and A. D. Wilson, "Isotope separation by radiation pressure of coherent pi pulses" Appl. Phys. Letts. **28**, 270-272 (1976)

A. P. Kazantsev, "Resonance light pressure" Sov. Phys. Usp. **21**, 58-76 (1978)

V. G. Minogin and O. T. Serimaa, "Resonant light pressure forces in a strong standing laser wave" Opt. Comm. **30**, 373-379 (1979)

D. Dalibard and C. Cohen-Tannoudji, "Dressed-atom approach to atomic motion in laser light: The dipole force revisited" J. Opt. Soc. Am. B **2**, 1707-1860 (1985)

P. W. Milonni, R. J. Cook and M. E. Goggin, "Radiation pressure from the vacuum: Physical interpretation of the Casimir force" Phys. Rev. A **38**, 1621-3 (1988)

A. P. Kazantsev, G. I. Durdotovich and V. P. Yakovlev, *Mechanical Action of Light on Atoms*, (World Scientific, Singapore, 1990)

K. Ellinger, J. Cooper and P. Zoller, "Light-pressure force in N-atom systems" Phys. Rev. A **49**, 3909-3933 (1994)

S. Chu, "Nobel Lecture: The manipulation of neutral particles" Rev. Mod. Phys. **70**, 685 - 706 (1998)

C. N. Cohen-Tannoudji, "Manipulating atoms with photons" Rev. Mod. Phys. **70**, 707-19 (1998)

[170] **Atomic deflection Hamiltonian** see also [171]

A. F. Bernhardt and B. W. Shore, "Coherent atomic deflection by resonant standing waves" Phys. Rev. A **23**, 1290 (1981)

A. P. Kazantsev, G. A. Ryabenko, G. I. Surdutovich and V. P. Yakovlev, "Scattering of atoms by light" Phys. Rep. **129**, 75-144 (1985)

A. Aspect, E. Arimondo, R. Kaiser, N. Vansteenkiste and C. Cohen-Tannoudji, "Laser cooling below the one-photon recoil energy by velocity-xselective coherent population trapping - theoretical analysis" J. Opt. Soc. Am. B, **6** 2112-2124 (1989)

E. M. Wright and P. Meystre, "Theory of an atomic interferometer in the Raman-Nath regime" Opt. Comm. **75**, 388-396 (1990)

B. W. Shore, P. Meystre and S. Stenholm, "Is a quantum standing wave composed of two traveling waves?" J. Opt. Soc. Am. B, **8**, 903-10 (1991)

[171] **Laser deflection of an atomic beam** see also [170]

P. L. Kapitza and P. A. M. Dirac, "Reflection of electrons from standing light waves" Proc. Camb. Phil. Soc. **29**, 297-300 (1933)

A. Ashkin, "Atomic-beam deflection by resonance-radiation pressure" Phys. Rev. Lett. **25**, 1321-24 (1970)

A. F. Bernhardt, D. E. Duerre, J. R. Simpson and L. L. Wood, "High resolution spectroscopy using photodeflection" Opt. Comm. **16**, 166-171 (1976)

E. Arimondo, A. Bambini and S. Stenholm, "Diffraction pattern of atoms in a resonant standing wave laser field" Opt. Comm. **37**, 103-107 (1981)

C. Tanguy, S. Reynaud and C. Cohen-Tannoudji, "Deflection of an atomic beam by a laser wave: Transition between diffractive and diffusive regimes" J. Phys. B **17**, 4623 (1984)

P. J. Martin, P. L. Gould, B. G. Oldaker, A. H. Miklich and D. E. Pritchard, "Diffraction of atoms moving through a standing light wave" Phys. Rev. A **36**, 2495-98 (1987)

P. Meystre, E. Schumacher and S. Stenholm, "Atomic beam deflection in a quantum field" Opt. Comm. **73** 443-7 (1989)

P. L. Gould, P. J. Martin, G. A. Ruff, R. E. Stoner, J.-L. Picque and D. E. Pritchard, "Momentum transfer to atoms by a standing light wave: Transition from diffraction to diffusion" Phys. Rev. A **43**, 585-90 (1991)

M. A. M. Marte, J. I. Cirac and P. Zoller, "Deflection of atoms by circularly polarized light beams in triple Laue configuration" J. Mod. 'Opt. **38**, 2265-2280 (1991)

S. M. Tan and D. F. Walls, "Atomic deflection in the transition between diffractive and diffusive regimes: A numerical simulation" Phys. Rev. A **44**, R2779-82 (1991)

T. Sleator, T. Pfau, V. Balykin, O. Carnal and J. Mlynek, "Experimental demonstration of the optical Stern-Gerlach effect" Phys. Rev. Lett. **68**, 1996-9 (1992)

[172] **Atomic beam splitter** see also [168]

P. Marte, P. Zoller and J. L. Hall, "Coherent atomic mirrors and beam splitters by adiabatic passage in multilevel systems" Phys. Rev. A **44**, R4118-21 (1991)

J. Lawall and M. Prentiss, "Demonstration of a novel atomic beam splitter" Phys. Rev. Lett. **72**, 993-996 (1994)

H. Theuer and K. Bergmann, "Atomic beam deflection by coherent momentum transfer and the dependence on weak magnetic fields" Euro. Phys. J. D **2**, 279-89 (1998)

[173] **Adiabaticity in scattering**

N. F. Mott and H. S. W. Massey, *The Theory of Atomic Collisions*, (Clarendon Press, Oxford, 1965)

E. E. Nikitin, *Theory of Elementary Atomic and Molecular Processes in Gases*, (Clarendon, Oxford, 1974)

H. S. W. Massey, *Atomic and Molecular Collisions*, (Taylor & Francis, London, 1979)

[174] **Multilevel adiabatic evolution** see also [77, 76, 78]

M. V. Kuz'min and V. N. Sazanov, "Complete population inversion in a multilevel quantum system on adiabatic application of an external resonance field" Sov. Phys. JETP **52**, 889-94 (1980)

F. T. Hioe, "Theory of generalized adiabatic following in multilevel systems" Phys. Lett. **99A**, 150 (1983)

J. Oreg, F. T. Hioe and J. H. Eberly, "Adiabatic following in multilevel systems" Phys. Rev. A **29**, 690-7 (1984)

G. L. Peterson and C. D. Cantrell, "Adiabatic excitation of multilevel systems" Phys. Rev. A **31**, 807-822 (1985)

B. R. Holstein, "The adiabatic propagator" Am. J. Phys. **57**, 714-20 (1989)

J. Vidal and J. Wudka, "Adiabatic evolution of quantum-mechanical systems" Phys. Rev. A **44**, 5383-89 (1991)

B. W. Shore, K. Bergmann, J. Oreg and S. Rosenwaks, "Multilevel adiabatic population transfer" Phys. Rev. A **44**, 7442-7447 (1991)

B. W. Shore, K. Bergmann, A. Kuhn, S. Schiemann, J. Oreg and J. H. Eberly, "Laser-induced population transfer in multistate systems: a comparative-study" Phys. Rev. A **45**, 5297-5300 (1992)

Y. B. Band, "Adiabatic approximation for the density matrix" Phys. Rev. A **45**, 6643-51 (1992)

A. V. Smith, "Numerical studies of adiabatic population inversion in multilevel systems" J. Opt. Soc. Am. B **9**, 1543-1551 (1992)

P. Pillet, C. Valentin, R.-L. Yuan and J. Yu, "Adiabatic population transfer in a multilevel system" Phys. Rev. A **48**, 845-848 (1993)

J. S. Melinger, S. R. Gandhi, A. Hariharan, D. Goswami and W. S. Warren, "Adiabatic population transfer with frequency-swept laser pulses" J. Chem. Phys. **101**, 6439-6454 (1994)

P. D. Featonby, G. S. Summy, J. L. Martin, H. Wu, K. P. Zetie, C. J. Foot and K. Burnett, "Adiabatic transfer for atomic interferometry" Phys. Rev. A **53**, 373-380 (1996)

A. Joye, F. Monti, S. Guérin and H. R. Jauslin, "Adiabatic evolution for systems with infinitely many eigenvalue crossings" J. Math. Phys. **40**, 5456-5472 (1999)

V. S. Malinovsky and J. L. Krause, "General theory of population transfer by adiabatic rapid passage with intense, chirped laser pulses" Eur. Phys. J. B **14**, 147-155 (2001)

S. Guérin, S. Thomas and H. R. Jauslin, "Optimization of population transfer by adiabatic passage" Phys. Rev. A **65**, 023409 (2002)

L. P. Yatsenko, S. Guérin and H. R. Jauslin, "Topology of adiabatic passage" Phys. Rev. A **65**, 043407 (2002)

S. Teufel, *Adiabatic Perturbation Theory in Quantum Dynamics*, (Springer, Berlin, 2003)

P. A. Ivanov and N. V. Vitanov, "Adiabatic evolution amidst dephasing" Phys. Rev. A **71**, 063407 (2005)

P. Král, I. Thanopulos and M. Shapiro, "Colloquium: Coherently controlled adiabatic passage" Rev. Mod. Phys. **79**, 53 (2007)

[175] **Adiabatic evolution with two states** see also [76, 77]

C. Zener, "Non-adiabatic crossing of energy levels" Proc. Roy. Soc. (Lond.) A **137**, 696-9 (1932)

A. M. Dykhne, "Quantum transitions in the adiabatic approximation" Sov. Phys. JETP **11**, 411-15 (1960)

D. Grischkowsky, "Adiabatic following and slow optical pulse propagation in rubidium vapor" Phys. Rev. A **7**, 2096-2101 (1973)

M. M. T. Loy, "Observation of population inversion by optical adiabatic rapid passage" Phys. Rev. Lett. **32**, 814-17 (1974)

R. T. Robiscoe, "Quasiadiabatic solution to the two-level problem" Phys. Rev. A **25**, 1178-1180 (1982)

C. Liedenbaum, S. Stolte and J. Reuss, "Inversion produced and reversed by adiabatic passage" Phys. Rep. **178**, 1-24 (1989)

J. S. Melinger, A. Hariharan, S. R. Gandhi and W. S. Warren, "Adiabatic population inversion in I2 vapor with picosecond laser pulses" J. Chem. Phys. **95**, 2210-13 (1991)

[176] **Adiabatic evolution with three states** see also [3, 98, 107]

J. R. Kuklinski, U. Gaubatz, F. T. Hioe and K. Bergmann, "Adiabatic population transfer in a three-level system driven by delayed laser pulses" Phys. Rev. A **40**, 6741-44 (1989)

M. Elk, "Adiabatic transition histories of population transfer in the lambda system" Phys. Rev. A **52**, 4017-4022 (1995)

N. V. Vitanov and S. Stenholm, "Non-adiabatic effects in population transfer in three-level systems" Optics Comm. **127**, 215-222 (1996)

N. V. Vitanov and S. Stenholm, "Analytic properties and effective two-level problems in stimulated Raman adiabatic passage" Phys. Rev. A **55**, 648-660 (1997)

[177] **Morris-Shore transformation for propagation**

F. E. Zimmer, J. Otterbach, R. G. Unanyan, B. W. Shore and M. Fleischhauer, "Dark-state polaritons for multi-component and stationary light fields" Phys. Rev. A **77**, 063823 (2008)